Modélisation de la dynamique des hydrocarbures aromatiques polycycliques (HAP) dans des sols soumis à un gradient de contamination allant d'un contexte agricole à un contexte industriel

Khaled Brimo

Modélisation de la dynamique des hydrocarbures aromatiques polycycliques (HAP) dans des sols soumis à un gradient de contamination allant d'un contexte agricole à un contexte industriel

Khaled Brimo

NNT : 2017SACLA0017

THESE DE DOCTORAT
DE
L'UNIVERSITE PARIS-SACLAY
PREPAREE A AGROPARISTECH
" L'INSTITUT DES SCIENCES ET INDUSTRIES DU VIVANT ET DE L'ENVIRONNEMENT "

ECOLE DOCTORALE n°581
Agriculture, alimentation, biologie, environnement et santé (ABIES)

Spécialité de doctorat : Science de l'Environnement

Par

Khaled BRIMO

Modélisation de la dynamique des hydrocarbures aromatiques polycycliques (HAP) dans des sols soumis à un gradient de contamination allant d'un contexte agricole à un contexte industriel

Thèse présentée et soutenue à Paris le 05 Mai 2017

Composition du Jury :

M. PERY Alexandre	ICPEF (HDR), AgroParisTech	Président
M. TRAPP Stefan	Professeur DTU, Danemark	Rapporteur
M. MARTINS Jean	Directeur de recherche, CNRS, LTHE Grenoble	Rapporteur
Mme DEPORTES Isabelle	Ingénieure ADEME, Angers	Examinateur
Mme DELOLME Cécile	IPEF, Université Paris-Est	Examinateur
Mme OUVRARD Stéphanie	Chargée de recherche HDR, INRA-LSE Nancy	Co-directeur de thèse
Mme GARNIER Patricia	Directrice de recherche, INRA-ECOSYS Grignon	Directeur de thèse

REMERCIEMENTS

Les travaux qui font l'objet de ce mémoire ont été réalisés en cotutelle entre le centre INRA de Grignon au sein de l'équipe « Sol » de l'unité ECOSYS et le laboratoire Sols et Environnement (LSE) à Nancy au sein l'équipe « Phytoremédiation », sous la direction de Patricia GARNIER, directrice de recherche à l'INRA de Grignon, et Stéphanie OUVRARD, chargée de recherche à l'INRA au LSE à Nancy. La thèse a bénéficié d'un cofinancement de l'ADEME et du département «Environnement et Agronomie » de l'INRA.

Tout d'abords, je tiens à exprimer ma profonde et sincère reconnaissance à mes deux directrices de thèse **Patricia GARNIER** et **Stéphanie OUVRARD** pour m'avoir fourni le cadre pour mener à bien ce travail. Un GRAND MERCI pour leurs conseils, leur disponibilité, leur soutien moral, leurs discussions constructives et pour avoir réussi à me redonner la confiance dans mes moments difficiles. Merci beaucoup pour tout !

Je tiens à remercier François LAFOLIE, chercheur à l'INRA d'Avignon pour avoir encadré le travail de mise au point du modèle sous la plateforme VSoil. Je tiens à lui adresser ma reconnaissance pour avoir pris le temps de répondre à mes questions fréquentes et pour avoir accepté de participer aux comités de pilotages de ma thèse. Je remercie également l'équipe informatique de VSoil, Nicolas MOITRIER, Nathalie MOITRIER, Cédric NOUGUIER du centre INRA d'Avignon et Valérie POT chercheur à l'INRA de Grignon pour leur aide précieuse à résoudre les problèmes techniques lors de l'utilisation de VSoil.

Je suis très reconnaissant aux membres de mon comité de thèse pour leurs conseils judicieux : Sabine HOUOT et Pierre BENOIT, chercheurs à l'INRA de Grignon, Jean Luc BERTRAND KRAJEWSKI, professeur de l'INSA de Lyon et Geoffroy SERE maître de conférences à l'université de Lorraine. Je les remercie chaleureusement du temps qu'ils ont consacré à cette thèse. Isabelle DEPORTS, ingénieur à l'ADEME, a accompagné cette thèse et à participé aux comités de pilotages. Je la remercie également pour avoir acceptée d'évaluer ce travail en participant au Jury de thèse.

Je tiens à remercier le professeur Enrique BARRIUSO, directeur de recherche à l'INRA de Grignon et le professeur Christophe SCHWARTZ, directeur du laboratoire LSE, pour

m'avoir accueilli au sein de leur laboratoire. Je tiens également à remercier tous les personnels scientifiques, administratifs et techniques qui m'ont souvent rendu service. Je remercie particulièrement Vincent MERCIER, Daniel POUDROUX et Anita BARAZER de centre INRA de Grignon, et Alain RAKOTO, Laetitia DESPOUY, Sylvia L'HUILLIER du LSE de Nancy. Mes remerciements vont aussi à Sophie LEGUEDOIS, chercheur à l'INRA de Nancy pour les discussions scientifiques constructives et pour m'avoir aidé à mon dossier de Bourse DEMOLON, Pierre LÉGLIZE, maître de conférences à l'université de Lorraine, pour son soutien moral, Noëlle RAOULT directrice de site GISFI pour son aide à chercher les données expérimentales du site GISFI, ainsi qu'à Marjolaine DESCHAMPS ingénieur à l'INRA de Grignon pour son aide précieuse dans le cadre des données de HAP du site QUALIAGRO..

Je tiens aussi à remercie Dr. Irina VASSILEVA et Corinne FIERS de l'Ecole Doctorale ABIES et Valérie PINEUX de ADEME pour leur disponibilité qu'elles apportent aux thésards et pour leur aide dans les démarches administratives.

Je remercie Monsieur Jean MARTINS, directeur de recherche à LTHE de Grenoble et Monsieur Stefan TRAPP, professeur à l'université Technique de Danemark, qui m'ont fait l'honneur en acceptant d'être rapporteurs de ce travail. Je tiens à adresser mes remerciements à Madame Cécile DELOME, directrice de recherche à l'université Paris-Est et Monsieur Alexandre PERY, professeur directeur de l'école doctorale ABIES AgroParisTech pour avoir acceptés de participer à mon jury de thèse.

Merci à toutes les personnes avec qui j'ai passé des bons moments. Merci beaucoup à tous mes amis thésards, post-doctorants et stagiaires présents et passés à Grignon ou à Nancy, à mes anciens colocataires pendant mon séjour à Grignon, et à toutes les personnes que j'ai oubliées de citer.

Enfin, il me reste à remercier mes très chers parents en Syrie, mes deux sœurs Roselyne et Rabab et mon frère Nabil ainsi qu'à ma copine Gihan pour leur soutien et leurs encouragements inconditionnels malgré l'horreur de la guerre, et à eux tous je dédie mon travail.

TABLE DES MATIERES

LISTE DES ABREVIATIONS

AIC = Akaike information criterion

BAP = Benzo(a)pyrene

BioW = Biowaste compost

cp = Compost

corr = Correlation coefficient

DCM =Dichloromethane

ds =Dry soil

DREAM =Differential evolution adaptive metropolis

ETP =Evapotranspiration

$\mathbf{f_C}$ =Lignin content dependence factor

FLT =Fluoranthene

$\mathbf{f_{oc}}$ =Organic carbon content in soil

fr =Correction factor

$\mathbf{f_T}$ =Temperature dependence factor

$\mathbf{f_W}$ =Water content dependence factor

GWS =Green waste and sludge compost

IPCC =Intergovernmental Panel on Climate Change

$\mathbf{K_d}$ =Sorption distribution coefficient

$\mathbf{K_{oc}}$ =Sorption distribution coefficient normalized to organic carbon

$\mathbf{K_{ow}}$ =Octanol-water partition coefficient

m =Number of model outputs

MSW =Municipal solid waste compost

n =Number of measured points

NER = Non-extractible residues

NS =Nash-Sutcliffe model efficiency index

OC =Organic carbon

P =Number of estimated parameters excluding fixed parameters

PAH =Polycyclic aromatic hydrocarbons

pdfs =Probability density functions

PHE =Phenanthrene

POP =Persistent organic pollutants

R =Rainfall

SOM =Soil organic matter

US-EPA = United States Environmental Protection Agency

T =Temperature

TDR =Time Domain Reflectometry probes

VSoil =Virtual Soil platform

x =Model inputs

y =Model outputs

$\mathbf{y_{calc,t,i}}$ =Predicted values at the tth observed time for the ith model output

$\mathbf{y_{obs,t,i}}$ = Observed values at the tth observed time for the ith model output

$\boldsymbol{\rho(y/x)}$ =Marginal likelihood

$\boldsymbol{\rho(y/\theta, x)}$ =Likelihood function

$\boldsymbol{\rho(\theta)}$ =Probability density of prior distribution of parameters

$\mathbf{U^2}$ =Inequality coefficient

χ^2 = Chi-square test

PAH model variables

$\mathbf{B_{SPE}}$ =Specific microbial biomasses

$\mathbf{PAH_{AV}}$ =PAH as available in soil solution

$\mathbf{PAH_{Bs}}$ =PAH as biogenic non-extractible residues

$\mathbf{PAH_{CO2}}$ =Carbon dioxide gas produced from the mineralization of PAH

$\mathbf{PAH_{CPWS}}$ =PAHs that is weakly sorbed onto organic carbon pools of compost

$\mathbf{PAH_{MET}}$ =PAH as metabolites

$\mathbf{PAH_{SS}}$ =PAH as strongly sorbed fraction

$\mathbf{PAH_{WS}}$ =PAH as weakly sorbed fraction

$\mathbf{X_{cp}}$ =Microbial biomass degrades the organic matter of the compost,

$\mathbf{X_{soil}}$ =Microbial biomass that degrades the soil organic matter

$\mathbf{X_{tot}}$ =Microbial biomass is the sum of the two previous microbial biomasses

OC module variables

$\mathbf{SDN_{SLOW}}$ =Proportion of organic C in the soluble fraction of pH-neutral detergent with slow degradation (pool Ci=1)

SDN_{FAST} =Proportion of organic C in the soluble fraction of pH-neutral detergent with fast degradation (pool Ci=2)

HCEL =Hemicelluloses-like fraction (pool Ci=3)

CEL =Cellulose-like fraction (pool Ci=4)

LIG =Lignin-like fraction (pool Ci=5)

DOC =Organic C soluble in hot water

Xcp =Microbial biomass in native compost

$CO2_{org}$ =Microbial biomass in native compost

$CO2_{org}$ =Organic carbon dioxide

HOC =Humified organic C

PAH model parameters

α =Magnitude of metabolites production by biodegradation for specific biomass

β =Magnitude of metabolites production by biodegradation for co-metabolism

μs_{max} =Maximum specific growth rate

k_{AW} =First order kinetic constant that goes from PAHAV into PAHWS compartment

k_{deg} =Kinetic constant of biodegradation for co-metabolism

k_{M} =Mortality rate constant

k_{MB} =First order kinetic constant that goes from PAHMET into PAHBs compartment

ks_{spe} =Half saturation of growth substrate for the specific biomass

k_{SW} =First order kinetic constant that goes from PAHSS into PAHWS compartment

k_{WA} =First order kinetic constant that goes from PAHWS into PAHAV compartment

k_{WS} =First order kinetic constant that goes from PAHWS into PAHSS compartment

Y_{spe} =Yield of specific biomass

OC module parameters

$\mu_{max\ cp}$ =Maximal growth rate for microbial biomass

k_{CEL} =Hydrolysis constant of $C_{i=4}$=CEL

k_{FAST} = Hydrolysis constant of $C_{i=2}$=SDN_{FAST}

k_{HCEL} = Hydrolysis constant of $C_{i=3}$=HCEL

k_{LIG} = Hydrolysis constant of $C_{i=5}$=LIG

Ks_{cp} =Saturation constant for Monod kinetic

k_{SLOW} =Hydrolysis constant of $C_{i=1}$=SDN_{SLOW}

m_{cp} =Death constant for microbial biomass

$\mathbf{w_{cp}}$ =Proportion of dead biomasses into HOC pool

$\mathbf{Y_{cp}}$ = Assimilation yield of organic C available for microbial biomass

$\mathbf{Y_{SW\,cp}}$ =Availability yield for dead microbial biomass

INTRODUCTION GENERALE

Du fait de la proximité d'activités industrielles passées ou anciennes, de la revalorisation agricole de sites modérément pollués ou de l'apport de matière organique exogène issue de déchets organiques, des contaminants organiques tels que les hydrocarbures aromatiques polycycliques (HAP) se retrouvent dans les sols. Ces composés reconnus comme toxiques présentent un risque de transfert vers les végétaux cultivés mais aussi vers les eaux souterraines par lixiviation et lessivage ou les eaux de surface par ruissellement. Néanmoins, les processus d'atténuation naturelle concourent à abaisser leur teneur dans les sols.

Des efforts importants sont actuellement réalisés pour décrire, comprendre et améliorer l'élimination des micropolluants, tels que les HAP au cours des différents procédés de traitements des déchets organiques (digestion anaérobie, compostage). Les traitements des produits résiduaires organiques conduisent à une stabilisation de la matière organique et dans une certaine mesure à un abattement des teneurs en micropolluants organiques (Lashermes et al., 2013). Toutefois peu de données existent sur leur devenir dans les sols (Kester et al., 2005; Monserie et al., 2009) et sur le lien qui existe entre leur traitement et leur devenir (Fragoulis et al., 2005; Pritchina et al., 2011). Par ailleurs, de nombreux travaux ont mis en évidence l'intérêt de la mise en culture pour accélérer les processus naturels de biodégradation des polluants organiques des sols contaminés (phytoremédiation), tels que les HAP (Haritash and Kaushik, 2009; Megharaj et al., 2011; Ouvrard et al., 2014) mais ces approches conduites *in situ* sur des terres anciennement contaminées peuvent se révéler moins efficaces du fait de la faible disponibilité des polluants. L'ancienneté de la contamination et sa forte association avec la matière organique sont mises en avant pour expliquer cette limitation (Ouvrard et al., 2014). La mise en œuvre des procédés de phytoremédiation des HAP nécessite alors une meilleure compréhension des mécanismes d'évolution de ces composés afin de i) prédire leur vitesse de dissipation et ainsi les durées de traitement attendues ; ii) vérifier leur transfert vers les autres compartiments de l'écosystème en particulier le compartiment eau afin de garantir la faible innocuité du système au cours du traitement ; iii) valoriser l'efficacité de stratégies d'atténuation naturelle en comparaison avec d'autres stratégies de restauration du sol (e.g., l'addition des solvants organiques pour accélérer la désorption).

En général, quel que soit le niveau et l'origine des contaminations en HAP dans le sol, très peu de travaux existent portant sur la modélisation de l'évolution de la disponibilité des HAP qui permettraient de mieux comprendre, de prédire les risques potentiels et d'apporter des solutions. La plupart des modèles de polluants organiques dans les sols sont des modèles de pesticides (FOCUS, 2006) et ne prennent pas en compte les interactions avec la matière

organique. De plus, les données cinétiques des divers HAP sont rares dans la littérature pour la prédiction du devenir des HAP dans le sol.

Les objectifs scientifiques de cette thèse sont alors la mise au point d'un modèle numérique décrivant des processus en interaction dans le sol afin de mieux comprendre les fonctions d'épuration du sol, de prévoir l'évolution d'une contamination organique potentielle, et de tester différentes stratégies de restauration des sols pollués ou de recyclage de déchets par rapport au devenir des HAP dans les sols.

Dans ce but, nous développons un nouveau model au sein de la plateforme SOL VIRTUEL de l'INRA (https://www6.inra.fr/vsoil) permettant de simuler la dynamique des HAP dans les sols dans deux contextes de contamination contrastés. Le contexte 1 étudie l'évolution de fortes concentrations de HAP dans des sols pollués de sites industriels où la mise en culture vise à remédier cette contamination pour la production de biomasse (site du GISFI, 54), et le contexte 2 étudie l'évolution de faibles concentrations de HAP apportés par des produits résiduaires organiques compostés en parcelles agricoles (site du QUALIAGRO, 78). Ces deux situations extrêmes offrent, au-delà de la concentration en contaminant, des contextes agronomiques et pédologiques, en particulier sur la nature des matières organiques, différents qu'il conviendra d'intégrer à l'approche de modélisation. Le modèle calibré et testé sera ensuite utilisé pour tester différentes stratégies de restauration des sols pollués ou de recyclage de déchets ce qui nous permettra de prédire à long terme des risques environnementaux liés à ces produits.

Initiée en Octobre 2013, cette thèse a été financée par l'ADEME (Agence de l'Environnement et de la Maîtrise de l'Energie) et par le département « Environnement et Agronomie » de l'Institut National de la Recherche Agronomique (INRA). Elle s'est déroulée, sous la direction de Patricia Garnier et Stéphanie Ouvrard dans deux équipes de recherches (l'équipe « Sol » de l'unité ECOSYS à Thiverval-Grignon (78), et l'équipe « Phytoremédiation des sols contaminés » du Laboratoire Sols et Environnement « LSE » de Nancy (54)) qui partagent une même préoccupation scientifique d'étude, à savoir le devenir des contaminants organiques dans les sols, mais dans des contextes très différents.

Ce mémoire comporte un chapitre de synthèse bibliographique (chapitre I) qui fait le point sur les sources de HAP dans les sols, les processus majeurs qui ont lieu, les modèles accessibles dans la littérature, et leurs contraintes d'utilisation. Cette synthèse conduit à la présentation des objectifs spécifiques de cette thèse ainsi qu'à la présentation de la démarche adoptée pour ce travail. Le manuscrit est composé ensuite de 4 chapitres (chapitres II à V) présentant les manuscrits de publications scientifiques issues de ce travail de thèse qui sont soient publiés,

soient soumis, soient en attente de soumission. Une conclusion générale et les perspectives sont données à la fin du mémoire.

Chapitre I. Devenir des HAP dans le sol : présentation des processus et approches de modélisation

1. Présentation des HAP dans les sols

Les hydrocarbures aromatiques polycycliques (HAP) sont des polluants organiques ubiquistes et toxiques produits principalement lors de la combustion incomplète des matières organiques (par exemple le charbon, l'huile, l'essence ou le bois).

Le nombre de HAP identifiés à ce jour est de l'ordre de 130. Parmi ceux-ci, une liste de 16 composés est généralement considérée pour les études environnementales. Ce sont les polluants retenus comme prioritaires par l'agence de protection de l'environnement des États-Unis (US-EPA). Cette sélection a été effectuée en prenant en compte leur toxicité, leur persistance et leur accumulation dans l'environnement. Les structures de ces molécules ainsi que quelques unes de leurs propriétés physico-chimiques sont résumées dans le Tableau I.1.

1.1. Propriétés physico-chimiques

Les hydrocarbures aromatiques polycycliques sont composés d'atomes de carbone et d'hydrogène dont la structure des molécules comprend au moins deux cycles aromatiques fusionnés par des arrangements linéaires, angulaires ou en coin (Toro et al., 2000). Les HAP angulaires, par exemple le pyrène, sont les plus stables (Blumer, 1976). Les propriétés physico-chimiques des HAP déterminent leur comportement dans l'environnement et particulièrement dans les sols (Chung and Alexander, 2002; Nam et al., 2003). Les HAP ayant été les plus étudiés dans la littérature et étant les plus couramment investigués sont l'anthracène et le benzo[a]pyrène (CCME, 2008). Les HAP sont souvent classés en fonction de leur poids moléculaire : les HAP avec deux ou trois cycles benzéniques sont les HAP à faible poids moléculaire (de l'ordre de 152-178 g mol^{-1}, par exemple le naphtalène et le phénanthrène) alors que les HAP avec quatre cycles benzéniques ou plus sont les HAP à fort poids moléculaire (de l'ordre de 228-278 g.mol^{-1}, par exemple fluoranthène et benzo[a]pyrène) (Iarc, 2010). Les HAP sont des composés hydrophobes et sont caractérisés

par une importante affinité pour les phases organiques (i.e. les matières organiques, les solvants apolaires). A l'inverse, la solubilité de HAP est très faible dans l'eau. Les HAP sont caractérisés par une solubilité décroissante avec l'augmentation du nombre de cycles benzéniques (Masih et al., 2010) et donc avec l'augmentation de leur poids moléculaire (Chen and Aitken, 1999; Thorsen et al., 2004). Le naphtalène (2 cycles) est le composé le plus léger (Tableau I.1) et donc le plus soluble. Sa solubilité est environ 10^5 fois supérieure à celle du benzo[g.h.i]perylène (6 cycles). Le coefficient de partage octanol/eau (Kow) permet de donner une estimation de l'affinité des HAP pour les phases organiques. Les valeurs de log K_{OW} pour les HAP sont comprises entre 3 et 8 (Miller et al., 1985). La tension de vapeur de HAP est relativement faible, mais les HAP légers avec deux cycles benzéniques sont considérées comme semi-volatils. Les HAP présentent une volatilité décroissante avec l'augmentation du poids moléculaire. Cette volatilité est estimée par la constante de Henry (K_H) qui exprime le ratio de la concentration dans l'air et dans l'eau à l'équilibre. Les valeurs de K_H pour les HAP sont comprises entre 0.0048 et 14.7 Pa m^3 mol^{-1}. Généralement, si la valeur de K_H est inférieure à la valeur seuil de 100 Pa m^3 mol^{-1}, la volatilisation du polluant n'est pas significative (Byrns, 2001). Du fait de leurs hydrophobie, lipophilie et faible volatilité, les HAP tendent à s'adsorber sur des particules minérales, magnétiques ou carbonées dans les cendres et la suie (Griest and Tomkins, 1986). Cette partition influe sur leur transport et leur réactivité dans l'environnement.

1.2. Sources et distribution dans les sols

Les HAP sont présents dans le sol du fait de différentes sources naturelles ou anthropiques dont : la biosynthèse par des organismes vivants (Seo et al., 2007), les feux de forêts (Mandalakis et al., 2005), l'enfouissement de la matière organique (Soclo et al., 2000) et la combustion des énergies fossiles (charbons, pétroles). Ce dernier processus constitue le plus grand contributeur d'apport de HAP dans les sols et résulte majoritairement d'activités industrielles, en particulier de cokeries et d'usines à gaz (Sharma, H. and Khan, 2007; Vane et al., 2014). Parmi les autres sources anthropiques des HAP on notera les contaminations localisées induites par des fuites de pétroles ou de goudrons, ainsi que le recyclage en agriculture de produits résiduaires organiques avec valeurs significatives de HAP.

Du fait de leurs proprietés physico-chimiques, le transfert atmosphérique est le moyen le plus important de dispersion des HAP dans l'environnement. La plupart des HAP atteignent le sol par les retombés atmosphériques sous des flux secs et humides (van Noort and Wondergem, 1985). Ceux-ci sont généralement reliés aux conditions météorologiques, la période de

l'année, l'heure du jour et les propriétés du site d'étude. Les retombés atmosphériques de HAP en France ont été investiguées dans plusieurs travaux (Azimi et al., 2005; Blanchard et al., 2007; Garban et al., 2002; Motelay-Massei et al., 2007). Par exemple, Garban et al. (2002) ont constaté des flux de 14 HAP de 5 à 6 fois supérieurs dans les zones urbaines par rapport à ceux dans les zones rurales en France. Ainsi, ils ont estimé des flux pour 14 HAP en zones urbaines à 2 g ha^{-1} an^{-1}.

Tableau I.1. Liste des 16 HAP appartenant à la liste des polluants prioritaires de l'US EPA et leurs principales propriétés chimiques (Source : Mackay et al., 2006)

HAP	Structure	Poids moléculaire (g mol^{-1})	Solubilité dans l'eau à 25 °C (mg L^{-1})	Constante de Henry à 25 °C (Pa m^3 mol^{-1})	Log K_{OW}
Acénaphthène		154,2	3,92	14,7	3,50
Acénaphtylène		152,2	3,927	11,5	3,78
Anthracène		178,2	1,3	5,04	4,30
Benzo[a]anthracène	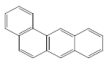	228,3	1,3	0,76	5,46
Benzo[a]pyrène		252,3	1,8	0,04	5,96
Benzo[b]fluoranthène	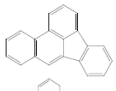	252,3	0,0061	0,051	5,80
Benzo[g,h,i]Perylène		276,3	0,00026	0,014	6,09
Benzo[k]fluoranthène	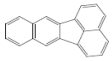	252,3	0,00076	0,069	5,97
Chrysène		228,3	3,9	0,26	5,43
Dibenzo[a,h]anthracène	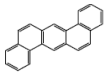	278,3	0,0006	0,0048	6,30
Fluoranthène		202,3	0,062	1,5	4,56
Fluorène		166,2	1,8	9,2	3,83
Indéno[1,2,3-c,d]pyrène	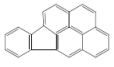	276,3	0,062	0,029	6,26
Naphtalène		128,2	32,0	48,9	3,05
Phénanthrène		178,2	1,2	3,98	4,20
Pyrène		202,3	0,135	1,25	4,57

1.3. Teneurs des HAP

Les teneurs individuelles des HAP dans les sols liées à des sources naturelles sont de l'ordre de 1 à 10 $\mu g\ kg^{-1}$ (Edwards, 1983). Ces valeurs peuvent augmenter si les sols sont arborés. Neilson (1998) a constaté des teneurs en HAP de 2 à 6 fois supérieures dans les sols de terrain arborés par rapport à celles dans des sites nus. Il a attribué cette différence à la synthèse et à l'accumulation de pollution atmosphérique par la végétation. En général, les teneurs des HAP dans les sols augmentent avec l'impact croissant de l'industrie, du trafic ou du chauffage domestique. Les teneurs en HAP dans les sols augmentent donc selon l'ordre suivant : sols arables < sols minéraux sous forêt < prairie permanente < sols urbains < sols industriels contaminés (Wilcke, 2000).

1.3.1. Teneurs dans les sols agricoles

Les teneurs en HAP dans les sols agricoles prouvent augmenter substantiellement avec l'application de boues d'épuration, de fumiers et de composts. Wilcke (2000) a rapporté des teneurs en HAP souvent 10 fois supérieures dans tous les types de boues d'épuration par rapport à celles dans le sol. Trente ans après l'application, Wild et al. (1992, 1991) ont constaté des teneurs en HAP encore 3 fois supérieures dans les sols amendés avec des boues d'épuration par rapport à ceux non amendés. Du fait de contraintes réglementaires sur les amendements dans les pays développés, dont la France, les flux de HAP apportés par les produits résiduaires organiques sont faibles. Houot et al. (2002) ont évalué les teneurs des micropolluants incluant les HAP dans les composts d'épandages à partir de résultats obtenus sur un essai au champ QualiAgro mis en place en 1998 (collaboration INRA-Véolia). Ils ont constaté que les flux de micropolluants organiques, dont les HAP, sont faibles par rapport aux stocks présents naturellement dans les sols ou même par rapport aux autres flux comme les dépôts atmosphériques. Ils ont également constaté que les concentrations de ces divers contaminants sont largement variables et dépendantes du type et de l'origine de l'amendement. Ils ont conclu que les effets éventuels ne seront observables qu'au long terme et en cas d'épandages répétés, pouvant générer des effets cumulatifs de faibles doses de HAP. Des exemples pour les concentrations maximales pour certains HAP selon la législation française sont mentionnés dans le Tableau I.2.

Tableau I.2. Concentrations maximales en HAP définies dans les normes NFU 44-051 et NFU 44-095, qualifiant respectivement les amendements organiques et les composts de boues d'épuration; flux maximum de polluants définis dans ces 2 normes pendant 10 ans et pour chaque épandage.

	NFU44-095	NFU44-051	2 normes	
	mg kg_{MS}^{-1}	mg kg_{MS}^{-1}	g ha^{-1} sur 10 ans	g ha^{-1} par épandage
Fluoranthène	4	4	60	6
Benzo(b)fluoranthène	2,5	2,5	40	4
Benzo(a)pyrène	1,5	1,5	20	2

1.3.2. Teneurs dans les sols de friches industrielles

Les teneurs en HAP rencontrées dans ce type de sol varient de quelques centaines à plusieurs milliers de mg kg^{-1} pour la somme des 16 HAP. Ces teneurs peuvent donc être supérieures de plusieurs ordres de grandeurs à la valeur de référence qui est de 50 mg HAP kg^{-1} préconisée au niveau national (BRGM, 2007). Les teneurs en HAP présentes dans les sols de friches dépendent également du type d'industrie (Tableau I.3). Juhasz and Naidu (2000) ainsi ont montré que l'industrie liée au stockage du bois représente la plus importante source de contamination en HAP apportant aux sols 18 704 mg kg^{-1}, contre plus de 7 000 mg kg^{-1} pour les usines à gaz.

Tableau I.3. Exemples de teneurs en HAP dans les sols de friches industrielles (source : Juhasz and Naidu, 2000)

HAP	Teneurs en HAP dans les sols en mg $kg^{-1}_{sol\ sec}$					
	P.Créosote	**P.Bois**	**T.Gas**	**P.Chimie**	**U.P.Gas**	**F.U.P.Gas**
NAP	1131	3925		186	97	
ACY	33	49			28	28
ACE		1368	2	43	49	2
FLU	650	1792	225	87	14	4
PHE	1595	4434	379	156	26	51
ANT	334	3307	156	53	11	58
FLT	682	1629	2174	137	73	195
PYR	642	1303	491	99	47	173
B[a]A		171	317	33	15	52
B[a]P		82	92	15	16	88
DBA			2451	12	21	
IP		23	207		33	46
Σ HAP	5863	18704	7337	821	451	974

NAP : naphthalène, ACY : acénaphtylène, ACE: acénaphtène, FLU : fluorène, PHE : phénanthrène, ANT : anthracène, FLT : fluoranthène, PYR : pyrène, B[a]A: benz[a]anthracène, B[a]P : benzo[a]pyrène, DBA : dibenzo[a,h]anthracène, IP : indéno[1,2,3-c,d]pyrène. P.Créosote: site de production de créosote (Ellis et al., 1991), T.Gas: site de travaux de gaz (Bewley et al., 1989), P.Chimie : site pétrochimique (Juhasz et al., 2000), P.Bois : site de préservation du bois (Mueller et al., 1991), U.B.Gas : site d'usines de production de gaz (Erickson et al., 1993), F.U.P.Gas: site français d'usines de production de gaz (Bogan et al., 1996)

1.4. Traitements des HAP dans les sols

Il existe plusieurs méthodes pour traiter les sols de friches industrielles contaminés par des HAP qui peuvent mettre en œuvre des processus aussi bien physico-chimiques que biologiques. Parmi les méthodes physico-chimique on trouve la désorption thermique, très efficace, qui consiste à chauffer le sol pour désorber et détruire les molécules organiques, l'oxydation chimique qui consiste à ajouter un oxydant (e.g. peroxyde d'hydrogène, permanganate) ou des procédé d'extraction par solvant. Ces méthodes peuvent pour certaines être réalisées *on site* (désorption thermique), voire *in situ* (oxydation chimique). Bien que ces méthodes soient très efficaces pour éliminer les polluants organiques nocifs, leur utilisation reste limitée aux cas de pollutions intenses et limitées géographiquement du fait de leurs coûts élevés (Beltran et al., 1996; Stehr et al., 2001).

Comparativement aux méthodes physico-chimiques, les méthodes de traitement biologiques sont moins coûteuses et peuvent être mise en œuvre pour de plus grandes surfaces. Toutefois elles présentent aussi quelques limites incluant : i) une durée d'intervention relativement longue pour atteindre les objectifs environnementaux, ii) une applicabilité uniquement dans les cas où le niveau de contamination est faible à moyen, et iii) une efficacitée limité pour certaines molécules, en particulier les plus lourdes (Cunningham et al., 1996; Ouvrard et al., 2014). Les différentes méthodes utilisées se distinguent principalement par les technologies utilisées et leur mode d'application (*in situ*, *on site* ou hors site) mais elles ont toutes comme objectif de favoriser l'activité biologique du sol afin d'accroître la biodégradation des composés organiques.

La biostimulation consiste à apporter de l'oxygène et/ou des nutriments non organiques, notamment l'azote, pour stimuler le développement des bactéries autochtones dégradant les HAP dans le site pollué (Bamforth and Singleton, 2005; Straube et al., 2003). Alors que la bioaugmentation consiste à introduire des souches microbiennes spécifiques, qui peuvent être des bactéries autochtones naturelles ou génétiquement modifiées en laboratoire, pour améliorer la capacité métabolique des micro-organismes indigènes dans le site pollué (Bamforth and Singleton, 2005; Straube et al., 2003). Ces deux stratégies peuvent d'ailleurs être utilisées de manière concomitante. La phytoremédiation est une forme de bioremédiation *in situ* reposant sur l'utilisation des plantes (Cunningham et al., 1996; Ouvrard et al., 2014; Pritchina et al., 2011). Dans ce cas, la présence de plantes stimule l'activité les microorganismes dégradant les polluants organiques en particulier par l'apport de carbone facilement assimilable au niveau des racines. La mise en œuvre de le phytoremédiation

s'accompagne également de pratiques culturales d'amendements et travail du sol qui sont également bénéfiques à l'activité biologique. Cependant, l'efficacité de la phytoremédiation, en particulier dans le cas des HAP, est limitée du fait de leur faible disponibilité. Il est alors important de mieux comprendre les processus qui contrôlent la biodisponibilité des HAP dans le sol en général et dans la rhizosphère en particulier, afin d'augmenter les rendements de ces techniques biologiques (Cunningham et al., 1996; Ouvrard et al., 2014).

2. Réactivité et modélisation du devenir des HAP dans le sol

Dans le sol, les HAP se distribuent entre les phases gazeuse, liquide et solide du sol en fonction de leurs propriétés physico-chimiques, mais également en fonction des conditions environnementales (pH, température, abondance de matières organique,…). La Figure I.1 présente les processus majeurs gouvernant le devenir de ces polluants organiques dans le sol. Ces processus comprennent la volatilisation vers l'atmosphère, le prélèvement et l'assimilation par les végétaux, la rétention physique (i.e. adsorption, désorption et diffusion) dont les interactions avec les matières organiques du sol, la biodégradation par les microorganismes, et la dispersion et le transport dans le sol par ruissellement et lixiviation.

Du fait du caractère hydrophobe des HAP, la volatilisation et le prélèvement par les plantes sont considérés comme intervenant très peu dans le devenir des HAP. On dispose de peu d'informations dans la littérature sur les taux de volatilisation des HAP dans les sols contaminés (Wilcke, 2000). Le taux de volatilisation d'un HAP dépend de ses propriétés physico-chimiques notamment la constante de Henry, les conditions climatiques (température de l'air et vitesse du vent), l'humidité et le potentiel redox du sol (Leduc et al., 1992; Ophoff et al., 1996). Dans une étude expérimentale par Park et al. (1990), les auteurs ont constaté que moins de 0,1 % de phénanthrène et d'anthracène (HAP de 3 cycles) incubés dans deux types de sol différents ont été volatilisés pendant deux jours d'incubation.

Du fait de leur lipophilie, les HAP peuvent s'adsorber sur les surfaces des racines des plantes, mais leur absorption par les racines est considérée comme très limitée (Binet et al., 2001). Bien que quelques HAP aient été détectés dans les tissus végétaux, on pense que les retombées atmosphériques sont la principale source pour ces polluants retrouvés dans les plantes et non pas le transfert direct depuis le sol (Wilcke, 2000). Les quantités de HAP transférés du sol vers la plante représentent en effet une très faible proportion des quantités de HAP présents dans les sols, en général moins de 0,01 % (Edwards, 1983; Goodin and Webber, 1995).

Les processus d'adsorption, de biodégradation et de transport sont quant à eux détaillés dans les paragraphes suivants ainsi que les modèles permettant de les représenter.

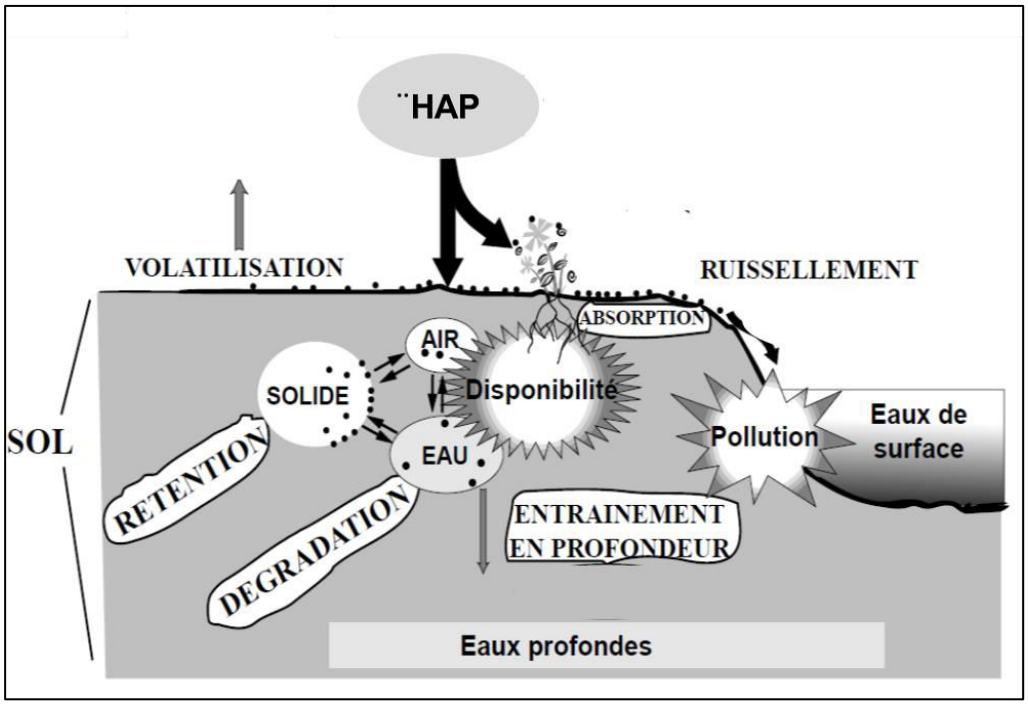

Figure I.1. Processus impliqués dans la dynamique des HAP dans le sol (modifiée de Barriuso et al., 1996)

2.1. Processus d'adsorption

2.1.1. Définition du processus

La rétention physique des HAP dans le sol est gouvernée par des processus diverses dont l'adsorption, processus physico-chimique interfacial relativement rapide, et la diffusion dans les agrégats ou dans les matières organiques du sol, généralement plus lente. Le passage de la fraction mobile et disponible de HAP en forme non disponible dans le sol est principalement induit par l'adsorption (Wilcke, 2000). Les matières organiques du sol sont le principal sorbant des polluants organiques (Gustafsson et al., 1996) et l'adsorption d'un polluant organique sur un sol est généralement considérée comme proportionnelle à sa teneur en matière organique (Means et al., 1980). L'adsorption des composés organiques peut aussi se faire sur la fraction minérale du sol, mais l'adsorption sur cette fraction n'est pas linéaire et dépend essentiellement de la surface spécifique de matériaux composants chacun de ses éléments (Rebhun et al., 1992). La contribution de la fraction minérale à la rétention physique du polluant peut alors être présentée par l'équation suivante :

$$K_p = (1-\theta)\, K_m + K_{OC}\, \theta f_{OC} \qquad \text{(I-1)}$$

Où K_p est le coefficient d'adsorption total sur la matrice minérale et organique du sol (L kg^{-1}), K_m est le coefficient d'adsorption globale sur la matrice solide (L kg^{-1}), K_{OC} (en L kg C^{-1}) est le coefficient d'adsorption normalisé à la teneur en carbone organique du sol, f_{OC} la fraction de carbone organique du sol (kg C kg^{-1}) et θ est la fraction minérale couverte par la matière organique humique du sol (-).

Outre la quantité de matière organique, l'intensité d'adsorption dépend également de la nature des matières organiques du sol. Ainsi, un sol qui contient des matières organiques matures avec beaucoup d'acides humiques est généralement caractérisé par une hystérésis de désorption significative, tandis qu'un sol dont la matière organique est essentiellement composée d'acides fulviques (*i.e.* matière organique immature) présente peu ou pas d'hystérésis de désorption (Johnson et al., 2001). Par ailleurs, l'affinité des HAP pour les matières organiques anthropogéniques, tel le charbon, est généralement 10 à 10 000 fois supérieure à celle pour les matières organiques naturelles (Cornelissen et al., 2004).

Les propriétés physico-chimiques des HAP influencent également l'intensité de l'adsorption. Celle-ci est d'autant plus élevée que la masse moléculaire du HAP est élevée (Johnson et al., 2001). La compétition entre les différents HAP (par exemple, entre le phénanthrène et le pyrène (White and Pignatello, 1999)) pour les sites d'adsorption est aussi un autre facteur pouvant influencer l'affinité d'adsorption dans le sol. Par ailleurs, étant donné que le processus d'adsorption est réversible, les composés adsorbés sur la matrice du sol sont susceptibles d'être libérés vers la solution du sol (désorption) mais cette réversibilité diminue avec l'augmentation du temps de contact dans le sol (*aging effect*). Les conditions d'humidité du sol peuvent aussi affecter l'intensité de la désorption. La présence de matières organiques dissoutes (MOD) peut jouer un double rôle facilitant ou au contraire augmentant la rétention. Elle peut en effet augmenter le transport du polluant dans le profil du sol en raison des effets de solubilisation et de concurrence sur les sites de sorption (Barriuso et al., 2011; Jardine et al., 1989; Xiu-hong et al., 2014) ou inversement favoriser l'adsorption si l'affinité du colloïde (MOD - polluant) pour la phase solide est supérieure à celle du colloïde seul.

2.1.2. Les types d'adsorption, lent rapide, forte faible

La rétention des HAP dans la matrice du sol se fait sur au moins deux phases d'adsorption. La première phase est rapide mais peu stable dans le temps (rétention faible) correspondant à la sorption vers des sites proches de la surface des sorbents organiques. La second phase est lente mais stable dans le temps (rétention forte) et qui peut s'expliquer par la diffusion des HAP au sein des agrégats du sol et / ou à l'intérieur de la matière organique du sol

(Weissenfels et al., 1992). Cette seconde phase peut durer plusieurs semaines voire plusieurs années. Elle correspond au processus de vieillissement (*aging*). C'est pour cette raison que les taux d'extraction des HAP par des solvants organiques diminuent avec l'augmentation du temps de contact des HAP dans le sol (Chung and Alexander, 2002; Hatzinger and Alexander, 1995). Il y a formation de résidus stabilisés et non-extractibles (Barriuso et al., 2008) qu'on appellera dans cette étude résidus liés d'origine physique en opposition aux résidus liée biogéniques produits par les biomasses microbienns dont on parlera plus tard.

2.1.3. Modélisation du processus d'adsorption

La modélisation du devenir des polluants organiques dans les sols a fait l'objet de nombreuses études et un grand nombre de modèles ont été proposés et testés (Barriuso et al., 2011; Johnson et al., 2001; Pomiès et al., 2013; Rav-Acha and Rebhun, 1992; Sabbah et al., 2004; Saffih-Hdadi et al., 1997; Shian Chee. Wu and Gschwend, 1986; Xiu-hong et al., 2014; Zarfl et al., 2009). Généralement, on distingue trois grands types de modèles : les modèles à l'équilibre, les modèles cinétiques et les modèles mixtes qui combinent les deux types précédents.

a) Modèles à l'équilibre

Dans les modèles à l'équilibre Figure I.2a, la rétention est assimilée à une adsorption instantanée, réversible. La modélisation est basée sur des lois de la forme :

$$C_{s,eq} = f\,(C_{w,eq}) \qquad \text{(I-2)}$$

où $C_{s,eq}$ est la quantité du polluant adsorbé à l'équilibre en kg kg^{-1}, $C_{w,eq}$ la concentration du polluant dans la phase aqueuse à l'équilibre en kg L^{-1}. Dans le cas le plus simple, $C_{s,eq}$ est considéré linéairement proportionnelles à $C_{w,eq}$ à l'équilibre. C'est l'isotherme la plus simple et donc l'équation précédente est réécrite comme :

$$C_{s,eq} = K_d\, C_{w,eq} \qquad \text{(I-3)}$$

Où K_d est le coefficient de partage entre la phase solide et la phase liquide exprimé en L kg^{-1}.

Lorsque la valeur de K_d pour un HAP est inconnue, le modélisateur peut fournir une valeur de ce coefficient à partir de l'équation suivante :

$$K_d = K_{OC}\, f_{OC} \qquad \text{(I-4)}$$

Où K_{OC} (en L kg C^{-1}) est le coefficient d'adsorption normalisé à la teneur en carbone organique du sol (f_{OC}, en kg C kg^{-1}). Ici, l'équation (I-4) est dérivée de l'équation (I-1) en faisant l'hypothèse que la contribution de la fraction minérale à l'adsorption total de matrice

du sol est négligeable. Les valeurs du paramètre K_{OC} peuvent également être estimées grâce aux expressions semi-empiriques disponibles dans la littérature et qui utilisent le coefficient de partage octanol/eau (K_{OW}), qui rend compte de l'affinité de la molécule pour une phase organique de référence, l'octanol. Nous donnons ci-dessous des exemples d'expressions semi-empiriques disponibles dans la littérature :

$$\log K_{OC} = 0{,}989 \log K_{OW} - 0{,}346 \qquad \text{(I-6, d'après Karickhoff et al., 1979)}$$

$$\log K_{OC} = \log K_{OW} - 0{,}317 \qquad \text{(I-7, (Means et al., 1980))}$$

$$\log K_{OC} = 0{,}62 \log K_{OW} + 0{,}7 \qquad \text{(I-8, (Walter et al., 2000))}$$

Ces relations semi-empiriques restent peu précises et leur utilisation doit toujours être considérée avec prudence. C'est la raison pour laquelle des auteurs ont récemment proposé une approche plus scientifique d'estimation du K_{OC} s'appuyant sur la structure moléculaire et énergétique des composés organiques (Nguyen et al., 2005).

Par ailleurs, et pour des concentrations en polluant organique élevées dans le sol, le coefficient K_d devient dépendant du nombre de sites d'adsorption et l'équation (I-3) n'est plus valide. Ce type d'isotherme est alors souvent modélisé par le modèle de Freundlich décrit par l'équation suivante :

$$C_{s,eq} = K_f C^{n}_{w,eq} \qquad \text{avec } n < 1 \qquad \text{(I-9)}$$

Où K_f est le coefficient de Freundlich et n est l'exposant de Freundlich. Si n=1 le modèle de Freundlich est équivalent à l'isotherme de sorption linéaire.

Les modèles de sorption à l'équilibre font l'hypothèse que le processus d'adsorption du polluant dans le sol est rapide par rapport aux autres processus affectant la dissipation de la fraction mobile du polluant dans la solution du sol. Des recherches au laboratoire et au terrain ont mis en évidence que les modèles d'équilibre simulent bien les isothermes d'adsorption pendant la première phase de l'adsorption mais simulent mal ce que se passe sur des temps plus longs. Ils négligent le phénomène de vieillissement et de stabilisation des résidus du polluant dans le sol.

b) Modèles cinétiques

Si l'hypothèse de la sorption à l'équilibre instantanée n'est pas valide, l'utilisation d'un modèle cinétique devient nécessaire. Généralement ces modèles considèrent que l'adsorption et la désorption d'un polluant sur la matrice du sol se produisent simultanément. Ils supposent

aussi que l'adsorption d'un polluant se fait en deux étapes, une étape initiale rapide suivie d'une étape lente. Ainsi, le polluant organique adsorbé sur la surface du sol doit se distribuer dans deux compartiments : le premier compartiment représente la fraction du polluant adsorbé sur les sites facilement accessibles de la phase solide du sol, donc les molécules facilement désorbables, et le deuxième compartiment peut, selon les cas, représenter soit la fraction du polluant qui diffuse dans les agrégats ou dans les matières organiques du sol, ou bien les résidus liés d'origine physique du polluant qui sont stabilisés dans le sol. Le nombre des compartiments pris en compte est variable allant de deux compartiments jusqu'au à des modèles multi-compartimentaux prenant en compte la formation de résidus liées d'origine physique. Un schèma du modèle cinétique de deux compartiments est présenté dans la Figure I.2b. Les équations différentielles prennent la forme suivante :

$$\frac{dC_w}{dt} = k_{-1}C_{s1} - k_1 C_w \qquad \text{(I-10)}$$

$$\frac{dC_{s1}}{dt} = k_1 C_w \quad (k_1 + k_2) C_{s1} + k_2 C_{s2} \qquad \text{(I-11)}$$

$$\frac{dC_{s2}}{dt} = k_2 C_{s1} \quad k_2 C_{s2} \qquad \text{(I-12)}$$

Avec :

C_w : la concentration du polluant mobile et dissoute dans le sol [kg L^{-1}]

C_{s1} : la concentration du polluant faiblement adsorbé dans le sol [kg kg^{-1}]

C_{s2} : la concentration du polluant fortement adsorbé dans le sol [kg kg^{-1}]

k_i : constantes du temps [s^{-1}]

Généralement, et en comparaison avec le modèle à l'équilibre, les modèles cinétiques multi-compartimentaux restituent mieux les conditions réelles d'adsorption-désorption des polluants organiques dans le sol. En outre, ce type de modèle est flexible dans la mesure où il peut être utilisé pour simuler différents cas. Par exemple, en Figure I.2b, k_{-2}=0 correspond au cas où le taux de désorption de HAP de la fraction fortement adsorbée vers la fraction faiblement adsorbée est nul (i.e. C_{S2} simule la fraction de HAP sous forme résidus liées non-extractible). Toutefois, un inconvénient majeur de ce modèle reste la définition arbitraire des différents compartiments du modèle. En effet, l'accessibilité expérimentale aux différentes phases est possible pour la fraction désorbable du HAP, mais il est actuellement encore impossible de

quantifier directement la part du HAP stabilisé sous la forme de résidus liés non extractibles sauf par bilan de masse ou par utilisation de traceurs isotopiques.

Johnson et al. (2001) ont testé la capacité de six modèles d'adsorption différents à restituer des données expérimentales représentant la rétention du phénanthrène dans différents cas en faisant varier la nature de la matière organique du sol, la concentration de phénanthrène dans le sol et le temps de contact. Selon eux, c'était le modèle cinétique à deux compartiments utilisant une cinétique du premier ordre qui a montré la meilleure aptitude à restituer les résultats expérimentaux dans les différentes situations. Ainsi, selon cette étude, l'utilisation d'un modèle cinétique à deux compartiments pour décrire les interactions physico-chimiques des HAP dans le sol devient cohérente. Cette étude a cependant montré une autre limite pour l'utilisation de ce type de modèle. Pour un HAP donné, il s'avère impossible de trouver un jeu de paramètres généralisable pour le modèle qui soit valide sur les différents systèmes d'étude. Pour un HAP, un jeu de paramètres peut donc varier selon le type de sol, la nature des matières organiques du sol, le temps de contact entre HAP et sol mais aussi suivant les ordres de grandeur des teneurs en HAP initiales. Cela rend donc le processus de calibration et de validation de ce type de modèle difficile.

c) Modèles mixtes

Dans ces modèles, Figure I.2c, la matrice sol est supposée avoir deux classes de sites où pour l'un la rétention est instantanée et pour l'autre la rétention est limitée cinétiquement. Ce dernier site est décrit par une cinétique du premier ordre tandis que le site avec rétention instantanée est représenté par une isotherme de sorption à l'équilibre. Ici les équations différentielles peuvent s'écrire sous la forme d'équations de modèles cinétiques mais en prenant en compte l'équation suivante (Pomiès et al., 2013):

$$K_d = \frac{C_w}{C_{s1}} = \frac{k_1}{k_{-1}} \qquad \text{(I-13)}$$

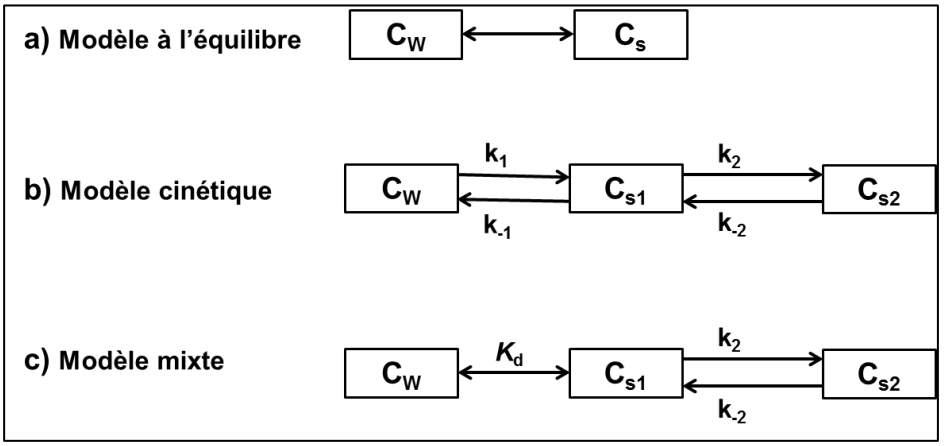

Figure I.2. Schéma des modèles simulant le processus d'adsorption/désorption dans le sol.

2.2. Processus de biodégradation

2.2.1. Minéralisation ou formation de métabolites

La biodégradation des polluants organiques par les microorganismes du sol est un des principaux processus contribuant à l'élimination des polluants dans le milieu naturel. Un certain nombre de microorganismes ont été isolés capables de dégrader totalement ou partiellement les HAP (Seo et al., 2007). Ce sont principalement des bactéries qui participent à cette dégradation. Certains champignons peuvent aussi dégrader les HAP, mais le rendement de la biodégradation par les champignons reste cependant inférieur à celui de bactéries (Kästner et al., 1999). La biodégradation d'un HAP peut conduire à la minéralisation au cours de laquelle le composé se décompose en CO2 et des produits intermédiaires, les « métabolites », peuvent également se former lors de la biodégradation partielle des HAP. La Figure I.3 illustre un exemple de métabolites produits lors de la biodégradation de pyrène (4 cycles) en milieu oxygéné par la bactérie Mycobacterium sp (Heitkamp et al., 1988). Les HAP sont également susceptibles d'être dégradés en absence d'oxygène si la quantité de nitrate dans le milieu est suffisante, mais le rendement de la biodégradation en condition anaérobie est plus faible que celui obtenu en condition aérobie.

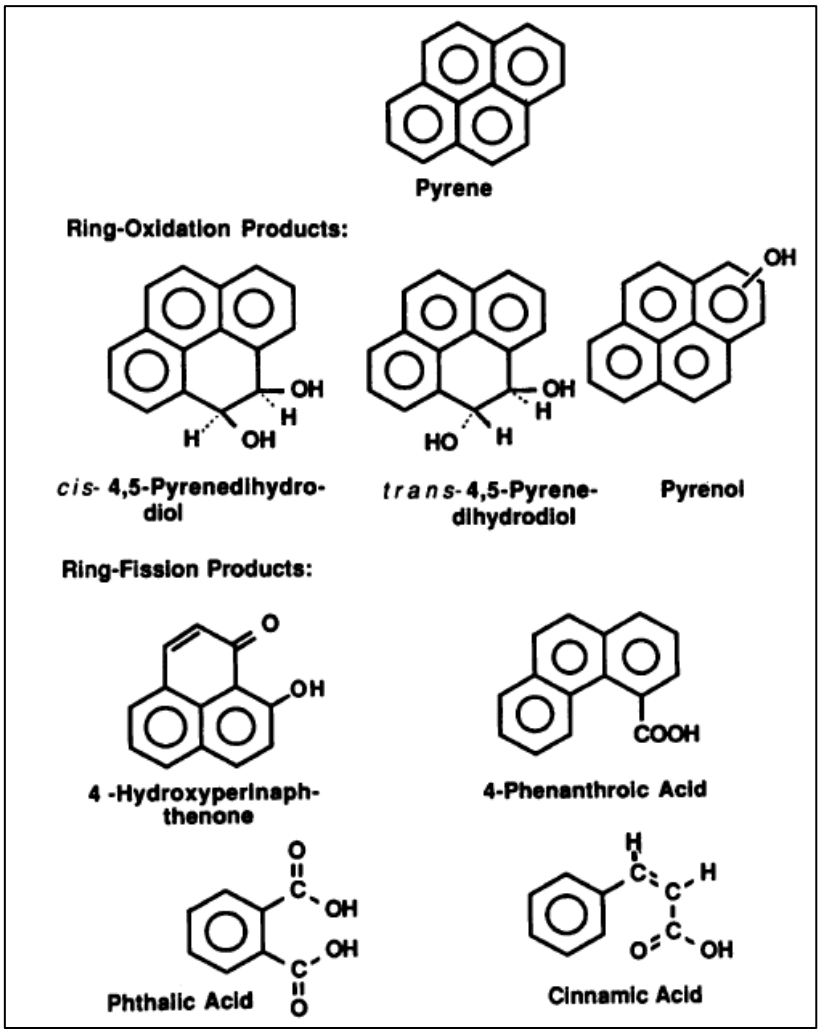

Figure I.3. Structures des métabolites du pyrène identifiés lors de la dégradation par *Mycobacterium* sp. (Heitkamp et al., 1988).

2.2.2. La notion de biodisponibilité

Semple et al. (2004) (Figure I.4) font la distinction entre trois fractions d'un composé organique dans le sol : i) la fraction biodisponible correspond à celle librement disponible pour traverser la membrane cellulaire d'un organisme, ii) la fraction bioaccessible est celle qui est disponible pour traverser la membrane cellulaire d'un organisme si l'organisme a l'accès au composé chimique, et iii) la fraction séquestrée correspondant à un composé chimique qui est occlus dans la matière organique du sol et n'est donc pas disponible à un moment donné ou qui occupe une aire spatiale différente de celle de l'organisme. La différenciation entre la fraction biodisponible d'un composé et celle bioaccessible est délicate (Semple et al., 2004). Le choix de la méthode d'extraction adoptée pour évaluer la biodisponibilité d'un composé organique (i.e. les méthodes d'extractions exhaustives ou non-exhaustive) peut aussi jouer un rôle dans l'estimation de la fraction biodisponible. De

nombreux résultats dans la littérature montrent qu'il y a une relation entre la méthode d'extraction utilisée et la quantité de composé récupérée (Kästner et al., 2014).

La disponibilité des HAP est faible car ils sont hydrophobes avec une affinité relativement élevée pour s'adsorber sur la matière organique du sol. De plus, cette affinité élevée pour l'adsorption peut augmenter significativement dans les sols de friches industrielles, du fait du phénomène de vieillissement des HAP (par augmentation de résidus non extractibles), mentionné au paragraphe 2.1.2. C'est la raison pour laquelle les HAP se trouvent majoritairement sous une fraction non disponible dans les sols. La désorption et deséquestration sont deux mécanismes qui peuvent rendre possible leur disponibilité dans le sol.

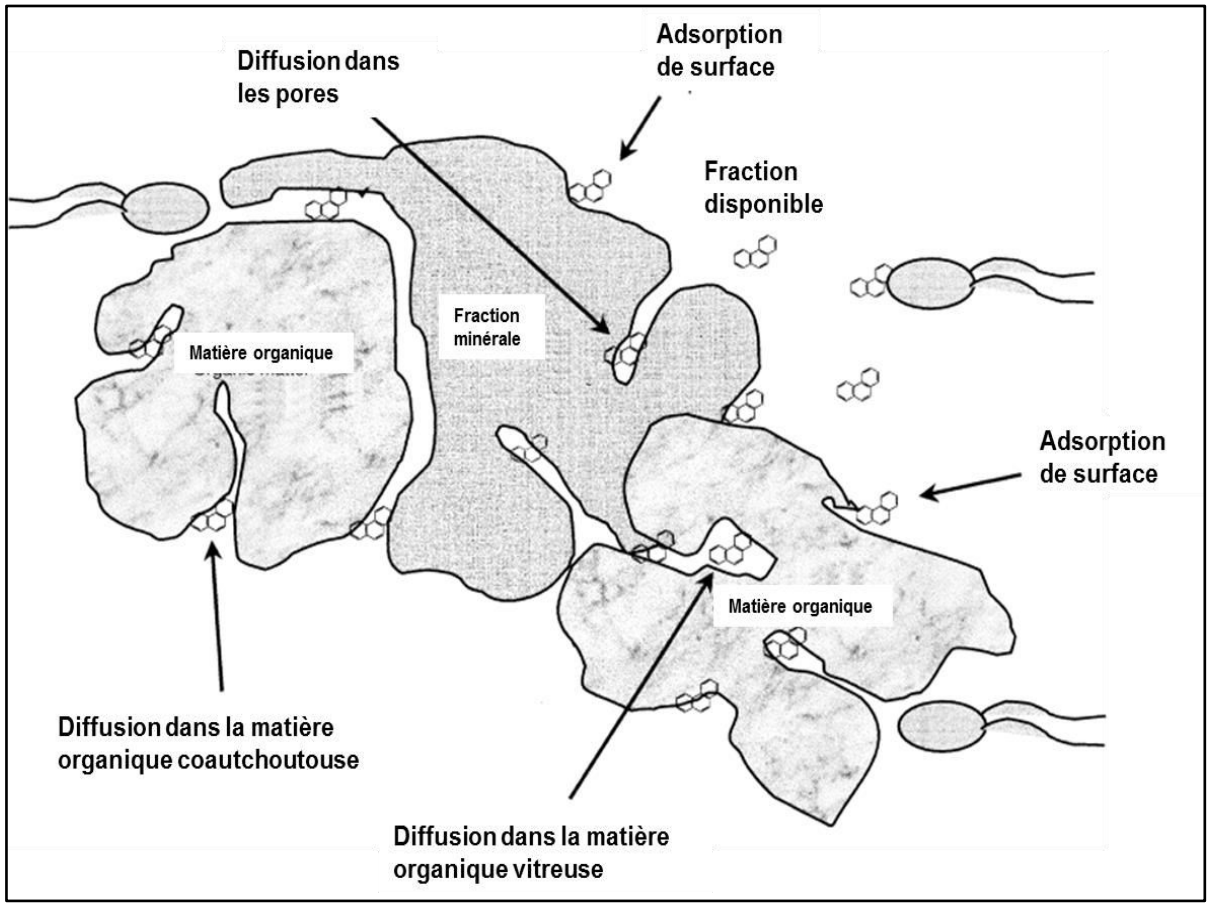

Figure I.4. Concept de biodisponibilité des HAP dans les sols (modifié de Semple et al., 2003)

2.2.3. Les voies de biodégradation

Deux voies principales de biodégradation sont décrites dans la littérature. La première met en jeu un type de communauté microbienne pour qui le substrat est la seule source de carbone et d'énergie. On parle alors de biodégradation par biomasse microbienne spécifique (Figure I.5). L'inconvénient majeur de cette hypothèse est que ce type de biomasse est difficilement

mesurable. La deuxième voie de biodégradation suppose que l'assimilation du substrat du polluant par les microorganismes se fait simultanément à l'assimilation d'un autre substrat, comme de la matière organique dissoute, qui est plus facilement accessible. On parle dans ce cas de biodégradation par co-métabolisme. L'intégration de la voie de biodégradation par co-métabolisme dans les modèles de polluants organiques permet de combiner la dynamique du polluant avec la dynamique de carbone organique présent dans le milieu.

L'apport de matières organiques extérieures comme lors de l'épandage de compost urbain augmente la teneur en matière organique du sol et stimule généralement l'activité microbienne du sol. La biodégradation dans un sol amendé peut être favorisée par l'augmentation de l'activité microbienne du sol car l'application d'amendement organique peut favoriser la dégradation par co-métabolisme (Hance, 1973). Le modèle COP-Soil développé par Geng et al. (2015) permet de simuler la croissance de la biomasse microbienne dégradant les polluants organiques dans le sol lors de la décomposition du compost.

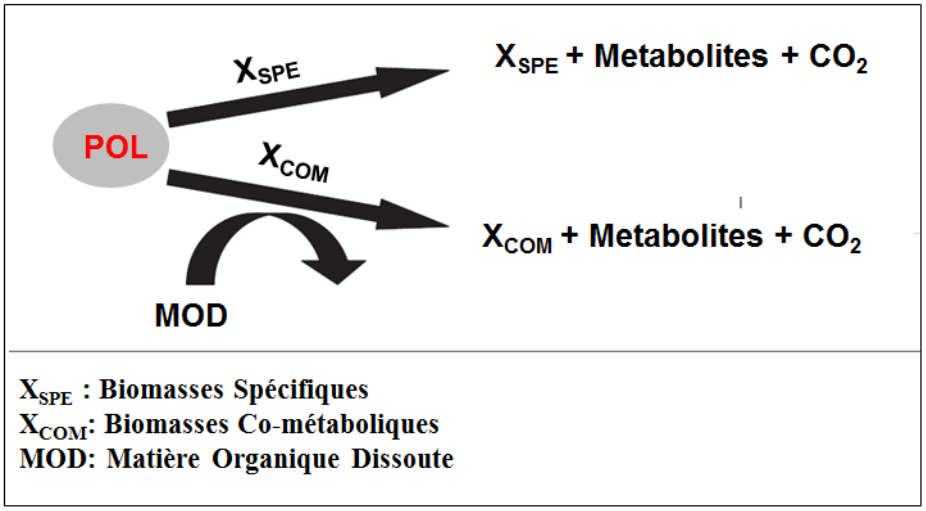

Figure I.5. Schéma des deux voies de biodégradation

2.2.4. Les résidus liés d'origine biogénique

La définition des résidus liés proposée par Roberts (1984) et adoptée par l'Union internationale de chimie pure et appliquée (IUPAC) est la suivante : « les résidus liés sont des espèces chimiques provenant d'un composé organique présent dans le sol qui ne peuvent pas être extraites par les méthodes d'extraction qui ne modifient pas la nature chimique de ces molécules » (Gevao et al., 2000). L'utilisation d'un marqueur (^{14}C ou ^{13}C) permet la mise en évidence de ces espèces non-extractibles par des méthodes de combustion qui analysent quantitativement le carbone marqué, mais qui ne permettent pas de connaitre la nature de ces

molécules. La formation des résidus liés peut être considérée comme un processus contribuant à l'élimination du polluant dans le sol du fait que le polluant n'est plus extractible. Ainsi la formation des résidus liés est souvent interprétée comme un processus de stabilisation. Cependant le polluant initial ou ses métabolites peuvent être encore dans le sol malgré leur non-extractibilité. Ainsi Lerch et al. (2009) ont mis en évidence qu'une petite quantité de résidus liés marqués pouvaient se libérer sur des temps longs dans le sol et être à nouveau extractibles (Lerch et al., 2009).

Généralement, les auteurs supposent que la formation de résidus liés se produit du fait de l'intervention de deux mécanismes d'interaction entre le polluant et la matrice du sol. Le premier est dû à des interactions chimiques et physiques correspondant aux liaisons covalentes ou liaisons hydrogènes et le piégeage et la diffusion du polluant ou de ses métabolites dans la matrice organique du sol. Cela conduit, par conséquent, à produire le composant chimique et physique des résidus liés d'origine physique. Le deuxième mécanisme est entrainé par l'activité biologique du sol qui conduit à la formation de résidus liées d'origine biologique appelés « biogéniques » puisque ils sont fabriqués totalement par les biomasses microbiennes du sol. De nombreux travaux dans la littérature (Aslam et al., 2014; Barriuso et al., 2008; Gevao et al., 2005; Kästner et al., 2013, 1999; Nowak et al., 2013; Richnow et al., 2000) montrent qu'il y a une corrélation directe entre l'activité microbienne et le taux de production des résidus liés dans le sol. La Figure I.6 met en évidence que l'inhibition de l'activité microbienne dans le sol *via* la stérilisation conduit à réduire la proportion des résidus liés.

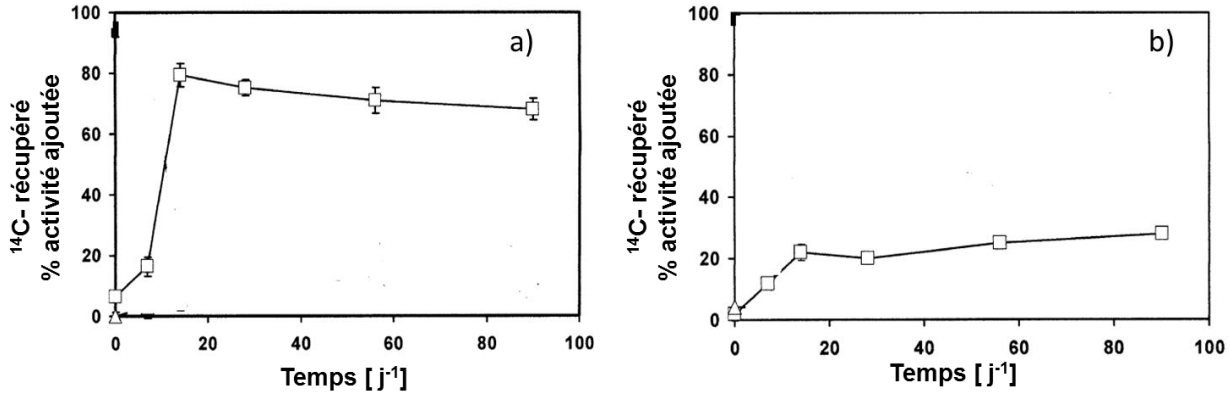

Figure I.6. Dynamique de la production de résidus liés dans le sol suite de l'incubation d'un herbicide marqué par ^{14}C « le Dicamba » avant (a) et (b) après la stérilisation (adapté de Gevao et al., 2005)

La contribution de la fraction biogénique aux résidus non extractibles totaux présents dans le sol peut être importante notamment pour les HAP de faible masse molaire. Richnow et al. (2000) ont trouvé pour le phénanthrène que cette contribution était d'au moins 11 % pendant

50 jours d'incubation dans un bioréacteur. Kästner et al. (2014) ont simulé la dynamique de l'anthracène (HAP à 3 cycles) dans le sol non modifié et ont estimé que 50 % des résidus non extractibles étaient d'origine biogénique après 50 jours de simulations. Du fait de la relation directe entre la formation de résidus liés biogéniques et l'activité microbienne du sol, les facteurs environnementaux (pH, température, humidité, pratique agricole..) qui modifient le taux de biodégradation du polluant organique dans le sol affectent aussi sa transformation en résidus liés biogéniques.

2.2.5. Modélisation de la cinétique de biodégradation

Dans la plupart des modèles de pesticide, la dégradation du polluant est modélisée à l'aide d'une cinétique du premier ordre qui représente une dégradation dominée par la voie co-métabolique du type :

$$\frac{dS}{dt} = K.S \qquad \text{(I.14)}$$

Avec, $\frac{dS}{dt}$, taux de dégradation du polluant (S) [$kg_{substrat}\ kg^{-1}\ s^{-1}$] et *K*, constante de dégradation du polluant.

Dans le modèle de Zhang et al. (2014), la dégradation dépend aussi de la taille de la biomasse dégradante ce qui permet de prendre en compte une évolution de la biomasse microbienne du sol si il y a un apport soudain et important de matière organique exogène. L'équation devient alors :

$$\frac{dS}{dt} = K.S.X \qquad \text{(I.15)}$$

Avec *X*, la biomasse dégradante.

Certains modèles considèrent une dégradation par biomasse spécifique ou le substrat est utilisé pour la croissance microbienne (Geng et al., 2015). Ces modèles utilisent alors les équations suivantes :

$$\frac{dS}{dt} = \frac{1}{Y}\frac{dX}{dt} \quad \text{(I-16)}$$

$$\frac{dX}{dt} = \mu X \quad mX \quad \text{(I-17)}$$

Avec :

$\frac{dX}{dt}$: taux de croissance de la biomasse dégradante (X) [$kg_{biomasse}\ kg^{-1}\ s^{-1}$]

Y : rendement d'assimilation avec Y<1 [-]

μ : taux de croissance de la biomasse [s^{-1}]

m : mortalité [s^{-1}]

La cinétique de croissance microbienne μ est généralement décrite par l'une des 4 cinétiques présentées dans le Tableau I.4, où μ_{max} est le taux maximum de croissance [s^{-1}] et K_s est la concentration en substrat nécessaire pour atteindre un taux de croissance égale à 50 % du taux de croissance maximum [$kg_{substrat}\ kg^{-1}$].

Tableau I.4. Les différents modèles de croissance microbienne.

Cinétique	μ	Remarque
Ordre zéro	$\mu = \mu_{max}$	La vitesse de dégradation est constante et indépendante de la concentration en substrat (S).
Premier ordre	$\mu = \mu_{max} S$	La vitesse de dégradation dépend de la concentration du substrat limitant (S).
Pseudo premier ordre	$\mu.X = \mu_{max} S.X$ $\mu.X = \gamma S$	Il y a un excès de biomasse dégradante (X) par rapport au substrat (S). La concentration de la biomasse (X) est incluse dans la valeur de la constante γ et le système est limité par S.
Monod	$\mu = \frac{\mu_{max} S}{K_S + S}$	En fonction de la value de K_S, on distingue 3 cinétiques : - si $S >> K_S$, le substrat est en excès, $\mu \quad \mu_{max}$ et le système est limité par la biomasse. - si $S << K_S$, le système est substat (S) limitant - si $S = K_S$, la vitesse de dégradation est constante avec $\mu = \frac{1}{2}\mu_{max}$

Les deux équations I-16 et I-17 montrent qu'une fraction (Y) du substrat dégradé est utilisée pour la fabrication des nouvelles cellules microbiennes ainsi que pour leur maintenance, alors que le reste du substrat est libéré dans le milieu sous la forme de CO_2 et métabolites (MET). Ceci s'exprime mathématiquement par :

$$\frac{dCO_2}{dt} + \frac{dMET}{dt} = (1 \quad Y)\frac{dS}{dt} \qquad \text{(I.18)}$$

2.2.6. Influence du milieu environnemental sur la biodégradation

Plusieurs facteurs physiques ou chimiques peuvent influencer le phénomène de biodégradation (Margesin and Schinner, 2001). Généralement, ces facteurs sont maîtrisés dans des conditions de laboratoire mais ils sont variables dans le milieu naturel (Leahy and Colwel, 1990). Ces divers facteurs sont par exemple la température ou l'humidité. D'autres facteurs physico-chimiques tels le pH, la salinité ou la présence de métaux lourds, peuvent affecter la biodégradation mais ils ne seront pas discutés ici.

a) Température

A des températures élevées, les réactions enzymatiques sont favorisées, ce qui augmente le taux de biodégradation (Atlas, 1981; Margesin and Schinner, 2001). Cependant des températures trop élevées peuvent diminuer la solubilité de l'oxygène, ce qui conduit à diminuer le taux de biodégradation microbienne en conditions aérobies (Atlas, 1981). L'effet de la température sur la biodégradation est considéré dans les modèles de dynamique des polluants organiques par le biais de fonctions mathématiques qui sont souvent des facteurs multiplicatifs de la constante de décomposition ou de croissance microbienne. Parmi les fonctions développées de température, on peut citer la fonction de Rosso et al. (1993) et aussi celles rapportées par Kaiser (1996) et par Stombaugh and Nokes (1996) pour le compost tandis que pour le sol on peut citer la fonction de Recous (1995) et celle d'Arrhenius (Coover and Sims, 1987). Ces fonctions ont d'abord été mises au point pour la dégradation des matières organiques du sol et ont été utilisées pour décrire la dégradation des contaminants organiques.

b) L'humidité

Le processus de biodégradation est aussi influencé par l'humidité du sol (Carter et al., 2010). L'humidité du sol est exprimée en masse ou volume d'eau par rapport au sol. Elle est corrélée à la granulométrie du sol et à la teneur en matières organique du sol (Yuandong et al., 2006). Elle peut varier entre 0 (sécheresse complète) et 100 % (saturation complète) dans le sol. L'humidité normale du sol se situe entre 60 % et 80 % de la capacité de rétention maximale en eau du sol. Les teneurs en eau faibles diminuent la diffusion des substrats vers les microorganismes et donc leur bioaccessibilité, les teneurs en eau fortes provoquent l'appauvrissement en oxygène dans le milieu ce qui a une influence négative sur l'activité microbienne (Yuandong et al., 2006). De même que pour l'effet de la température, des fonctions mathématiques sont développées pour prendre en compte l'humidité du sol dans les modèles. A ce titre, on peut citer la fonction de Andrén et al. (1992).

2.3. Processus de transport

2.3.1. Généralités et définitions

L'eau peut entrainer le déplacement des polluants organiques dans le sol par le ruissellement, par la lixiviation et par le lessivage (Fernandes et al., 2006). Le ruissellement est le phénomène décrivant l'écoulement de l'eau et des matières dissoutes et colloïdales qu'elle contient à la surface du sol. Le lessivage concerne le transport des particules solides non

solubles (i.e. les colloïdes) tandis que la lixiviation concerne le transport d'éléments dissous comme par exemple, les polluants dissouts dans la solution du sol et les matières organiques dissoutes. Le ruissellement des contaminants sur le sol peut entrainer la pollution des eaux de surface comme les lacs, ruisseaux, rivières. La lixiviation et le lessivage peuvent contribuer à la pollution des eaux du sol et de la nappe.

La migration des polluants vers les eaux profondes dépend à la fois des propriétés du polluant et de celles du sol. En ce qui concerne les propriétés du polluant, les polluants les plus persistants peuvent présenter des risques accrus de mobilité vers les eaux souterraines. D'après Jones et al. (1989), la quantité transportée des HAP ne décroit pas avec l'augmentation de la masse molaire car les matières organiques dissoutes servent de vecteurs à ces polluants vers les eaux profondes. En terme de propriétés du sol, un sol drainant à faible capacité de rétention (avec peu de matière organique) ou encore la présence d'écoulements préférentiels rapides (Jarvis, 2007) favorisent l'entrainement des polluants par lixiviation vers les eaux profondes.

2.3.2. Modélisation du transport des HAP en solution

Le transport d'un composé dissous dans la porosité du sol se produit principalement par l'association de trois processus qui sont la convection, la diffusion moléculaire et la dispersion mécanique. L'équation de la convection-dispersion (ou l'équation générale du transport) est utilisée dans la plupart des modèles mécanistiques pour décrire le transport des solutés en milieu poreux. On citera à titre d'exemple les modèles PEARL (Leistra et al., 2001), PRZM (Carsel et al., 1998) et MACRO (Larsbo and Jarvis, 2003)). L'équation générale de transport est la combinaison des équations de transfert de matière et de la loi de conservation de la masse. Ainsi, pour un transport unidirectionnel, elle a la forme suivante :

$$\frac{\partial(\rho C_S)}{\partial t}+\frac{\partial(\theta C_w)}{\partial t}=\frac{\partial(vC_w)}{\partial z}+\frac{\partial}{\partial z}\left(D_L\frac{\partial C_w}{\partial z}\right) \qquad \text{(I-19)}$$

Où t est le temps (s), z est la profondeur (m), ρ est la masse volumique apparente sèche du sol ($kg_{sol}\ m^{-3}_{sol}$), θ est la teneur en eau volumique du sol ($m^3_{eau}\ m^{-3}_{sol}$), C_w est la concentration de la substance dissoute (HAP) dans la solution du sol ($kg_{sub}\ m^{-3}_{eau}$), C_s est la concentration de la substance adsorbée sur la phase solide du sol ($kg_{sub}\ kg^{-3}_{sol}$) et D_L est le coefficient de dispersion ($m^2\ s^{-1}$).

Le premier terme à droite de l'équation (I-19) représente le transport du soluté par advection ou convection ; c'est-à-dire par le mouvement de flux d'eau au travers du milieu poreux.

Ainsi, la quantité de soluté transporté par advection est fonction de sa concentration et de la vitesse de l'eau. La variable *v* est donnée par l'équation suivante :

$$v = \frac{K}{\theta_e}\frac{dh}{dz} \qquad \text{(I-20)}$$

Avec *dh/dz* qui est le gradient hydraulique, *K* la conductivité hydraulique et θ_e la porosité effective (-). Celle-ci correspond à la partie de la porosité dans laquelle l'eau pourra circuler.

Le deuxième terme à droite de l'équation (I-19) représente le transport par le biais de la dispersion liée au coefficient de dispersion apparent D_L qui associe le coefficient de diffusion moléculaire D_e ($m^2\ s^{-1}$) basé sur la diffusion de soluté dans un milieu poreux et le coefficient de dispersion mécanique qui est égale à une propriété de la géométrie du milieu poreux, la dispersivité longitudinale du sol λ (-), multiplié par la vitesse linéaire moyenne *v*. On a alors :

$$D_L = D_e + \lambda v \qquad \text{(I-21)}$$

Le premier terme à gauche de l'équation (I-19) est un terme correcteur qui permet de décrire les processus de sorption et désorption des solutés avec la phase solide du sol. Il est également possible, et selon les conditions environnementales gouvernant le milieu d'étude, d'introduire d'autres termes correcteurs qui rendent compte de processus supplémentaires qui peuvent modifier la réactivité du soluté dans la solution du sol (par exemple, la dégradation, le prélèvement par les racines des végétaux, les précipitations atmosphériques).

2.3.3. Modélisation du co-transport des HAP avec la MOD

Le transport de contaminants hydrophobes comme les HAP est souvent décrit en prenant en compte la phase adsorbée sur la matière organique dissoute (MOD) qui peut co-transporter le polluant plus en profondeur dans le sol.

Les matières organiques dissoutes (MOD) sont des molécules organiques dont la taille n'excède pas 0,46 µm (Zsolnay et al., 1999). Elles représentent une faible fraction des quantités totales de matières organiques. D'après Nierop et al. (2002), cette quantité ne dépasse pas les 1 % de quantité totale de la matière organique du sol. Leur première source est l'activité des plantes et la production d'exsudats racinaires. Leur seconde source définie par McDowell (2003) est l'activité biologique et la décomposition de la matière organique par les micro-organismes du sol.

Rav-Acha and Rebhun, (1992) ont proposé un modèle (Figure I.7) basé sur des équilibres de sorption entre le polluant organique, la MOD et la phase solide du sol. Les interactions prises en compte sont les équilibres de sorption : i) entre le polluant organique libre (POL) dans la solution du sol et lorsqu'il est adsorbé sur les MOD, ii) entre le polluant organique libre et le

polluant organique adsorbé sur la phase solide du sol et iii) entre la MOD dans la solution du sol et celle adsorbée sur la phase solide du sol, selon les relations suivantes :

$$K_{POL\ MOD} = \frac{C_{POL\ MOD}}{C_{POL} C_{MOD}}; K_{POL\ SOL} = \frac{S_{POL}}{C_{POL}}; K_{MOD} = \frac{S_{MOD}}{C_{MOD}} \quad \text{(I-22)}$$

Avec $C_{POL\text{-}MOD}$, C_{POL} et C_{MOD} qui sont les concentrations dans la solution du sol des POL associés à la MOD, des POL libres et du COD respectivement ; S_{POL} et S_{MOD} représentent les quantités de polluants organiques libres et de COD adsorbés sur la phase solide du sol, et $K_{\text{POL-MOD}}$, $K_{\text{POL-sol}}$ et K_{MOD} représentent les coefficients de distribution des différentes interactions. En se basant sur des relations additives des concentrations des deux formes de polluants organiques (libres et associées à la MOD) en phase aqueuse et en solution respectivement. Les auteurs calculent alors un coefficient de distribution du polluant total entre la phase liquide et la phase solide du sol, K_{POL}^{T} selon :

$$K_{POL}^{T} = \frac{S_{POL}^{T}}{C_{POL}^{T}} = \frac{S_{POL} + S_{POL\ MOD}}{C_{POL} + C_{POL\ MOD}} = \frac{K_{POL\ SOL} + K_{MOD} K_{POL\ MOD} C_{MOD}}{1 + K_{POL\ MOD} C_{MOD}} \quad \text{(I-23)}$$

Avec $S_{POL\text{-}MOD}$ la quantité de POL-MOD adsorbée sur la phase solide du sol. La relation a été établie en faisant l'hypothèse simplificatrice que l'objet associé POL-MOD a les mêmes propriétés d'adsorption sur le sol que la MOD.

Selon l'équation (I-23), si C_{MOD}=0 (i.e. absence MOD), alors $K_{POL}^{T} = K_{POL\ SOL}$. C'est-à-dire que le coefficient de distribution du polluant total devient équivalent au coefficient de distribution du polluant libre sur la surface du sol.

Si $K_{POL\ SOL} >> K_{POL\ MOD}$, alors l'équation (I-23) peut être réécrite comme :

$$K_{POL}^{T} = \frac{K_{POL\ SOL}}{1 + K_{POL\ MOD} C_{MOD}} \quad \text{(I-24)}$$

Ici, l'équation (I-24) entraîne que l'adsorption du POL total en présence de la matière organique est réduite pour des concentrations croissantes de MOD ($K_{POL}^{T} < K_{POL\ SOL}$). Ceci explique l'effet de solubilisation observé dans certaines études qui ont rapporté que la capacité d'adsorption des polluants organiques diminue avec une concentration croissante de MOD, tandis qu'en présence d'une MOD fortement réactive (une valeur de $K_{POL\ MOD}$ élevée), l'inverse se produit. Cette approche d'interaction polluant-MOD a été utilisée par la suite par Sabbah et al.(2004) dans un modèle de transport convectif dispersif prenant en compte un modèle de sorption à deux types de sites, instantanés et cinétiques. Ils ont pu montrer

comment la matière organique dissoute pouvait faciliter le transport de HAP par son effet sur les taux de sorption et de désorption.

La décomposition de la matière organique de compost épandu entraine la formation de MOD qui peut favoriser leur solubilité apparente dans la solution du sol par le biais des interrelations entre les polluants organiques et la MOD et donc un entrainement en profondeur par transport facilité (Xiu-hong et al., 2014). Chabauty et al. (2016) ont mis en évidence ce phénomène pour divers contaminants organiques sur des colonnes de sol.

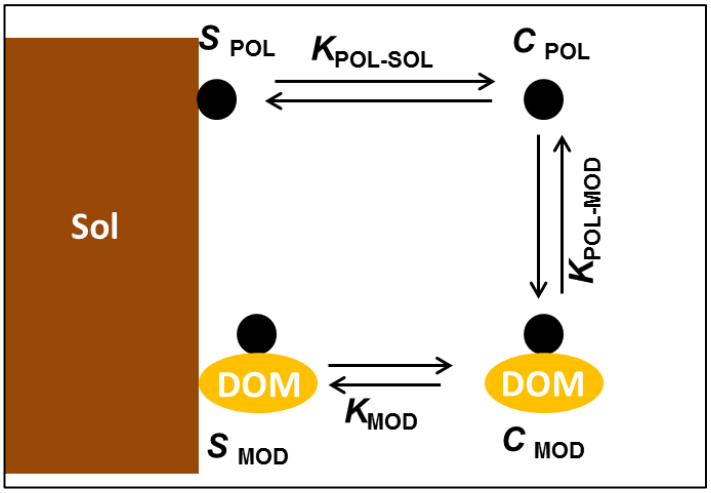

Figure I.7. Schéma des interactions entre les polluants libres dans la phase soluble (POL), adsorbés sur les MOD et sur les phases solides du sol (modifié de Barriuso et al. (2011)).

3. Les modèles de dynamique des HAP

Assez peu de modèles présentés dans la littérature sont dédiés aux HAP dans le sol. Nous présentons ici une synthèse sur un ensemble de modèles décrivant la dynamique des HAP dans le sol (voir le Tableau I.5). L'analyse des différents modèles conduit alors aux remarques suivantes :

1) Tous les modèles, à l'exception de celui de Thiele-Bruhn and Brümmer (2005), ont été testés en conditions de laboratoire. La structuration et l'application du modèle sont généralement conduites sur des réacteurs de type batch, excepté pour le modèle de Sabbah et al. (2004) qui a été appliqué à une colonne de sol. A ce jour, aucun modèle global dédié aux HAP incluant l'ensemble des processus majeurs contrôlant le devenir de HAP dans les sols (i.e. adsorption, biodégradation, transport , interaction avec la matière organique (MO) du sol naturelle ou exogène) n'a été proposé et appliqué sur le terrain.

2) Les HAP de faible poids moléculaire (3 ou 4 cycles benzéniques) sont souvent les molécules utilisées dans les modèles (Tableau I.5). Ces molécules sont choisies du fait de leur mobilité significative en comparaison avec les autres molécules de HAP. Les données de la littérature sur les cinétiques de HAP sont très peu renseignées. Ces cinétiques sont souvent déterminées à l'aide de données expérimentales mesurées sur des périodes qui varient entre quelques semaines et quelques mois (excepté dans Thiele-Bruhn and Brümmer (2005) où elles sont éstimées sur une période de 168 semaines). Néanmoins, la validité de ces cinétiques déterminées dans les conditions de laboratoire n'a pas été testée à l'échelle du terrain.
3) Tous ces modèles ont été testés pour une seule situation (soit un sol agricole, soit un sol de friche industrielle). Il n'y a pas de modèle dont l'aptitude a été testée pour des gammes de concentrations étendues.
4) Le problème de la libération des HAP avec l'incorporation d'amendement organique dans le sol est rarement traité. Parmi les 8 modèles examinés, le modèle de Geng et al.(2015) est le seul qui a permis de simuler la dynamique des HAP dans un sol amendé par du compost. Le couplage entre le sous-modèle de dynamique de la matière organique et celui du polluant organique (Figure I.8) a permis de modéliser l'effet de la décomposition du compost sur la croissance de la biomasse dégradant les HAP (par voie co-métabolique), et il a également permis de modéliser l'effet du compost sur l'affinité des HAP pour la matrice solide en intégrant l'adsorption sur la matrice « sol-compost ». Cependant, le modèle montre certaines limitations. Par exemple, il est basé sur une structure utilisant un compartiment unique pour le sol amendé et le compost apporté alors que ce mélange pourrait être représenté par deux compartiments distincts. Il est possible d'utiliser le modèle pour simuler la dynamique des HAP lors d'une expérience de laboratoire dans lequel le mélange sol-compost peut être considéré comme une seule phase, mais le modèle avec sa structure actuelle n'est pas applicable dans le cas où le sol reçoit au champs des apports répétés de compost au cours du temps.
5) Le modèle de Kästner et al.(2014) est le seul qui permet de simuler le compartiment biogénique des résidus non extractibles de polluant dans le sol (Figure I.9). Les modèles de polluants organiques ne font souvent pas la différence entre les compartiments physico-chimiques et biogéniques des résidus liés.
6) L'adsorption et la biodégradation, qui sont les deux principaux processus responsables de la dynamique des HAP dans le sol, ont été modélisés différemment

suivant les modèles. Cela indique qu'il n'existe pas de consensus entre les modélisateurs sur la façon de modéliser les processus de biodégradation et d'adsorption. Les hypothèses, les concepts et les unités des paramètres sont assez différents entre modèles. Il est donc difficile de comparer les différentes structures des modèles et de comparer les valeurs des paramètres entre les modèles.

- Concernant la biodégradation, les deux différences majeures entre les modèles sont :
  - 1) le choix de la fraction bio-disponible utilisable par les biomasses microbiennes dégradantes, c'est souvent la fraction liquide (libre & associée aux colloïdes) qui est considérée comme la fraction biodisponible pour les biomasses microbiennes. Dans certains modèle (comme Fragoulis et al., 2005)), la fraction adsorbée est biodisponible).
  - 2) la modélisation des voies de biodégradation : il peut s'agir d'une seule voie (Kästner et al., 2014; Thiele-Bruhn and Brümmer, 2005; Wick et al., 2001) ou de deux voies de biodégradation (Fragoulis et al., 2005; Geng et al., 2015)) et leur description mathématique (certains modèles utilisent seulement la cinétique de Monod (Kästner et al., 2014; Wick et al., 2001) et d'autres utilisent la cinétique de Monod combinée avec une cinétique du premier ordre (Fragoulis et al., 2005; Geng et al., 2015).

Concernant l'adsorption, les modèles utilisent souvent deux phases d'adsorption (Geng et al., 2015; Johnson et al., 2001; Kästner et al., 2014; Sabbah et al., 2004) dont une cinétique réversible du premier ordre. Il n'existe pas de consensus sur la façon de définir les différents compartiments du modèle par rapport aux fractions adsorbées.

Tableau I.5. Synthèse des 8 modèles de dynamique des HAP dans le sol identifiés dans la littérature

Référence	Type de modèle	Processus majeurs modélisés✱				Type de HAP†	Échelle d'application	Échelle de temps (semaines)	Commentaires
		Ads	Biodg	Tra	MO				
Rav-Acha and Rebhun, 1992	équilibre	oui				PHE	Batch	-	L'adsorption se fait sur trois phases : la surface du sol, le polluant libre et la MOD+ dans la solution du sol
Johnson et al., 2001	dynamique	oui				PHE	Batch laboratoire	36	Tester 6 modèles différents d'adsorption
Sabbah et al., 2004	dynamique	oui		oui		PHE FLT	Colonne laboratoire	-	
Wick et al., 2001	dynamique		oui			ANT	Batch laboratoire	3.5	
Thiele-Bruhn and Brümmer, 2005	dynamique		oui			15HAP	Batch (jar)	168	Les données sont issues d'incubations de sols de friches qui sont réalisées en conditions atmosphériques extérieures
Fragoulis et al., 2005	dynamique	oui	oui			PHE	Batch laboratoire	58	
Geng et al., 2015	dynamique	oui	oui		oui	FLT	Batch laboratoire	20	sol agricole
Kästner et al., 2014	dynamique	oui	oui			ANT	Batch laboratoire	1.5	sol de friche le modèle est aussi utilisé dans Adam et al. (2014) et Rein et al. (2016)

✱ Ads : adsorption, Biodg : biodégradation, Tra : transport, MO : matières organiques

† PHE : phénanthrène, FLT : fluoranthène, ANT : anthracène

+ MOD : matière organique dissoute

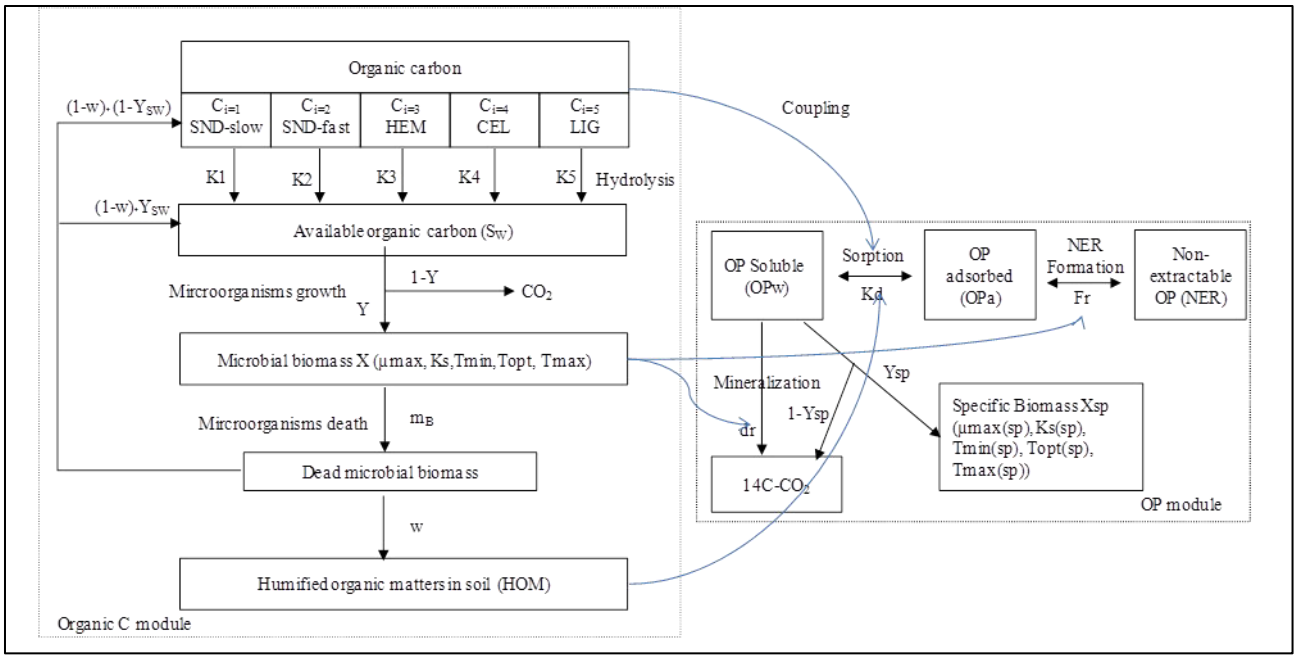

Figure I.8. Structure générale du modèle de Geng et al. (2015)

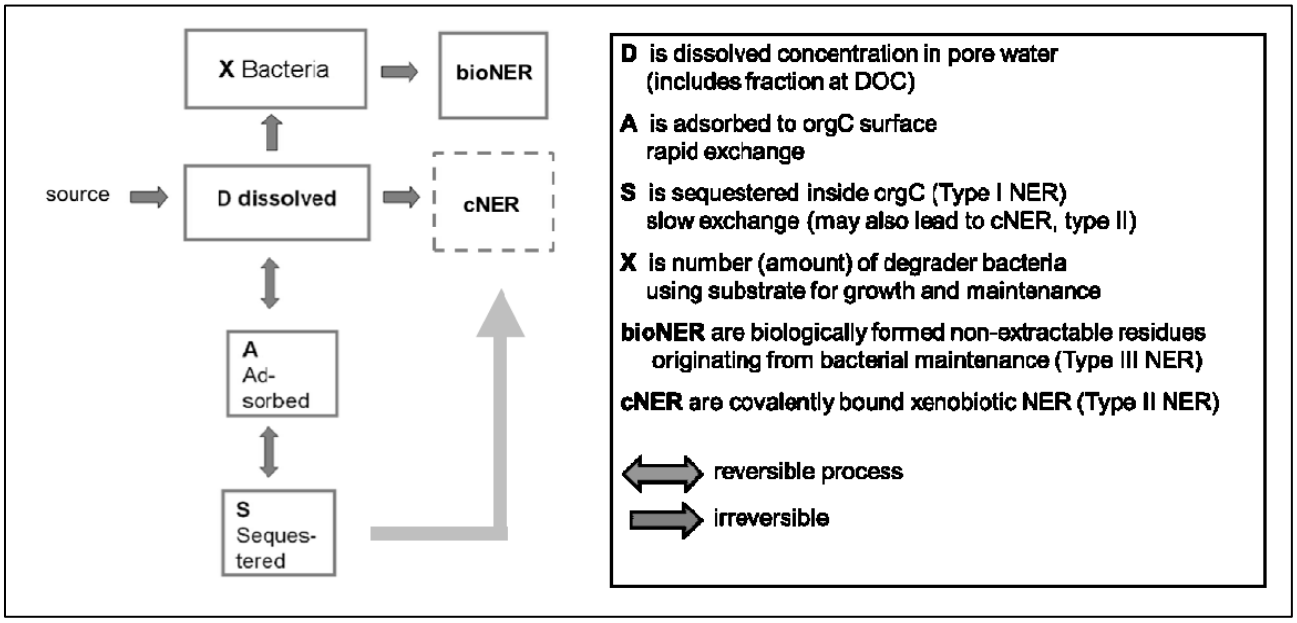

Figure I.9. Structure générale du modèle de Kästner et al. (2014)

4. Objectifs de la thèse

Ce travail de thèse a deux principaux objectifs : le premier objectif est la mise au point d'un outil de modélisation mécanistique qui permette de décrire les processus de la dynamique des HAP à l'échelle du champ en interaction avec i) la matière organique sur laquelle les polluants vont s'adsorber ; ii) les microorganismes du sol qui dégradent les HAP ou

participent à la formation des résidus liés soit par métabolisme spécifique soit par co-metabolisme ; iii) la lixiviation en tant que puits *via* le transfert des HAP vers les eaux souterrains ; et iv) le climat en tant que source *via* les retombées atmosphériques mais également en tant que conditions aux limites à l'échelle du champ (pluie, evatranspiration, température de l'air..). Le deuxième objectif est d'utiliser cet outil de modélisation pour décrire des scénarios concernant le devenir des HAP afin de répondre à des questions plus finalisées pour les deux situations contrastées de l'étude :

- Pour le site de GISFI (54) lié à de fortes concentrations de HAP dans un sol contaminé de site industriel. Il s'agit d'étudier l'impact à long terme de la décontamination du sol pour différentes prévisions climatiques.
- Pour le site de QUALIAGRO (78) lié à de faibles concentrations de HAP apportées par de composts en parcelles agricoles. Il s'agit d'étudier l'influence à long terme d'un apport répété de composts sur l'accumulation de HAP, en fonction du type des déchets organiques et de la nature du polluant.

Ce travail s'est alors déroulé en trois grandes étapes, répondant chacune à des objectifs spécifiques :

I. Identification des processus à modéliser et développement de modules qui décrivent la dynamique des HAP et qui incluent les processus 1) d'adsorption des HAP sur la matrice organique et solide du sol et la formation des résidus liés physiques, 2) de biodégradation en fonction de l'environnement organique et microbien et la production de résidus liés biogéniques, et qui tiennent également en compte la qualité des matières organiques compostées sur le relargage des HAP.
II. Développement de nouveaux modules sous MATLAB (Mathwork, USA) en leur associant un algorithme Bayésien « DREAM » (Vrugt, 2016) permettant de paramétrer les modules en utilisant des données expérimentales de laboratoire. Ces données expérimentales ont été sélectionnées et considérées comme complémentaires aux données de terrain pour calibrer les nouveaux modules HAP proposés.
III. Proposer un modèle global adapté aux HAP et pouvant s'adapter aux dispositifs expérimentaux aux champs pour les deux situations d'étude. Ce modèle a été établi sous la plateforme SOL Virtuel de l'INRA et comprend des modules qui représentent les principaux processus influençant le devenir des HAP dans le sol. Ce modèle a ensuite été utilisé pour simuler des scenarios sur le devenir des HAP dans les deux situations d'étude.

Le choix des HAP étudiés a été basé sur la disponibilité des données expérimentales : trois HAP listés comme prioritaires par l'agence de protection de l'environnement américaine US-EPA et l'Union Européenne ont été retenus comme HAP modèles pour la situation de QUALIAGRO (78) : le phénanthrène (un HAP léger à 3 cycles), le fluoranthène (un HAP moyen à 4 cycles) et le benzo[a]pyrène (un HAP lourd à 5 cycles). Pour la situation du GISFI (54), l'étude s'est limitée au phénanthrène.

Lorsque l'effet du compost a été considéré, trois types de composts d'origine urbaine ont été étudiés:

- Un compost issu d'ordures ménagères résiduelles après collecte sélective des emballages propres et sacs papiers (cartons, verres et emballages) (MSW) ;
- Un compost issu de la fraction fermentescible des ordures ménagères collectées sélectivement (déchets de cuisine, fleurs) (BioW) ;
- Un compost issu d'un mélange de déchets verts et de boues de station d'épuration (GWS).

La démarche générale adoptée pour ce travail de thèse est synthétisée dans la Figure I.10.

La **partie I** est consacrée au développement et au paramétrage des nouveaux modules HAP en utilisant des données expérimentales de laboratoire. Elle est présentée dans deux chapitres de ce mémoire de thèse :

- Dans le **chapitre n°2**, les modules décrivant les processus d'adsorption et biodégradation des HAP dans le sol sont proposés et paramétrés sur les données expérimentales acquises pour la situation d'étude de sol pollué industriel (GISFI, 54). Un jeu de paramètres est établi pour le phénanthrène dans un sol sans plante sur la base d'une expérience d'incubation de phénanthrène marqué au ^{13}C (Cébron et al., 2011).
- Dans le **chapitre n°3**, un module complémentaire simulant l'évolution des HAP des composts pendant leur décomposition et qui tient compte de la qualité des matières organiques compostées sur le relargage des HAP est proposé. Des hypothèses de couplage représentant les interactions entre ce module et les modules d'adsorption et de biodégradation des HAP présentés au chapitre précédant sont ensuite formulées. Les modules sont paramétrés sur la base d'expériences d'incubation de trois HAP marqués au ^{14}C (thèse de Verge-Leviel, 2001) représentant la situation d'étude de sol agricole recevant un apport de compost (QUALIAGRO, 78). Trois jeux de paramètres ont été identifiés pour le phénanthrène, le fluoranthène et le benzo [a] pyrène.

Pour ces deux approches une analyse de sensibilité des paramètres est effectuée à l'aide de l'algorithme DREAM. Celle-ci permet de mettre en évidence les processus contrôlant le devenir des HAP dans ces systèmes et nous amene à proposer des simplifications de formalisme par rapport aux modules proposés.

La **partie II** consiste à implémenter les modules de réactivité des HAP développés et paramétrés sous Matlab dans la partie I dans la structure de la plateforme SOL VIRTUEL et à évaluer son aptitude à rendre compte des observations mesurées dans les deux situations *in situ*. Le modèle HAP couplé est ensuite utilisé pour décrire des scenarios sur le devenir des HAP *in situ* pour les deux situations d'étude. Cette partie est également composée de deux chapitres:

- Dans le **chapitre n°4**, deux scenarios pour le site du GISFI (54) sont réalisés. Les données expérimentales acquises sur 10 ans d'observation ayant montré qu'il n'y a pas d'influence de la végétation sur la dynamique des HAP dans le sol, nous avons uniquement appliqué le modèle sur la condition de sol nu. Il s'agit en particulier i) d'évaluer l'influence des conditions climatiques à long terme sur le potentiel de stockage du phénanthrène dans le sol, ii) d'estimer l'effet de la modification de disponibilité du polluant (par exemple par l'addition de solvants organiques) sur la dissipation du phénanthrène.
- Dans le **chapitre n°5**, des scenarios d'épandage pour le site QUALIAGRO (78) sont réalisés. Il s'agit i) d'étudier l'influence de l'apport répété à long terme de déchets organiques compostés sur l'accumulation de HAP dans le sol agricole, ii) d'évaluer l'influence du type de compost sur cette accumulation, et iii) d'estimer le potentiel de stockage des HAP sous la forme de résidus liés physiques et biogéniques.

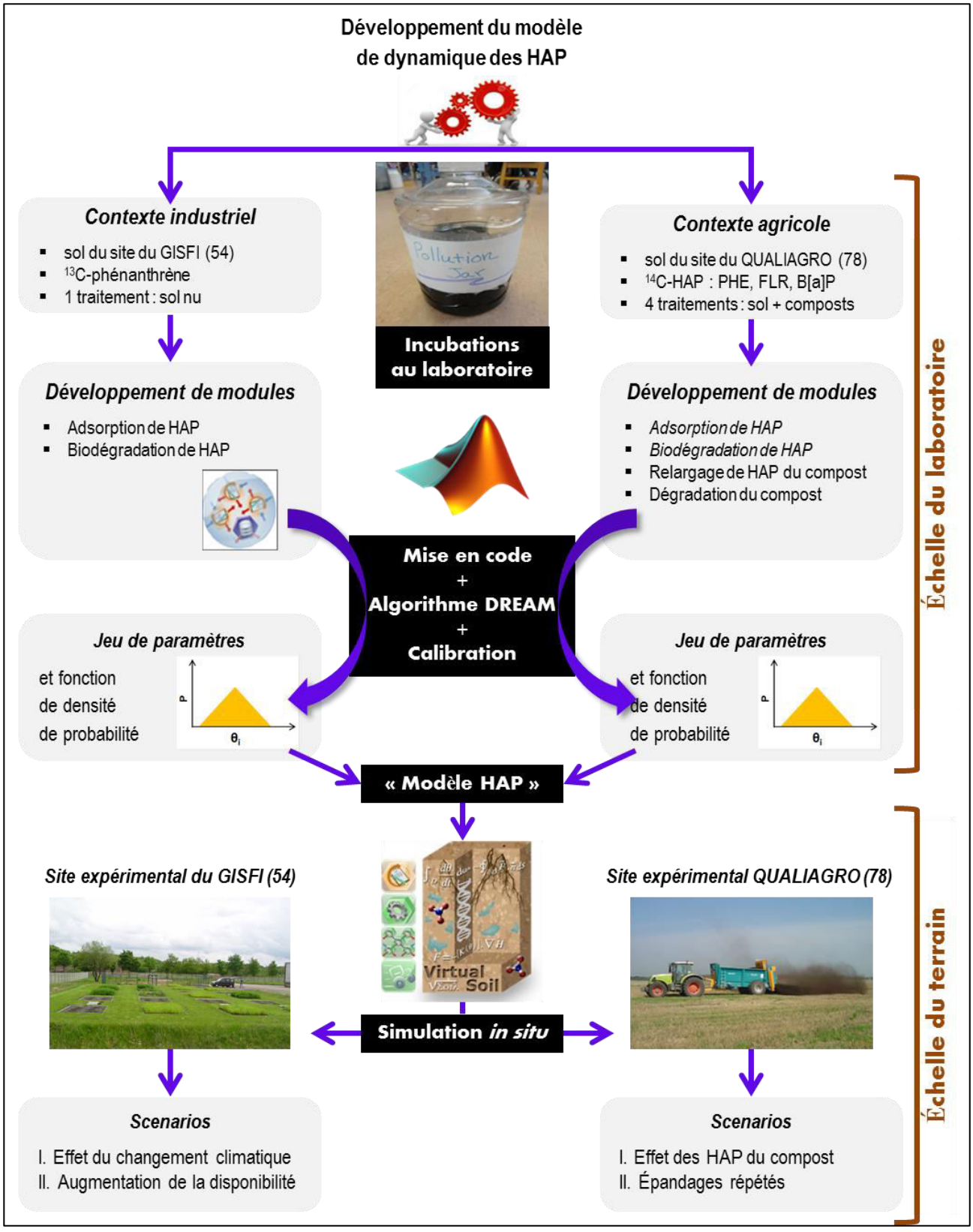

Figure I.10. Schéma de la démarche générale adoptée pour ce travail de these

5. Références bibliographiques

Adam, I.K.U., Rein, A., Miltner, A., Fulgêncio, A.C.D., Trapp, S., Kästner, M., 2014. experimental results and integrated modeling of bacterial growth on an insoluble hydrophobic substrate (Phenanthrene). Environ. Sci. Technol. **48**, 8717–8726. doi:10.1021/es500004z

Andrén, O., Steen, E., Rajkai, K., 1992. Modelling the effects of moisture on barley straw and root decomposition in the field. Soil Biol. Biochem. **24**, 727–736. doi:10.1016/0038-0717(92)90246-T

Aslam, S., Benoit, P., Chabauty, F., Bergheaud, V., Geng, C., Vieubl, L., Garnier, P., 2014. Modelling the impacts of maize decomposition on glyphosate dynamics in mulch. Eur. J. Soil Sci. **65**, 231–247. doi:10.1111/ejss.12126

Atlas, R.M., 1981. Microbial degradation of petroleum hydrocarbons: an environmental perspective. Microbiol Rev. **45**, 180–209.

Azimi, S., Rocher, V., Muller, M., Thevenot, D.R., 2005. Sources , distribution and variability of hydrocarbons and metals in atmospheric deposition in an urban area (Paris , France). Sci. Total Environ. **337**, 223–239. doi:10.1016/j.scitotenv.2004.06.020

Bamforth, S., Singleton, L., 2005. Review: Bioremediation of polycyclic aromatic hydrocarbons: Current knowledge and future directions. J. Chem. Technol. Biotechnol. **80**, 723–736.

Barriuso, E., Andrades, M.S., Benoit, P., Houot, S., 2011. Pesticide desorption from soils facilitated by dissolved organic matter coming from composts: Experimental data and modelling approach. Biogeochemistry **106**, 117–133. doi:10.1007/s10533-010-9481-y

Barriuso, E., Benoit, P., Dubus, I.G., 2008. Formation of pesticide nonextractable (bound) residues in soil: Magnitude, controlling factors and reversibility. Environ. Sci. Technol. **42**, 1845–1854. doi:10.1021/es7021736

Barriuso, E., Clavet, R., Schiavon, M., Soulas, G., 1996. Les pesticides et les polluants organiques des sols :tranformations et dissipation. Etude et gestion des sols. **3**, 279–296.

Beltran, F.J., Overjero, G., Rivas, J., 1996. Oxidation of polynuclear aromatic hydrocarbons in water. 3. UV radation combined with hydrogen peroxide. Ind. Eng. Chem. Res. **35**, 883–890.

Bewley, R., Ellis, B., Theile, P., Viney, I., Rees, J., 1989. Microbial clean up of contaminated soil. Chem. Ind. **23**, 778–783.

Binet, P., Portal, J., Leyval, C., 2001. Dissipation of 3-6-ring polycyclic aromatic hydrocarbons in the rhizosphere of ryegrass. Soil Biol. Biochem. **32**, 2011–2017. doi:10.1016/S0038-0717(00)00100-0

Blanchard, M., Teil, M., Guigon, E., Ollivon, D., Garban, B., Chevreuil, M., 2007. Persistent toxic substance inputs to the river Seine basin (France) via atmospheric deposition and urban sludge application. Sci. Total Environ. **375**, 232–243. doi:10.1016/j.scitotenv.2006.12.012

Blumer M, 1976. Polycyclic aromatic compounds in nature. Sci. Am. 234, 34–45.

Bogan, B.W., Schoenike, B., Lamar, R.T., Cullen, D., 1996. Expression of LiP genes during growth in soil and oxidation of anthracene by Phanerochaete chrysosporium. Appl. Environ. Microbiol. **62**, 3697–3703.

BRGM (Bureau de Recherches Géologiques et Minières), 2007. Bases de données relatives à la qualité des sols : Contenu et utilisation dans le cadre de la gestion des sols pollués.

Byrns, G., 2001. The fate of xenobiotic organic compounds in wastewater treatment plants. Water Res. **35**, 2523–2533.

Carsel, R., Imhoff, J., Hummel, P., Cheplick, J., Donigian, J.A., 1998. PRZM-3: a model for predicting pesticide and nitrogen fate in the crop root and unsaturated soil zones: user's manual for release 3.12. Athens, GA: GA: National Exposure Research Laboratory,Office of Research and Development, US Environmental Protection Agency

Carter, D., Yellowlees, D., Tibbette, M., 2010. Moisture can be the dominant environmental parameter governing cadaver decomposition in soil. Forensic Sci. Int. **200(1-3)**:60-6. doi: 10.1016/j.forsciint.2010.03.031

CCME (Canadian Council of Ministers of Environment), 2008. Canadian soil quality guidelines for carcinogenic and other polycyclic Aromatic hydrocarbons: scientific criteria document. Winnipeg: CCME.

Cébron, A., Louvel, B., Faure, P., France-lanord, C., Chen, Y., Murrell, J.C., Leyval, C., 2011. Root exudates modify bacterial diversity of phenanthrene degraders in PAH-polluted soil but not phenanthrene degradation rates. Environ. Microbiol. **13**, 722–736. doi:10.1111/j.1462-2920.2010.02376.x

Chabauty, F., Pot, V., Deschamps, M.B., Bernet, N., Labat, C., Benoit, P., 2016. Transport of organic contaminants in subsoil horizons and effects of dissolved organic matter related to organic waste recycling practices. Environ. Sci. Pollut. Res. **23**, 6907–18. doi:10.1007/s11356-015-5938-9.

Chen, S.-H., Aitken, M.D., 1999. Salicylate Stimulates the Degradation of High-Molecular Weight Polycyclic Aromatic Hydrocarbons by Pseudomonas saccharophila P15. Environ. Sci. Technol. **33**, 435–439.

Chung, N., Alexander, M., 2002. Effect of soil properties on bioavailability and extractability of phenanthrene and atrazine sequestered in soil. Chemosphere **48**, 109–115. doi:10.1016/S0045-6535(02)00045-0

Coover, M.P., Sims, R.C., 1987. The effect of temperature on polycyclic aromatic hydrocarbon persistence in an unacclimated agriculturalsoil. Hazard. Waste Hazard. Mater. **4**, 69–82.

Cornelissen, G., Elmquist, M., Groth, I., Gustafsson, Ö., 2004. Effect of sorbate planarity on environmental black carbon sorption. Env. Sci Technol. **38**, 3574–3580.

Cunningham, S.D., Anderson, T.A., Schwab, A.P., Hsu, F.C., 1996. Phytoremediation of Soils Contaminated with Organic Pollutants. Adv. Agron. **56**, 55–114. doi:10.1016/S0065-2113(08)60179-0

Edwards, N.T., 1983. Polycyclic Aromatic Hydrocarbons (PAH's) in the Terrestrial Environment-A Review. J. Environ. Qual. **12**, 427–441.

Ellis, B., Harold, P., Kronberg, H., 1991. Bioremediation of a creo- sote contaminated site. Environmental Technology. Environ. Technol. **12**, 447–459.

Erickson, D.C., Loehr, R.C., Neuhauser, E.., 1993. PAH loss during bioremediation of manufactured gas plant site soil. Water Res. **27**, 911–919.

Fernandes, M., Cox, L., Hermosín, M., Cornejo, J., 2006. Organic amendments affecting sorption, leaching and dissipation of fungicides in soils. Pest Manag Sci **62 (12)**, 1207-1215. 12 2006.

Fragoulis, G., Trevisan, M., Puglisi, E., Capri, E., 2005. A model assessing bioavailability of persistent organic pollutants in soil, Reactive Transport in Soil and Groundwater. Springer-Verlag, Berlin/Heidelberg. doi:10.1007/3-540-26746-8_3

Garban, B., Blanchoud, H., Motelay-massei, A., Chevreuil, M., Ollivon, D., 2002. Atmospheric bulk deposition of PAHs onto France : trends from urban to remote sites. Atmos. Environ. **36**, 5395–5403.

Geng, C., Haudin, C.-S., Zhang, Y., Lashermes, G., Houot, S., Garnier, P., 2015. Modeling the release of organic contaminants during compost decomposition in soil. Chemosphere **119**, 423–431. doi:10.1016/j.chemosphere.2014.06.090

Gevao, B., Jones, K.C., Semple, K.T., 2005. Formation and release of non-extractable14C-Dicamba residues in soil under sterile and non-sterile regimes. Environ. Pollut. **133**, 17–24. doi:10.1016/j.envpol.2004.04.007

Gevao, B., Semple, K.T., Jones, K.C., 2000. Bound pesticide residues in soils: A review. Environ. Pollut. **108**, 3–14. doi:10.1016/S0269-7491(99)00197-9

Goodin, J.D., Webber, M.D., 1995. Persistence and Fate of Anthracene and Benzo(a)pyrene in Municipal Sludge Treated Soil. Waste Manag. **24**, 271–278.

Griest, W.H., Tomkins, B.A., 1986. Influence of carbonaceous particles on the interaction of coal combustion stack ash with organic matter. Env. Sci. Technol. **20**, 291–295.

Gustafsson, Ö., Haghseta, F., Chan, C., MacFarlane, J., Gschwend, P.M., 1996. Quantification of the dilute sedimentary soot phase: implications for PAH speciation and bioavailability. Env. Sci. Technol. **31**, 203–209.

Hance, R.J., 1973. The e†ects of nutrients on the decomposition of the herbicides atrazine and linuron incubated with soil. Pestic. Sci. **4**, 817–22.

Hatzinger, P.B., Alexander, M., 1995. Effect of aging of chemicals in soil on their biodegradability and extractability. Environ. Sci. Technol. **29**, 537–545. doi:10.1021/es00002a033

Heitkamp, M.A., Freeman, J.P., Milelr, D.W., Cerniglia, C.E., 1988. Pyrene degradation by a mycobacterium sp.: identification of ring oxidation and ring fission products. Appl. Environ. Microbiol. **54**, 2556–2565.

Houot S. et al. (2002) Agronomic value and environmental impacts of urban composts used in agriculture. In: Insam H., Riddech N., Klammer S. (eds) Microbiology of Composting. Springer, Berlin, Heidelberg ,

Iarc, 2010. IARC Monographs on the evaluation of carcinogenic risks to humans: some non-heterocyclic polycyclic aromatic hydrocarbons and some related exposures. Iarc Monogr. Eval. Carcinog. Risks To Humans **92**, 1–868.

Jardine, P.M., McCarthy, J.F., Weber, N.L., 1989. Mechanisms of Dissolved Organic Carbon Adsorption on Soil. Soil Sci. Soc. Am. J. **53**, 1378-1385.doi:10.2136/sssaj1989.03615995005300050013x

Jarvis, N.., 2007. A review of non-equilibrium water flow and solute transport in soil macropores: principles, controlling factors and consequences for water quality. Eur. J. Soil Sci. **58**, 523–546.

Johnson, M.D., Keinath, T.M., Weber, W.J., 2001. A distributed reactivity model for sorption by soils and sediments. 14. Characterization and modeling of phenanthrene desorption rates. Environ. Sci. Technol. **35**, 1688–1695. doi:10.1021/es001391k

Jones, K.C., Stratford, J.A., Tidridge, P., Waterhouse, K.S., 1989. Polynuclear aromatic hydrocarbons in an agricultural soil: Long-term changes in profile distribution. Environ. Pollut. **56**, 337–351.

Juhasz, A., Stanley, G., Britz, M., 2000. Microbial degradation of high molecular weight polycyclicaromatic hydrocarbons by Stenotrophomonas maltophilia strain VUN 10,003. Lett Appl Microbiol .**30(5)**, 396-401. doi: 10.1046/j.1472-765x.2000.00733.x

Juhasz, A., Naidu, R., 2000. Bioremediation of high molecular weight polycyclic aromatic hydrocarbons: a review of the microbial degradation of benzo[a]pyrene. Int. Biodeterior. Biodegradation **45**, 57–88.

Kaiser, J., 1996. Modelling composting as a microbial ecosystem: a simulation approach. Ecol. Modell. **91**, 25–37.

Karickhoff, S.W., Brown, D.S., Scott, T.A., 1979. Sorption of hydrophobic pollutants on natural sediments. Water Res. **13**, 241–248.

Kästner, M., Nowak, K.M., Miltner, A., Trapp, S., Schäffer, A., 2014. Classification and modelling of non-extractable residue (NER) formation of xenobiotics in soil—a synthesis. Crit. Rev. Environ. Sci. Technol. **44**, 2107–2171. doi:10.1080/10643389.2013.828270

Larsbo, M., Jarvis, N., 2003. MACRO 5.0. A model of water flow and solute transport in macroporous soil. Technical description. Rep EmergoUppsala, Sweden: Swedish University of Agricultural Sciences. [49 pp.].

Lashermes, G., Zhang, Y., Houot, S., Steyer, J.P., Patureau, D., Barriuso, E., Garnier, P., 2013. Simulation of Organic Matter and Pollutant Evolution during Composting: The COP-Compost Model. Environ. Qual. **42(2)**, 361–372. doi:10.2134/jeq2012.0141

Leahy, J.G., Colwel, R., 1990. Microbial Degradation of Hydrocarbons in the Environment. Microbiol. Rev. **54**, 305–315.

Leduc, R., Samson, R., Al-Bashir, B., Al-Hawari, J., Cseh, T., 1992. Biotic and abiotic disappearance of four PAH compounds from flooded soil under various redox conditions. Wat. Sci. Tech. **26**, 51-60.

Leistra, M., van der Linden, AMA., Boesten, JJTI., Tiktak, A., van den Berg, F., 2001. PEARL model for pesticide behaviour and emissions in soil-plant systems: description of the processes. Alterra Rep 13. The Netherlands: Wageningen University and Research Centre, Wageningen. [115 pp.].

Lerch, TZ ; Dignac, MF; Nunan, N; Barriuso, E; Mariotti, A. 2009. Ageing processes and soil microbial community effects on the biodegradation of soil C-13-2,4-D nonextractable residues. Environ. Pollut, **157**, 2985-2993

MacKay D., Shiu W.Y., Ma K.-C., Lee S.C. 2006. Handbook of physical-chemical properties and environmental fate for organic chemicals. 2nd ed. CRC Press, Boca Raton (FL).

Mandalakis, M., Gustafsson, O., Alsberg, T., Egeback, A.L., Reddy, C.M., Xu, L., Klanova, J., Holoubek, I., Stephanou G., E., 2005. Contribution of biomass burning to atmospheric poly-cyclic aromatic hydrocarbons at three European background sites. Env. Sci. Technol. **39**, 2976–2982.

Margesin, R., Schinner, F., 2001. Biodegradation and bioremediation of hydrocarbons in extreme environments. Appl. Microbiol. Biotechnol. **59**, 650–663.

Masih, J., Masih, A., Kulshrestha, A., Singhvi, R., Taneja, A., 2010. Characteristics of polycyclic aromatic hydrocarbons in indoor and outdoor atmosphere in the North central part of India. J. Hazard. Mater. **177**, 190–198. doi:10.1016/j.jhazmat.2009.12.017

McDowell, W.., 2003. Dissolved organic matter in soils—future directions and unanswered questions. Geoderma **113**, 179–186.

Means, J.C., Wood, S.G., Hassett, J.J., Banwart, W.L., 1980. Sorption of polynuclear aromatic hydrocarbons by sediments and soils. Env. Sci. Technol **14**, 1524–1528.

Miller, M.M., Wasik, S.P., Huang, G.L., Shiu, W.Y., Mackay, D., 1985. Relationships between octanol-water partition coefficient and aqueous solubility. Environ. Sci. Technol **19**, 522–529. doi:10.1021/es00136a007

Motelay-Massei, A., Ollivon, D., Garban, B., Tiphagne-Larcher, K., Chevreuil, M., 2007. Fluxes of polycyclic aromatic hydrocarbons in the Seine estuary , France : mass balance and role of atmospheric deposition. Hydrobiologia **588**, 145–157. doi:10.1007/s10750-007-0659-9

Mueller, J.G., Lantz, S.E., Blattmann, B.O., Chapman, P.J., 1991. Bench-scale evaluation of alternative biological treatment process for the remediation of pentachlorophenol and creosote contami- nated materials: solid phase bioremediation. Environ. Sci. Technol. **25**, 1045–1055.

Nam, K., Kim, J.Y., Oh, D.I., 2003. Effect of soil aggregation on the biodegradation of phenanthrene aged in soil. Environ. Pollut. **121**, 147–51.

Neilson, A.N., 1998. PAHs and Related Compounds. Springer-Verlag Berlin Heidelberg. doi:10.1007/978-3-540-49697-7

Nguyen, T.H., Goss, K.-U., Ball, W.P., 2005. Polyparameter linear free energy relationships for estimating the equilibrium partition of organic compounds between water and the natural organic matter in soils and sediments. Environ. Sci. Technol. **39**, 913–924. doi:10.1021/es048839s

Nierop, K.G., Jansen, B., Verstraten, J.M., 2002. Dissolved organic matter, aluminium and iron interactions: precipitation induced by metal/carbon ratio, pH and competition. Sci. Total Environ. **300**, 201–2011.

Nowak, K.M., Girardi, C., Miltner, A., Gehre, M., Schäffer, A., Kästner, M., 2013. Contribution of microorganisms to non-extractable residue formation during biodegradation of ibuprofen in soil. Sci. Total Environ. **445–446**, 377–384. doi:10.1016/j.scitotenv.2012.12.011

Ophoff, H., Stork, A., Veerkamp, W., Fuhr, F., 1996. Volatilization and mineralization of [3-C-14]fluoranthene after: Soil incorporation and soil surface application. Int. J. Environ. Anal. Chem. **64**, 97–109. doi:10.1080/03067319608028339

Ouvrard, S., Leglize, P., Morel, J.L., 2014. PAH phytoremediation : rhizodegradation orrhizoattenuation ? Int. J. Phytoremediation 16, **37–41**. doi:10.1080/15226514.2012.759527

Pomiès, M., Choubert, J.-M., Wisniewski, C., Coquery, M., 2013. Modelling of micropollutant removal in biological wastewater treatments: A review. Sci. Total Environ. **443**, 733–748. doi:10.1016/j.scitotenv.2012.11.037

Pritchina, O., Ely, C., Smets, B.F., 2011. Effects of PAH-contaminated soil on rhizosphere microbial communities. Water Environ. J. **222**, 17–25. doi:10.1007/s11270-011-0800-2

Puglisi, E., Cappa, F., Fragoulis, G., Trevisan, M., Del, A.A.M., 2007. Bioavailability and degradation of phenanthrene in compost amended soils. Chemosphere. **67**, 548–556. doi:10.1016/j.chemosphere.2006.09.058

Rav-Acha, C., Rebhun, M., 1992. Binding of organic solutes to dissolved humic substances and its effects on adsorption and transport in the aquatic environment. Water Res. **26**, 1645–1654.

Rebhun, M., Kalabo, R., Grossman, L., Manka J., Rav-Acha, C., 1992. Sorption of organics on clay and synthetic humic-clay complexes simulating aquifer processes. Wat. Res. **26**, 79-84.

Recous, S., 1995. Soil inorganic N availability: effect on maize residue decomposition. Soil Biol. Biochem. **27**, 1529–1538.

Rein, A., Adam, I.K.U., Miltner, A., Brumme, K., Kästner, M., Trapp, S., 2016. Impact of bacterial activity on turnover of insoluble hydrophobic substrates (phenanthrene and pyrene)— Model simulations for prediction of bioremediation success. J. Hazard. Mater. **306**, 105–114. doi:10.1016/j.jhazmat.2015.12.005

Richnow, H.H., Annweiler, E., Koning, M., Lüth, J.C., Stegmann, R., Garms, C., Francke, W., Michaelis, W., 2000. Tracing the transformation of labelled [1-13C]phenanthrene in a soil bioreactor. Environ. Pollut. **108**, 91–101. doi:10.1016/S0269-7491(99)00205-5

Roberts, T.R., 1984. Non-extractable pesticide residues in soils and plants. Pure Appl. Chem. **56**, 945–956.

Rosso, L., Lobry, J.R., Flandrois, J.P., 1993. An unexpected correlation between cardinal temperatures of microbial growth highlighted by a new model. J. Theor. Biol. **162**, 447–463.

Sabbah, I., Rebhun, M., Gerstl, Z., 2004. An independent prediction of the effect of dissolved organic matter on the transport of polycyclic aromatic hydrocarbons. J. Contam. Hydrol. **75**, 55–70. doi:10.1016/j.jconhyd.2004.04.003

Saffih-Hdadi, K., Bruckler, L., Barriuso, E., 1997. Modeling of sorption and biodegradation of parathion and its metabolite paraoxon in soil. J. Environ. Qual. **32**, 2207–2215. doi:10.2134/jeq2003.2207

Semple, K., Doick, K., Jones, K., Burauel, P., Craven, A., Harms., H., 2004. Defining bioavailability and bioaccessibility of contaminated soil and sediment is complicated. Env. Sci. Technol. **35**, 228A–231A.

Semple, K.T., Morriss, A.W.J., Paron, G.I., 2003. Bioavailability of hydrophobic organic contaminants in soils: fundamental concepts and techniques for analysis. Eur. J. Soil Sci. **54**, 809–818. doi: 10.1046/j.1351-0754.2003.0564.x

Seo, J.-S., Keum, Y.-S., Harada, R.M., Li, Q.X., 2007. Isolation and characterization of bacteria capable of degrading polycyclic aromatic hydrocarbons (PAHs) and organophosphorus pesticides from PAH-contaminated soil in Hilo, Hawaii. J. Agric. Food Chem **55**, 5383–5389. doi:10.1021/jf0637630

Sharma, H., V.K.J., Khan, Z.H., 2007. Characterization and source identification of polycyclic aromatic hydrocarbons (PAHs) in the urban environment of Delhi. Chemosphere **66 (2)**, 302–310.

Shian Chee. Wu, Gschwend, P.M., 1986. Sorption Kinetics of Hydrophobic Organic Compounds to Natural Sediments and Soils. Env. Sci Technol **20**, 717–725.

Sims, R.C., Dupont, R.R., Doucette, W.J., 1990. Fate of PAH compounds in two soil types : influence of volatilization, abiotic loss, and biological activity. Environ. Toxicol. Chem. **9**, 187–195.

Soclo, H.., Garrigues, P., Ewald, M., 2000. Origin of Polycyclic Aromatic Hydrocarbons (PAHs) in coastal marine sediments: case studies in Cotonou (Benin) and Aquitaine (France) areas. Mar. Pollut. Bull. **40**, 387–396.

Stehr, J., Muller, T., Svensson, K., Kamnerdpetch, C., Scheper, T., 2001. Basic examination on chemical preoxydation by ozone for enhancing bioremediation of phenanthrene contaminated soils. appl Microbiol. Biotechnol. **57**, 803–809.

Stombaugh, D.P., Nokes, S.E., 1996. Development of a biologically based aerobic composting simulation model. Trans. ASAE. **39**, 239–250.

Straube, W.L., Nestler, C.C., Hansen, L.D., Ringleberg, D., Pritchard, P.H., Jones-Meehan, J., 2003. Remediation of polyaromatic hydrocarbons (PAHs) through landfarming with biostimulation and bioaugmentation. Acta Biotechnol J. **23**, 179–196.

Thiele-Bruhn, S., Brümmer, G.W., 2005. Kinetics of polycyclic aromatic hydrocarbon (PAH) degradation in long-term polluted soils during bioremediation. Plant Soil **275**, 31–42. doi:10.1007/s11104-004-0265-9

Thorsen, W.A., Cope, W.G., Shea, D., 2004. Bioavailability of PAHs: effects of soot carbon and PAH source. Environ. Sci. Technol. **38**, 2029–2037.

Toro, D.M. DI., McGrath, J.A., Hansen, D.J., 2000. Technical basis for narcotic chemicals and polycyclic aromatic hydrocarbon criteria. I . Water and tissue. Environ. Toxicol. Chem. **19**, 1951–1970.

Vane, C.H., Kim, A.W., Beriro, D.J., Cave, M.R., Knights, K., Moss-hayes, V., Nathanail, P.C., 2014. Applied Geochemistry Polycyclic aromatic hydrocarbons (PAH) and polychlorinated biphenyls (PCB) in urban soils of Greater London, UK. Appl. Geochemistry **51**, 303–314.doi:10.1016/j.apgeochem.2014.09.013

Vane, C.H., Kim, A.W., Beriro, D.J., Cave, M.R., Knights, K., Moss-hayes, V., Nathanail, P.C., 2014. Applied Geochemistry Polycyclic aromatic hydrocarbons (PAH) and polychlorinated biphenyls (PCB) in urban soils of Greater London , UK. Appl. Geochemistry **51**, 303–314. doi:10.1016/j.apgeochem.2014.09.013

Verge-Leviel, C., 2001. Les micropolluants organiques dans les composts d'origine urbaine: étude de leur devenir au cours du compostage et biodisponibilité des résidus après épandage des composts au sol (Thèse de doctorat, Institut National Agronomique Paris Grignon, FRA).

Vrugt, J.A., 2016. Markov chain Monte Carlo simulation using the DREAM software package : Theory , concepts , and MATLAB implementation. Environ. Model. Softw. **75**, 273–316. doi:10.1016/j.envsoft.2015.08.013

Walter, T., Ederer, H.., Först, C., Stieglitz, L., 2000. Sorption of selected polycyclic aromatic hydrocarbons on soils in oil-contaminated systems. Chemosphere **41**, 387–397.

Weissenfels, W.D., Klewer, H.-J., Langhoff, J., 1992. Adsorption of polycyclic aromatic hydrocarbons (PAHs) by soil particles: influence on biodegradability and biotoxicity. Environ. Biotechnol. **36**, 689–696.

White, J.C., Pignatello, J.J., 1999. Influence of bisolute competition on the desorption kinetics of polycyclic aromatic hydrocarbons in soil. Env. Sci Technol **33**, 4292–4298.

Wick, L.Y., Colangelo, T., Harms, H., 2001. Kinetics of mass transfer-limited bacterial growth on solid PAHs. Environ. Sci. Technol. **35**, 354–61.

Wilcke, W., 2000. SYNOPSIS Polycyclic aromatic hydrocarbons (PAHs) in soil — a Review. J. Plant Nutr. Soil Sci. **163**, 229–248. doi:10.1002/15222624(200006)163:3<229::AID-JPLN229>3.0.CO;2-6

Wild, S.R., Berrow, M.L., McGrath, S.P., Jones, K.C., 1992. Polynuclear aromatic hydrocarbons in crops from long-term field experiments amended with sewage sludge. Environ. Pollut. **76**, 25–32.

Wild, S.R., Obbard, J.P., Munn, C.I., Berrow, M.L., Jones, K.C., 1991. The long-term persistence of polynuclear aromatic hydrocarbons (PAHs) in an agricultural soil amended with metal-contaminated sewage sludges. Sci. Total Environ. **101**, 235–253.

Xiu-hong, Y., Garnier, P., Shi-zhong, W., Bergheaud, V., Xiong-fei, H., 2014. PAHs sorption and desorption on soil influenced by pine needle litter-derived dissolved organic matter. Pedosphere **24**, 575–584. doi:10.1016/S1002-0160(14)60043-6

Yuandong, Z., Shirong, L., Jiangming, M., 2006. Water-holding capacity of ground covers and soils in alpine and sub-alpine shrubs in western Sichuan, China. Acta Ecol. Sin. **26**, 2775–2782.

Zarfl, C., Klasmeier, J., Matthies, M., 2009. A conceptual model describing the fate of sulfadiazine and its metabolites observed in manure-amended soils. Chemosphere **77**, 720–726. doi:10.1016/j.chemosphere.2009.08.035

Zsolnay, A., Baigar, E., Jimenez, M., Steinweg, B., Saccomandi, F., 1999. Differentiating with fluorescence spectroscopy the sources of dissolved organic matter in soils subjected to drying. Chemosphere **38**, 45–50.

PARTIE I. SIMULATIONS A L'ECHELLE DU LABORATOIRE

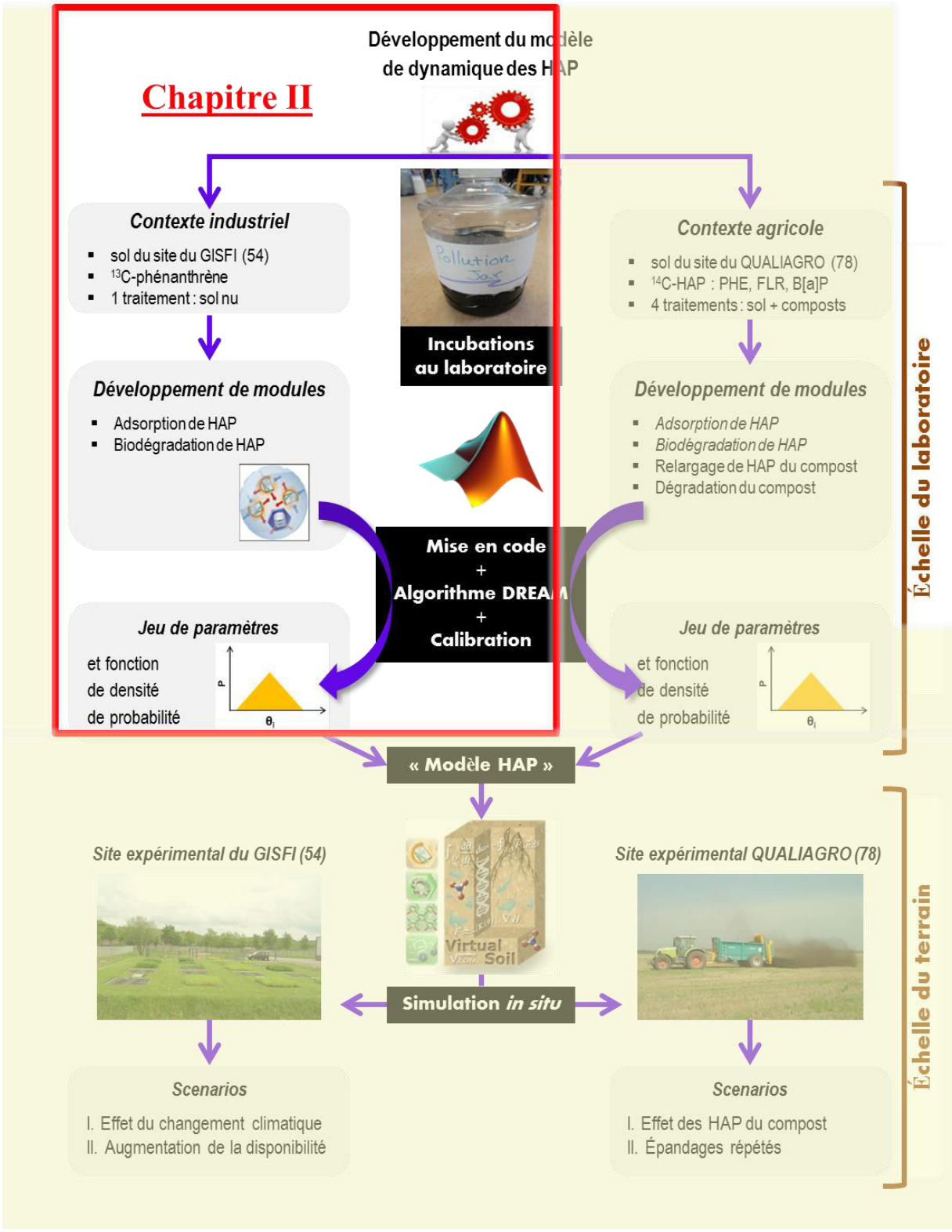

Place du chapitre II dans l'ensemble du travail de thèse

Chapitre II. Paramétrage et validation du modèle de dynamique des HAP sur un sol anciennement contaminé à l'échelle du laboratoire

Résumé du contenu du chapitre en français

Ce chapitre présente les deux modules du modèle de dynamique des HAP proposés pour simuler les processus de biodégradation et d'adsorption dans le sol. Les modules sont basés sur les hypothèses suivantes: i) la fraction soluble de HAP est la seule qui peut être métabolisée par l'activité microbienne du sol ; ii) la minéralisation des HAP se fait suivant deux voies de biodégradation : la voie co-métabolique utilisant une cinétique du pseudo premier ordre et la voie de biodégradation spécifique modélisée par une cinétique de Monod ; iii) la formation de résidus liés biogéniques est obtenue soit par la mort de la biomasse microbienne spécifique ou par la sorption irréversible de métabolites issus de la voie de biodégradation co-métabolique ; et iv) les HAP peuvent s'adsorber sur deux compartiments définis respectivement par des cinétiques d'adsorption rapides et lentes. Le premier compartiment correspond à la fraction de HAP adsorbés sur les sites facilement accessibles de la phase solide du sol et se caractérise donc par une faible stabilité dans le sol. Le second compartiment correspond à la fraction de HAP qui diffuse lentement dans la porosité ou dans les matières organiques du sol et se caractérise donc par une forte stabilité dans le sol. Des données expérimentales issues d'incubations de phénanthrène marqué au ^{13}C ajouté dans un sol industriel (cokerie de Neuves-Maisons, 54) pré-contaminé par des HAP ont été utilisées pour calibrer les paramètres du modèle. Le module HAP a été développé sous MatLab et associé à une procédure d'optimisation de paramètres par approche Bayésienne (DREAM). Cette démarche a permis d'estimer les fonctions de densité de probabilité des paramètres du modèle. Cela a également conduit à des simplifications importantes dans la structure du modèle. Les résultats de la calibration ont également mis en évidence que la voie

de biodégradation spécifique était la plus efficace pour expliquer les données expérimentales, comme on pouvait s'y attendre pour un sol industriel anciennement contaminé. L'analyse globale de la sensibilité a montré que la quantité de HAP finalement dégradée était principalement régie par des interactions physico-chimiques plutôt que par une activité biologique. Les résultats ont conduit à la rédaction d'un article publié qui fait l'objet du présent chapitre : Brimo K., Garnier P., Sun S., Bertrand-Krajewski J.-L., Cébron A., Ouvrard S. 2016. Using a Bayesian approach to improve and calibrate a dynamic model of polycyclic aromatic hydrocarbons degradation in an industrial contaminated soil. *Environmental Pollution* 215, 27-37. doi : 10.1016/j.envpol.2016.04.094

Using a Bayesian approach to improve and calibrate a dynamic model of polycyclic aromatic hydrocarbons degradation in an industrial contaminated soil

Khaled Brimo[a,b,c,d], Patricia Garnier[a], Siao Sun[e], Jean-Luc Bertrand-Krajewski[e], Aurélie Cébron[f,g], Stéphanie Ouvrard[b,c]

[a]INRA, EcoSys, UMR1405, Université Paris-Saclay, 78850, Thiverval-Grignon, France

[b]INRA, Laboratoire Sols et Environnement, UMR 1120, F-54518 Vandoeuvre-lès-Nancy, France

[c]Université de Lorraine, Laboratoire Sols et Environnement, UMR 1120, F-54518 Vandoeuvre-lès-Nancy, France

[d]Agence de l'Environnement et de la Maîtrise de l'Energie, 20 avenue du Grésillé, BP 90406, F-49004 Angers Cedex 01, France

[e]Université de Lyon, INSA Lyon, DEEP, F-69621 Villeurbanne Cedex, France

[f]CNRS, LIEC, UMR 7360, Faculté des Sciences et Technologies, BP 70239, F-54506 Vandoeuvre-lès-Nancy Cedex, France

[g]Université de Lorraine, LIEC, UMR 7360, Faculté des Sciences et Technologies, BP 70239, F-54506 Vandoeuvre-lès-Nancy Cedex, France

*Corresponding authors: Stéphanie Ouvrard

Tel: + 33 383 595 762

E-mail: stephanie.ouvrard@univ-lorraine.fr

Fax: +33 383 595 791

Article published in journal of Environmental Pollution (2016)

1. Abstract

A novel kinetics model that describes the dynamics of polycyclic aromatic hydrocarbons (PAHs) in contaminated soils is presented. The model includes two typical biodegradation pathways: the co-metabolic pathway using pseudo first order kinetics and the specific biodegradation pathways modeled using the Monod kinetic. The sorption of PAHs to the solid soil occurs through bi-phasic fist order kinetics, and two types of non-extractible bound residues are considered: the biogenic and the physically sequestered into soil matrix. The PAH model was developed in Matlab, parameterized and tested successfully on batch experimental data using a Bayesian approach (DREAM). Preliminary results led to significant model simplifications. They also highlighted that the specific biodegradation pathway was the most efficient at explaining experimental data, as would be expected for an old industrial contaminated soil. Global analysis of sensitivity showed that the amount of PAHs ultimately degraded was mostly governed by physicochemical interactions rather than by biological activity.

Keywords: DREAM, PAH reactivity, biodegradation pathways, global sensitivity analysis

Highlights

- A new dynamic model for PAHs in soil is presented.
- The probability density functions of model parameters have been determined.
- PAHs mineralization was predicted using the specific biodegradation pathway alone.
- The long-term fate of PAHs is controlled by physicochemical interactions.

2. Introduction

The wide exploitation and use of fossil energy and its by-products have caused the dispersion of original and transformed fossil organic compounds in the environment. These pollutants accumulate in soils causing acute or more diffuse contamination. Among them, polycyclic aromatic hydrocarbons (PAHs) pose a serious threat to the human health and the environment owing to their carcinogenicity, bioaccumulation and persistence (Iarc, 2010). Their general behavior and impact on all environmental compartments, *e.g.* transfer from soil to water resources or into the food chain, need to be addressed in the general context of contaminated soil risk assessment and safe land-reuse. Thus, models predicting the dissipation rate of PAHs over a wide range of environmental conditions with sufficient accuracy are necessary for environmental risk assessment and decision support.

Models dedicated to the description and prediction of organic pollutants behavior in soils remain scarce. Most existing tools have been developed and applied for pesticides in the context of cultivated lands (Beulke et al., 2000; Köhne et al., 2009). Only very few models deal with other organic pollutants such as PAHs (Geng et al., 2015) or pharmaceutical products (Moenickes et al., 2011; Zarfl et al., 2009). These models display a great variety of assumptions and mathematical formalisms and for most of them they have not been validated or tested in the field (except those developed for pesticides).

We develop a new modeling tool to predict the general behavior of PAHs in soil that might be applicable in a wide range of situations from agricultural land, with low concentration values, to highly contaminated soils from industrial sites. To achieve this goal, a specific module describing PAHs reactivity in soil systems including physical and biological processes has been developed and calibrated with laboratory data corresponding to extreme situations of contamination.

First, we propose a new dynamic model accounting for the different biological and chemical processes governing general PAHs behavior in contaminated soils. The model is then calibrated using previously published data from a laboratory incubation experiment, with a global optimization algorithm called DREAM based on the Bayesian approach. This method helps identifying the controlling processes governing PAHs behavior under several hypotheses of degradation pathways of PAHs. Finally we present a sensitivity analysis of model parameters that strengthen the ranking of controlling processes.

3. Modeling

3.1. Model description and assumptions

3.1.1. PAHs reactivity in soils

PAHs dissipation in soil is mostly driven by two processes: adsorption and biodegradation (White et al., 1999; Wilcke, 2000). When PAHs enter the soil, they rapidly sorb on minerals and organic matters in soil aggregates. Due to their hydrophobicity and strong interaction with soil organic matters, only a minor part moves into soil solution where PAHs can associate to colloids or remain. The fixed fraction can diffuse into small pores where it remains being scarcely accessible for microorganisms, forming what is called physical non-extractible residues (NER). Kinetics of adsorption and desorption of pollutant depends on different many factors such as soil properties (e.g. texture, structure, organic matter content) (Chung and Alexander, 2002; Nam et al., 2003), pollutant hydrophobicity, initial loading level (Johnson et al., 2001; Pignatello, 1990), climate (Dagois et al., 2015) and the biological activity (Gevao et al., 2005). Moreover, results from both lab-scale and field experiments show that the potential rate of desorption decreases with increasing contact time. This phenomenon also referred to "aging" actually encompasses multiple processes including the diffusion and sorption of PAHs into the soil organic and inorganic fractions. It highlights the fact that (bio)availability decreases with increasing contact time (Hatzinger and Alexander, 1995; White et al., 1999).

The biodegradation of PAHs occurs through two main pathways corresponding to two different biological strategies for microorganisms. The adapted microorganisms use the target compound as the sole carbon and energy sources; they are referred as specific biomass (B_{SPE}). The non-growing microorganisms rely on another substrate for their growth and maintenance; they are referred to as co-metabolic biomass (Janke and Fritsche, 1985; Pomiès et al., 2013). Recent works have highlighted the importance of microbial activity in increasing the amount of NER of PAHs in soil, suggesting the need of distinguishing between NER by physical processes (aging), and the biogenic NER resulting from microorganisms transformation of pollutants and further incorporation in soil organic matters (SOM) (Barriuso et al., 2008; Kästner et al., 2014; Richnow et al., 2000).

In such a soil ecosystem, plants only represent a minor sink term but their indirect effect may however have a significant impact through water uptake, microbial activity enhancement and fresh carbon input.

3.1.2. Model modules

The different processes described in the previous section were modeled using 2 submodules: the sorption module and the biodegradation module (Figure II.1). The model equations including kinetics and stoichiometry for PAHs transformations are presented in the form of a Petersen matrix in Table II.1, whereby the rate equations are read both down and across (Russell, 2006). The model includes 7 compartments and 12 parameters. For all compartments the concentration unit is $mg^{13}C/kg_{ds}$, where the subscript "ds" refers to dry soil.
The PAHs adsorption mechanism is described by a bi-phasic first order kinetics module, which was commonly used in the literature (Johnson et al., 2001). We thus assume that the adsorption occurs in two compartments with two adsorption rates: the first one is characterized by a fast rate and weak stability (PAH_{WS}, where "ws" stands for weak sorption) (Processes I and II) followed by a second one characterized by a slower reactivity exchange but strong stability (PAH_{SS}, where "ss" stands for strong sorption) (Processes III and IV). Based on these assumptions, the formation of PAH_{SS} directly via the aqueous fraction is neglected.
The biodegradation module is built on the basis of four assumptions. Compounds in the aqueous phase (PAH_{AV}, where "av" stands for available) are the only substrates available for microbial biomass (Ogram et al., 1985; Thomas et al., 1986; Wodzinski and Coyle, 1974). The available fraction may contain both free dissolved PAHs and those complexed with colloids. Having no information about different compound speciation in solution we decided to merge two forms in a common compartment assuming that microorganisms use them at the same rate (Delgadillo-Mirquez et al., 2011; Laor et al., 1996).

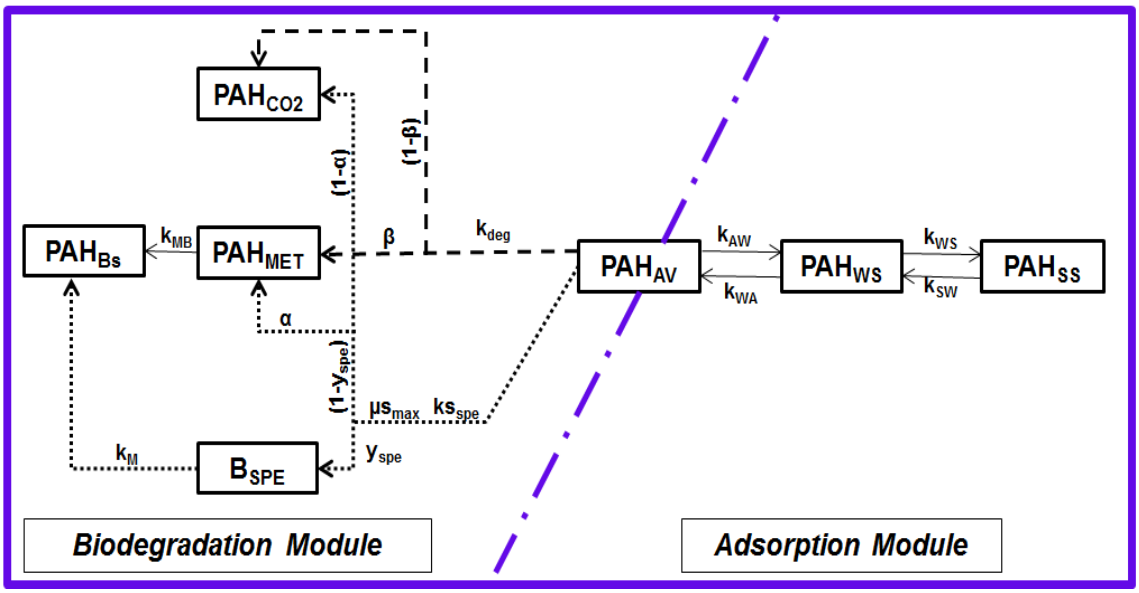

Figure II.1. Structure of the PAHs model. Cometabolism pathway is plotted by dashed lines whereas the pathway driven by specific biomass is marked by points, with k_{ij}: first order kinetic constant with the first subscript denoting the source and the second the sink of the corresponding process (A: PAH_{AV}; B: PAH_{Bs}; M: PAH_{MET} S: PAH_{SS} and W: PAH_{WS}) (d^{-1}); μs_{max}: maximum specific growth rate (d^{-1}); ks_{spe}: half saturation of growth substrate for the specific biomass ($mg^{13}C/kg_{ds}$); Y_{spe}: yield of specific biomass (-); k_M: mortality rate constant (d^{-1}); α: magnitude of metabolites production by biodegradation for specific biomass (between 0 and 1); k_{deg}: pseudo first order kinetic constant of biodegradation for co-metabolism (d^{-1}); β: magnitude of metabolites production by biodegradation for co-metabolism (between 0 and 1)

Table II.1. PAHs model equations described by Petersen matrix (Russell, 2006)*

Process \ Variable			PAH_{AV}	PAH_{CO2}	PAH_{MET}	PAH_{WS}	PAH_{SS}	PAH_{Bs}	B_{SPE}	Rate ($mg\ ^{13}C/kg_{ds}/d$)
I	Weak sorption	sorption	-1			1				$k_{AW}.PAH_{AV}$
II		desorption	1			-1				$k_{WA}.PAH_{AV}$
III	Strong sorption	sorption				-1	1			$k_{WS}.PAH_{SS}$
IV		desorption				1	-1			$k_{SW}.PAH_{SS}$
V	Substrate uptake by co-metabolism		-1	(1-β)	β					$k_{deg}.PAH_{AV}.f_T.f_W$
VI	Growth of specific biomass		$\frac{-1}{Y_{spe}}$	$(1-\alpha).\frac{(1-Y_{spe})}{Y_{spe}}$	$\alpha.\frac{(1-Y_{spe})}{Y_{spe}}$				1	$\frac{\mu s_{max}.PAH_{AV}}{ks_{spe}+PAH_{AV}}.B_{SPE}.f_T.f_W$
VII	Biogenic production	Metabolites transformation			-1			1		$k_{MB}.PAH_{MET}$
VIII		Specific biomass mortality						1	-1	$k_m.B_{SPE}$
			PAHs available $mg\ ^{13}C/kg_{ds}$	PAHs mineralized into CO_2 $mg\ ^{13}C/kg_{ds}$	Metabolites $mg\ ^{13}C/kg_{ds}$	Weakly sorbed $mg\ ^{13}C/kg_{ds}$	Strongly sorbed $mg\ ^{13}C/kg_{ds}$	Biogenic residues $mg\ ^{13}C/kg_{ds}$	Specific biomass $mg\ ^{13}C/kg_{ds}$	

* $\mathbf{f_T}$: Temperature dependence factor(-); $\mathbf{f_W}$: water content dependence factor (-); additional notations are defined in Figure II.1.

Biodegradation occurs according to two pathways. The first one is driven by the specific biomass (B_{SPE}) whose growth and maintenance is described by the Monod equation (Monod, 1949; Wick et al., 2001) (Process VI, plotted in dotted line Figure II.1). The second pathway is the biodegradation by the co-metabolic microorganisms (plotted in dashed line Figure II.1). We chose herein to exclude modeling the growth of co-metabolic microorganisms because they have different and more complex growth and maintenance rates than B_{SPE}. Instead, the biodegradation rate is calculated using the pseudo first order kinetic formalism whereby the available substrate (PAH_{AV}) is the only rate limiting factor for PAHs biodegradation in soil (Govind et al., 1991) (Process V) (i.e. the amount of co-metabolic microorganisms is not a limiting factor.

The metabolism of substrate by microorganisms by the two aforementioned pathways leads to mixed products of metabolites and biological wastes, in addition to CO_2 production (PAH_{CO2}). For simplifications, all biological products are later described by one model compartment and referred to as "metabolites" (PAH_{MET}).

According to Kästner et al.(2014), biogenic NER are obtained by incorporating dead microbial cells in SOM, whereas the metabolites resulting from co-metabolic degradation lead to the formation of physical NER. To avoid confusion, we defined PAH_{Bs} (where "Bs" stands for biogenics) corresponding to biogenic NER that include both dead specific biomass (Process VIII) and irreversible PAH_{MET} in soil (Process VII).

Soil biodegradation rates are related to temperature and water content using the correction factors f_T, f_W following equations proposed by Recous (1995) and Andrén et al. (1992) respectively:

$$f_T = e^{0.085(T - T_{ref})} \qquad \text{(II.1)}$$

Where T is the actual soil temperature in °C and T_{ref} is the reference temperature (15 °C).

$$f_w = \frac{\log(\quad) - \log(\quad_{min})}{\log(\quad_{opt}) - \log(\quad_{min})} \qquad \text{(II.2)}$$

Where Φ is the water potential in cm H_2O, Φ_{min} is the minimum water potential (-75800 cm H_2O) at which the microbial activity ceases and Φ_{opt} is the optimum water potential (100 cm H_2O).

3.2. Experimental data

Data used for model calibration were taken from the experimental study of Cébron et al. (2011). It was an incubation experiment of freshly added fully ^{13}C labeled phenanthrene (PHE) in an aged PAH contaminated soil from a former coking plant site.

All incubation experiments were performed in triplicates at a controlled temperature of 24 °C. The moisture level of homogenized soil samples was adjusted to 80% of the soil water holding capacity. The concentration of ^{13}C-PHE spiked in soil was 250 $mg^{13}C/kg_{ds}$. The distribution of ^{13}C-PHE among the extractible, non-extractible and the mineralized fractions was assessed on days 0, 4, 8 and 12. Mass balances of the total ^{13}C recovery were within 80-106% of the initial ^{13}C-PHE added to the soil. We therefore applied a weight on the three aforementioned fractions at each time step to reach 100% recovery.

The amount of ^{13}C recovered by dichloromethane (DCM) using accelerated solvent extraction was considered as the extractible fraction, including the labelled phenanthrene present in soil/solution interface as well as its metabolites. No significant ^{13}C-labelled intermediate compounds were found in this DCM extract, we therefore considered the metabolites concentration (PAH_{MET}) to be zero. The amount of soluble ^{13}C-PHE (PAH_{AV} in the model) was calculated from the total ^{13}C-PHE in DCM extracts considering that the total ^{13}C-PHE recovered by DCM was sorbed on soil (*i.e.* neglecting contribution of soluble PHE, being 1/1000 to 1/960 of the total) using the sorption distribution coefficient K_d (L/kg_{ds}) as follows:

$$K_d = \frac{\text{sorbed labelled phenanthrene revovered by DCM } (mg\,^{13}C / kg_{ds})}{PAH_{AV}} \quad \text{(II.3)}$$

The K_d value was obtained using:

$$K_d = K_{OC} f_{OC} \quad \text{(II.4)}$$

Where f_{oc} is the organic carbon content in soil (here 63 g C kg_{ds}^{-1}) and K_{oc} is the sorption distribution coefficient normalized to f_{oc}, which can be calculated using the correlation taken from Nguyen et al. (2005):

$$\log K_{OC} = 1.14 \log K_{ow} \quad 1.02 \quad \text{(II.5)}$$

Where K_{ow} is the octanol-water partition coefficient equal to 4.57 for phenanthrene (Mackay et al., 2006).

The amount of ^{13}C remaining in the soil after DCM extraction was considered as the NER, from both physical and biogenic origins. This fraction, PAHNER, corresponded to the three model compartments pooled together: PAHSS, PAHBS and BSPE. Indeed, due to its polarity the specific microbial biomass B_{SPE} was supposed to remain in the soil after DCM extraction and to contribute to the NER. The concentrations of B_{SPE} on days 4, 8 and 12 were estimated from the measured bacterial population densities assimilating carbon derived from ^{13}C labeled phenanthrene using the hypothesis that a microbial cell is equivalent to 10^{10} carbon atoms (Troussellier et al., 1997).

Finally, the mineralized fraction was estimated from the difference between CO_2 released in incubations with and without labelled phenanthrene addition, and was considered corresponding to PAH_{CO2} values.

3.3. Procedure for parameters estimation

3.3.1. Numerical solution and optimization method

The model differential equations were solved numerically within a MATLAB code using Crank Nicolson finite different scheme with a varying time step to assure the computational stability (Crank and Nicolson, 1996).

The DREAM (DiffeRential Evolution Adaptive Metropolis) algorithm (Vrugt, 2016; Vrugt et al., 2008) based on the Markov Chain Monte Carlo method applied within Bayesian framework was used for estimating model parameters thanks to the dual advantage: (1) ensuring global optimum in the given searching range, instead of local optimum by a numerical nonlinear regression algorithms (Aster et al., 2013), and (2) determining uncertainty in parameters in the posterior probability density functions (pdfs) shown in equation (II.6) (Sun and Bertrand-Krajewski, 2013):

$$\left(\quad / y, x \right) = \frac{\left(y / \quad , x \right) \quad \left(\quad \right)}{\left(y / x \right)} \quad \text{(II.6)}$$

Where x and y are the observed values of model inputs and outputs, $\rho(\theta)$ is the probability density of prior distribution of parameters, $\rho(y/\theta, x)$ is the likelihood function returning the probability density for model results for given values of parameters and inputs, and $\rho(y/x)$ is the marginal likelihood.

For this work, the matrix of input variables (x) was composed of the 4 compartments: PAH_{WS}, B_{spe}, PAH_{NER} and PAH_{CO2} measured on days 0, 4, 8 and 12. The model outputs matrix (y) was the corresponding values computed numerically by daily time step. Hence, the DREAM software written in MATLAB (Vrugt et al., 2008) was used to fit our model. The prior

distribution of each parameter was assigned to follow a uniform distribution reflecting the limited prior information about parameters values. A maximum number of 200,000 model evolutions (based on an error-and-trial approach) was set. The likelihood function was chosen to have the form an exponential power density function as described by Box and Tiao (1992). After DREAM terminated, the last 50% of the evaluated parameter samples from all the chains were selected to generate histograms of probability density functions of the evaluated model parameters.

3.3.2. Setting up

The searching ranges of model parameters are listed in Table II.2. They were chosen based on available literature studies (Delgadillo-Mirquez et al., 2011; Fragoulis et al., 2005; Geng et al., 2015; Johnson et al., 2001; Köhler et al., 1994; Tao et al., 2007; Weissenfels et al., 1990; Wick et al., 2001) and further adjusted using a stepwise trial and error strategy. The model was run with the initial conditions observed a few minutes after the beginning of the experiment: PAH_{CO2}, PAH_{Bs}, PAH_{SS} and PAH_{MET} were null; all ^{13}C-PHE in soil was PAH_{WS} and PAH_{AV} as described in section 3.2. The initial specific biomass concentration was 0.575 mg $^{13}C/kg_{ds}$ calculated from data reported by Cébron et al. (2009).

Table II.2. Prior ranges, optimal values and confidence intervals (CI) for PAHs model parameters as obtained with DREAM by running the model with the two different biodegradation pathways independently.

Parameter	Unit	Range	Calibarated parameters			
			Biodegradation via specific biomass		Biodegradation via co-metabolism	
			Optimum	95% CI	Optimum	95% CI
k_{AW}*	d^{-1}	NA	55.725	[55.39, 56.70]	44.534	[44.18, 44.91]
k_{WA}	d^{-1}	[0, 0.2]	0.0567	[0.058, 0.059]	0.0453	[0.0449, 0.0456]
k_{WS}	d^{-1}	[0, 0.2]	0.0582	[0.058, 0.059]	0.0584	[0.0582, 0.0585]
k_{MB}	d^{-1}	[0, 0.5]	$60\ 10^{-5}$	[$10\ 10^{-5}$, $440\ 10^{-5}$]	$20\ 10^{-5}$	[$3\ 10^{-5}$, $126\ 10^{-5}$]
μs_{max}	d^{-1}	[0, 12]	4.89	[2.99, 9.50]	-	-
ks_{spe}	$mg^{13}C/kg_{ds}$	[001, 0.15]	0.0024	[0.0012, 0.0384]	-	-
Y_{spe}	-	[0.05, 0.3]	0.127	[0.122, 0.131]	-	-
k_M	d^{-1}	NA	NA	NA	-	-
α	-	[0, 1]	0.0121	[0.0015, 0.150]		
k_{deg}	d^{-1}	[0, 200]	-	-	133.05	[128.24, 137.83]
β	-	[0, 1]	-	-	0.016	[0.015, 0.018]

***the parameter k_{AW} was calculated by k_{WA} using equation (II.9).**

3.3.3. Goodness of fit criteria

Both the Nash Sutcliffe index (NS) (Nash and Sutcliffe, 1970) and the Akaike information criterion (AIC) (Burnham and Anderson, 2004) are used to quantitatively evaluate the model performance in reproducing the observations:

$$NS_{i\to m} = 1 - \frac{\sum_{t=1}^{n}\left(y_{obs,t,i} - y_{calc,t,i}\right)^2}{\sum_{t=1}^{n}\left(\bar{y}_{obs,i} - y_{obs,t,i}\right)^2} \qquad \text{(II.7)}$$

$$AIC = nm\ln\left(\frac{\sum_{i=1}^{m}\sum_{t=1}^{n}\left(y_{obs,t,i} - y_{calc,t,i}\right)^2}{nm}\right) + 2p \qquad \text{(II.8)}$$

Where $y_{obs,t,i}$ and $y_{calc,t,i}$ are respectively the observed and predicted values at the t^{th} observed time step for the i^{th} model output, $\bar{y}_{obs,i}$ represents the mean observed value of the i^{th} model output, p is the number of estimated parameters excluding constant parameters, n is the number of measured points, and m is the number of model outputs, as defined in paragraph 3.3.1. The effect of the model outputs PAH_{MET} and PAH_{AV} on the goodness of fit is neglected due to lack of observed data. The best fit is assessed by the closest to one NS value. AIC is used to compare models with different levels of complexity as it includes the number of parameters in addition to the information about the accuracy of the model outputs compared to experimental data. The smallest AIC value indicates the best compromise between model complexity and model accuracy.

4. Model simplifications

Some simplifications were performed on the model structure by eliminating the appearing non-significant processes for our case study. The slow desorption of the phenanthrene from the strongly sorbed compartment (PAH_{SS}) to the weakly one (PAH_{WS}) was considered negligible (*i.e.* k_{SW}=0), meaning that PAH_{SS} corresponded effectively to an irreversibly bound (*i.e.* NER) compartment of phenanthrene. This simplification was consistent with previous studies reporting that the effective time scale required for slow desorption process is in the order of magnitude of months or years (Johnson et al., 2001) instead of a few days as in our case study.

The first model runs using DREAM and all the parameters initially defined but with k_{SW} set to 0 showed that the histogram of the pdfs for the mortality rate constant (k_M) was concentrated to the lower bound around 10^{-5} d^{-1} (results not shown). When this lower bound was relaxed,

the distribution was uniform meaning that this parameter was not sensitive to explain our experimental data. Thus the mortality phase for the specific biomass turnover was negligible during the few days experiment and the k_M value was set to 0. This simplification seems biologically realistic since a 12 days monitoring period might be insufficient for the microbial biomasses to reach their maximum growth, starving and then cellular death.

Independent optimization of k_{WA} and k_{AW} also led to inconsistent results. Correlation matrix between the two parameters showed that they were not linearly linked (linear correlation coefficient, r = 0.04) and that the most likely values for k_{WA} were generally much higher than those of $k_{AW,}$ which is physically unrealistic. Such modeling discrepancies could be attributed to the lack of data on the compound fraction in solution. Thus, we decided to keep k_{AW} as a calibration parameter and to calculate k_{WA} using the K_d value and the dynamic definition of adsorption (Pomiès et al., 2013) giving:

$$K_d = \frac{k_{AW}}{k_{WA}} \quad \text{(II.9)}$$

5. Biodegradation pathways discrimination

The model based on the simplifications described in the previous section was then run using DREAM. However, the model including both pathways of biodegradation at the same time led to ambiguous fits pertaining to the microbial rates. Indeed, experimental data did not give any indication on relative implications of both pathways and it was not possible to define constant or even narrow ranges for most of biodegradation kinetic values, such as μs_{max} and k_{deg} (see Supplementary Information (SI), Figure SI II.1). We thus chose to run the model alternatively with the separate pathways alone (2 scenarios) and to use the results to discriminate between both pathways to identify the most probable or most effective one. From a mathematical point of view, this approach also resulted in a model with less parameters to be calibrated. The scenario 1 driven by co-metabolic biomass led to a model with 5 parameters and the scenario 2 driven by specific biomass led to a model with 7 parameters. Three parameters are used in both scenarios (k_{WA}, k_{WS} and $k_{MB.}$

5.1. Scenario 1: co-metabolic biodegradation pathway

The histograms representing the posterior probability density functions (pdfs) of model parameters against the parameters searching ranges, as well as the correlations among the parameters are presented in Figure II.2a. The parameter searching range and the most likely

parameter estimated value together with the 95% confidence interval for each parameter are all summarized in Table II.2. Results showed that most of the model parameters tended to display a Gaussian distribution with 95% confidence intervals covering only relatively small ranges within the uniform prior distributions. Only k_{MB} seems to be log-normally distributed. Thus experimental data contain sufficient information for model parameter estimation. The relatively small linear correlations between most of the parameters indicate that model parameters are rather independent each other, with the unique exception of the negative correlation between the parameters k_{deg} and k_{WA} (r = -0.775), which could be described by the following empirical formula:

$$k_{\deg} = 587.18 \quad 10024 k_{WA} \quad \text{(with } R^2=0.78\text{)} \quad \text{(II.10)}$$

This correlation illustrates the close link interconnection between adsorption and biodegradation processes on the fate of the target compound. It also shows that k_{WA} with tolerance error might be used to calculate k_{deg} and thus Equation II.10 can be used to further reduce the number of model parameters necessary to describe the observations. Moreover, this result reveals that k_{WA} is a key parameter within scenario 1 being correlated to both k_{deg} (Equation II.10) and k_{AW} (Equation II.9). This raises the question of whether these three parameters actually represent an invariant mechanism of the underlying physiochemical and biological processes, or whether they correlate due to structural defaults in the model proposed within this scenario.

Using calibration results in Table II.2, predicted model outputs along with their 95% confidence intervals were calculated and are presented in Figure II.3. These curves were obtained by stochastic simulation through running the model in the direct way using the 95% confidence intervals previously estimated fir the five calibrated parameters. At the simulation starting time, the uncertainty in the measured PAH_{WS} was assumed to apply to a uniform distribution and the no uncertainty was considered for other model compartments with the values given in section 3.3.2

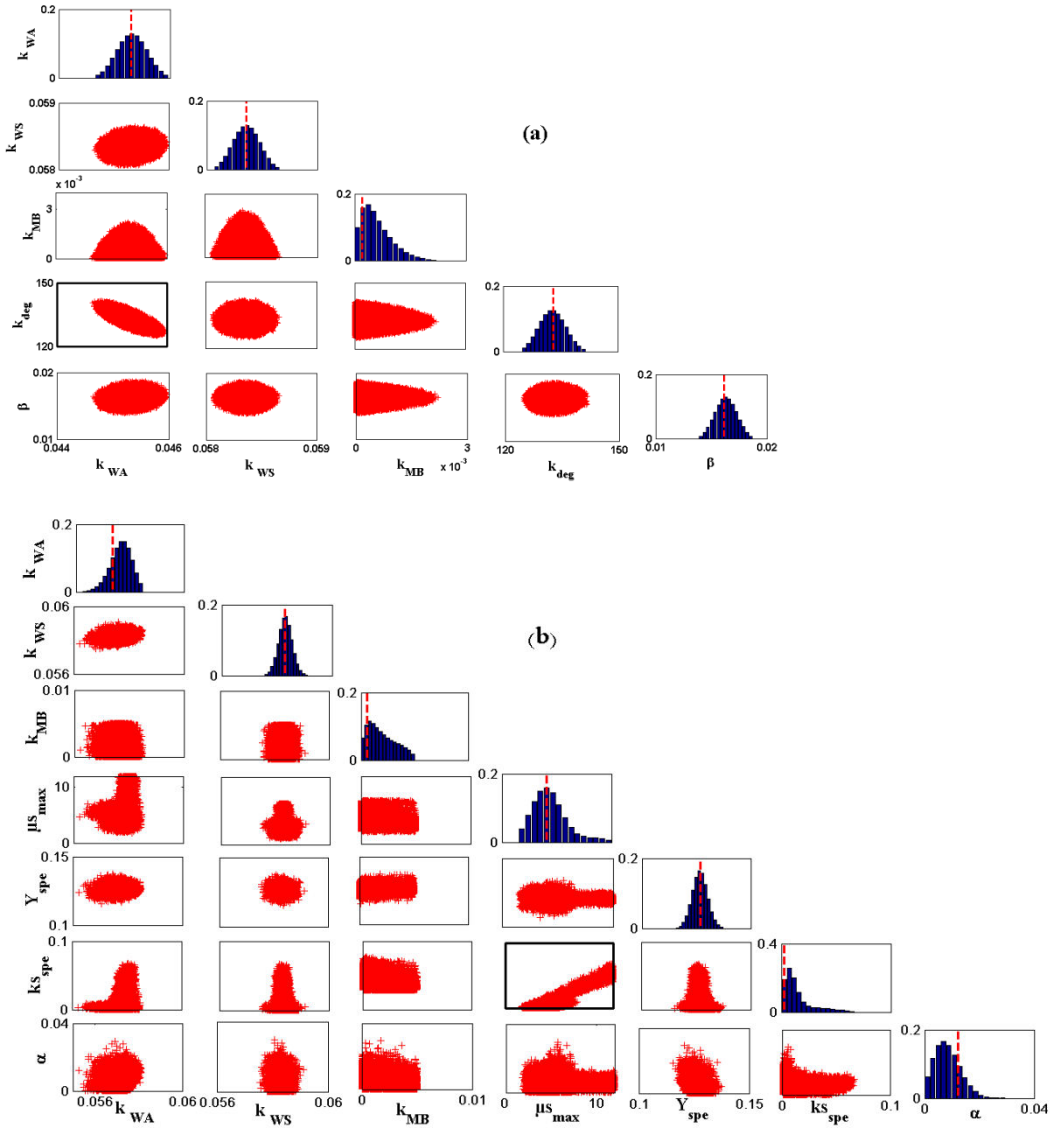

Figure II.2. Histograms of the evaluated model parameters (diagonal panels) and correlations between parameters (off-diagonal panels) for the PAH model, supposing biodegradation by (a) co-metabolism biomass and (b) specific biomass. The y-axis refers to the probability distribution value in diagonal panels and to the parameter searching range in off-diagonal panels while x-axis indicates the parameter searching range. The panels plotted with a solid line denote a high linear correlation between the parameters. Dashed lines indicate the most likely parameter values

For the mineralized fraction of labelled phenanthrene in soil, the model underestimates the observations as confirmed by a low value of the Nash Sutcliff index (NS=0.56) (Figure II.3b). The weakly sorbed fraction matches well the observed values with NS values close to 0.85 (Figure II.3c). For the total non-extractible fraction (PAH_{NER}) in soil simulation is also satisfactory with NS equal to 0.69 (Figure II.3e). However, at the end of incubation time, the model tends to over estimate the NER value, predicting a still increasing amount with time

whereas experimental data displayed a plateau. The model prediction for solution concentrations (Figure II.3a) and metabolites (Figure II.3d) are both within the range of experimental error tolerance. The recorded Akaike information criterion value for this scenario is 79.84.

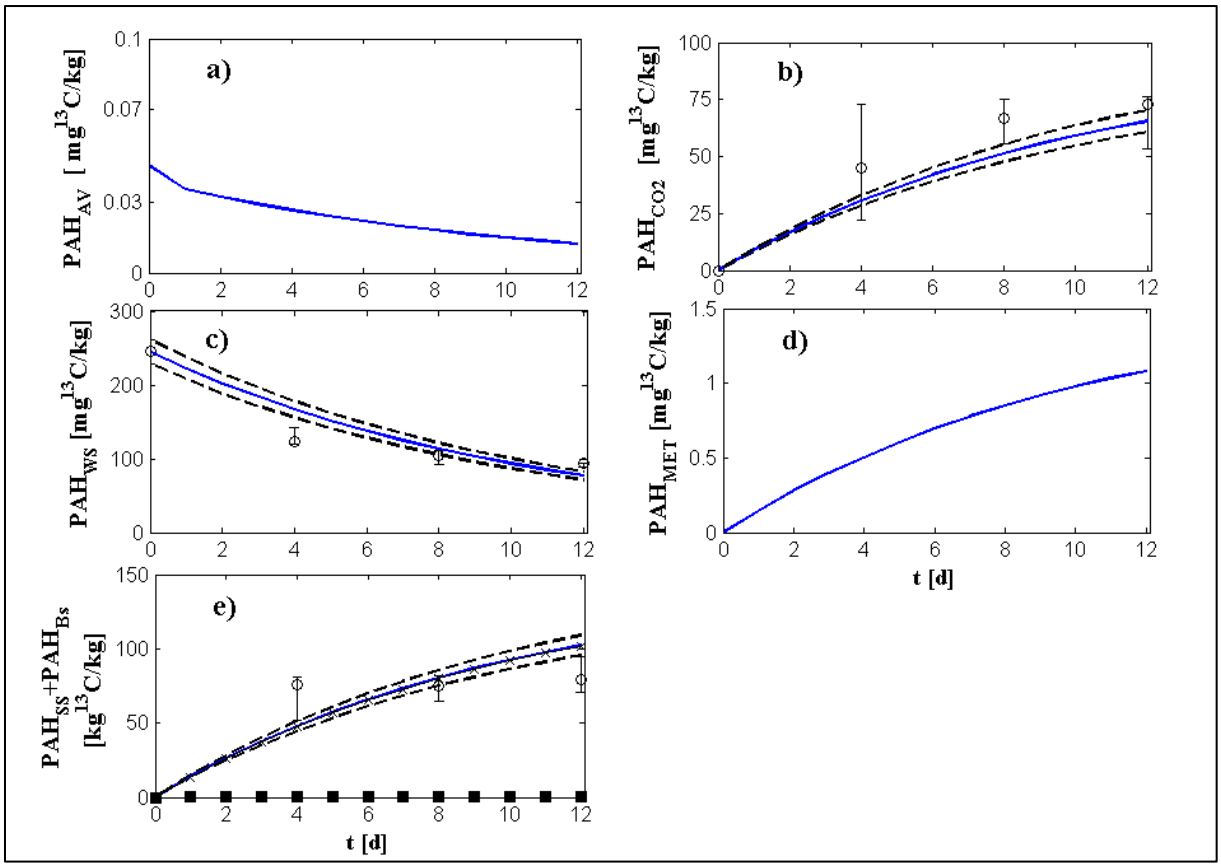

Figure II.3. Comparison between simulated (—) and observed (ǫ) phenanthrene concentration over time using the first scenario with co-metabolism biomass. From top left: a) available PAH in solution, b) mineralized PAH into CO_2, c) weakly sorbed on soil, d) metabolites, e) non-extractible residues as the sum of two fractions: strongly sorbed (—×—), biogenic (—■—). 95% confidence intervals for simulated concentrations are plotted with broken lines. Error bars indicate minimum and maximum values (n=3).

5.2. Scenario 2: specific biodegradation pathway

Following the same approach as used for the previous scenario, the model was run using the specific biodegradation pathway alone (i.e. 7 fitting parameters, see Table II.2). For most parameters, 95% confidence intervals cover narrow ranges of their prior distributions with the exception of μs_{max} (Table II.2), moreover most histograms appeared approximately Gaussian with the exception of ks_{spe} which tends to concentrate near its lower bound (Figure II.2b). Such a behavior can be at least partially ascribed to the positive correlation between μs_{max} and

ks_{spe} (r =0.84). No significant correlations among parameters are otherwise detected. We thus propose an empirical relationship between μs_{max} and ks_{spe} that can be used to further simplify the model:

$$ks_{spe} = 0.0099 - 0.0048\,\mu s_{max} + 0.0007\,\mu s_{max}^{2} \quad (\text{with } R^2=0.91) \quad (II.11)$$

It indicates that the half saturation substrate concentration in solution (ks_{spe}) could be a suitable monitoring parameter for deriving the growth rate (μs_{max}).

The 95% confidence intervals of simulation evolutions of the labelled phenanthrene compartments together with the measured ones are shown in Figure II.4. With this scenario, the simulation of the mineralized fraction (Figure II.4b) is improved compared to scenario 1 and an almost perfect fit is obtained, with high a Nash Sutcliffe of 0.92. Minor improvements are obtained for other model compartments with NS values equal to 0.86, 0.70, and 0.72 for PAH_{WS}, PAH_{NER} and PAH_{Bs} respectively. A sharp decrease of the initial concentration of labelled phenanthrene in solution is predicted (Figure II.4a), illustrating that a fast sorption equilibrium state for phenanthrene in solution is achieved at the end of the first incubation day. The model also predicts that less than 0.6 mg $^{13}C/kg_{ds}$ metabolites production is obtained at the end of incubation. For this scenario, the Akaike information criterion value is 82.61. This is a little bit higher than for scenario 1, which means that the increase in accuracy (higher NS values) is partly obtained thanks to a higher level of model complexity with seven parameters instead of five in the previous scenario. In addition, Figure II.4f shows that B_{SPE} is not very well simulated (NS = 0.72).

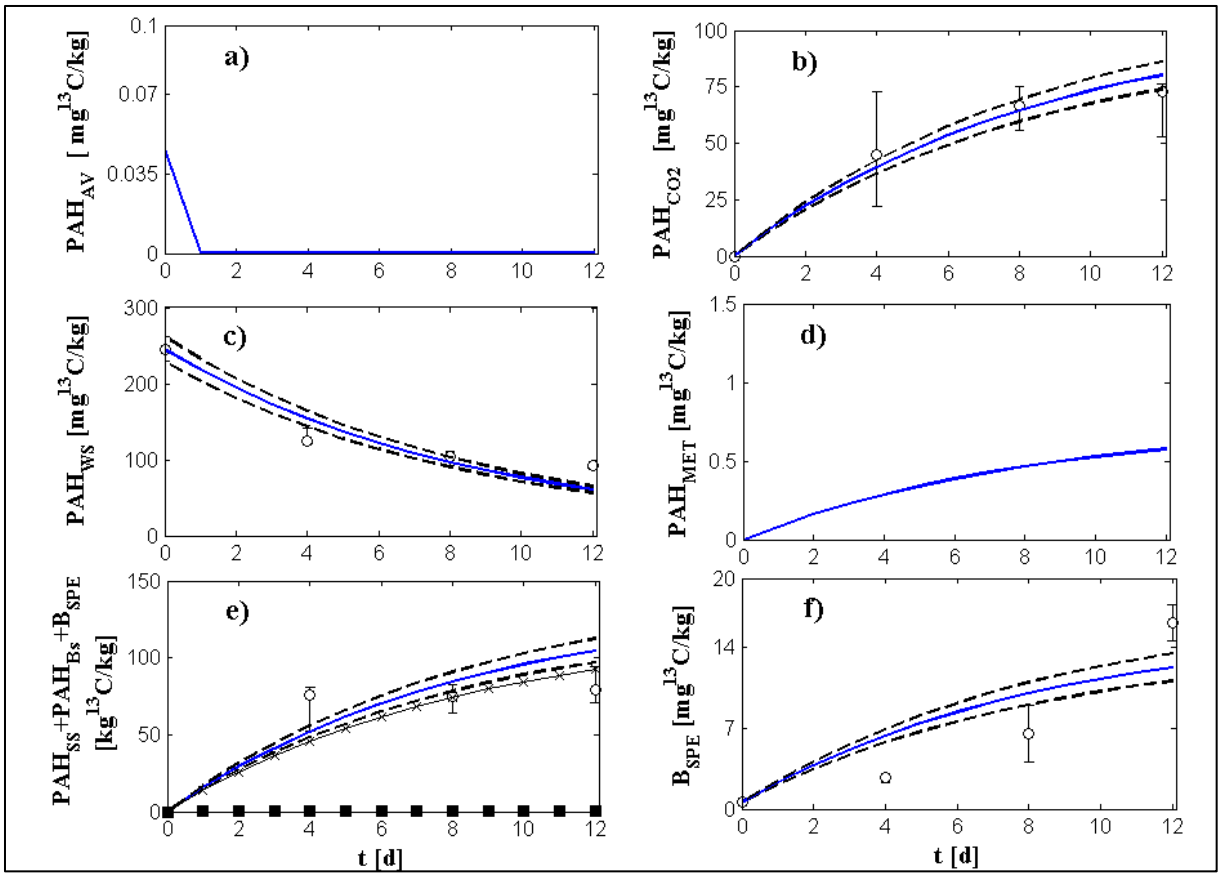

Figure II.4. Comparison between simulated (—) and observed (ϙ) phenanthrene concentration evolutions over time using the second scenario with specific biomass. From top left: a) available PAH in solution, b) mineralized PAH into CO_2, c) weakly sorbed on soil, d) metabolites, e) non-extractible residues as the sum of 3 fractions: strongly sorbed (—×—), biogenic (—■—) and specific biomass, f) phenanthrene assimilated by specific biomass. 95% confidence intervals for simulated concentrations are plotted with broken lines. Error bars indicate minimum and maximum values (n=3).

5.3. Final choice for model and behaviour analysis

Results obtained for both scenarios show that the model using the specific biomass degradation pathway (scenario 2) gives the best fit according to the NS values, with a small increase of the AIC criterion. Our selection of the specific biodegradation pathway is corroborated by the values of the calibrated microbial rates. The obtained value of 133 d^{-1} for k_{deg} in scenario 1, corresponding to a half degradation time of 1 hour, is not biologically realistic. In contrast, kinetic values obtained with scenario 2 approach those found in the literature and increase thereby the confidence in the model predictions. Indeed, the model predicts that the specific biomass doubles within 5 h, which is in accordance with the values published by Tao et al. (2007) for a microbial biomass using the phenanthrene as the sole source of carbon and energy in PAHs contaminated soil. The most likely biomass yield, $Y_{spe,}$ is equal to 0.127, which is about half of the value found by Weissenfels et al. (1990) for

phenanthrene within a pure bacterial culture, but was close to the value of 0.158 proposed by Kästner et al. (2014)for the anthracene (knowing that anthracene is 3-cycles PAHs close to phenanthrene). Similarly, the value of Ks_{spe} measured for anthracene by Wick et al. (2001) lies within the 95% confidence interval obtained for phenanthrene in this study.

Furthermore, simulation results showed that the fitting of empirical values of PAH_{CO2} is not improved when both biodegradation pathways are run simultaneously, meaning that the specific biodegradation pathway is most likely the main biodegradation mechanism for the labelled phenanthrene in our case study (see SI, Figure SI II.2 and

Table SI II.1). This result is further supported by the fact that a modification of the diversity of phenanthrene degrading bacterial population does not increase phenanthrene mineralization rate in this same contaminated soil (Cébron et al., 2011).

Consequently, based on above discussion and for further *in situ* experiments, we suggest to use the model only with the biodegradation pathway driven by specific biomass (i.e. scenario 2 with 7 parameters). The specific pathway might, with a reasonable compromise between model complexity and model accuracy to represent processes in the soil, be used alone for further simulations at different time scales, especially with lack of information about the microbial biomass uptake rates which might never be measured in reality. It is important to underline that our findings do not mean by itself that the co-metabolic biomass is a negligible contribution to the overall labelled phenanthrene mineralization: it only indicates that the pathway driven by the specific biomass and modeled within the Monod kinetic is the best way to predict the degradation of PAHs in the studied soil.

For scenario 2, the highest efficiency of biodegradation is associated with the prediction of an exponential growth for the specific biomass (Figure II.4f). Such a prediction might appear in contradiction to the typical observations made for the growth of specific biomass, usually preceded by an initial lag period. A biological explanation of this finding could be related to the preliminary presence of phenanthrene degrading microbial biomasses in the aged contaminated soil but with limited accessibility for the PAHs due to the aging process. Once the labelled phenanthrene was added to the soil, an immediate use of the added compound by the specific biomass occurred, which was reflected by intense release of CO_2 with simultaneous sharp decrease of the concentration of labelled phenanthrene during the first two days of incubation.

Another important result is that the calibrated parameters for the adsorption module are all within the ranges reported by Johnson et al. (2001) with only slight differences for both scenarios (Table II.1). Finally, the model predicts that the metabolites production would be

less than 1%, and that the contribution of the biogenic non-extractible residues to the total extractible residues could be neglected at such short time scale. This finding would be in agreement with results indicating that sorption occurs more rapidly than the biodegradation in the soil (Adam et al., 2014).

6. Sensitivity analysis

One objective of this work was to identify the main factors controlling the biodegradation of PAHs in the studied soil. A global sensitivity analysis was therefore carried out to identify the sensitivity of three of the model outputs to the model parameters for the selected model (scenario 2). The selected outputs were PAH_{CO2}, PAH_{AV} and $r_{PAH_{AV}/PAH_{WS}}$, representing the kinetics of sorption and desorption of the labelled phenanthrene between the available compartment (PAH_{AV}) and the weakly sorbed one (PAH_{WS}):

$$r_{PAH_{AV}/PAH_{WS}} = k_{AW} PAH_{AV} \quad k_{WA} PAH_{WS} \qquad \text{(II.12)}$$

The sensitivity analysis performed using the FAST 99 function (Saltelli et al., 1999) of the R package "sensitivity" (Pujol et al., 2015) with 400 model runs per parameter (i.e. 400 x 5 = 2000 model runs in total). This method, also called the "extended-FAST" method, estymates the first order and total Sobol' indices for all the factors. In other words, it evaluates the sensitivity to the chosen parameters when acting alone (first order) or when combined with the other parameters (total orders). We chose to keep the parameter α set to its value to avoid any compensation with the two Monod kinetic constants (i.e. μs_{max}, Y_{spe}). A uniform distribution was used for the tested parameters in the following ranges: $k_{WA} = k_{WS}$ = [0.00086, 0.086], μs_{max} = [0.0, 8.6], Y_{spe} = [0.1, 0.3], ks_{spe} = [0.001, 0.1].

Figure II.5 shows the first orders and the total orders characterizing the relative importance of those parameters on the three outputs. The first and the total orders of ads/desorption rates k_{WA}, k_{AW} are very high for both PAH_{AV} and $r_{PAH_{AV}/PAH_{WS}}$, indicating that those two parameters have the major effects on the mass of hydrophobic compound in solution, while Y_{spe}, μs_{spe} and k_{SW} are the second most important ones with interactions with other parameters. The maximum growth rate μs_{max} is the critical factor during mineralization, while the parameters k_{WA} and k_{AW} have the main effect with interactions with other parameters (Figure II.5b). The parameters ks_{spe} and k_{MB} have negligible impacts on the three outputs and can thus be set to their calibrated values. These results illustrate that for longer time periods, the amount of ultimately degraded PAHs depends more on adsorption rates than on the Monod kinetics and

that more generally in such systems physical interactions dominate the biological mechanisms in controlling the fate of PAHs.

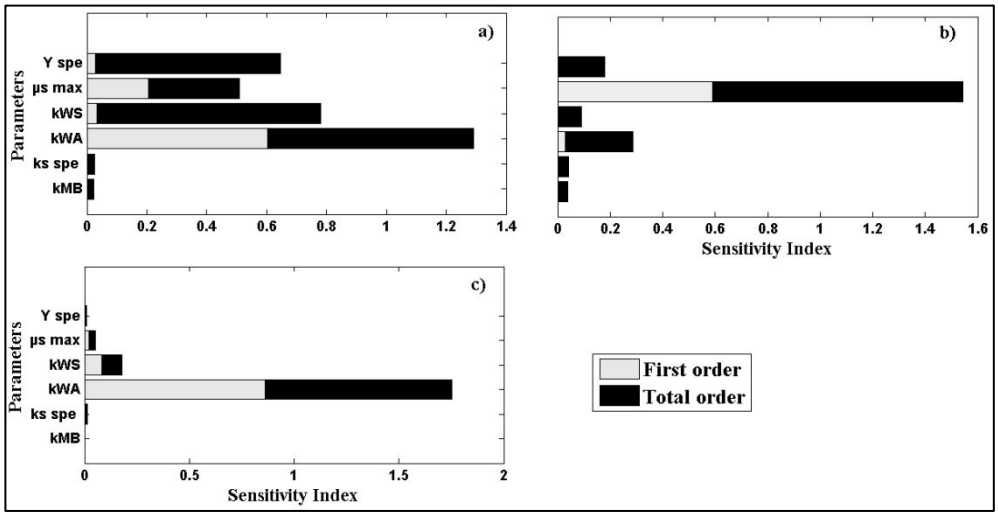

Figure II.5. Sensitivity indices for the parameters **of the selected PAH model with respect to the variables: a) PAH_{AV}, b) PAH_{CO2} c)** $r_{PAH_{AV}/PAH_{WS}}$

7. Conclusion

The kinetic model proposed for simulating the dynamics of PAHs in soil is appropriate for describing the underlying biological and physical transformation of PAHs in soil for a few days aboratory incubation experiment. Model calibration was achieved by coupling the model to the Bayesian method (DREAM) that allowed us to estimate the probability density functions for all the model kinetic values. Results appear in good agreement with literature studies. The calibration procedure led to model simplifications retaining the specific biodegradation pathway as the predominant biological process. A global sensitivity analysis of the model parameters shows that the amount of PAHs ultimately degraded is mostly governed by the adsorption/desorption kinetics rather than biological kinetics. In future work, this module will be included in a global modeling framework including dynamic water transfer, heat transfer and solute transport under climatic conditions in the Vsoil modeling platform to be applied on long term *in situ* experimental plots of agricultural soils or industrial soils.

Nomenclature

AIC Akaike information criterion

B_{SPE} specific microbial biomasses

corr correlation coefficient

DCM dichloromethane

DREAM differential evolution adaptive metropolis

ds dry soil

f_{oc} organic carbon content

f_T temperature dependence factor

f_W water content dependence factor

K_d sorption distribution coefficient

k_{deg} pseudo first order kinetic constant of biodegradation for co-metabolism

k_{AW} first order kinetic constant that goes from PAH_{AV} into PAH_{WS} compartment

k_{MB} first order kinetic constant that goes from PAH_{MET} into PAH_{Bs} compartment

k_{SW} first order kinetic constant that goes from PAH_{SS} into PAH_{WS} compartment

k_{WA} first order kinetic constant that goes from PAH_{WS} into PAH_{AV} compartment

k_{WS} first order kinetic constant that goes from PAH_{WS} into PAH_{SS} compartment

k_M mortality rate constant

K_{oc} sorption distribution coefficient normalized to f_{oc}

K_{ow} octanol-water partition coefficient

ks_{spe} half saturation of growth substrate for the specific biomass

m number of model outputs

n number of measured points

NER non-extractible residues

NS Nash Sutcliffe index

p number of estimated parameters excluding fixed parameters

PAH polycyclic aromatic hydrocarbons

PAH_{AV} PAH as available in soil solution

PAH_{BS} PAH as biogenic NER

PAH_{CO2} carbon dioxide gas produced from the mineralization of PAH

PAH_{MET} PAH as metabolites

PAH_{SS} PAH as physically NER

PAH_{WS} PAH sorbed extracted by DCM

pdfs probability density functions

SOM soil organic matter

x model inputs

y model outputs

$y_{calc,t,i}$ predicted values at the t^{th} observed time for the i^{th} model output

$y_{obs,t,i}$ observed values at the t^{th} observed time for the i^{th} model output

$\bar{y}_{obs,i}$ mean observed for the i^{th} model output

Y_{spe} yield of specific biomass

α magnitude of metabolites production by biodegradation for specific biomass

β magnitude of metabolites production by biodegradation for co-metabolism

μs_{max} maximum specific growth rate

$\rho(y/x)$ marginal likelihood

$\rho(y/\theta, x)$ likelihood function

$\rho(\theta)$ probability density of prior distribution of parameters

8. Acknowledgements

This research was financially supported by the French Environment and Energy Management Agency (ADEME) and the Environment and Agronomy division of the French National Institute for Agricultural Research (INRA). We are grateful to Dr. François Lafolie for his assistance in performing the sensitivity analysis and to Dr. Delphine Derrien for the fruitful discussion.

9. References

Adam, I.K.U., Rein, A., Miltner, A., Fulgêncio, A.C.D., Trapp, S., Kästner, M., 2014. Experimental Results and Integrated Modeling of Bacterial Growth on an Insoluble Hydrophobic Substrate (Phenanthrene). Environ. Sci. Technol. **48**, 8717–8726. doi:10.1021/es500004z

Andrén, O., Steen, E., Rajkai, K., 1992. Modelling the effects of moisture on barley straw and root decomposition in the field. Soil Biol. Biochem. **24**, 727–736. doi:10.1016/0038-0717(92)90246-T

Aster, R.C., Borchers, B., Thurber, C.H., 2013. Nonlinear Regression, in: Parameter Estimation and Inverse Problems. Elsevier, pp. 217–238. doi:10.1016/B978-0-12-385048-5.00009-4

Barriuso, E., Benoit, P., Dubus, I.G., 2008. Formation of pesticide nonextractable (bound) residues in soil: Magnitude, controlling factors and reversibility. Environ. Sci. Technol. **42**, 1845–1854. doi:10.1021/es7021736

Beulke, S., Dubus, I.G., Brown, C.D., Gottesburen, B., 2000. Simulation of pesticide persistence in the field on the basis of laboratory data : A review. Environ. Qual. **29**, 1371–1379. doi:10.2134/jeq2000.00472425002900050001x

Box, G.E.P., Tiao, G.C., 1992. Bayesian Assessment of Assumptions 1. Effect of Non-Normality on Inferences about a Population Mean with Generalizations, in: Bayesian Inference in Statistical Analysis. John Wiley & Sons, Inc., Hoboken, NJ, USA, pp. 149–202. doi:10.1002/9781118033197.ch3

Burnham, K.P., Anderson, D.R., 2004. Multimodel Inference: Understanding AIC and BIC in Model Selection. Sociol. Methods Res. **33**, 261–304. doi:10.1177/0049124104268644

Cebron, A., Beguiristain, T., Faure, P., Norini, M.-P., Masfaraud, J.-F., Leyval, C., 2009. Influence of Vegetation on the In Situ Bacterial Community and Polycyclic Aromatic Hydrocarbon (PAH) Degraders in Aged PAH-Contaminated or Thermal-Desorption-Treated Soil. Appl. Environ. Microbiol. **75**, 6322–6330. doi:10.1128/AEM.02862-08

Cébron, A., Louvel, B., Faure, P., France-lanord, C., Chen, Y., Murrell, J.C., Leyval, C., 2011. Root exudates modify bacterial diversity of phenanthrene degraders in PAH-polluted soil but not phenanthrene degradation rates. Environ. Microbiol. **13**, 722–736. doi:10.1111/j.1462-2920.2010.02376.x

Chung, N., Alexander, M., 2002. Effect of soil properties on bioavailability and extractability of phenanthrene and atrazine sequestered in soil. Chemosphere **48**, 109–115. doi:10.1016/S0045-6535(02)00045-0

Crank, J., Nicolson, P., 1996. A practical method for numerical evaluation of solutions of partial differential equations of the heat-conduction type. Adv. Comput. Math. **6**, 207–226. doi:10.1007/BF02127704

Dagois, R., Schwartz, C., Coussy, S., Lorgeoux, C., Ouvrard, S., Faure, P., 2015. Climatic influence on mobility of organic pollutants in Technosols from contrasted industrial activities. J. Soils Sediments **16**, 1306–1315. doi:10.1007/s11368-015-1108-4

Delgadillo-Mirquez, L., Lardon, L., Steyer, J.P., Patureau, D., 2011. A new dynamic model for bioavailability and cometabolism of micropollutants during anaerobic digestion. Water Res. **45**, 4511–4521. doi:10.1016/j.watres.2011.05.047

Fragoulis, G., Trevisan, M., Puglisi, E., Capri, E., 2005. A model assessing bioavailability of persistent organic pollutants in soil, Reactive Transport in Soil and Groundwater. Springer-Verlag, Berlin/Heidelberg. doi:10.1007/3-540-26746-8_3

Geng, C., Haudin, C.-S., Zhang, Y., Lashermes, G., Houot, S., Garnier, P., 2015. Modeling the release of organic contaminants during compost decomposition in soil. Chemosphere **119**, 423–431. doi:10.1016/j.chemosphere.2014.06.090

Gevao, B., Jones, K.C., Semple, K.T., 2005. Formation and release of non-extractable14C-Dicamba residues in soil under sterile and non-sterile regimes. Environ. Pollut. **133**, 17–24. doi:10.1016/j.envpol.2004.04.007

Govind, R., Lai, L., Dobbs, R., 1991. Integrated model for predicting the fate of organics in wastewater treatment plants. Environ. Prog. **10**, 13–23. doi:10.1002/ep.670100111

Hatzinger, P.B., Alexander, M., 1995. Effect of Aging of Chemicals in Soil on Their Biodegradability and Extractability. Environ. Sci. Technol. **29**, 537–545. doi:10.1021/es00002a033

Iarc, 2010. IARC monographs on the evaluation of carcinogenic risks to uumans: some non-heterocyclic polycyclic aromatic hydrocarbons and some related exposures. Iarc Monogr. Eval. Carcinog. Risks To Humans **92**, 1–868.

Janke, D., Fritsche, W., 1985. Nature and significance of microbial cometabolism of xenobiotics. J. Basic Microbiol. **25**, 603–619.

Johnson, M.D., Keinath, T.M., Weber, W.J., 2001. A distributed reactivity model for sorption by soils and sediments. 14. Characterization and modeling of phenanthrene desorption rates. Environ. Sci. Technol. **35**, 1688–1695. doi:10.1021/es001391k

Kästner, M., Nowak, K.M., Miltner, A., Trapp, S., Schäffer, A., 2014. Classification and modelling of non-extractable residue (NER) formation of xenobiotics in soil—a synthesis. Crit. Rev. Environ. Sci. Technol. **44**, 2107–2171. doi:10.1080/10643389.2013.828270

Köhler, A., Schüttoff, M., Bryniok, D., Knackmuß, H.-J., 1994. Enhanced biodegradation of phenanthrene in a biphasic culture system. Biodegradation **5**, 93–103. doi:10.1007/BF00700634

Köhne, J.M., Köhne, S., Šimůnek, J., 2009. A review of model applications for structured soils: b) Pesticide transport. J. Contam. Hydrol. **104**, 36–60. doi:10.1016/j.jconhyd.2008.10.003

Laor, Y., Strom, P.F., Farmer, W.J., 1996. The effect of sorption on phenanthrene bioavailability. J. Biotechnol. **51**, 227–234. doi:10.1016/S0168-1656(96)01600-8

Mackay, D., Shiu, W.Y., Ma, K., Lee, S.C., 2006. Handbook of physical-chemical properties and environmental fate for organic chemicals, 2nd ed. ed. CRC Press, Boca Raton (FL).

Moenickes, S., Höltge, S., Kreuzig, R., Richter, O., 2011. Process dominance analysis for fate modeling of flubendazole and fenbendazole in liquid manure and manured soil. Sci. Total Environ. **410–411**, 226–234. doi:10.1016/j.scitotenv.2011.09.047

Monod, J., 1949. The Growth of Bacterial Cultures. Annu. Rev. Microbiol. **3**, 371–394. doi:10.1146/annurev.mi.03.100149.002103

Nam, K., Kim, J.Y., Oh, D.I., 2003. Effect of soil aggregation on the biodegradation of phenanthrene aged in soil. Environ. Pollut. **121**, 147–51.

Nash, J.E., Sutcliffe, J.V., 1970. River flow forecasting through conceptual models part I — A discussion of principles. J. Hydrol. **10**, 282–290. doi:10.1016/0022-1694(70)90255-6

Nguyen, T.H., Goss, K.-U., Ball, W.P., 2005. Polyparameter Linear Free Energy Relationships for Estimating the Equilibrium Partition of Organic Compounds between Water and the Natural Organic Matter in Soils and Sediments. Environ. Sci. Technol. **39**, 913–924. doi:10.1021/es048839s

Ogram, A. V, Jessup, R.E., Ou, L.T., Rao, P.S., 1985. Effects of sorption on biological degradation rates of (2,4-dichlorophenoxy) acetic acid in soils. Appl. Environ. Microbiol. **49**, 582–587.

Pignatello, J.J., 1990. Slowly reversible sorption of aliphatic halocarbons in soils. II. Mechanistic aspects. Environ. Toxicol. Chem. **9**, 1117–1126. doi:10.1002/etc.5620090902

Pomiès, M., Choubert, J.-M., Wisniewski, C., Coquery, M., 2013. Modelling of micropollutant removal in biological wastewater treatments: A review. Sci. Total Environ. **443**, 733–748. doi:10.1016/j.scitotenv.2012.11.037

Pujol, A.G., Iooss, B., Janon, A., Veiga, D., Fruth, J., Gilquin, L., Guil-, J., Gratiet, L. Le, Lemaitre, P., Ramos, B., Touati, T., 2015. Package " sensitivity " [WWW Document]. URL https://cran.r-project.org/web/packages/sensitivity/sensitivity.pdf

Recous, S., 1995. Soil inorganic N availability: effect on maize residue decomposition. Soil Biol. Biochem. **27**, 1529–1538.

Richnow, H.H., Annweiler, E., Koning, M., Lüth, J.C., Stegmann, R., Garms, C., Francke, W., Michaelis, W., 2000. Tracing the transformation of labelled [1-13C]phenanthrene in a soil bioreactor. Environ. Pollut. **108**, 91–101. doi:10.1016/S0269-7491(99)00205-5

Russell, D.L., 2006. Elements of Biological Treatment, in: Practical Wastewater Treatment. John Wiley & Sons, Inc., Hoboken, NJ, USA, pp. 91–124. doi:10.1002/0470067926.ch6

Saltelli, A., Tarantola, S., Chan, K.P.-S., 1999. A Quantitative Model-Independent Method for Global Sensitivity Analysis of Model Output. Technometrics **41**, 39–56. doi:10.1080/00401706.1999.10485594

Sun, S., Bertrand-Krajewski, J.L., 2013. Separately accounting for uncertainties in rainfall and runoff: Calibration of event-based conceptual hydrological models in small urban catchments using Bayesian method. Water Resour. Res. **49**, 5381–5394. doi:10.1002/wrcr.20444

Tao, X.-Q., Lu, G.-N., Dang, Z., Yi, X.-Y., Yang, C., 2007. Isolation of phenanthrene-degrading bacteria and characterization of phenanthrene metabolites. World J. Microbiol. Biotechnol. **23**, 647–654. doi:10.1007/s11274-006-9276-4

Thomas, J.M., Yordy, J.R., Amador, J.A., Alexander, M., 1986. Rates of dissolution and biodegradation of water-insoluble organic compounds. Appl. Environ. Microbiol. **52**, 290–296.

Troussellier, M., Bouvy, M., Courties, C., Dupuy, C., 1997. Variation of carbon content among bacterial species under starvation condition. Aquat. Microb. Ecol. **13**, 113–119.

Vrugt, J.A., 2016. Markov chain Monte Carlo simulation using the DREAM software package : Theory , concepts , and MATLAB implementation. Environ. Model. Softw. **75**, 273–316. doi:10.1016/j.envsoft.2015.08.013

Vrugt, J. a., ter Braak, C.J.F., Clark, M.P., Hyman, J.M., Robinson, B. a., 2008. Treatment of input uncertainty in hydrologic modeling: Doing hydrology backward with Markov chain Monte Carlo simulation. Water Resour. Res. **44**, 1–15. doi:10.1029/2007WR006720

Weissenfels, W.D., Beyer, M., Klein, J., 1990. Degradation of phenanthrene, fluorene and fluoranthene by pure bacterial cultures. Appl. Microbiol. Biotechnol. **32**, 479–484. doi:10.1007/BF00903787

White, J.C., Hunter, M., Nam, K., Pignatello, J.J., Alexander, M., 1999. Correlation between biological and physical availabilities of phenanthrene in soils and soil humin in aging experiments. Environ. Toxicol. Chem. **18**, 1720–1727. doi:10.1002/etc.5620180816

Wick, L.Y., Colangelo, T., Harms, H., 2001. Kinetics of mass transfer-limited bacterial growth on solid PAHs. Environ. Sci. Technol. **35**, 354–61.

Wilcke, W., 2000. SYNOPSIS Polycyclic Aromatic Hydrocarbons (PAHs) in Soil — a Review. J. Plant Nutr. Soil Sci. **163**, 229–248. doi:10.1002/1522-2624(200006)163:3<229::AID-JPLN229>3.0.CO;2-6

Wodzinski, R.S., Coyle, J.E., 1974. Physical state of phenanthrene for utiliszation by bacteria. Appl. Microbiol. **27**, 1081–1094.

Zarfl, C., Klasmeier, J., Matthies, M., 2009. A conceptual model describing the fate of sulfadiazine and its metabolites observed in manure-amended soils. Chemosphere **77**, 720–726. doi:10.1016/j.chemosphere.2009.08.035

10. Supplementary Information (SI)

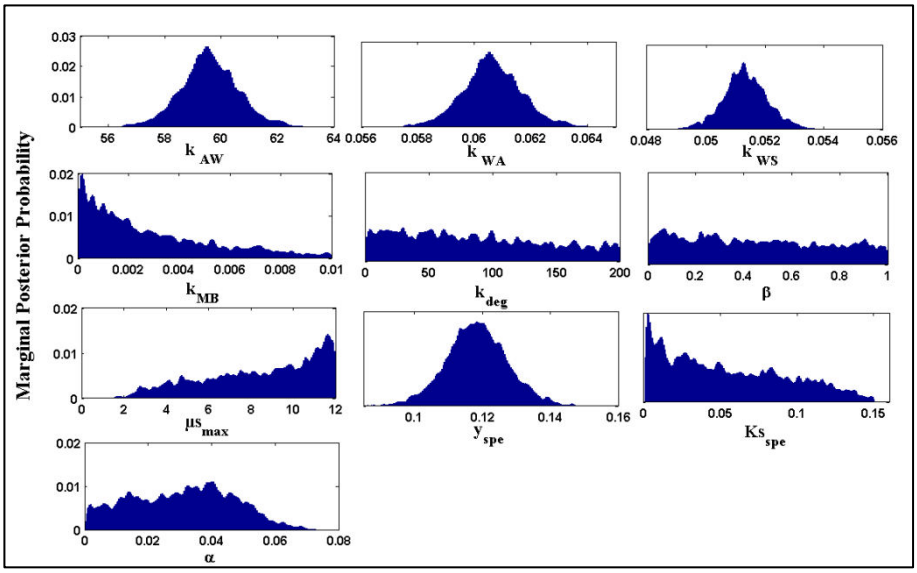

Figure SI II.1. Histograms of the evaluated model parameters for the PAH model supposing biodegradation occurred by both biodegradation pathways: cometabolism and specific biomass. The y-axis refers to the probability distribution while x-axis indicates to the parameter searching range.

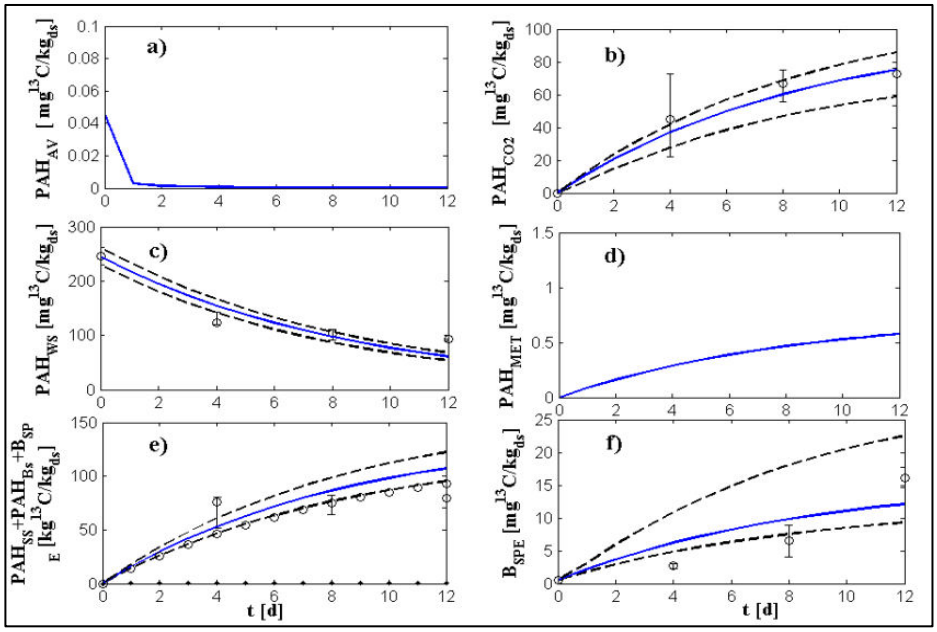

Figure SI II.2. Comparison between simulated (—) and observed (ϙ) phenanthrene concentrations evolutions over time assuming biodegradation occurred by both pathways of biodegradation: cometabolism and specific biomass. From top left: a) available in solution, b) mineralized into CO_2, c) weakly sorbed on soil, d) metabolites, e) non-extractible residues as the sum of 3 fractions: strongly sorbed (——×——), biogenic (—■—) and the specific biomass, f) phenanthrene assimilated by specific biomass. 95% confidence intervals for simulated concentrations are plotted in (– – –). Error bars indicate minimum and maximum (3 replicates).

Table SI II.1. Comparison of Nash Sutcliffe index values biodegradation pathways scenarios

Biodegradation pathways	PAH_{CO2}	PAH_{NER}	PAH_{WS}
Both pathways	0.92	0.69	0.87
Specific biomass	0.92	0.7	0.87
Cometabolic biomass	0.56	0.69	0.85

Before starting with DREAM package

An introduction to the PAH model is provided in the paper:

Brimo K., Garnier P., Sun S., Bertrand-Krajewski J.L, Cébron A., Ouvrard S. Using a Bayesian approach to improve and calibrate a dynamic model of polycyclic aromatic hydrocarbons degradation in an industrial contaminated soil. Environmental Pollution 215, 27-37. doi : 10.1016/j.envpol.2016.04.094
We recommend reading this paper before getting started. To get information about DREAM code, we recommend reading these two papers:

1. *Vrugt, J. a., ter Braak, C.J.F., Clark, M.P., Hyman, J.M., Robinson, B. a., 2008. Treatment of input uncertainty in hydrologic modeling: Doing hydrology backward with Markov chain Monte Carlo simulation. Water Resour. Res. 44, 1–15.*
2. *Vrugt, J.A., 2016. Markov chain Monte Carlo simulation using the DREAM software package : Theory , concepts , and MATLAB implementation. Environ. Model. Softw.*

How to get started

Our script follows the operating instructions and data inputs and outputs of the script "runDREAM" in DREAM code written by Jasper.A. Vrugt

To get started using PAH model, the user has to open the script "runDREAM" and run the script step by step. The script includes comments giving short description of the DREAM method and the steps of our case study model, as well as how to obtain the posterior "pdf" of model parameters after termination of DREAM script.

If the user still has not clear idea of how to back out the "pdf" of model parameters, we suggest running the short MATLAB-code

```
S=[];
for i=1:11 % 11=12-1 is the number of model parameters
   S=[S;Sequences(:,:,i)]; % returns i by n matrix S
end
[a,b]=sort(S(:,13),'descend');% 13=i+2
R=S(b,:);% values of PAH model parameters:
kwa/kws/ksw/kmb/kdeg/µmax/km/yspe/Kspe/beta/alpha
```

Furthermore, the package includes additional scripts:

- *PAH: is a function script returns the model output matrix whose elements are the corresponding values of these in input matrix, and computed numerically at daily step.*
- *PAH_model_Code_to_run_simulation:" to perform a simulation and visualize the model outputs using a model parameters sets*

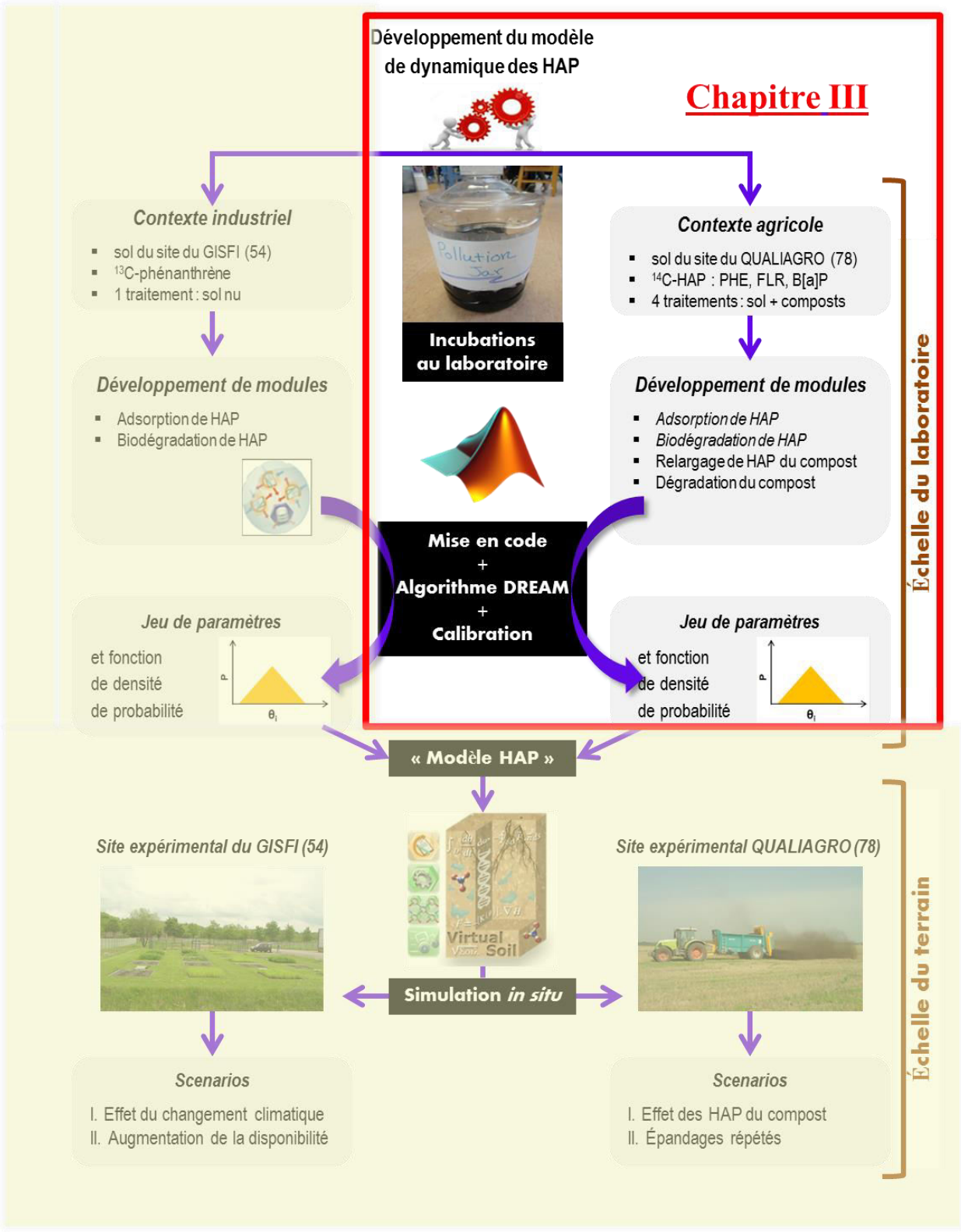

Place du chapitre III dans l'ensemble de travail de thèse

Chapitre III. Modélisation du devenir des HAP apportés avec les composts dans un sol agricole en fonction de la nature des matières organiques exogènes à l'échelle du laboratoire

Résumé du contenu du chapitre en français

Ce chapitre porte sur la modélisation d'expériences de laboratoire étudiant la dynamique des HAP marqués au carbone 14 apportés dans des composts urbains après ajout de ces composts dans un sol agricole. Le modèle a été construit à partir des modules présentés au chapitre 2 en leur associant un nouveau module qui décrit le relargage des HAP des composts au fur et à mesure de leur décomposition. Le modèle a été paramétré sur la base d'expériences d'incubations au laboratoire de trois HAP marqués au ^{14}C : le phénanthrène (3 cycles), le fluoranthène (4 cycles) et le benzo(a)pyrene (5 cycles). La dynamique de chaque HAP a été suivie pour 4 qualités de compost différentes. De manière similaire qu'au chapitre précédent, la calibration du modèle a été réalisée en utilisant l'approche bayésienne « DREAM », programmé sous MATLAB. Pour chaque HAP, il a été possible de définir un seul jeu de paramètres permettant de simuler de manière correcte la dynamique d'un HAP pour les différents traitements, excepté pour le fluoranthène où le modèle a mis en évidence une biomasse microbienne spécifique différente pour chaque traitement. Les résultats expérimentaux montrent que la qualité du compost a influencé la dynamique de transformation des HAP dans le sol. Nos résultats de simulations ont mis en évidence que la dissipation des HAP par minéralisation dans le sol amendé était davantage contrôlée par la limitation de la biodisponibilité des HAP plutôt que par l'activité biologique. Le modèle a prédit une forte augmentation de la formation des résidus biogéniques pour le HAP le moins hydrophobe (le phénanthrène).

Ce chapitre fait l'objet d'un article en préparation présenté dans ce chapitre : Khaled Brimo, Stéphanie Ouvrard, Sabine Houot, François Lafolie, Patricia Garnier. Modelling the fate of

PAH added with composts in amended soil according to the origin of the exogeneous organic matter, to be submitted to *Science of the Total Environment*.

Modelling the fate of PAH added with composts in amended soil according to the origin of the exogeneous organic matter

Khaled Brimo[a,b,c], Stéphanie Ouvrard[b], Sabine Houot[a], François Lafolie[d], Patricia Garnier[a]

[a]UMR EcoSys, INRA, AgroParisTech, Université Paris-Saclay, 78850, Thiverval-Grignon, France

[b]UMR Laboratoire Sols et Environnement, INRA, Université de Lorraine, 54518 Vandoeuvre-lès-Nancy, France

[c]Agence de l'Environnement et de la Maîtrise de l'Energie, 20 avenue du Grésillé, BP 90406, F-49004 Angers Cedex 01, France

[d]UMR EMMAH, INRA, UAPV, 84914 Avignon 9, France

*Corresponding author: Patricia Garnier

Tel: + 33 130 815 314

E-mail: patricia.garnier@inra.fr

Article prepared for submission in Science of the Total Environment

1. Abstract

A new model able to simulate the behaviors of polycyclic aromatic hydrocarbons (PAH) added with compost in agricultural soil is presented. This model associates modules describing the physical, biological and biochemical processes involved in PAH dynamics in soils, along with a module describing compost degradation resulting in PAH release. The model was calibrated from laboratory soil incubations using three ^{14}C-PAH in three different compost types. Parameter estimation was carried out using a Bayesian approach. For each PAH, a single parameter set enabled to simulate adequately the observed dynamics of PAH for all compost. Processes occurring before compost application to soil strongly influenced the fate of PAHs in soil. Our simulations showed that PAHs dissipation during composting was higher in mature composts while PAH dissipation in amended soil was higher in the non-mature compost.

Keywords: PAH reactivity, model, amended soil, compost, bounded residue, Bayesian approach

Highlights

- Dynamic of the PAHs added with composts in soil were influenced by the processes occurring during composting
- The model simulates the release of PAH included in compost expressed as a function of the organic carbon decomposition rates of the added composts.
- Parameter estimation using a Bayesian approach produces one set of parameters for each PAH relevant for all composts
- The model calculates the proportion of biogenic and physical bound residues in the non-extractable compartment of PAHs.

2. Introduction

The recycling of composted organic residues in soils is a practice increasingly used in agriculture. It helps to prevent the loss of soil fertility by restoring the soil organic matter contents as well as improving soil physical properties (Tejada et al., 2009, Annabi et al., 2011; Goss et al., 2013;). However, certain persistent organic pollutants (POPs), among them polycyclic aromatic hydrocarbons (PAH), may be present in the feedstock materials of these composts, leading to soil contamination risk when they are recycled in agricultural areas (Brändli et al., 2005; Wilcke, 2000; Wild et al., 1991). Several works have reported the effects of quantity and quality of soil organic matter on the environmental behavior of POPs in soil (Gunasekara and Xing, 2003; Wang et al., 2010; Xing, 1997; Xiu-hong et al., 2014). It is of special importance to know how and to which extent the dissipation of PAH is affected by the addition of composted organic residues in soil. Kästner et al. (1999) and Haudin et al. (2013) showed that compost addition in soils had a stimulation effect on desorption and thus on the degradation of PAHs. However, some other authors such as Puglisi et al. (2007) found that compost application could promote the formation of sequestered fractions of compounds, leading to reduce its bioavailability for microorganisms in soil.

Most of the reviewed studies in literature deal with the effects of a certain type of composts (often green waste compost) on a single PAH molecule (often low molecular weight compounds, with three fused benzene rings, such as phenanthrene or anthracene). Moreover, little is known about the fate of PAH in soil when the dissipation becomes controlled simultaneously by the quality of amended compost and the physico-chemical properties of the contaminant. Kinetic data for various PAH are scarce in literature until now for the prediction of PAH fate in soil-compost mixtures system.

A number of models have been developed to explore the fate of POPs in amended soils (eg: Zarfl et al., 2009, Wu et al., 2013, Morais et al., 2013) but the models that consider explicitly the impacts of organic matter decomposition on sorption and mineralization or dissipation of POPs are very scarce. Lashermes et al. (2013) simulated the mineralization of four organic pollutants during the composting of green waste and sludge. Geng et al. (2015) simulated the mineralization of these four organic pollutants after their incorporation with the compost in soil. Both studies considered the interactions between the pollutants and the organic matter explicitly. The impact of the composting process and the type of composted organic matter on organic pollutant fate after their addition in soil has never been simulated.

The aims of the present work were twofold: (i) propose a new coupled model adapted to study the dynamics of PAH in soil-compost mixtures systems that takes into account explicitly the type of organic amendments on the fate of PAH during the decomposition of compost in soil and (ii) quantify with the model the kinetics of three different ^{14}C-labeled PAH (phenanthrene, PHE, fluoranthene, FLT and benzo(a)pyrene, BAP) from experimental data of soil amended with three different composts.

3. Modeling

3.1. Model description

3.1.1. General structure

The PAH model is made of 3 modules: PAH biodegradation/adsorption module, OC module and PAH release module. The structure of the PAH biodegradation/adsorption module is based on the model described by Brimo et al. (2016). The specific module of OC dynamic and its interaction with the PAH module were added following the models developped in Lashermes et al. (2013) and Geng et al. (2015) that simulate the interactions between organic matter and organic pollutant dynamic (like PAH) during composting and after compost application in soil. The novelty of our model here is to add a "release" module to simulate the release of PAH from compost into soil during the decomposition of compost.

We used the PAH biodegradation/adsorption module associated to OC module to simulate the fate of PAH dynamic during compost incubation. We used the PAH biodegradation/adsorption module alone to simulated the PAH dynamic in soil without compost and the 3 modules together to simulate the PAH dynamic in soil amended with compost.

In our previous model described in Brimo et al., (2016), the biological and chemical mechanisms controlling PAH behavior in soil are modeled using two sub-modules showed in Figure III.1: the adsorption module and the biodegradation module. The adsorption module is based on bi-phasic first order kinetic model with an initial fast kinetics characterized by weak sorption (PAH_{WS}, where "ws" refers to weakly sorbed), and a slower kinetics with strong sorption (PAH_{SS}, where "ss" refers to strongly sorbed). The biodegradation module assumes that biodegradation uses only the soluble PAH (PAH_{AV}, where "av" refers to available) with specific degradation pathways from a specific microbial biomass (B_{SPE}) whose growth and maintenance is described by the Monod equation (dotted lines for the biodegradation module in Figure III.1 and co-metabolic degradation pathways modeled using a second order kinetic

from the microbial biomass degrading the compost (X_{cp}) (dashed lines in Figure III.1). Degradation of PAH produces CO_2 emission (PAH_{CO2}), metabolites (PAH_{MET}), and biogenic non-extractible residues (PAH_{Bs}). The influence of temperature and water content on biological processes is taken into account using the correction factors f_T and f_W for temperature and water content respectively (see Table SI III.1 in Supporting Information).

The OC dynamic module was based on the module proposed by Lashermes et al. (2013) and Geng et al. (2015) which describes organic matter transformations during composting and during the compost decomposition in soil, respectively. The organic carbon in compost was divided into several pools measured using the Van Soest fractionation method (Van Soest and Wine, 1967) and characterized by their specific degradability. All organic pools are hydrolysed into available substrates (DOC) for growth of compost degrading microbial biomass (X_{cp}) according to their specific hydrolysis constants. The micro-organisms die at a specific death rate and dead cells are recycled into either the compost organic compartment SND_{slow} (with slow degradation rate) or directly into the compartment DOC. Humified organic C (HOC) was assumed to be derived from dead microbial biomass to simulate "Soil" condition, while for "compost" condition this part of the model is not activated and the whole dead biomass is recycled. The PAH available in solution PAH_{AV} (calculated in PAH module) can be degraded through co-metabolism by microorganisms X_{cp} that use the compost organic matter as their primary energy source (calculated in the OC module). We assumed that the contribution of PAH_{AV} to X_{cp} growth and maintenance can be neglected because PAH_{AV} has low concentrations compared to the total quantity of organic carbon substrates of compost. The evolution of microbial biomass in a soil-compost mixture system is essentially driven by the decomposition of fresh organic matter added with the compost.

A new PAH Release module was developed in this work to describe the release of PAH contained in compost during the decomposition of the applied compost in soil. This module is used only for amended soil simulations and not for compost incubation. The PAH_{CPWS} (where "cpws" refers to PAHs that is weakly sorbed onto organic carbon pools of compost) is subject to dual processes (Figure III.1). We assumed that PAH are distributed among the OC fractions proportionally to the relative mass of each fraction. One fraction of PAH moves into soil solution (PAH_{AV}), with the hydrolysis of organic pools of compost to become an available substrate for microorganisms (Processes XI, XII, XIII, XIV, XV in Table SI III.1). We assume that the releasing rates of PAH into the solution are proportional to the hydrolysis of compost pool they belong as PAH are closely associated with organic carbon pools of compost. For simplicity, we assumed the irreversibility of this process. The other fraction of

PAH becomes much more strongly sorbed on surface of soil-compost mixture (process IV in Table SI III.1) and goes directly from PAH_{CPWS} of compost compartment into PAH_{SS} soil compartment. This process was simulated because experimental results described below showed from some treatments high bound residues formation in spite of low organic matter decomposition and then low PAH release by hydrolysis.

The releasing rate of PAH_{CPWS} (µg/kg_{ds}) added with compost as function of the organic pools hydrolysis kinetics is calculated using equation III.1:

$$\frac{dPAH_{CPWS}}{dt} = \sum_{i=1}^{i=5}\left[\frac{\left(k_{Ci}C_{i,t} \quad fr_{i,t}\right) f_{Ci}}{\sum_{i=1}^{i=5} C_{i,t}} PAH_{CPWS}\right] \quad k_{CS}PAH_{CPWS} \qquad \text{(III.1)}$$

$C_{i,t}$ is the carbon mass concentration of organic pool i of the applied compost at time t as defined in Table SI III.3 with (C_1=SDN_{SLOW}, C_2=SDN_{FAST}, C_3=HCEL, C_4=CEL and C_5=LIG) [kg C/kg_{cp} C]; k_{Ci} is the hydrolysis constant of pool Ci in [d^{-1}] (see Table SI III.3); k_{CS} is the first order kinetic constant from PAH_{CPWS} to PAHss compartment [d^{-1}]; f_{Ci} is the lignin content dependence factor proposed by Corbeels et al. (1999) (see Iqbal et al., 2014) and $fr_{i,t}$ is a correction factor defined by :

$$fr_{i,t} = \begin{cases} 0 & \text{when } i \neq 1 \\ w_{CP}\left(1 \quad Y_{SWCP}\right) m_{CP} X_{CP,t} & \text{when } i = 1 \end{cases} \qquad \text{(III.2)}$$

For i=1 (SDN_{SLOW}), the flux of the dead co-metabolic microorganisms that might be recycled into the organic pool C_1 does not contain any PAH anymore.

The microbial biomass X_{cp} degrades the organic matter of the compost, the microbial biomass X_{soil} degrades the soil organic matter and the microbial biomass X_{tot} is the sum of the two previous microbial biomasses. The native microorganisms in soil X_{soil} remained stable across time. We used the organic carbon module (OC) to simulate the dynamics of co-metabolic microbial biomass (X_{cp}) associated with decomposition of composted organic carbon in soil-compost mixture system (to simulate the "Compost" system, $X_{tot} = X_{cp}$, to simulate the "soil" system, $X_{tot} = X_{soil}$ = constant, to simulate the "amended soil" system, $X_{tot} = X_{cp} + X_{soil}$). Only X_{cp} activity is simulated and X_{soil} is considered as a constant.

The mathematical model uses a set of nonlinear ordinary differential equations that are solved numerically within a MATLAB code. All model equations are presented in SI Table SI III.1.

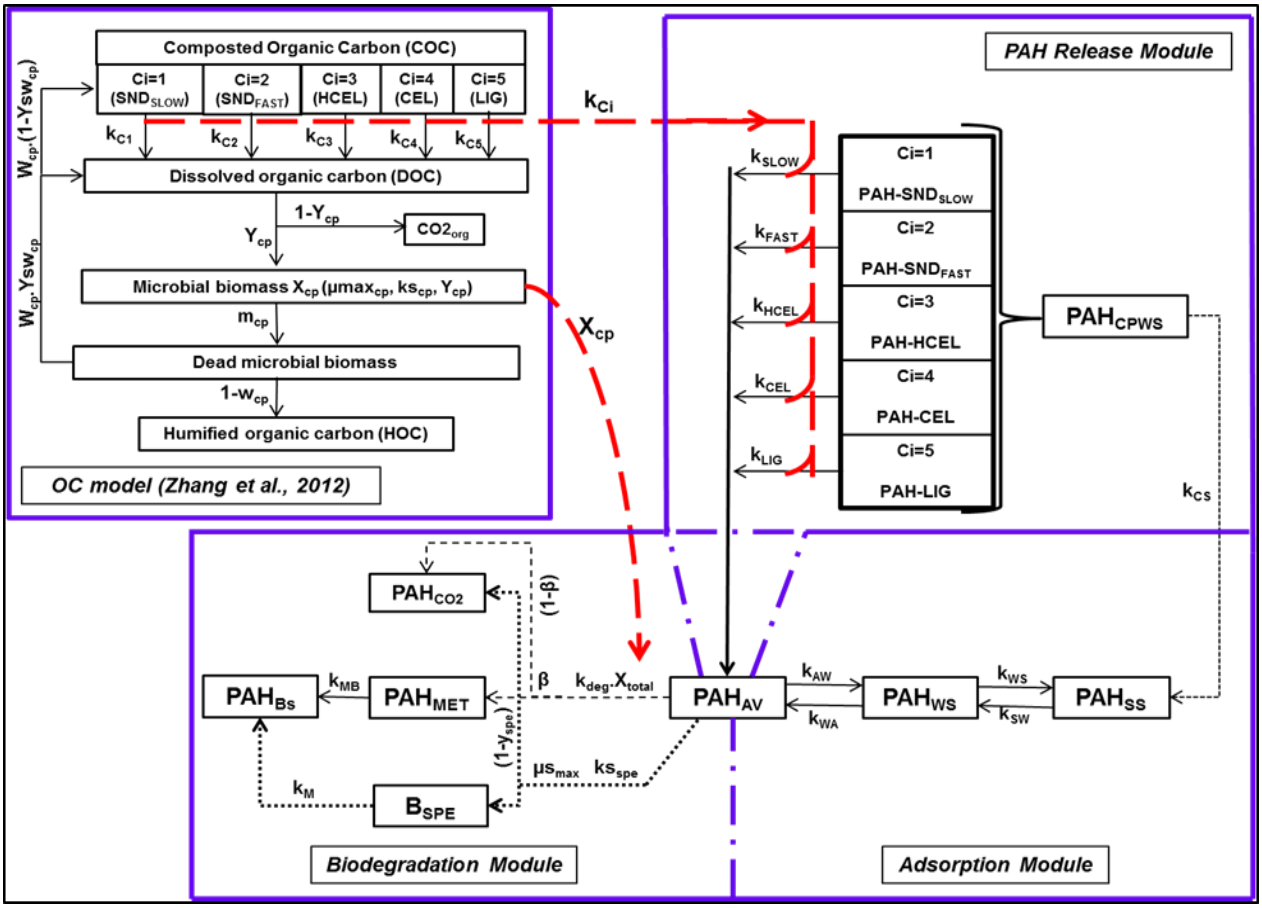

Figure III.1. Diagram of coupling between OC model (in the upper left corner) and the different modules of the PAH model (including PAH release module in the upper right corner and the biodegradation /adsorption modules placed on the left below and the right below corners respectively). Dashed bold arrows indicate the interaction points between modules. k_{ij}: first order kinetic constant with the first subscript denoting the source and the second the sink of the corresponding process (A: PAH_{AV}; B: PAH_{Bs}; C: PAH_{CPWS}; M: PAH_{MET} S: PAH_{SS} and W: PAH_{WS}) (d^{-1}); k_{deg}: kinetic constant of biodegradation for co-metabolism (mg C/kg_{dw}.d), considering that the concentration of the co-metabolism biomass is given by (mg C/kg_{dw}) ; β: magnitude of metabolites production by biodegradation for co-metabolism (between 0 and 1); μs_{max}: maximum specific growth rate (d^{-1}); ks_{spe}: half saturation of growth substrate for the specific biomass (mg C/kg_{dw}); Y_{spe}: yield of specific biomass (-); k_M: mortality rate constant (d^{-1})

Table SI III.1. PAH model equations described by Petersen matrix (Russell, 2006)*

Process \ Variable			PAH_{AV}	PAH_{CPWS}	PAH_{CO2}	PAH_{MET}	PAH_{WS}	PAH_{SS}	B_{SPE}	PAH_{Bs}	Rate (kg C/kg_{dw}/d)
I	Weak sorption	sorption	-1				1				$k_{AW}.PAH_{AV}$
II		desorption	1				-1				$k_{WA}.PAH_{AV}$
III	Strong sorption	Sorption reversible					-1	1			$k_{WS}.PAH_{SS}$
IV		Sorption irreversible		-1				1			$k_{CS}.PAH_{CPWS}$
V		Desorption reversible					1	-1			$k_{SW}.PAH_{SS}$
VII	Substrate uptake by co-metabolism		$-X_{total}$		$(1-\beta).X_{total}$	$\beta.X_{total}$					$k_{deg}.PAH_{AV}.f_T.f_W$
VIII	Growth of specific biomass		$\frac{-1}{Y_{spe}}$		$\frac{(1-Y_{spe})}{Y_{spe}}$				1		$\frac{\mu s_{max}.PAH_{AV}}{ks_{spe}+PAH_{AV}}.B_{SPE}.f_T.f_W$
IX	Biogenic NER production	Metabolites transformation				-1				1	$k_{MB}.PAH_{MET}$
X		Specific biomass mortality							-1	1	$k_m.B_{SPE}$
XI	Hydrolysis	$C_1 = SDN_{SLOW}$ $PAH - SDN_{SLOW}$	1	-1							$\frac{(k_{SLOW}.C_{SLOW}-fr_{i,t}).f_{Ci}}{\sum_{i=1}^{i=5}C_i}.PAH_{CPWS}$
XII		$C_2 = SDN_{FAST}$ $PAH - SDN_{FAST}$	1	-1							$\frac{(k_{FAST}.C_{FAST}-fr_{i,t}).f_{Ci}}{\sum_{i=1}^{i=5}C_i}.PAH_{CPWS}$
XIII		$C_3 = HCEL$ $PAH - HCEL$	1	-1							$\frac{(k_{HCEL}.C_{HCEL}-fr_{i,t}).f_{Ci}}{\sum_{i=1}^{i=5}C_i}.PAH_{CPWS}$
XIV		$C_4 = CEL$ $PAH - CEL$	1	-1							$\frac{(k_{CEL}.C_{CEL}-fr_{i,t}).f_{Ci}}{\sum_{i=1}^{i=5}C_i}.PAH_{CPWS}$
XV		$C_5 = LIG$ $PAH - LIG$	1	-1							$\frac{(k_{LIG}.C_{LIG}-fr_{i,t}).f_{Ci}}{\sum_{i=1}^{i=5}C_i}.PAH_{CPWS}$

*f_T: Temperature dependence factor(-); f_W, water content dependence factor (-); f_{Ci}, the lignin content dependence factor $fr_{i,t}$, correction factor given by equation (III.2)

3.2. Experimental data (From Verge-Leviel, 2001)

The impact of origin and characteristics of compost on PAH dynamics in soil was assessed experimentally by Verge-Leviel (2001). These data are used here to calibrate the PAH model. Three types of incubation containing the PAH have been done (Figure III.2a):

❶ Incubations of composts spiked with PAH: to stabilize PAH in compost before its addition to soil and then to create conditions closer to reality

❷ Incubations of soil amended with PAH in compost: to study the effect of compost type on PAH fate in soil

❸ Incubation of soil spiked directly with PAH: as a control to see the effect of the stabilization of PAHs in the compost compared to its direct addition in soil

3.2.1. Soil and composts

A silt loam soil was collected from the upper horizon of an agricultural experimental farm located at Palaiseau, near Paris (91, France). Ten sub-samples were collected and mixed to obtain a homogeneous representative composite sample. The soil was sieved at 5 mm and stored fresh at 4 °C before use. Its main characteristics were (g/kg_{dw}): clay, 187; silt, 756; sand, 57; organic C content, 11.9. The soil pH in water was 5.5.

The experiments were performed with three composts sampled from Veolia composting plants in France during the maturation phase: green waste and sludge compost (GWS), biowaste compost (BioW) and municipal solid waste compost (MSW). The main characteristics of these composts are detailed in Houot et al. (2012). Composts were sieved at 5 mm.

3.2.2. Incubations setup

The following ^{14}C-PAH were used: [9C-ring-14C] phenanthrene (PHE; 1459 MBq/mmol; > 98 % purity), [3C-ring-14C] fluoranthene (FLT; 1665 MBq/mmol; 98 % purity) and [7C-ring-14C] benzo(a)pyrene (BAP; 984 MBq/mmol; > 98 % purity). ^{14}C-labeled and non-labeled PAH were purchased from Sigma (St. Quentin Fallavier, France). Solutions of the labeled pollutants were first prepared in methanol. The radioactivity of the prepared solutions was 29.899, 34.481 and 47.709 MBq/L for PHE, FLT and BAP respectively. The final concentrations were adjusted with non-labelled PAH at 13 mg/L for each PAH.

Incubation experiments were performed as follows. Hundred µL of each ^{14}C-PAH solution were added to 1 g_{fw} of compost in 100 mL glass jars. The closed jars were then pre-incubated for 28 days at 28 °C. On the 28th day, 20 g_{fw} soil (water content equivalent to pF=2.5) were

added and the incubation of the soil-compost mixtures (20:1) were carried out for 55 additional days at 28 °C (series 2 in Figure III.2a). Control incubations containing only ^{14}C-PAH solution with compost or soil were run simultaneously under the same conditions for 83 days (series 1 and 3 in Figure III.2a). All experiments were run in triplicates.

3.2.3. Analysis (See SI for details)

The C-CO_{2org} and ^{14}C-CO_2 from the mineralization of the total organic carbon and ^{14}C-PAH respectively, were periodically measured at days 3, 7, 10, 14, 21, 28, 31, 36, 41, 47, 54, 61, 67, 74 and 83. The distribution of ^{14}C-PAH among the metabolites, parent pollutant extractible and the non-extractible and mineralized fractions was assessed on the days 28 and 83 for each incubation.

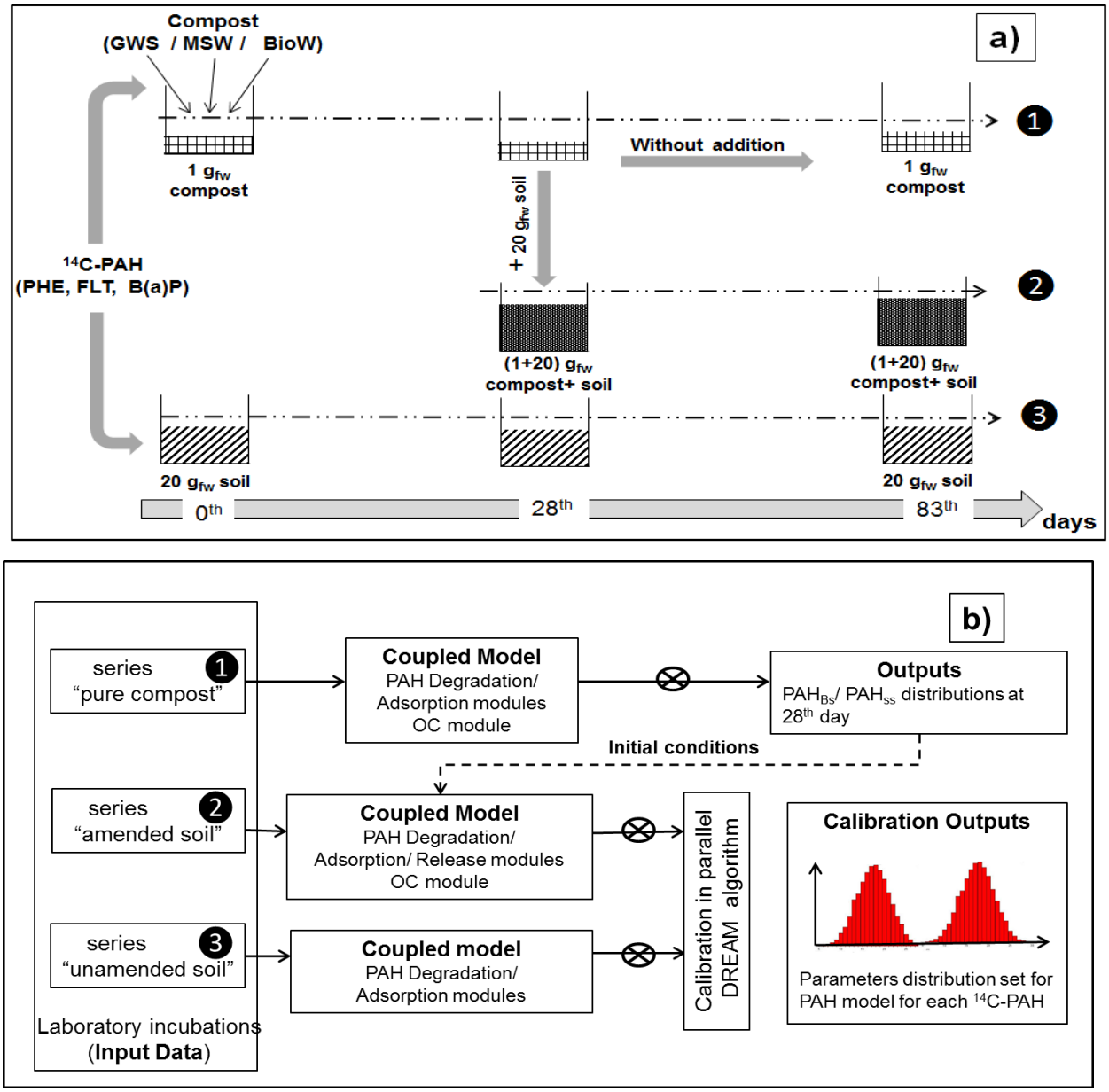

Figure III.2. (a) Schematic design of incubation experiments over 83 days. Three incubations series: ❶ pure compost; ❷ soil-compost mixtures; ❸ control unamended soil. For each of the first and second incubations, three different composts were incubated independently: GWS, MSW and BioW. Each incubation was performed with each of the labeled pollutants (PHE, FLT and BAP). All incubations were run in triplicates. (b) Schematic overview of the modeling methodology. 83 days of simulation of the data in series ❶ (3 treatments corresponding to 3 composts) for determining the mass ratio between the biogenic, PAH_{Bs}, and the physical, PAH_{ss}, non-extractible residues at 28th incubation day, being the initial day of the incubations of compost-soil mixtures. Run the model simultaneously in calibration mode over 55 days and 83 days, using respectively the data of series ❷ (3 treatments corresponding to 3 amended soils) and the data of series ❸ (control unamended soil), to determine the parameters distribution set of PAH model for each PAH.

Supporting Information (SI) 1. Analysis during compost and soil/compost incubations

The $C\text{-}CO_{2org}$ and $^{14}C\text{-}CO_2$ from the mineralization of the total organic carbon and ^{14}C-PAH respectively, were trapped in 10 mL of NaOH (0.1 N) which was periodically sampled and replaced at days 3, 7, 10, 14, 21, 28, 31, 36, 41, 47, 54, 61, 67, 74 and 83. The trapped $C\text{-}CO_{2org}$ was analyzed by colorimetric continuous flow analyser (Skalar, Breda, Netherland) whereas $^{14}C\text{-}CO_2$ was measured by liquid scintillation counting on 0.5 mL aliquots of NaOH after adding 4 mL of scintillation liquid (Ultimagold XR, Packard, USA).

The distribution of ^{14}C-PAH among the extractible and non-extractible fractions was assessed on days 28 and 83. The overall incubated samples (equivalent to 1 g_{fw} of compost for 21 g_{fw} of soil-compost mixtures or 20 g_{fw} of soil) were first removed and placed in Corex glass centrifuged tubes (25 mL for samples equivalents to 1 g_{fw} or 150 mL for 20 g_{fw}). Extraction was performed with 10 mL or 100 mL of methanol for 24 h (end-over-end shaker, 20 °C), followed by centrifugation at 5000 g for 15 min to recover supernatants. The ^{14}C-PAH activity in the supernatants was quantified by liquid scintillation counting. Three successive methanol extractions were conducted. After the 3rd extraction, the three methanol extracts were pooled and concentrated by evaporation and filtered at 0.45 µm. Distributions of the ^{14}C extractible fractions between parent molecule and its metabolites were assessed using HPLC (Nova-Pack C18 (4.6 x 250 mm) equipped with a radioactive flow detector (Radiomatic Flo-One Bêta A-500, Packard). The mobile phase for PHE and FLT: 60:40 (v/v) methanol/water (held for 10 min), increasing to 100 % methanol over a 10 min period and held for 5 min, whereas for BAP: 60:40 (v/v) methanol/water, increasing to 100 % methanol over a 8 min period and held for 17 min.

After extractions, samples containing non-extractible ^{14}C-PAH residues were dried at ambient temperature. Their radioactivity content was measured by combustion in an Oxidizer 307 (Packard, USA) and trapping of $^{14}C\text{-}CO_2$ with Carbosorb and mixing with Permaflour prior to liquid scintillation counting.

3.2.4. Experimental data handling

Assuming the mineralized fraction was precisely measured compare to the measured extractable and non-extractable fractions, the yiel of the three fractions were adjusted to 100% recovery by applying a weight distribution error on the metabolites, parent extractible and non-extractible fractions at each of the two extraction times. To assess the suitability of raw data for the modeling purpose, a two factor analysis of variance (ANOVA) with replication was performed to verify whether a significant difference existed between the four treatments

(i.e. the 3 different compost + soil, besides to the control soil without amendment) across both days and the type of analyzed fraction on the dissipation of labeled ^{14}C-PAH through soil-compost mixtures system.

The model parameters were fitted to the experimental fractions. The measured mineralized fraction was assigned to the simulated PAH_{CO2}, the metabolites extractible fraction corresponded to the simulated PAH_{MET}, whereas the non-extractible fraction corresponded to the three model compartments pooled together: B_{SPE}, PAH_{Bs} and PAH_{ss}. The extractible fraction of the parent compound in soil-compost mixtures system corresponded to three model variables pooled together: PAH_{AV}, PAH_{WS}, PAH_{CPWS}. The initial soil microbial biomass, X_{soil}, was taken equal to 244 mg C/kg_{dw} as reported by Chalhoub et al. (2013) for similar soil.

Supporting Information (SI) 2. Adsorption coefficients

The amount of compounds in soil solution, PAH_{AV}, was estimated using the sorption distribution coefficient Kd as following:

$$K_d(L/kg_{dw}) = \frac{EXT_{parent}(kg/kg_{dw})}{PAH_{AV}(kg/L)} \quad (III.SI.1)$$

The values of Kd of the three labeled ^{14}C-PAH for the different treatments through series 1 and 3 were experimentally determined by sorption batch experiments from Verge-Leviel (2001), whereas the sorption distribution coefficients in soil-compost mixtures system, $Kd_{mixture}$, were calculated as:

$$K_{d_{mixture}} = K_{OC_{mixture}} f_{OC,t} \quad (III.SI.2)$$

Where $f_{OC,t}$ (kg C/kg_{dw}) was the organic carbon content in soil-compost mixtures system, accounting for the reducing of organic carbon content across time t due to the mineralization and can be expressed as:

$$f_{OC,t} = \frac{f_{OC,s,t}W_s + f_{OC,cp,t}W_{cp}}{W_s} \quad (III.SI.3)$$

W_{cp}, W_s were the dry weight of compost and soil respectively in (kg_{dw}); $f_{OC,cp,t}$ and $f_{OC,s,t}$ were the organic carbon contents in compost and soil respectively at time step t in (kg C/kg_{dw}).

$K_{OC,mixture}$, in (L/kg C), was the sorption distribution coefficient normalized to organic content f_{OC}, and was derived as follows:

$$K_{OC_{mixture}} = \frac{K_{OCcp} f_{OCcp,0} W_{cp} + K_{OCs} f_{OCs,0} W_s}{f_{OCcp,0} W_{cp} + f_{OCs,0} W_s} \quad (III.SI\ 4)$$

Where, $f_{OC,cp,0}$ and $f_{OC,s,0}$ were the initial organic carbon contents in compost and soil respectively (kg C/kg_{dw}) before applying compost onto soil; K_{OCcp}, K_{OCs} were the sorption distribution coefficients normalized to organic content for the labeled ^{14}C-PAH in compost and soil respectively. The values of $K_{OCcp,}$ K_{OCs} and $K_{OCmixture}$ for each labeled ^{14}C-PAH for the different treatments are summarized in Table SI III.2.

Table SI III.2. K_{OC} measured and calculated for soil, composts and soil-compost mixtures

^{14}C-PAH	Incubation series number	Treatment	Log K_{OC} Measured L/kg C	Log $K_{OC,\ mixture}$ Calculated L/kg C
Phenanthrene	Series 1	GWS	4.38	
	Series 1	BioW	4.23	
	Series 1	MSW	4.01	
	Series 3	Soil Control	4.33	
	Series 2	GWS + Soil		4.35
	Series 2	BioW + Soil		4.30
	Series 2	MSW + Soil		4.23
Fluoranthene	Series 1	GWS	4.31	
	Series 1	BioW	4.36	
	Series 1	MSW	3.99	
	Series 3	Soil control	4.76	
	Series 2	GWS + Soil		4.62
	Series 2	BioW + Soil		4.68
	Series 2	MSW + Soil		4.59
Benzo(a)pyrene	Series 1	GWS	4.79	
	Series 1	BioW	4.62	
	Series 1	MSW	4.75	
	Series 3	Soil Control	6.49	
	Series 2	GWS + Soil		6.26
	Series 2	BioW + Soil		6.35
	Series 2	MSW + Soil		6.25

* K_{OC} values were determined by sorption batch experiments by Verge-Leviel (2001), whereas $K_{OC,\ mixture}$ values were calculated by applying the equation (III.SI.4)

3.3. Modeling methodology

While the two first runs 1 and 2 were conducted with OC model alone, the two others runs 3 and 4 were implemented with PAH model coupled to OC model. The runs of modelling 1 and 3 were carried out to simulate the compost incubations in order to calculate at 28 days, the amount and distribution of non-extractable PAH between biogenic and strongly sorbed fractions (PAH_{Bs} and PAH_{ss}, respectively) that were not available from the experiments. The two runs of modelling 2 and 4 were used to estimate a set of parameters able to simulate all the treatments of soil-compost mixtures for each PAH. In run 3 of soil amended with composts, the initial data of PAH compartments was obtained from the experimental data

obtained at 28th days of the compost experiments. The four groups of runs were carried out sequentially as summarized in Table III.1.

Table III.1. The **calibration** procedures

# Run	Data set	Objectives
N° 1 OC Model In compost 3 composts	CO2 mineralized Figure III.2, serie ❶	Calibration of OC model parameters to be used by run **N° 3** Table SI III.3 and Figure III.3a,b
N° 2 OC Model In soil-compost mixture 3 composts	CO2 mineralized Figure III.2, serie ❷	Calibration of OC model parameters to be used by run **N° 4** Table SI III.3 and Figure III.3c,d
N° 3 Coupling model OC×PAH In compost **3** composts × 3 PAH	^{14}C-CO_2 mineralized ^{14}C-PAH fractions Figure III.2, serie ❶	Determining the ratio between biogenic NER PAH_{BS} and strongly sorbed PAH_{SS} at 28^{th} day of compost incubations / initial time of soil-compost incubations run **N° 4** Table III.3 and Figure SI III.1
N° 4 Coupling model OC× PAH In soil-compost mixture In soil control 3 composts × 3 PAH 1 sol× 3 PAH	^{14}C-CO_2 mineralized ^{14}C-PAH fractions Figure III.2, serie ❷ ^{14}C-PAH fractions Figure III.2, serie ❸	Get 1 set of parameters able to simulate each PAH for the 3 composts-soil mixtures and soil control Table III.3 and Figure III.4

In run 4, the algorithm DREAM (Vrugt, 2016) was inserted in the code of the coupled model and used for estimating the probability density functions of PAH model parameters in soil (see more details in Brimo et al., 2016). The parameter ranges required by DREAM as prior parameters distributions were chosen based on literature survey and further adjusted using step trial and error strategy. Each run included a maximum total of 5000 model simulations, and only the best 50% of the simulations were chosen (see Brimo et al. (2016)) and used to build the histograms of probability density functions of the model parameter values. Nash Sutcliffe index (Nash and Sutcliffe, 1970) was calculated for the quantitative evaluation of the model accuracy.

4. Results and discussion

4.1. Calibration of OC model for control compost and amended soil

The OC model was not able to simulate correctly the experimental mineralized carbon using the parameters of Geng et al (2015). Therefore, the OC model required parameter calibration prior to use (Table SI III.3). We chose to re-optimize the hydrolysis rates of cellulose (CEL)

and hemicellulose (HCEL) pools in such a way that k_{CEL} is equal to k_{HCEL} because Iqbal et al. (2014) found that the CEL and HCEL organic pools have similar decomposition rates. The calibration of OC yielded an estimated value of 0.03 d^{-1} for both parameters k_{CEL} and k_{HCEL} model in pure composts and quite similar value of 0.02 d^{-1} in amended soil. The updated values of k_{CEL}, k_{HCEL} obtained through this study were very close to that reported by Iqbal et al. (2014) of 0.028 $d^{-1}$for crop residue decomposition in soil. Zhang et al. (2012) reported that the soluble organic pool would have very different characteristics in the fast pool (SDN_{fast}), and the slow pool (SDN_{slow}) depending on the origin of compost. Consequently, in compost incubation, we chose to re-adjust also the parameter k_{fast} (hydrolysis rate of the fast soluble pool) and found an estimated value of 0.212 d^{-1} for k_{fast}. In amended soil we chose also to fit both parameters linked to microbial biomass, the mortality rate and the proportion of recycling dead microbial biomass (m_{cp}, and w_{cp} respectively) because Zhang et al.(2012) found that the organic mineralized fraction (CO_{2org}) was very sensitive to the parameters linked to microbial biomass. The calibration in amended soil yielded an estimated value of 0.085 d^{-1} for m_{cp}, and two different estimated values for w_{cp}: 0.1% in GWS and BioW, which also was the same as that obtained by Geng et al., (2015) for GWS treatment, whereas the estimated value with MSW was 99.9%. These results indicated that microbial biomass was recycled in the immature compost MSW treatments while the more stable composts like GWS and BioW led directly to soil humified organic matter. The updated sets of parameters for the OC model are summarized in Table SI III.3. A single set of parameters was found to simulate adequately the dynamics of OC in all composts for each type of incubation in pure composts and amended soils. The evolutions of organic carbon mineralization into CO_2, $CO2_{org}$, and microbial biomass are displayed on Figure III.3. According to this Figure III.3 (a and c), a very good agreement between simulated and experimental data is obtained for CO_{2org} as confirmed by the high Nash Sutcliffe efficiency index of 0.97, 0.84, 0.89 for the treatments MSW, BioW, GWS, respectively, in the pure composts, and of 0.99, 0.98, 0.90 for MSW, BioW, GWS, respectively, in the amended soils. During the initial step of incubations in control composts (Figure III.3 a and b), a rapid mineralization and a significant increase in microbial biomass are observed. At the end of simulation period, the CO_{2org} mineralized in the treatment driven by MSW is 1.7 to 3.8 times higher than that observed in BioW and GWS treatments respectively. The maximum predicted peak for biomass growth is higher in BioW treatment than in MSW and GWS treatments. However, after the maximum peak, the microbial biomass in MSW treatment remains much higher than in BioW and GWS (Figure III.3b). Following compost application in soil (Figure III.3 c and d), the dynamics of OC

decomposition for the different treatments in amended soil followed the same order than those previously found in the pure compost incubations but with much higher mineralization and microbial growth in MSW in comparison to the other treatments. This result showed that the MSW compost was not matured when sampled on the composting plants neither after 28 days of incubation alone, compared to the other. These varying behaviors for the different composts during incubations can be attributed to the origin and the maturity degree of the applied compost as reported by Francou et al., (2008), Zhang et al., (2012) and Chalhoub et al., (2014).

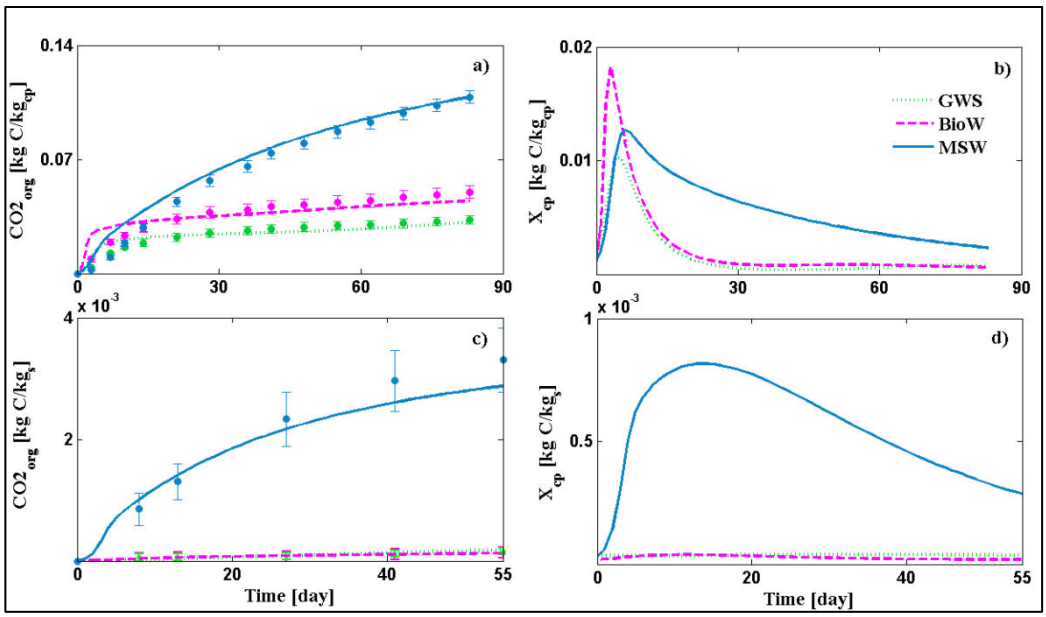

Figure III.3. Experimental (○) and simulated results obtained using the OC model for the three treatments. The figures in the first line are the simulated results obtained during the 83 days of compost incubations, whereas those in the second line are obtained from the incubation of the amended soil during 55 days. a) carbon emission, $CO2_{org}$, b) microbial biomass, X_{cp} c) $CO2_{org}$ emission from the decomposition of compost in the amended soil, d) microbial biomass, X_{cp}. Error bars indicate the standard deviation (3 replicates).

Table SI III.3. The variables and parameters of the OC module for A: incubations of pure compost, B: incubations of compost-soil mixtures

Symbol	Description	Parameter value	Unit
Variables			
$C_{i=1}$=SDN_{SLOW}	Proportion of organic C in the soluble fraction of pH-neutral detergent with slow degradation		kg C/kg_{cp}
$C_{i=2}$=SDN_{FAST}	Proportion of organic C in the soluble fraction of pH-neutral detergent with fast degradation		kg C/kg_{cp}
$C_{i=3}$=HCEL	Hemicelluloses-like fraction		kg C/kg_{cp}
$C_{i=4}$=CEL	Cellulose-like fraction		kg C/kg_{cp}
$C_{i=5}$=LIG	Lignin-like fraction		kg C/kg_{cp}
DOC	Organic C soluble in hot water		kg C/kg_{cp}
X_{cp}	Microbial biomass in native compost		kg C/kg_{cp}
$CO2_{org}$	Organic carbon dioxide		kg C/kg_{cp}
HOC	Humified organic C		kg C/kg_{cp}
Parameters			
A: incubation with compost alone			
k_{SLOW}	Hydrolysis constant of $C_{i=1}$=SDN_{SLOW}	0.0001[a]	d^{-1}
k_{FAST}	Hydrolysis constant of $C_{i=2}$=SDN_{FAST}	**0.0212**[b]	d^{-1}
k_{HCEL}	Hydrolysis constant of $C_{i=3}$=HCEL	**0.0300**[b]	d^{-1}
k_{CEL}	Hydrolysis constant of $C_{i=4}$=CEL	**0.0300**[b]	d^{-1}
k_{LIG}	Hydrolysis constant of $C_{i=5}$=LIG	0.0001[a]	d^{-1}
Y_{cp}	Assimilation yield of organic C available for microbial biomass	0.500[a]	-
μmax_{cp}	Maximal growth rate for microbial biomass	5.9900[a]	d^{-1}
Ks_{cp}	Saturation constant for Monod kinetic	101.07[a]	% of initial TOC[c]
m_{cp}	Death constant for microbial biomass	0.2290[a]	d^{-1}
$Y_{SW\,cp}$	Availability yield for dead microbial biomass	0.4069[a]	-
B: incubation with soil compost mixtures system			
k_{SLOW}	Hydrolysis constant of $C_{i=1}$=SDN_{SLOW}	0.0001[a]	d^{-1}
k_{FAST}	Hydrolysis constant of $C_{i=2}$=SDN_{FAST}	0.0612[a]	d^{-1}
k_{HCEL}	Hydrolysis constant of $C_{i=3}$=HCEL	**0.0200**[b]	d^{-1}
k_{CEL}	Hydrolysis constant of $C_{i=4}$=CEL	**0.0200**[b]	d^{-1}
k_{LIG}	Hydrolysis constant of $C_{i=5}$=LIG	0.0001[a]	d^{-1}
Y_{cp}	Assimilation yield of organic C available for microbial biomass	0.5000[a]	-
μmax_{cp}	Maximal growth rate for microbial biomass	5.9900[a]	d^{-1}
Ks_{cp}	Saturation constant for Monod kinetic	101.07[a]	% of initial TOC[c]
m_{cp}	Death constant for microbial biomass	**0.0850**[b]	d^{-1}
$Y_{SW\,cp}$	Availability yield for dead microbial biomass	0.4069[a]	-
w_{cp}	Proportion of dead biomasses into HOC pool	0.1/ **99.9**[d]	%

[a]The default parameter values were taken from (Geng et al., 2015)
[b]The new parameter values optimized in the present study using the three compost: GSW, MSW and BioW (in bold text)
[c] TOC: total organic carbon
[d] The w_{cp} value of 0.1% for GWS and BioW , whereas a value of 99.9 % for MSW

4.2. Simulation of PAH fractions in compost

As previously mentioned, we first predict the dynamics of ^{14}C-PAH during the 83 days of compost incubations but we identified the initial conditions of the compost added to soil at the

28th day. All simulations were carried out using the PAH model coupled to the OC model. The model was calibrated for each compost and each PAH. Table SI III.4 gives the Nash-Sutcliffe efficiency for the extractible PAH, the metabolites, the total non-extractible and the mineralized fractions for each of the three ^{14}C-PAH. The performance of the model to reproduce the experimental measurements was good as confirmed by the Nash Sutcliff efficiency index generally greater than 0.60. Nevertheless, the efficiency of the model to match the experimental data for metabolite fractions measured in MSW treatment was poor with Nash Sutcliff index values of -0.12, -3.09, -0.5 for PHE, FLT and BAP, respectively. The discrepancy between simulations and experiments in MSW treatment was mainly due to the model overestimation of the data at the end of the incubation. The consequences of this discrepancy are discussed later in section 4.4.

The simulated results for the non-extractible residues (PAH_{SS} +PAH_{BS}) and the mineralized fraction (PAH_{CO2}) for each ^{14}C-PAH over all treatments are presented in Figure SI III.1. The amount of CO_2 mineralized increased in the following order: BAP, FLT and PHE because of the higher microbial degradation due to their lower number of benzene rings. We found that the highest mineralization intensity was obtained in the treatments with BioW and GWS composts for all PAH. Lower mineralization was observed in the incubations with MSW compost. These observations are in contrast with results on the organic decomposition of the three composts, where the mineralization was significantly higher for MSW than for GWS and BioW composts. This suggests that the potential amounts of microorganisms degrading the organic pollutants by co-metabolism pathway should have been smaller in the treatment with MSW compost in comparison to GWS and BioW as already mentioned in Houot et al., (2012). We assumed therefore that the biodegradation of the labeled pollutants into ^{14}C-CO_2, PAH_{CO2}, occurred through the pathway driven by specific biomass and not only by the co-metabolism pathway. This assumption is supported by the study of Cerniglia (1997)who reported that composts rich in lignin including ligninolytic fungi can be efficient in the bioremediation of PAH in contaminated wastes. Houot et al. (2012) found higher PAH mineralization in GWS and BioW than in MSW and concludes that the maturation microflora was more efficient than the thermophilic microflora for mineralizing organic pollutants. The PAH mineralization were well simulated in the treatments with BioW and GWS composts when considering both biodegradation pathways. In contrast, regarding the treatment with MSW compost, the model predicted that the mineralized fraction was produced only through the specific biomasses pathway and not from the co-metabolic one. This result was corroborated by the observed initial lag-phases of the mineralized fraction with this treatment.

The percentages of biogenic non-extractible residues, PAH_{BS} (referring to the total non-extractible residues fractions, PAH_{NER}) after 28th day of composting (day where composts were amended into the soil) are given in Table III.2. A low percentage of biogenic non-extractible residues were predicted for FLT and PHE in MSW compost. The model estimated much higher PAH_{BS} for BAP with about 18.7%. We observed that the higher the mineralization rates of ^{14}C-PAH were, the higher the model estimation of the biogenic contribution to the total non-extractible residues was (Figure SI III.1 and Table III.2). These findings are in agreement with results reported in literature about the biogenic bounded residues formation. There are numerous references reporting that microbial activity has a direct and significant effect on the formation of the non-extractible residues for POP (Barriuso et al., 2008; Gevao et al., 2005; Kästner et al., 1999; Nowak et al., 2013). However, the biogenic rates of formation during incubations remain unknown as no chemical analyses were carried out and very little works can be found in literature about the quantification or the modeling of biogenic residues formation during compost incubations or in compost amended soil. Richnow et al. (2000) found for PHE that the contribution of the biogenic fraction to the total non-extractible residues was at least 11% after 50 days of incubation in a batch bioreactor. Kästner et al. (2013) simulated the dynamics of anthracene (PAH with 3 cycles) in non-amended soil and predicted that 50% of non-extractible residues were biogenic after 50 days of simulations.

Table III.2. Distributions between PAHCO2, PAH_{AV}, PAH_{WS} and PAH_{NER} at 28th incubation day for each ^{14}C-PAH incubated with composts (expressed in % of initial amount)

	phenanthrene			fluoranthene			benzo(a)pyrene		
	GWS	**BioW**	**MSW**	**GWS**	**BioW**	**MSW**	**GWS**	**BioW**	**MSW**
PAH_{CO2}	53	52.5	0.1	1.85	37.26	<<1	<<1	<<1	<<1
PAH_{AV}	<<1	<<1	<<1	<<1	0.26	<<1	<<1	<<1	<<1
PAH_{WS}	5.7	6.4	86.9	90.3	32.8	93	42.6	61.6	65.7
PAH_{NER}	32.7	32.9	13	6.4	22.1	6.4	56.9	38.0	30.3
PAH_{ss}*	74.90	75.40	100	94.1	60.7	96.3	100	100	81.3
PAH_{Bs}*	25.10	24.60	<< 1	5.9	39.3	2.9	<< 1	<< 1	18.7

* Distributions between PAH_{Bs} and PAH_{ss} at 28th incubation day for each ^{14}C-PAH incubated with composts (% of PAH_{NER})

Table SI III.4. Nash Sutcliff values for PAH model simulations efficiency for the simulations performed in control composts

Treatment	^{14}C-PAH fraction	^{14}C-PAH		
		phenanthrene	**fluoranthene**	**benzo(a)pyrene**
GWS (control compost)	Extractible fraction PAH_{CPWS}	0.89	0.91	0.85
	Non-extractible fraction PAH_{SS}+PAH_{Bs}	0.90	0.76	0.99
	Metabolites PAH_{MET}	0.90	0.87	0.99
	Mineralized fraction PAH_{CO2}	0.92	0.98	0.75
BioW (control compost)	Extractible fraction PAH_{CPWS}	0.98	0.97	0.999
	Non-extractible fraction PAH_{SS}+PAH_{Bs}	0.78	0.91	0.99
	Metabolites PAH_{MET}	0.98	0.90	0.99
	Mineralized fraction PAH_{CO2}	0.97	0.98	0.85
MSW (control compost)	Extractible fraction PAH_{CPWS}	0.87	0.96	0.99
	Non-extractible fraction PAH_{SS}+PAH_{Bs}	0.78	0.99	0.97
	Metabolites PAH_{MET}	-0.12	-3.09	-0.5
	Mineralized fraction PAH_{CO2}	0.65	0.635	0.826

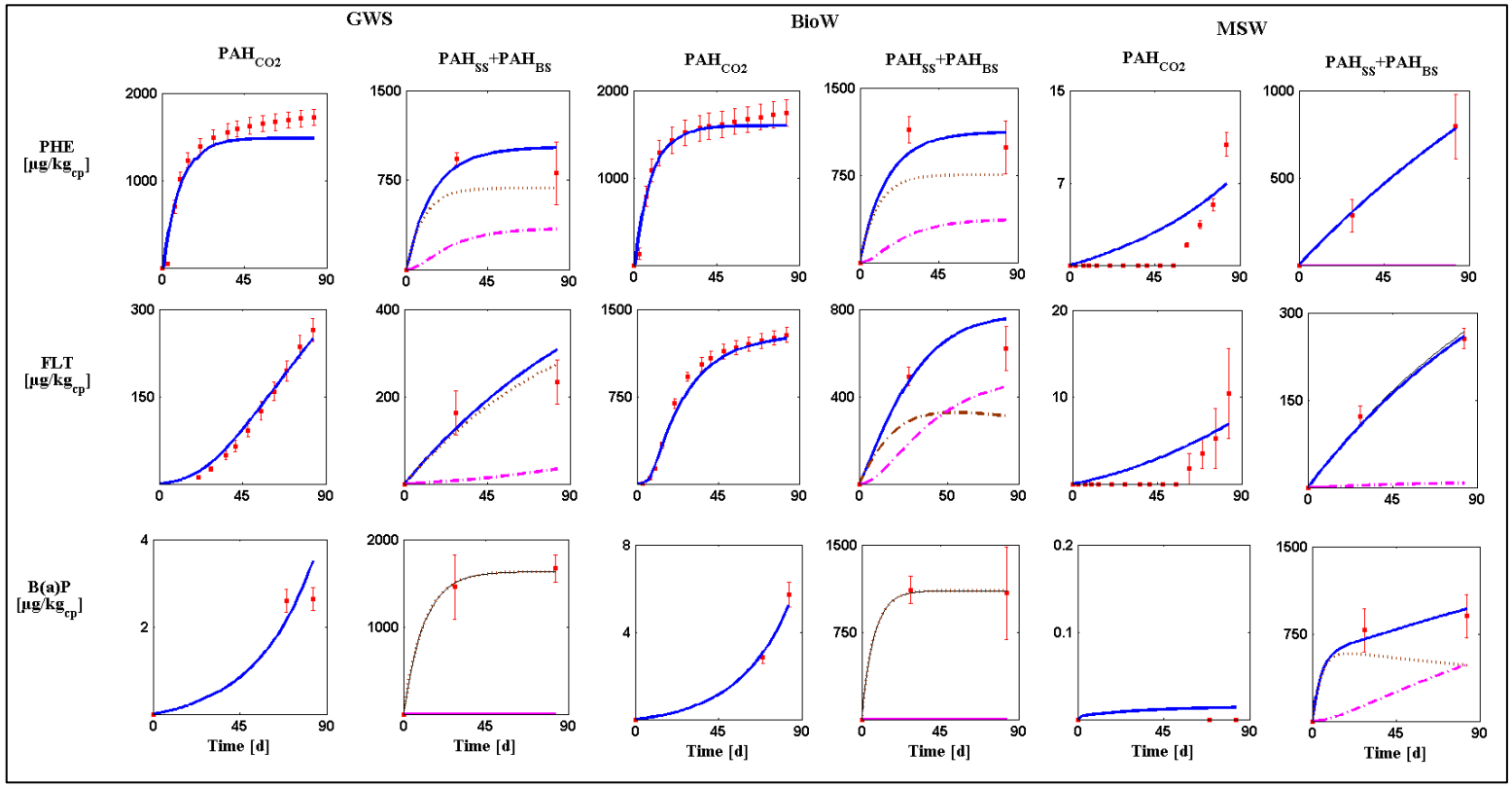

Figure SI III.1. Simulation of ^{14}C-PAH in control composts. Pane line up in (3x6) matrix, where the three rows define the three ^{14}C-PAH: PHE, FLT, and BAP respectively. Simulation results are marked in lines, whereas the experimental data are represented by dots. Error bars indicate the standard deviation (3 replicates). The panels entitled "PAH$_{SS}$+PAH$_{BS}$" include the total simulated non-extractible fraction (in soild line, blue), the simulated strongly sorbed (in pointed line, brown) and the simulated biogenic NER (in pointed dashed line, violet). All data are given in µg/kg$_{cp}$ (dry weight).

4.3. Simulation of PAH fractions in amended soils

The PAH model coupled with DREAM algorithm was run in order to determine the best set of model parameter values for soil-compost incubations for each PAH. The initial conditions were obtained from the ^{14}C-PAH distribution between biogenic and strongly sorbed fractions at the 28th day of pure compost incubations. The best set of model parameters was the one that simulated as accurately as possible the observed data recorded for one pollutant for the amended soil with the three different composts and the unamended soil treatments (Table III.3). A single parameters set for all compost types was found to simulate the dynamics of PHE and BAP independently. However, such single parameter set could not be determined for FLT where different values were found for the parameter K_{cs} (rate of strongly sorbed compartment formation from compost PAH) and μ_{max} (maximum growth rate of specific biomass).

4.3.1. Performance of the model

Two Nash Sutcliff efficiency index (NS) values were calculated for each ^{14}C-PAH and each treatment (Table III.4). While the first one, NS_{global}, was used to evaluate the goodness of fit for all model variables together, the second one, NS_{CO2}, accounted for the goodness of fit for the mineralised variable PAH_{CO2} alone. In general, the overall performance demonstrated good ability of the model to describe the observed PAH transformation in soil, as confirmed by the relatively high NS_{global} values that were above 0.75 for most of the simulation situations. The performance of the model to simulate the mineralised fractions was generally good and NS_{CO2} values close to 1 for many simulations. Still, for some situations, a poor performance was achieved like with BAP for unamended soil (NS_{CO2}=0.28) or with FLT for biowaste (NS_{CO2}=0.01). Indeed, the simulated curves were obtained using a unique parameter set that corresponded to the best compromise over the whole treatments, thus resulting in high discrepancies for some cases.

Table III.3. Optimal values and confidence intervals (CI) of PAH model parameters obtained with DREAM for the three ^{14}C-PAH in amended soils

Par	Unit	Phenanthrene		Fluoranthene		Benzo(a)pyrene	
		Optimum	95% CI	Optimum	95% CI	Optimum	95% CI
k_{AW}	d^{-1}	1.770	[0.484, 3.865]	26.428	[1.44, 28.06]	24.810	[15.04, 28.15]
k_{WA}	d^{-1}	0.230	[0.079, 0.238]	0.932	[0.0124, 0.94]	0.218	[0.075, 0.354]
k_{WS}	d^{-1}	0.065	[0.030, 0.10]	0.021	[0.021, 0.114]	0.029	[0.0274, 0.036]
k_{SW}	d^{-1}	0.032	[0.027, 0.045]	0.042	[0.037, 0.199]	0.007	[0.005, 0.012]
k_{MB}	d^{-1}	0.037	[0.037, 0.149]	0.065	[0.017, 0.096]	0.138	[0.079, 0.184]
k_{CS}	d^{-1}	0.238	[0.10, 0.570]	0.002[a] 0.016[b] 0.06[c]	[$5x10^{-4}$, $2x10^{-2}$]	$6x10^{-4}$	[$1x10^{-4}$, $1x10^{-3}$]
k_{deg}	mg C/kg_{dw}.d	$2.7x10^{-3}$	[$2x10^{-3}$, $2x10^{-2}$]	$2.2x10^{-4}$	[$1x10^{-2}$, $2 x10^{-3}$]	$1.7x10^{-4}$	[$6x10^{-5}$, $3x10^{-4}$]
β	-	0.478	[0.385, 0.498]	0.59	[0.445, 0.597]	0.59	[0.356, 0.597]
μs_{max}	d^{-1}	2.606	[1.786, 11.29]	8.423[d] 0.54[e]	[0.394, 11.237]	0.908	[0.227, 1.685]
ks_{spe}	$\mu g\ ^{14}C/kg_{dw}$	36.627	[25.52, 71.26]	12.133	[3.82, 73.3]	46.256	[16.65, 58.56]
Y_{spe}	-	0.251	[0.13, 0.275]	0.274	[0.112, 0.289]	0.166	[0.124, 0.246]
k_M	d^{-1}	0.035	[0.005, 0.088]	0.043	[0.0044, 0.0897]	0.018	[0.015, 0.087]

[a, b, c]Optimum values for k_{CS} for the amended soil with GWS, BioW, MSW respectively.

[d]Optimum value for μs_{max} for the amended soil with GWS and BioW.

[e]Optimum value for μs_{max} for the amended soil with MSW.

Table III.4. Nash Sutcliff index values calculated in soils for CO_2 alone and for all compartments together

Treatment	Phenanthrene		Fluoranthene		Benzo(a)pyrene	
	NS_{global}	NS_{CO2}	NS_{global}	NS_{CO2}	NS_{global}	NS_{CO2}
GWS	0.98	0.78	0.99	0.99	0.9	0.84
BioW	0.97	0.60	0.75	0.01	0.99	0.99
MSW	0.95	0.92	0.98	0.88	0.99	0.98
Unamended soil	0.98	0.95	0.99	0.96	0.99	0.28

4.3.2. Comparison between experimental and simulated results

The observed and simulated dynamics of the three PAH in the soil amended with the three composts and in the unamended soil are presented in Figure III.4, SI.2, SI.3. These results could be explained by i) the physiochemical properties of the PAH, ii) the initial amount and distribution of PAH in compost fractions and iii) the degradability of the composts.

As already observed in compost (section 4.2), the amount of CO_2 mineralised for BAP and FLT was much lower than CO_2 mineralised for PHE because their higher number of benzene rings compare to PHE more difficult to degrade by microorganisms. For PHE, a decrease in the mineralisation was observed in the following order: unamended soil > MSW > BioW = GWS. Similar orders were obtained for BAP but for FLT a higher mineralisation was obtained with BioW treatment in comparison to the three others but with no significant difference. For BAP and PHE, the total amount of PAH brought with MSW was higher than this brought with GWS and BioW because of the low PAH mineralization observed in MSW during composting process. The higher microbial growth stimulated by the high decomposition of MSW compare to BioW/GWS (Figure III.3) may enhance degradation by co-metabolism in this compost. PHE was localized in adsorbed fractions for unamended soil and MSW and thus was available for microorganisms, while it was initially present mainly in NER fractions of BioW and GWS and thus was less available for microorganisms. Mineralization in unamended soils was higher than in amended soils because the bioavailability of PAH_{AV} in the soil alone was much higher than this of PAH_{AV} coming from the release of PAH from compost PAH_{CPWS} in amended soil. For FLT, we observed higher mineralisation for BioW compared to GWS and MSW although a lower amount was added with BioW. The BioW compost was also the treatments that mineralized more the FLT during composting, as shown in section 4.2. Degradation by specific biomass from BioW may explain this higher mineralisation in this treatment, as explained below.

For PHE and BAP, the results highlighted that the biodegradation of PAH was mainly driven by co-metabolic microbial biomass in compost treatments while PAH degradation was driven by the specific microbial biomass in soil (Figure III.4, SI.2, SI.3 in last columns). For FLT, the model predicted that an important part of the mineralisation fraction was formed through the specific biodegradation pathway for GWS and BIOW. For FLT, because we could not use the same parameters for all treatments and we had to estimate the growth rate of specific microorganisms (μS_{max}) for each treatment as shown in Table III.3. Indeed, Geng et al. (2015) found possible degradation of FLT by specific biomass pathway and Brimo et al. (2016) found that the model output is very sensitive to this parameter. We found higher growth rate of specific microorganisms for BioW compared to MSW. Houot et al. (2012) showed that specific microflora was higher in mature composts and affected FLT mineralisation. Haudin et al. (2013) pointed also the possible involvement of specific biomasses during FLT mineralization in GWS-soil mixtures depending on the latency period (lag phase) observed in the mineralization curves.

NER fraction decreased or stayed constant in most treatments with GWS and BioW and highly increased for MSW and soil treatments. Simulated PAH_{SS} decrease was always accompanied by an increase in PAH_{BS}. The increase of NER in MSW was due to the increase in biogenic NER that was stimulated by the higher microbial biomass growth in this treatment (see Table III.3). Indeed, in the model, microbial activity controls both mineralisation and biogenic NER production (Eq. IX and X in Table SI III.1). The biogenic productions of NER estimated by the model for PHE were in the following order: unamended soil > MSW> BioW > GWS. This order was comparable to the order obtained for the mineralisation of PHE. Similar results were also obtained for FLT but for BAP little biogenic NER production was simulated because the rate of biogenic NER formation from PAH_{MET} (k_{MB}) was much lower for this PAH (see Figure SI III.2, Figure SI III.3, Table III.3). The model predicted that almost 50% and 30% of the total non-extractible residues of PHE and FLT respectively were biogenic at the end of the simulation period (55 days). The difference between PAH pointed out that the biogenic NER production rates were lower for PAH with high number of benzene rings. However, this result of the simulations could not be confirmed by this experiment and additional measurements of the biogenic NER fraction using the recent methods proposed by Nowak et al. (2013) could be used in the future.

The decrease of adsorbed compartments (PAH_{CPWS}+PAH_{WS}) with time was more pronounced in the following order PHE> FLT> BAP due to the increase in hydrophobicity of PAH, which increased adsorption on soil and composts. At the final day, much less PAH was adsorbed for PHE than for FLT and BAP. For each PAH, the decrease of adsorbed fractions was more marked in the following order: Soil> MSW> BioW-GWS. For BAP, we even had an increase of adsorbed compartments in BioW and GWS compartments. The adsorption of hydrophobic contaminant is higher on mature organic matter as shown by Aslam et al. (2013) and was much more marked on amended than on unamended soil. We obtained the inverse order than for mineralization curves where soil and MSW treatments displayed more carbon mineralization. In all treatments, the simulated PAH_{WS} compartment increased at the expense of simulated "compost" compartment (PAH_{CPWS}) that diminished. This effect was more marked for less hydrophobic PAH like PHE. These results were quite well simulated with the model. It was able to simulate the difference between treatments for each PAH using a unique set of parameters except for FLT where two parameters had to be optimized for each treatment.

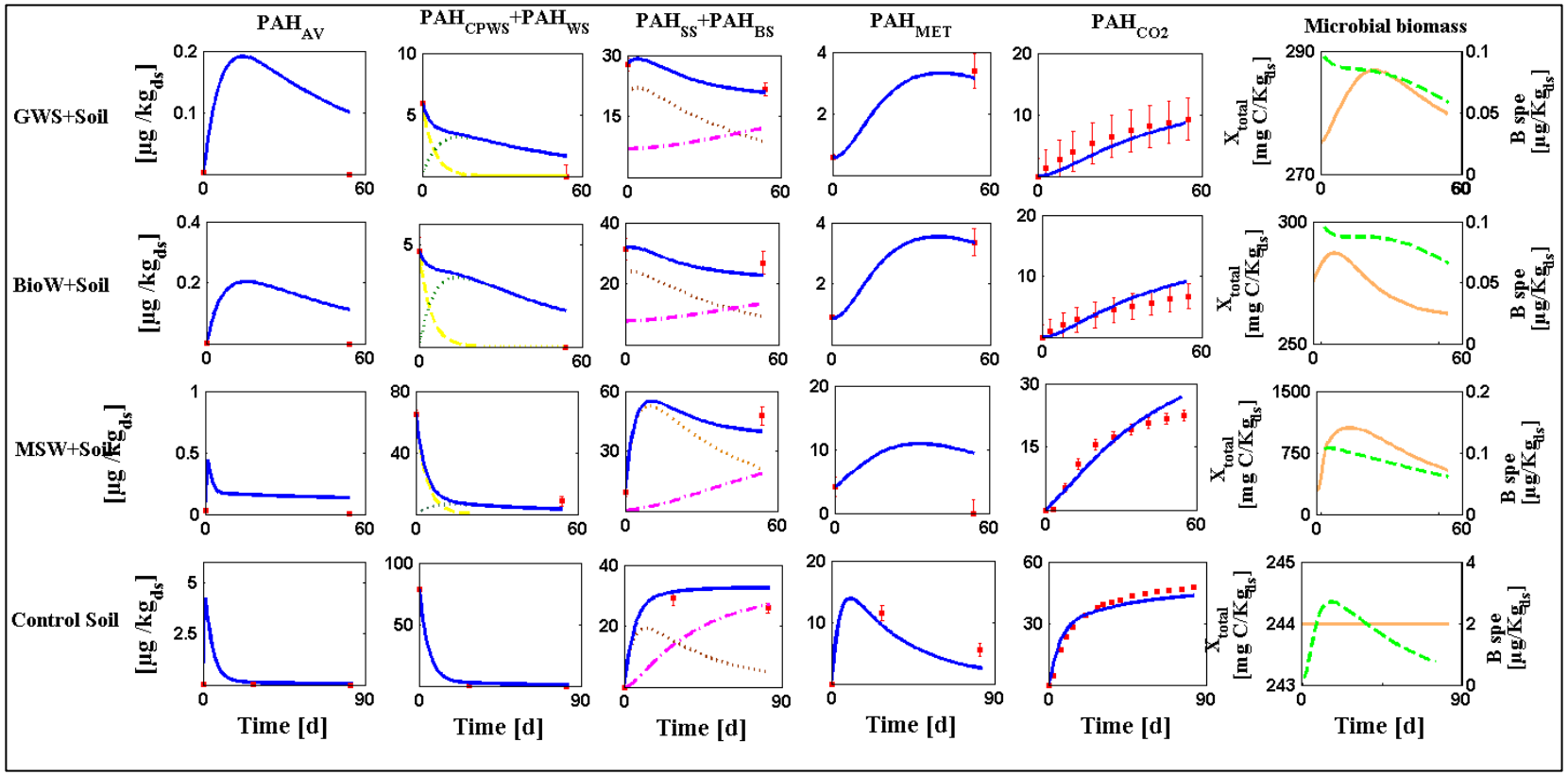

Figure III.4. Simulated and observed phenanthrene concentrations over time in amended soils for all treatments. Simulation results are marked in lines, whereas the experimental data are represented by red dots. Error bars indicate the standard deviation (3 replicates). The column entitled "PAH_{CPWS}+PAH_{WS}" included the total simulated weakly sorption fraction in solid blue line with PAH_{CPWS} in dashed yellow line and PAH_{WS} in pointed green line. The column entitled "PAH_{SS}+PAH_{BS}" include the total simulated non extractible fraction in solid blue line, with the simulated strongly sorbed in pointed brown line and the simulated biogenic NER in pink pointed dashed line. The last column presents the dynamics of two microbial biomasses: X_{total} (Left y-axis, bold solid line) and B_{SPE} (right y-axis, dashed line)

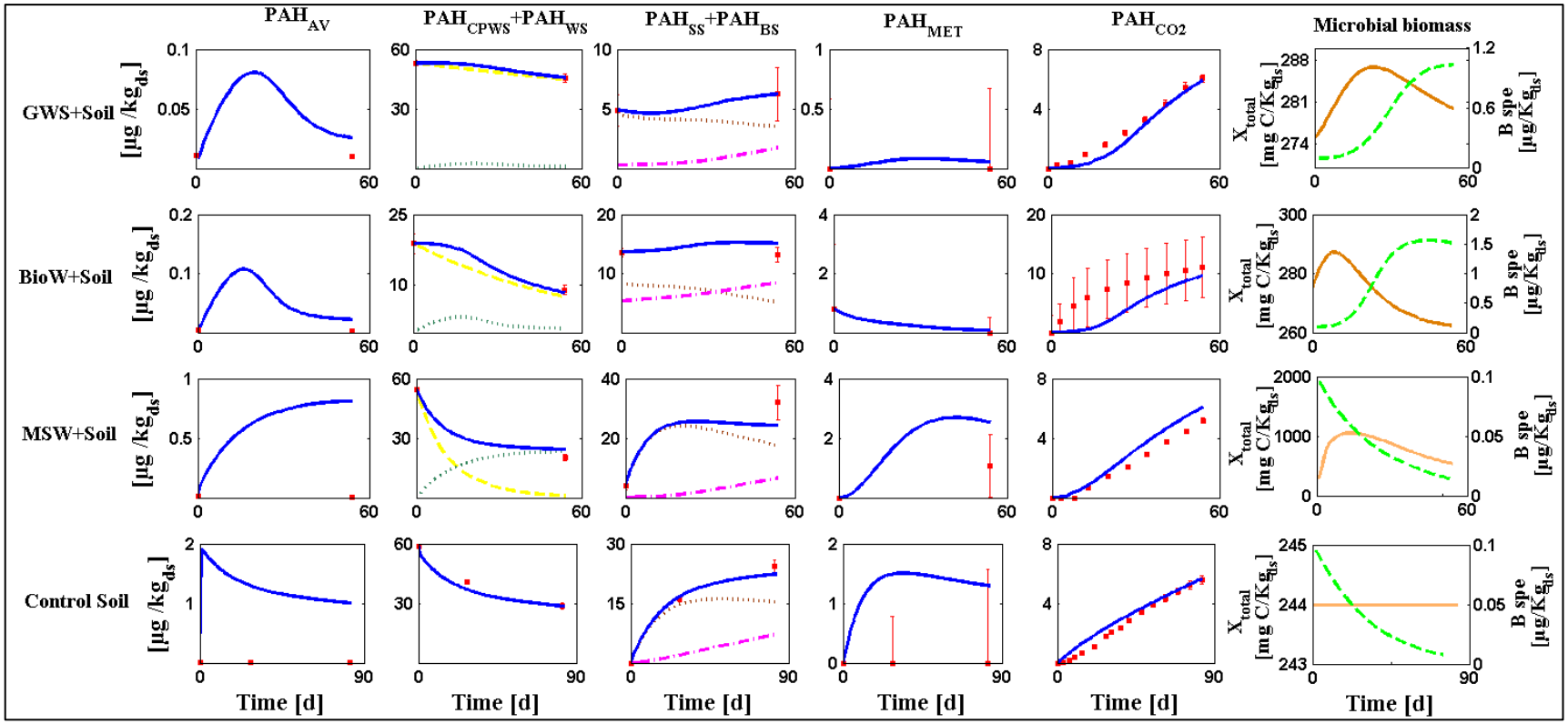

Figure SI III.2. Simulated and observed <u>fluoranthene</u> concentrations over time in amended soils for all treatments. Simulation results are marked in lines, whereas the experimental data are represented by red dots. Error bars indicate the standard deviation (3 replicates). The column entitled "PAH_{CPWS}+PAH_{WS}" included the total simulated weakly sorption fraction in solid blue line with PAH_{CPWS} in dashed yellow line and PAH_{WS} in pointed green line. The column entitled "PAH_{SS}+PAH_{BS}" include the total simulated non extractible fraction in solid blue line, with the simulated strongly sorbed in pointed brown line and the simulated biogenic NER in pink pointed dashed line. The last column presents the dynamics of two microbial biomasses: X_{total} (Left y-axis, bold solid line) and B_{SPE} (right y-axis, dashed line)

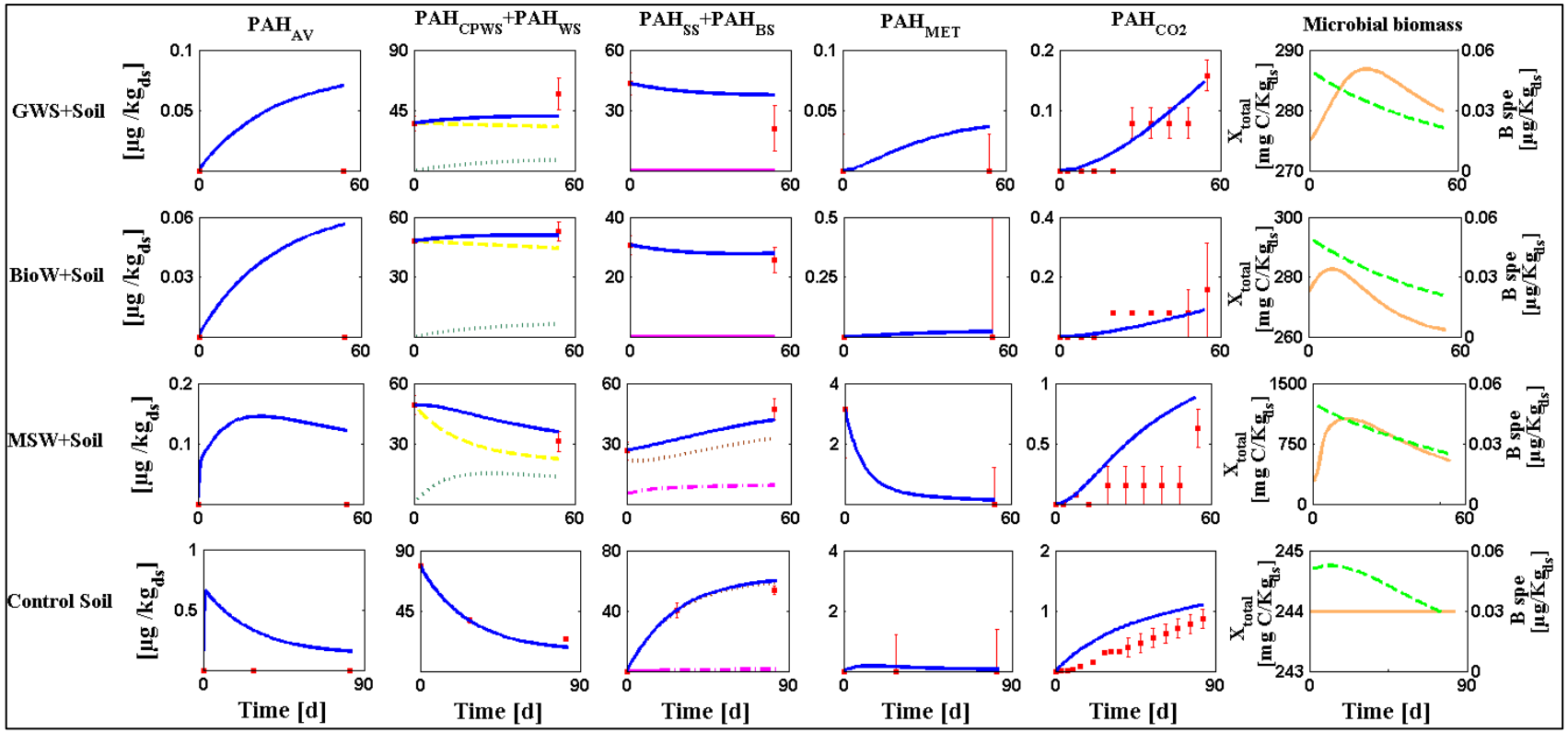

Figure SI III.3. Simulated and observed benzo(a)pyrene concentrations over time in amended soils for all treatments. Simulation results are marked in lines, whereas the experimental data are represented by red dots. Error bars indicate the standard deviation (3 replicates). The column entitled "PAH_{CPWS}+PAH_{WS}" included the total simulated weakly sorption fraction in solid blue line with PAH_{CPWS} in dashed yellow line and PAH_{WS} in pointed green line. The column entitled "PAH_{SS}+PAH_{BS}" include the total simulated non extractible fraction in solid blue line, with the simulated strongly sorbed in pointed brown line and the simulated biogenic NER in pink pointed dashed line. The last column presents the dynamics of two microbial biomasses: X_{total} (Left y-axis, bold solid line) and B_{SPE} (right y-axis, dashed line)

4.3.3. Estimated parameters

The histograms of Figure III.5 present the probability density functions (PDF) of model parameters against parameter ranges. The most appropriate parameter estimated values with their 95% confidence intervals are listed in Table III.3. Results show that some parameters were very well defined since their histograms of values display Gaussian distributions with 95% confidence intervals occupying small ranges inside uniform prior distributions (example the parameters k_{SW}, $k_{WS,}$ k_{CS} and k_{MB} for PHE). However, some other parameters, in contrast, had more uniform PDF and/or concentrated most of their probability mass at their lower or higher limits. Such parameters are linked to the biodegradation pathway driven by specific biomasses (μs_{max}, k_M ,y_{spe}, ks_{spe}) probably due to the lack of data to measure the specific degradation. Low correlations were found between parameters except between sorption parameters k_{SW} and $k_{WS,}$ with a correlation coefficient of 0.75. Comparison of the parameter values obtained in this current study with their values published in literature was difficult because of the differences between models. The fitted parameter values of the co-metabolism biodegradation pathway k_{deg} were found to be in the following order: PHE >FLT > BAP which was correlated to the bioavailability of pollutant itself linked to its chemical hydrophobicity. The fitted value for μs_{max} of FLT in GWS of 0.54 d^{-1} was close to the value obtained by Geng et al., (2015) for the same PAH in the same compost. The optimized values of y_{spe} for PHE and FLT (0.251 and 0.274 [-] respectively) were found to be close to that proposed by Weissenfels et al. (1990) (0.24 and 0.23 [-] for PHE and FLT respectively).

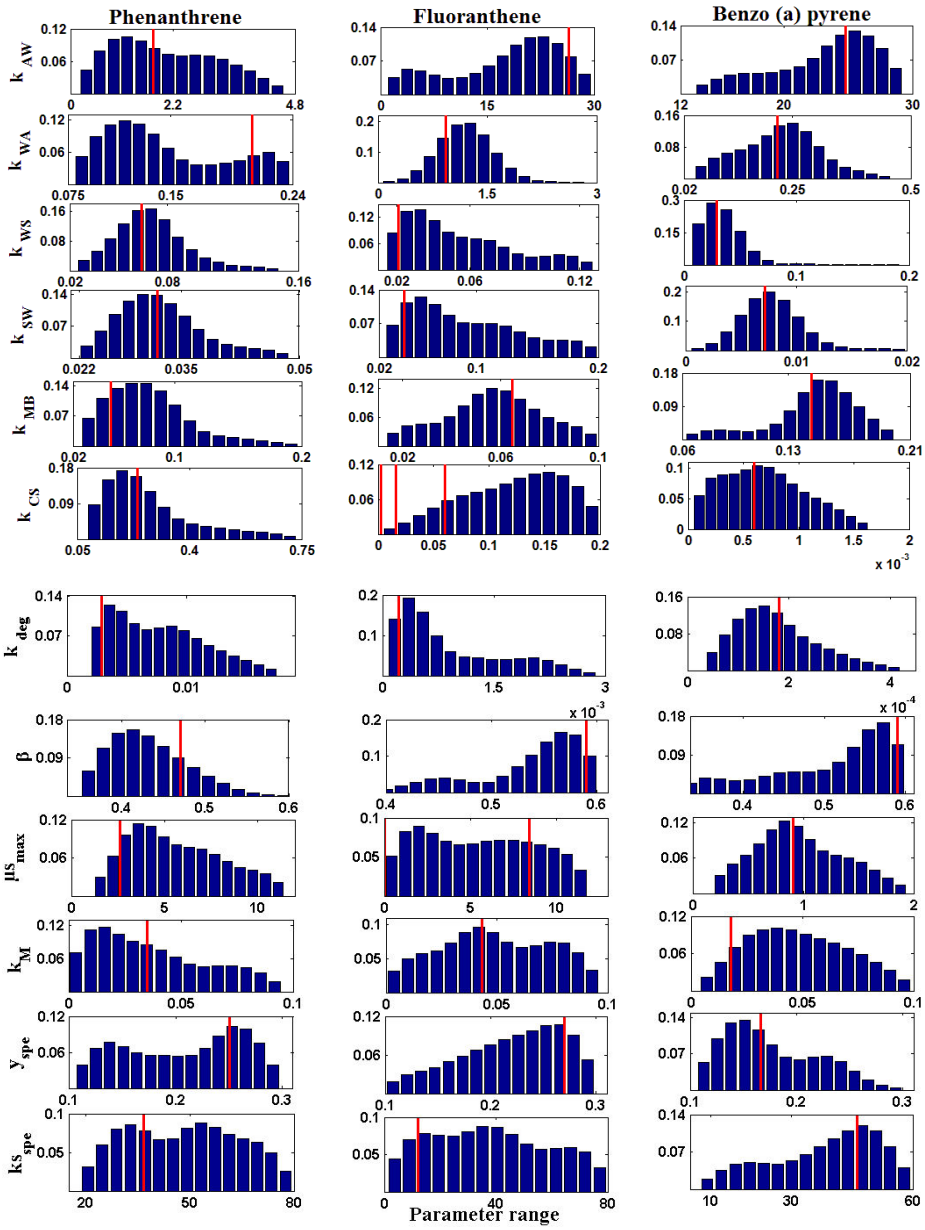

Figure III.5. Probability density distribution of the evaluated model parameters for the three PAH. The y-axis refers to the probability distribution value and the x-axis indicates the parameter searching range. Red solid lines indicate the most appropriate parameters values.

4.4. Model sensitivity to some key initial variables

4.4.1. Sensitivity of PAH mineralization to the mass of added compost

Figure III.6 shows a comparison between the mineralisation simulated for each PAH with different treatments under the hypothesis of a 5-fold increase of applied compost mass while keeping the pollutant concentration in the compost unchanged. The goal of the simulation was to explain the processes controlling the mineralisation of PAH in amended soil. Indeed,

although the size of co-metabolic microbial biomass degrading PAH highly increased, the results showed that the mineralisation of ^{14}C-PAH was only slightly increased (see Figure III.6). For PHE, the amount of compost had no effect on mineralisation. On the opposite, for BAP, all the curves increased when increasing the added organic matter. For FLT only the MSW treatment increased with the increase of organic matter. The PHE availability for potential mineralisation was not very high (see compartments: CPWS+WS in Figure III.4) compare to FLT and BAP (see compartments: CPWS+WS in Figure SI III.2 and Figure SI III.3) and only 2 µg/kg of PHE was still available for extra mineralisation at the end of the incubation. BAP and FLT mineralisation was more sensitive to the amount of compost and the co-metabolism activity. Their effects were higher in MSW for both PAHs and in all composts for BAP because these treatments showed increase of co-metabolic biomass moreover more PAHs were still available for more mineralisation as we can see in Figure SI III.2 and Figure SI III.3.

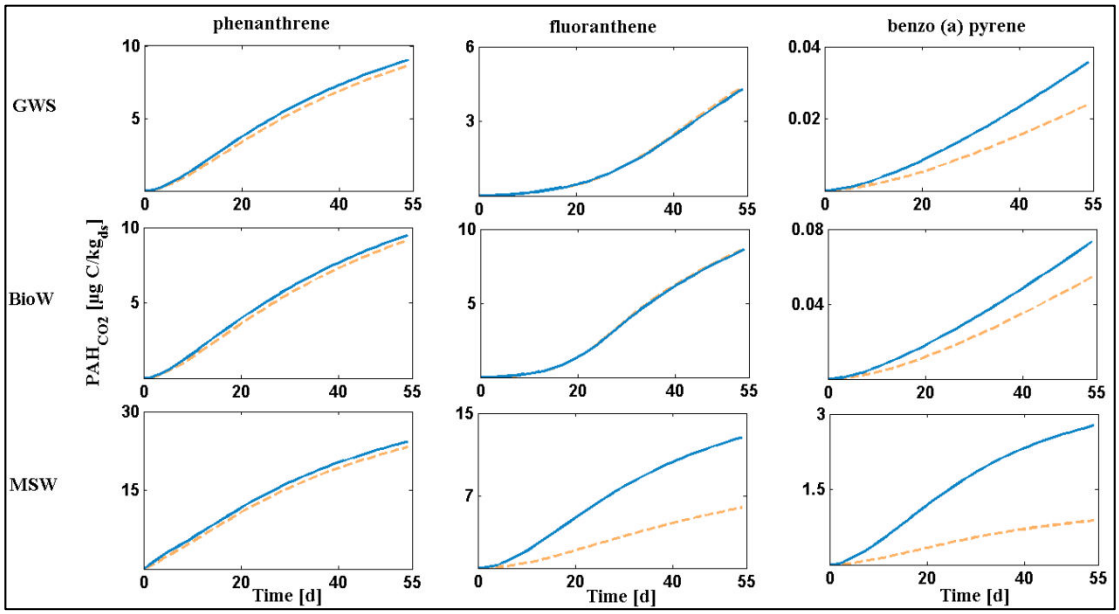

Figure III.6. Effect of the increase of organic load of applied compost on the mineralization of PAH in amended soil. Simulations with solid lines were run with a five-fold increase of applied organic load. Simulations with dashed lines were run without modification of compost amount

4.4.2. Sensitivity of PAH mineralisation to the composition of non-extractible residues

The impact of the initial conditions of biogenic fraction to the total non-extractible residues on the model output PAH_{CO2} was evaluated. The initial values of the percentage of biogenic contribution to the total non-extractible residues varied between 0 and 100%. The CO_2

mineralization at the end of the incubations is presented for PHE and BAP for both GWS and MSW treatments in Figure III.7.

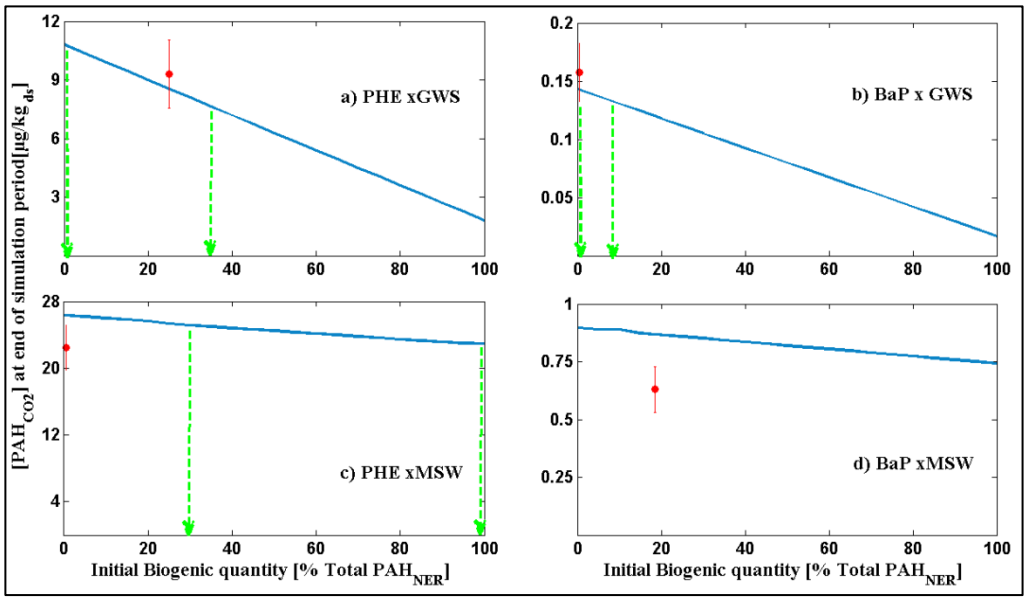

Figure III.7. Mineralized fraction PAH_{CO2} calculated at the end of simulation periods as function of the initial percentage of biogenic residue. (⊖) represents the mean value of the measured mineralized fraction PAH_{CO2} with its error bars (± standard deviation) versus the default biogenic residue percentage value reported in Table III. 2. Dashed green arrows shows the range acceptable initial biogenic residue percentage calculated from the experimental error of the final mineralized values and the simulated mineralization (blue line).

Results show that the simulated PAH_{CO2} at the end of simulation periods is highly impacted by the initial values of the biogenic fraction. We found that the PAH_{CO2} emission increased when decreasing the initial contribution of biogenic NER for all treatments. This result was related to the model hypothesis which assumed that the amount of PAH strongly sorbed on soil matrix, PAH_{ss}, might become bio-accessible for the microorganisms following a desorption process (because ksw≠0) in contrast to the NER biogenic fraction, PAH_{BS}, that could not be remobilised. The relative difference between the simulated mineralised fraction into CO_2, PAH_{CO2}, at the end of the simulation period for 0% and 100% of biogenic residue showed in the following decreased order: BAP×GWS > PHE×GWS > BAP×MSW > PHE×MSW. The impact of biogenic NER initial fraction on the CO_2 emission was higher for GWS treatment than for MSW, suggesting that the model was less sensitive of the initial biogenic NER fraction with MSW treatment. The compost GWS created more initial non-extractable residues (PAH_{BS}+PAH_{SS}) than MSW for both PAH (see Figure SI III.1) and thus changes in initial composition of PAH NER led to higher differences in PAH final

mineralization for GWS. This result underlined the assumption on the significant role of composts quality in the dissipation of PAH in the amended soil. The reliability of our assumption about the non-extractible residues distribution has not yet been fully assessed and further validation is still needed in the future.

As the simulations performed in the composts did not provide uncertainties related to the predicted values of the biogenic fraction of NER, we evaluated the ranges of these values for which the model remains able to reproduce correctly the observed mineralised fractions. Using Figure III.7 we estimated the range of initial biogenic NER values that simulated the mineralised fraction inside its experimental error bars. Hence, for the simulations performed with GWS treatments, the acceptable ranges of the initial biogenic NER proportion values were between 0 and 36% for PHE, and between 0 and 9% for BAP. The initial predicted values of biogenic NER fractions with GWS treatment given in Table III.2 were included within these ranges. For the simulations performed with MSW treatment, the range for PHE was between 30 and 100% and the initial predicted value for biogenic NER distribution did not belong to this range (Figure III.7c). It was also found that whatever the initial predicted biogenic NER quantity was, the model tended to overestimate the mineralised fraction observed at the end of the incubation period performed with BAP (Figure III.7d). However, as the highest relative difference was less than 14.5 % for MSW, we might conclude that there was no significant effect of initial biogenic NER proportion on uncertainties derived from the compost incubation simulations on CO_2 emission in amended soils.

5. Conclusion

The PAH-OC model was appropriate to describe, under laboratory conditions, the interactions between the main physical, biological and biochemical processes influencing the dissipation of PAH included in compost and after compost application to soil. The most significant features of this model were to take into account the organic matter characteristics of the applied compost, the production of non-extractible residues and the biodegradation pathway. A single parameter set for all compost types was found to simulate adequately the dynamics of PHE and BAP in the different composts. For FLT, because a specific biomass biodegradation pathway had to be considered for mature composts, such unique set of parameter could not be established. The modeling study confirmed that the processes occurring during composting had a strong impact on the fate of PAHs entering in soils with composts. During compost incubation, the PAH dissipation was higher with mature composts while in soil/compost incubations, the PAH dissipation was higher in the non-mature compost

partly because more PAHs were bio-available. Investigating how the biogenic and physical processes contribute to the total non-extractible residues formation from recent methods reported in literature is one of perspectives of this work. Further work should also be devoted to the application of the model in field under long term studies.

6. Acknowledgements

This research was financially supported by the French Environment and Energy Management Agency (ADEME) and the Environment and Agronomy division of the French National Institute for Agricultural Research (INRA). The experimental data were obtained during Christine Vergé-Leviel PhD financed by Veolia Recherche & Innovation.

7. References

Annabi, M., Bissonnais, Y. Le, Villio-poitrenaud, M. Le, Houot, S., 2011. Improvement of soil aggregate stability by repeated applications of organic amendments to a cultivated silty loam soil. "Agriculture, Ecosyst. Environ. **144**, 382–389. doi:10.1016/j.agee.2011.07.005

Barriuso, E., Benoit, P., Dubus, I.G., 2008. Formation of pesticide nonextractable (bound) residues in soil: Magnitude, controlling factors and reversibility. Environ. Sci. Technol. **42**, 1845–1854. doi:10.1021/es7021736

Brändli, R.C., Bucheli, T.D., Kupper, T., Furrer, R., Stadelmann, F.X., Tarradellas, J., 2005. Persistent organic pollutants in source-separated compost and its feedstock materials--a review of field studies. J. Environ. Qual. **24**, 735–60. doi:10.2134/jeq2004.0333

Brimo, K., Garnier, P., Sun, S., Bertrand-krajewski, J., Cébron, A., Ouvrard, S., 2016. Using a Bayesian approach to improve and calibrate a dynamic model of polycyclic aromatic hydrocarbons degradation in an industrial contaminated soil. Environ. Pollut. **215**, 27–37. doi:10.1016/j.envpol.2016.04.094

Cerniglia, C.E., 1997. Fungal metabolism of polycyclic aromatic hydrocarbons : past , present and future applications in bioremediation. J. Ind. Microbiol. Biotechnol. **19**, 324–333.

Chalhoub, M., Garnier, P., Coquet, Y., Mary, B., Lafolie, F., Houot, S., 2013. Increased nitrogen availability in soil after repeated compost applications : Use of the PASTIS model to separate short and long-term effects. Soil Biol. Biochem. **65**, 144–157. doi:10.1016/j.soilbio.2013.05.023

Corbeels, M., Hofman, G., Van Cleemput, O., 1999. Simulation of net immobilization and mineralization in substrate-ammended soils by the NCsoil computer model. Biol. Fertil. Soils **28**, 422–430.

FOCUS, 2006. Guidance Document on Estimating Persistence and Degradation Kinetics from Environmental Fate Studies on Pesticides in EU Registration" Report of the FOCUS Work Group on Degradation Kinetics, EC Document Reference Sanco/1005, 1–436.

Geng, C., Haudin, C.-S., Zhang, Y., Lashermes, G., Houot, S., Garnier, P., 2015. Modeling the release of organic contaminants during compost decomposition in soil. Chemosphere **119**, 423–431. doi:10.1016/j.chemosphere.2014.06.090

Gevao, B., Jones, K.C., Semple, K.T., 2005. Formation and release of non-extractable14C-Dicamba residues in soil under sterile and non-sterile regimes. Environ. Pollut. **133**, 17–24. doi:10.1016/j.envpol.2004.04.007

Goss, M.J., Tubeileh, A., Goorahoo, D., 2013. A review of the use of organic amendments and the risk to human health. Adv. Agron. **120**, 275–379.

Gunasekara, A.S., Xing, B., 2003. Sorption and desorption of naphthalene by soil organic matter: importance of aromatic and aliphatic components. J. Environ. Qual. **32**, 240–246.

Hartlieb, N., Marschner, B., Klein, W., 2001. Transformation of dissolved organic matter (DOM) and 14C-labelled organic contaminants during composting of municipal biowaste. Sci. Total Environ. **278**, 1–10. doi:10.1016/S0048-9697(01)00902-0

Haudin, C.S., Zhang, Y., Dumény, V., Lashermes, G., Bergheaud, V., Barriuso, E., Houot, S., 2013. Fate of 14C-organic pollutant residues in composted sludge after application to soil. Chemosphere **92**, 1280–1285. doi:10.1016/j.chemosphere.2013.02.041

Houot, S., Verge-Leviel, C., Poitrenaud, M., 2012. Potential mineralization of various organic pollutants during composting. Pedosphere **22**, 536–543. doi:10.1016/S1002-0160(12)60038-1

Iqbal, A., Garnier, P., Lashermes, G., Recous, S., 2014. A new equation to simulate the contact between soil and maize residues of different sizes during their decomposition. Biol. Fertil. Soils **50**, 645–655. doi:10.1007/s00374-013-0876-5

Kästner, M., Nowak, K.M., Miltner, A., Trapp, S., Schäffer, A., 2014. Classification and modelling of non-extractable residue (NER) formation of xenobiotics in soil—a synthesis. Crit. Rev. Environ. Sci. Technol. **44**, 2107–2171. doi:10.1080/10643389.2013.828270

Kästner, M., Streibich, S., Beyrer, M., Richnow, H.H., Fritsche, W., 1999. Formation of bound residues during microbial degradation of [14C]anthracene in soil. Appl. Environ. Microbiol. **65**, 1834–1842.

Nash, J.E., Sutcliffe, J.V., 1970. River flow forecasting through conceptual models part I — A discussion of principles. J. Hydrol. **10**, 282–290. doi:10.1016/0022-1694(70)90255-6

Nowak, K.M., Girardi, C., Miltner, A., Gehre, M., Schäffer, A., Kästner, M., 2013. Contribution of microorganisms to non-extractable residue formation during biodegradation of ibuprofen in soil. Sci. Total Environ. **445–446**, 377–384. doi:10.1016/j.scitotenv.2012.12.011

Peltre, C., Christensen, B.T., Dragon, S., Icard, C., Kätterer, T., Houot, S., 2012. RothC simulation of carbon accumulation in soil after repeated application of widely different organic amendments. Soil Biol. Biochem. **52**, 49–60. doi:10.1016/j.soilbio.2012.03.023

Puglisi, E., Cappa, F., Fragoulis, G., Trevisan, M., Del, A.A.M., 2007. Bioavailability and degradation of phenanthrene in compost amended soils. Chemosphere. **67**, 548–556. doi:10.1016/j.chemosphere.2006.09.058

Richnow, H.H., Annweiler, E., Koning, M., Lüth, J.C., Stegmann, R., Garms, C., Francke, W., Michaelis, W., 2000. Tracing the transformation of labelled [1-13C]phenanthrene in a soil bioreactor. Environ. Pollut. **108**, 91–101. doi:10.1016/S0269-7491(99)00205-5

Russell, D.L., 2006. Elements of Biological Treatment, in: Practical Wastewater Treatment. John Wiley & Sons, Inc., Hoboken, NJ, USA, pp. 91–124. doi:10.1002/0470067926.ch6

Tejada, M., Hernandez, M.T., Garcia, C., 2009. Soil restoration using composted plant residues: Effects on soil properties. Soil Tillage Res. **102**, 109–117. doi:10.1016/j.still.2008.08.004

Van Soest, P.J., Wine, R.H., 1967. Use of detergents in the analysis of fibrous feeds.

IV. Determination of permanganate. Journal of AOAC **50 (1)**, 50–55.

Vrugt, J.A., 2016. Markov chain Monte Carlo simulation using the DREAM software package : Theory , concepts , and MATLAB implementation. Environ. Model. Softw. **75**, 273–316. doi:10.1016/j.envsoft.2015.08.013

Wang, H., Lin, K., Hou, Z., Richardson, B., Gan, J., 2010. Sorption of the herbicide terbuthylazine in two New Zealand forest soils amended with biosolids and biochars. J Soils Sediments **10**, 283–289. doi:10.1007/s11368-009-0111-z

Weissenfels, W.D., Beyer, M., Klein, J., 1990. Degradation of phenanthrene, fluorene and fluoranthene by pure bacterial cultures. Appl. Microbiol. Biotechnol. **32**, 479–484. doi:10.1007/BF00903787

Wilcke, W., 2000. SYNOPSIS Polycyclic Aromatic Hydrocarbons (PAHs) in Soil — a Review. J. Plant Nutr. Soil Sci. **163**, 229–248. doi:10.1002/1522-2624(200006)163:3<229::AID-JPLN229>3.0.CO;2-6

Wild, S.R., Obbard, J.P., Munn, C.I., Berrow, M.L., Jones, K.C., 1991. The long-term persistence of polynuclear aromatic hydrocarbons (PAHs) in an agricultural soil amended with metal-contaminated sewage sludges. Sci. Total Environ. **101**, 235–253.

Xing, B., 1997. The effect of the quality of soil organic matter on sorption of naphthalene. Chemosphere **35**, 633–642.

Xiu-hong, Y., Garnier, P., Shi-zhong, W., Bergheaud, V., Xiong-fei, H., 2014. PAHs sorption and desorption on soil influenced by pine needle litter-derived dissolved organic matter. Pedosphere **24**, 575–584. doi:10.1016/S1002-0160(14)60043-6

Zhang, Y., Lashermes, G., Houot, S., Doublet, J., Steyer, J.P., Zhu, Y.G., Barriuso, E., Garnier, P., 2012. Modelling of organic matter dynamics during the composting process. Waste Manag. **32**, 19–30. doi:10.1016/j.wasman.2011.09.008

PARTIE II. SIMULATIONS A L'ECHELLE DU TERRAIN

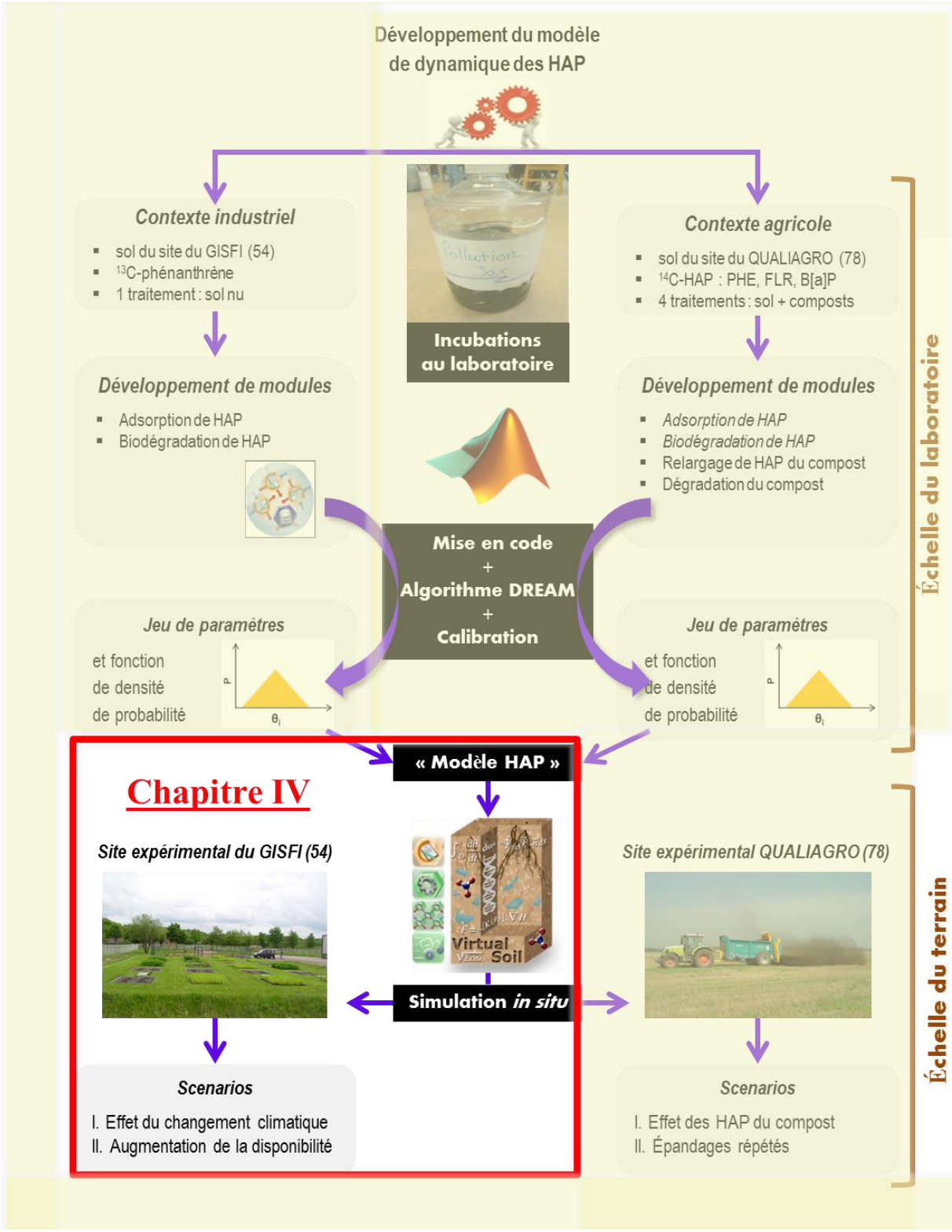

Place du chapitre IV dans l'ensemble du travail de thèse

Chapitre IV. Simulations de la dynamique *in situ* des HAP dans un sol historiquement contaminé ; évaluation de l'impact de scenarios de changement climatique et de modification de la disponibilité sur le long terme

Résumé du contenu du chapitre en français

Ce chapitre propose une extension à l'échelle du terrain des résultats obtenus dans le chapitre 2. L'objectif était de prédire, sous certaines hypothèses, le devenir du phénanthrène (PHE) dans des parcelles de terres industrielles anciennement contaminées, mises en place sur le site expérimental du GISFI. Dans ce contexte, et en utilisant les modules calibrés et présentés précédemment, un modèle couplé HAP-atmosphère -eau-sol de la prévision de la dynamique des HAP a été développé au sein de la plateforme SOL VIRTUEL de l'INRA. Ce modèle unidimensionnel est composé de 5 modules principaux : le transport de chaleur, le transfert hydrique, le transport de soluté de HAP, l'adsorption de HAP et le module de biodégradation de HAP. Les données climatiques sont fournies par des modules spécifiques et considérées comme conditions aux limites dans le modèle. Les données expérimentales de terrain acquises dans la modalité de traitement sans végétation du dispositif de 24 parcelles lysimétriques sur des périodes de plusieurs années ont été utilisées pour affiner la calibration des différents modules du modèle HAP. Le modèle calibré et testé a ensuite été utilisé pour réaliser deux scenarios distincts. Le premier vise à prédire l'évolution des concentrations de PHE en conditions de sol nu selon différentes conditions climatiques prédites à long terme (entre 2010 et 2039) suivant les projections climatiques du groupe d'experts intergouvernemental sur l'évolution du climat. Les deux projections climatiques retenues sont définies sous les appellations A2 (scénario le plus intense) et B1 (scénario le plus modeste). Le second scenario testé vise à estimer l'effet de

l'augmentation de la disponibilité du polluant, sous l'effet par exemple de l'addition de solvants organiques. Les simulations de ces différentes situations ont globalement mis en évidence que i) la minéralisation du PHE se caractérise par deux phases de dégradation, ii) l'élimination du PHE du sol est régie par la limitation au transfert de matière et non par l'activité microbienne , iii) les facteurs météorologiques sont importants et devraient donc être pris en compte dans chaque stratégie de gestion et iv) l'augmentation de la disponibilité du polluant, toutes choses égales par ailleurs, conduit à une réduction significative des HAP au cours du temps. Cette partie du travail fait l'objet d'un article en cours de préparation et présenté dans ce qui suit : Khaled Brimo, Patricia Garnier, François Lafolie, Geoffroy Séré, Stéphanie Ouvrard, *In situ* long-term modeling of phenanthrene dynamics in an aged contaminated soil using the "VSOIL" platform, to be submitted to *Science of the Total Environment*

In situ long-term modeling of phenanthrene dynamics in an aged contaminated soil using the "VSOIL" platform

Khaled Brimo[a,b,c,d], Patricia Garnier[a], François Lafolie[e], Geoffroy Séré[b,c], Stéphanie Ouvrard[b,c]

[a]INRA, EcoSys, UMR1405, Université Paris-Saclay, 78850, Thiverval-Grignon, France

[b]INRA, Laboratoire Sols et Environnement, UMR 1120, F-54518 Vandoeuvre-lès-Nancy, France

[c]Université de Lorraine, Laboratoire Sols et Environnement, UMR 1120, F-54518 Vandoeuvre-lès-Nancy, France

[d]Agence de l'Environnement et de la Maîtrise de l'Energie, 20 avenue du Grésillé, BP 90406, F-49004 Angers Cedex 01, France

EMMAH, Université d'Avignon et des Pays de Vaucluse, INRA, 84914, Avignon, France

*Corresponding author: Stéphanie Ouvrard

Tel: + 33 383 595 762

E-mail: stephanie.ouvrard@univ-lorraine.fr

Fax: +33 383 595 791

Article prepared for submission in journal of Science of the Total Environment

1. Abstract

Management and remediation actions of polycyclic aromatic hydrocarbon (PAH) contaminated sites require an accurate knowledge of the dynamics of these chemicals in situ under real conditions. Here we developed, under the Virtual Soil Platform, a global model for PAH that describes the principal physical and biological processes controlling the dynamics of PAH in soil under climatic conditions. The model was applied first to simulate the observed dynamics of phenanthrene in situ and then to predict scenarios of the fate of phenanthrene in soil. Our results show that the model can adequately predict the fate of phenanthrene and can contribute to clarify some of unexplored aspects regarding the behavior of phenanthrene in soil like its degradation mechanism and stabilization. Scenarios showed that addition solvent or surfactants resulted in significant increasing in substrate transfer rate, hence reducing time remediation. However, also increases in toxicity and risk of leaching were noticed. It clearly appeared that meteorological factors were important and should also be accounted for in each management strategy.

Keywords: Virtual Soil platform, PAH reactivity, industrial contaminated soil, future climate change

Highlights

- The fate of PHE in a soil from a former coking plant was predicted in situ under real conditions
- The effects of projected future climate conditions on the fate of PHE were investigated.
- Biodegradation of PHE at long term in aged contaminated soil is determined by two degradation phases
- In situ, remediation by addition of solvent and surfactants appeared to have the highest removal efficiency yield.

2. Introduction

Industrial sites formerly associated with coal exploration and gasworks have frequently been reported to be highly contaminated by persistent organic pollutants (Edwards, 1983; Wilcke, 2000). Among many pollutants, the sixteen polycyclic aromatic hydrocarbons (PAH) defined by the US Environmental Protection Agency (EPA) have been given great interest due to their carcinogenicity, bioaccumulation and persistence in the environment (Iarc, 2010; Tsibart and Gennadiev, 2013). Thus the remediation of sites contaminated by PAH is an essential practice because of environmental concerns, and also to avoid any potential contamination of water aquifer (Broholm et al., 1998). While a number of conventional techniques such as thermal desorption can be applied for the cleanup of such contaminated sites, phytoremediation compared to other techniques has gained popularity in the last decades because of its reduced cost, ease of implementation as well as its eco-friendliness with no damage to the neutral and texture structure of the soil (Cunningham et al., 1996; Ouvrard et al., 2014). Nevertheless, there has only been limited success with this technique in sites contaminated with PAH compounds and these unsatisfactory results have been mainly attributed to bioavailability limitation (Ouvrard et al., 2014; Wilson and Jones, 1993). Indeed, information about PAH compounds distribution among the physical phases that comprise a soil system as well as about the processes and the mechanisms by which PAH compounds are interacting in soil should allow a better understanding of conditions that lead to bioavailability problem as well as similar others ones. Moreover, additional information of the rates by which these simultaneous processes proceed in a soil system can help to obtain important management factors, including: i) the long time required to attain clean up goals; ii) the effects of environmental conditions on the course of remediation; iii) the impact on the decontamination rate of solvents or surfactants following application on soil.

For addressing these issues concerning remedial actions, there is an increasing need of development of complex models that mimic increasingly the relevant processes occurring in a soil. A number of reviews have appeared in the literature presenting simulation models that describe the dynamics of PAH in polluted soils. However, these models are few and they have either focused on one of the major processes influencing PAH behavior in soil (e.g. the degradation process in (Thiele-Bruhn and Brümmer, 2005; Wick et al., 2001), the sorption and aging process in (Johnson et al., 2001) and plant uptake and rhizosphere activity in (Takaki et al., 2014)) , or a two or more of the main processes as in (Adam et al., 2014; Fragoulis et al., 2005; Geng et al., 2015; Peters et al., 1999; Rein et al., 2016). Actually, with

the exception of (Peters et al., 1999; Thiele-Bruhn and Brümmer, 2005) these models have only been tested using experimental laboratory data. Therefore, reliable kinetic data for PAH at field conditions is very scarce. Moreover, as the exploration of laboratory kinetics data to field conditions is still not clearly valid as reported by Beulke et al.(2000), the use of these kinetics for predictions at field scale may lead to results far of reality. Generally, two major obstacles have limited the availability of such kinetics for PAH at field scale i) absence of appropriate data on long term (i.e. with time scale of several years) that are required for models development; ii) the lack of coupled model tools able to simulate simultaneously numerous processes occurring in a soil system due either to a little understanding of the interaction between the processes or technology difficulties for implementing coupled models or both. Recently, our group of research has developed kinetics modules for PAH that tested successfully at laboratory conditions (Brimo et al., 2016). This paper considers the second part of a work devoted to simulate in situ the fate of a PAH compound in an aged soil of a former coking plant under real conditions. We used data set from a long term experimental contaminated field described in (Ouvrard et al., 2011).

Our first objective here is to present and to evaluate a new coupled model for PAH developed by coupling modules for transport and transformation processes using a modeling platform. Our second objective is to use the validated model to formulate two individual scenarios for a model compound of the 16 US-EPA PAH "phenanthrene (PHE)" in order i) to predict at long term of forty years period (2010-2039) the implications of the future climatic changes on decontamination rate of PHE in soil, i) to explore the effect of increase the mass transfer rate of PHE several times on its fate in soil. In order to simplify our preliminary work, the scope of the study is limited only on the bare soil (i.e. the uncultivated plots in situ). This is because plants can represent a potential source for PAH attenuation in soil across the rhizosphere induced by the roots (Ouvrard et al., 2014) and this process *in situ* is poorly understood both quantitatively and qualitatively.

3. Materiel and methods

3.1. Case study

3.1.1. General field conditions

Data set used for modeling comes from a long-term field experiment initiated in 2005 in order to study, under various management practices, the remediation efficiency of an aged contaminated soil collected from a former coking plant (Ouvrard et al., 2011). The field is located in north-eastern France (49°213N, 5°996E). Mean annual air temperature is 10 °C and mean annual rainfall amounts to 805 mm $year^{-1}$ (average data between 2007 and 2014). Atmospheric bulk deposition of 14 PAH (16 US EPA PAH except naphthalene and acenaphthylene) is estimated to be between 19-93 ng m^{-2} d^{-1} (Garban et al., 2002). The field devices used for the present study consist in four stainless steel lysimetric plots, and two large-scale lysimeters.

3.1.2. Field plots

The lysimetric plots were implemented in June 2005. Each plot (surface area of 2x3 m^2 and depth of 0.7 m) was filled with an industrial contaminated soil in the top 40 cm depth while the bottom 30 cm was filled with a gravel layer for drainage. In this study we considered the four plots left without vegetation. This soil studied has a silty sand texture, neutral pH and relatively high organic carbon content of 62 g C kg_{ds}^{-1} (where *ds* subscript refers to dry soil). The initial 16 US-EPA PAH content was 1924 ± 258 mg kg_{ds}^{-1}. Soil was sampled twice a year, in September and in April/May from September 2005 till 2012. For each plot, a representative soil sample is obtained from 6 sampling points. At each sampling time, two extraction methods were employed in order to identify and quantify the total and available PAH concentrations. Total concentrations were classically determined by GC-MS analysis following accelerated solvent extraction using dichloromethane and available concentrations were quantified by solid phase extraction using Tenax® (Barnier et al., 2014; Ouvrard et al., 2011)

Drainage water was collected in a tank (0.4 x0.48 m and 0.6 m deep) and quantitatively and qualitatively characterized. Water volume was estimated by regular measurement of water level in collection tank. After each measurement, the tanks were emptied until the following one. Thus data correspond to average values over variable time periods, depending on climatic conditions and filling tank rates. Occasionally, for high drainage events, water outflows exceeded the tank storage capacity leading to some uncertainty on the drainage

volume. To avoid such data inconsistency, each plot was equipped in 2011 with a tipping counter to measure water outflows volumes with a one-hour time step. Water sampling was performed twice a year in March/April and in September/October for chemical assessment. PAH total dissolved concentrations were estimated using the AquaMS PAH probe (AquaMS, France).

3.1.3. Lysimeter device

Two lysimeters (Umwelt-Gerate-Technik, Müncheberg, Germany) (1 m^2 x 2 m) were filled with the same material in April 2008. One was sown with alfalfa and the other, used in this study, was left bare. These columns were equipped with time domain reflectometry probes (TDR) and temperature sensors installed at depths 50, 100, 150 cm for volumetric water content and temperature monitoring in soil profile respectively. At the bottom, a tipping counter measured the water outflow from the lysimeter. All data were recorded at one-hour time step using a data logger (Séré et al., 2012).

3.1.4. Climatic data

Real climatic data were collected with a weather station located at the experimental site (WS STD1, Delta-T Devices). Air temperature, humidity, global incoming solar radiation, rainfall and wind speed were recorded with a one-hour time step. Complementary data collected at Rombas (Meurthe et Moselle, France) weather station located about 9 km from the experimental field were also used to make up for *on site* device failure.

Prospective climatic data, representing future climate conditions in the next decades (between the years 2020 and 2049), have been obtained on the basis of the outputs of global climate model (ALADIN) provided by ANR-SCAMPEI project (http://www.cnrm-game-meteo.fr/scampei/). Among the greenhouse gas emission scenarios developed on the basis of future economic, social and environmental developments for the zone of the study (Meurthe et Moselle, France), two scenarios of future climate changes proposed by IPCC (Intergovernmental Panel on Climate Change) were selected. The Scenario A2 (the most intense) assumes a high anthropogenic emissions level in a context of rapid economic growth and based on regional development levels, B1 (the most modest) describes a low emissions level in a context of greater environmental with introduction of clean and resource-efficient technologies and global development. The monthly and annual averages of main climatic variables (rainfall, evapotranspiration and air temperature) for the both scenarios were summarized in Table SI IV.1.

Table SI IV.1. Monthly and annual average rainfall, evapotranspiration (ETP), mean air temperature (T_{mean}), maximum air temperature (T_{max}) and minimum air temperature (T_{min}) predicted within the both future climatic changes scenarios A2 and B1 between 2020 and 2049

Month	Scenario A2					Scenario B1				
	Rainfall mm	ETP mm	T_{mean} °C	T_{max} °C	T_{min} °C	Rainfall mm	ETP mm	T_{mean} °C	T_{max} °C	T_{min} °C
January	66.51	13.03	2.30	4.37	0.24	64.90	12.81	1.98	4.03	-0.07
February	51.47	19.62	3.97	7.19	0.74	57.57	20.39	4.74	7.93	1.56
March	59.76	38.08	6.54	9.96	3.12	44.82	40.91	6.70	10.39	3.01
April	60.24	58.51	9.66	13.95	5.37	47.86	60.71	9.91	14.52	5.30
May	80.37	80.26	13.72	18.73	8.71	57.27	86.90	13.14	18.46	7.82
June	75.62	90.53	16.69	20.52	12.86	81.96	95.37	16.83	20.90	12.76
July	64.01	100.51	18.56	22.92	14.21	56.23	114.97	19.29	24.39	14.18
August	49.38	90.63	19.83	25.04	14.61	57.09	99.78	20.36	26.11	14.61
September	63.75	53.47	15.82	20.87	10.78	63.07	53.98	15.69	20.92	10.45
October	68.21	25.28	11.00	14.86	7.14	74.94	24.61	10.82	14.50	7.13
November	71.04	11.69	6.42	8.73	4.11	82.20	11.89	7.09	9.15	5.03
December	66.25	11.22	2.71	4.94	0.47	71.25	11.51	3.25	5.44	1.06
Mean annual	776.60	592.83	10.60	14.34	6.86	759.16	633.84	10.82	14.73	6.90

3.1.5. Statistical analysis

Statistical analyses were performed using R software (Version 3.2.3). Analysis of variance (ANOVA) and the Tukey Kramer HSD test were performed to test if the PHE fractions and the percolated water volumes differed significantly among the four replicates of the bare plots.

3.2. Model description

Model building and simulations were achieved using the INRA Virtual Soil Platform (Lafolie et al., 2014). Detailed information about the platform and how the model was built within this platform is available in the Supporting Information (SI).

Briefly, the coupled PAH model is one-dimensional and is composed of five main modules: heat transport, water flow, solute transport, PAH sorption and PAH biodegradation. The climatic data (evapotranspiration (ETP), rainfall (R), air temperature (T)) are provided by specific modules considered as boundary conditions. This study focused on soil processes without any plant effect and no modules associated to plant processes were implemented at this stage. PAH atmospheric deposits was considered minor compared to PAH soil concentrations, and not considered as well. Figure IV.1a shows the relationships between the modules and the information they exchange as input variables and output variables. Heat transport module computes heat flow and soil temperature distributions in the soil profile using the convection diffusion equation. Water flow module computes water outflow, water

content and water potential distributions in the soil profile using Richard equation. Solute transport module simulates the transport of the solute species, here PAH, in the soil solution using the advection-dispersion equation. The mathematical algorithms and numerical solutions adopted for these three aforementioned modules were taken from Lafolie (1991). The PAH biodegradation and sorption modules simulate PAH dynamics in soil including biodegradation and sorption processes. These were developed specifically and previously published by Brimo et al. (2016). Biodegradation module simulates the degradation of the solute species of PAH (PAH_{AV}, where "av" subscript refers to available) using two biodegradation pathways. The co-metabolic pathway (plotted in dashed lines Figure IV.1b) uses first order kinetics and the specific biodegradation pathway uses Monod equation (plotted in pointed lines Figure IV.1b). Coefficients controlling soil water content and temperature dependence of degradation proposed respectively by Recous (1995) and Andrén et al.(1992) were also considered in the development of this module. The module computes the growth of the specific biomasses, B_{SPE}, the metabolites formation, PAH_{MET}, the production of CO_2, PAH_{CO2}, and the formation of biogenic bounded residues, PAH_{BS}. Sorption module computes both the weakly sorbed (PAH_{WS}, where "ws" refers to weakly sorbed) and the strongly sorbed (PAH_{SS}, where "ss" refers to strongly sorbed) fractions for PAH as result of sorption on soil solid fraction. Both processes are described using bi-phasic first order kinetics model.

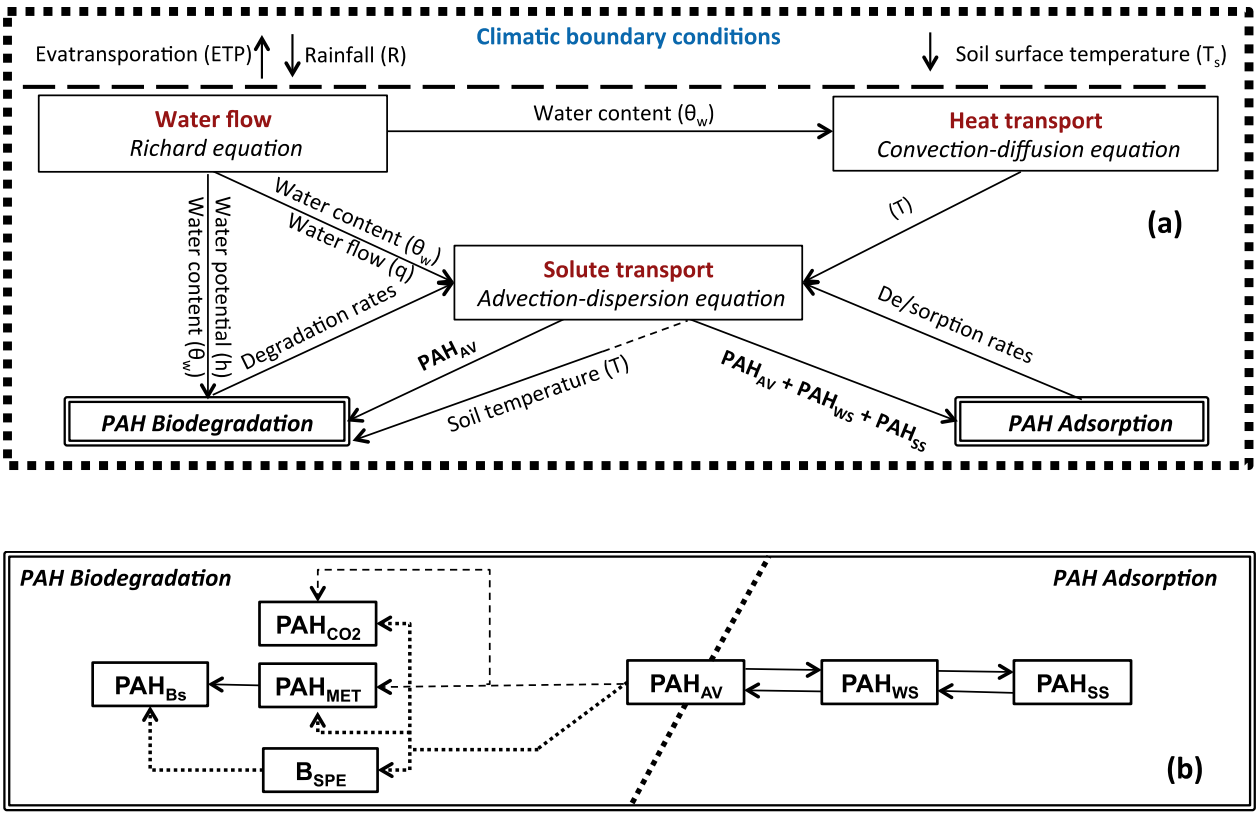

Figure IV.1. (a) The PAH model coupling scheme: the limited conditions as well as the defined processes (in bold text), the corresponding mathematical modules (" ") and their related variables required as input variables and produced as output variables with focus on the PAH biodegradation and adsorption modules. (b) Structure of the adsorption and biodegradation modules.

PAH model development in the Virtual Soil platform (SI)

All information about the Virtual Soil platform (VSoil) can be consulted on the dedicated web page: https://www6.inra.fr/vsoil/. Only the most relevant information about the basic structure of the platform with a description of the PAH model building process within the platform are presented below.

General description of the VSoil platform (SI)

The platform is an open modeling software that enables users to: (i) smooth the development and the share of models linked to a variety of bio-chemical and physical processes occurring in the soil; ii) facilitate the coupling of models to build a larger integrated model in order to address complex problems in soil system.

*In general, model building in VSoil is performed by successive use of four softwares termed VSoil_Processes, VSoil_Modules, VSoil_Models and VSoil_Player respectively (*Figure SI IV.1*). VSoil_Processes is dedicated at defining the elementary processes and their related*

variables required as inputs variables and produced as outputs variables. VSoil_Modules aims at developing a new module or modifying an existing module in the platform. The module provides the mathematical description of a process. Each module is associated to only one process but several modules can be proposed for a given process (each represents an alternative conceptualization to describe that process). A model for a specified problem can be created or modified by assembling the appropriate modules thanks to VSoil_Models. VSoil_Player enables users to run the models, to achieve simulation results, and to compare previous achieved outputs for several runs. Recently, a new functionality has been implemented in the platform that allows users to perform global sensitivity analysis based on R-sensitivity package (Pujol et al., 2015) .

PAH model construction in the VSoil platform (SI)

We present here the process of developing the PAH coupled model within the Virtual Soil platform. In the current study, dealing with a bare soil, the following processes have been taken into account: soil heat flow, soil water flow and solute transport that are all viewed as "transport processes". As well, the biodegradation and sorption processes for PAH that describe the major mechanisms affecting PAH dissipation in soil. At the beginning, the aforementioned processes and their associated variables had to be identified in "VSoil_Processes" software. Indeed, while the transport processes were already existed in the platform, no specific processes linked to PAH biodegradation and PAH sorption was available. Thus, two new processes accounting for the biodegradation and the sorption of PAH were created (added) in "VSoil_Processes". The input/ output variables associated by the new added processes were also created (i.e. the variables describing the dynamics of PAH in soil such like PAH_{SS}*,* PAH_{WS}*, and* PAH_{CO2}*…).*

The next step was attaching an appropriate module for each of those processes using "VSoil_Modules" software. We used the official modules already available in the platform to account for the transport processes. We thus selected a module that describes the convection-diffusion equation for heat flow process, a module describes the Richard equation for water flow process, and a module describes the advection-dispersion equation for the solute transport process. We had only to adapt those modules with the variables associated to the new added processes. In contrast, two new modules with their algorithms were created and inserted in the platform to be used for representing the biodegradation and sorption processes. The source and the computational functions of those modules were described in the paper. In fact, the platform is designed so that once a module is selected, the upstream

processes required to provide the input variables for that module are automatically identified by the platform. As a result, several processes which were connected by default with the selected processes were also identified ("canopy water transfer", "mulch water transfer", "mulch solutes leaching", "mulch dynamics" , " surface energy and balance", "soil hydraulic properties", "preferential water flow", "soil structure" and "organic matter dynamics" as showed in Figure SI IV.2*). Consequently, in the current study, a module that provides the metrological information was set for the process "surface energy and balance". A module that provides constant values for the soil properties (soil bulk density, soil porosity) was set for the process "soil structure". A module that provides determined values of the hydraulic soil properties (saturated hydraulic conductivity, saturated volumetric water content, etc.....) was set for the process "soil hydraulic properties". The remained processes which were not actually simulated by the current study were represented by specific modules in which the output variables were simply set to 0 ("no-mulch", "no-canopy", etc.…).*

The last step in model building process was the production of the numerical model by coupling the previous modules using "VSoil_Models" software. This step was readily performed since the coupling was automatically achieved by the platform. Figure SI IV.2 *illustrates the PAH coupled model at end of this stage.*

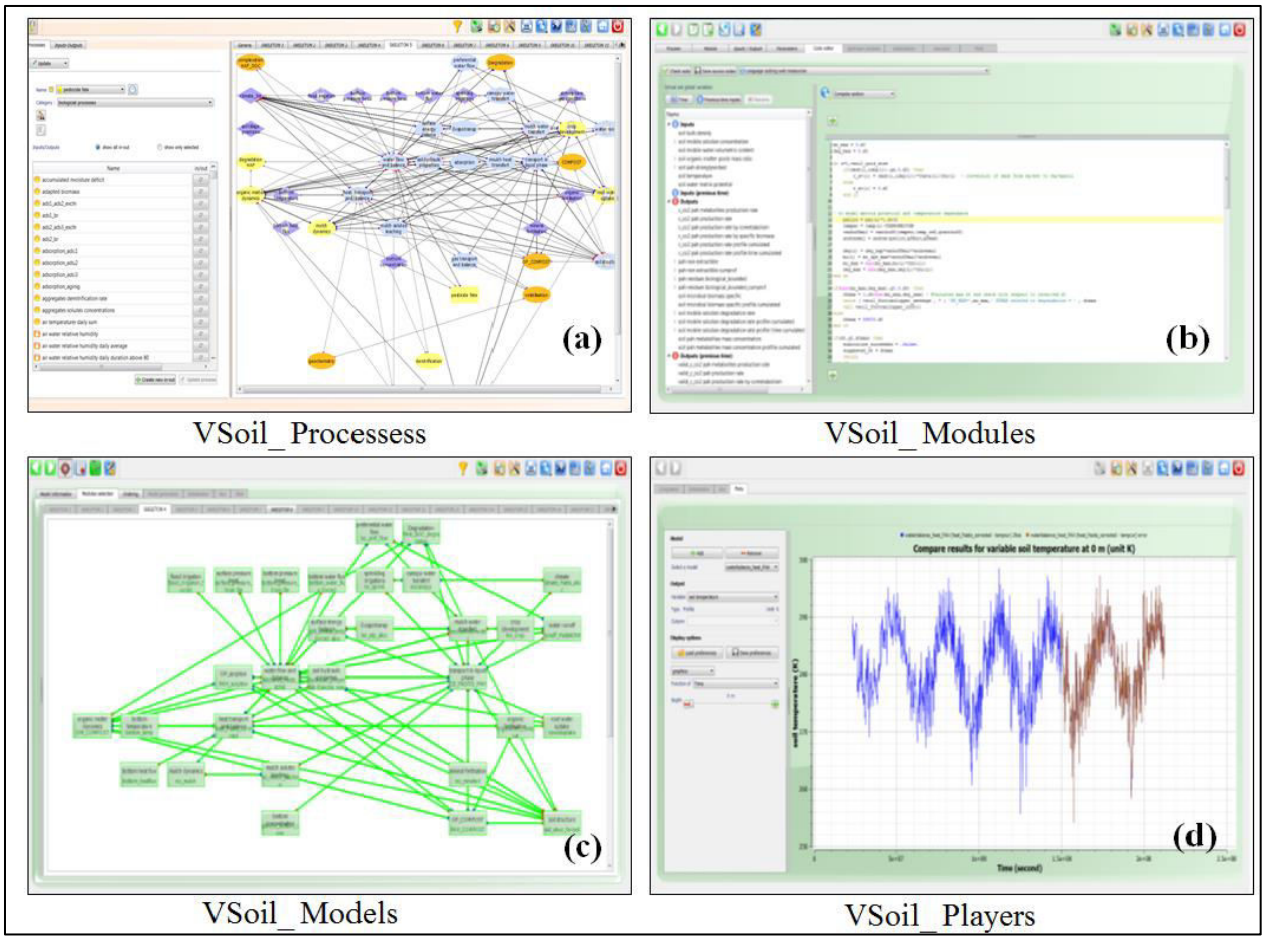

Figure SI IV.1. The four softwares of the Virtual Soil platform. From top left: a) VSoil_Processess aims at defining the processes and their input/outputs associated variables, b) VSoil_Modules aims at providing the appropriate module algorithm to each defined process, c) VSoil_Models is dedicated to assembling the modules to create a larger model, d) VSoil_Players aims at restoring and comparing achieved data.

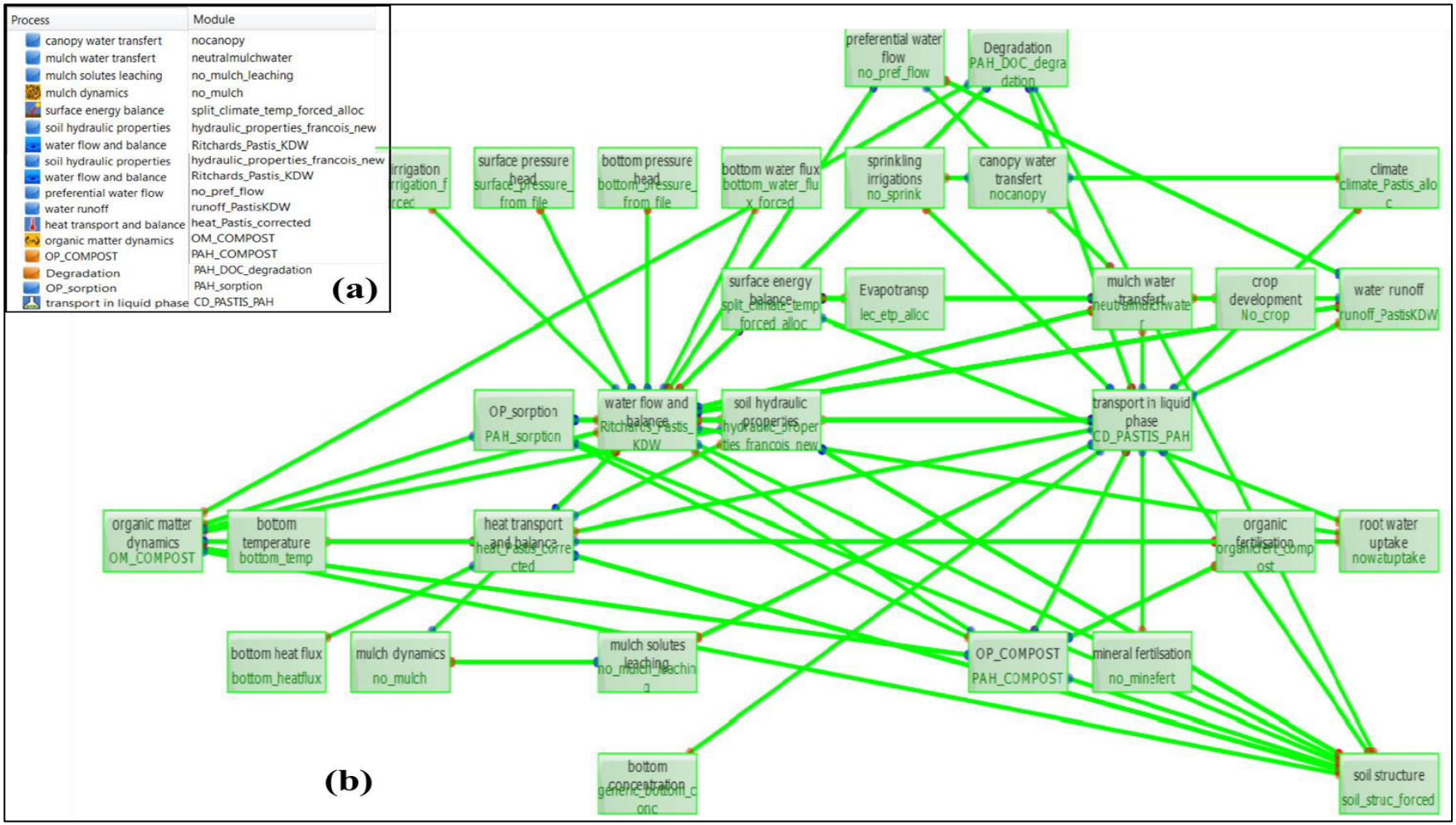

Figure SI IV.2. (a) The text part in the top left indicates the list of the simulated processes and their relevant modules. (b) Scheme of the interconnection (green bold lines) of the different processes (process name is given in black text) and their corresponding modules (in green text) considered in PAH coupled model, as appeared in VSoil_Modules software. Blue points indicate input variable(s) provided by an upstream module, whereas the red points indicate output variable(s) computed by that module.

3.3. Modelling methodology

The objectives of the present work were i) to propose a model (i.e. structure + set of parameters) able to correctly represent long-term PAH behavior in industrial contaminated soils under realistic conditions and ii) to use this model to predict potential future behavior under variable climatic conditions as might be expected from global warming effect, or forceful increase in contaminant availability. Thus the model was first calibrated and validated on past time series to be then used for prediction scenarios using modeled climatic data and alternative kinetic constant.

To start with, both water flow and heat transport modules were calibrated. Indeed, their outputs are compulsory input variables for other modules. This step was performed using the hydraulic and thermal experimental data collected from the lysimetre device. The Van Genuchten (1980) soil hydraulic functions with the model of Mualem (1976) were implemented to describe the soil water retention and the hydraulic conductivity functions. A polynomial formulation linking soil thermal conductivity to soil water content taken from Garnier et al. (2001) was selected to describe the thermal conductivity curves. The water flow parameters thus optimized were then checked against the lysimetric plots data.

Model calibration continued by calibrating the PAH modules (corresponding to the biodegradation and sorption modules) to simulate PHE data obtained on the lysimetric plots over the first eight measurement points of our data set (from May 16, 2006 until April 26, 2010). Then, starting from the default parameter values obtained from calibration study using laboratory data (Brimo et al., 2016), a new set of parameters was derived by fitting three parameters: k_M, k_{SW} and μs_{max} while fixing the other parameters to their default values. The parameters k_M and k_{SW} were chosen because they were not optimized in the previous study due to short experimental time (they were left fixed to zero). The parameter μs_{max} was also chosen as it proved to have significant influence both independently and in conjunction with other model parameters including k_{SW} and k_M on the model simulation results, as previously assessed by a global sensitivity test (Brimo et al., 2016). We chose to set μs_{max} to a realistic value taken from the literature describing *in situ* PHE degradation in a soil of a former coke plant to improve the model prediction due to lack experimental data on the mineralisation quantities. The model was then validated using the last five measurement points of our data set (from September 27, 2010 until September 27, 2012).

Finally, the validated model was further used to explore the effect of two factors: climate and pollutant availability.

In the first case, we aimed at evaluating climate change impact on long-term (40 years) fate of PHE. To do so and using as initial conditions the data measured in September 27, 2010, we run two identical model simulations during the period from September 27, 2010 to December 31, 2049. The only difference between the two simulations was the input meteorological data sets. The meteorological data used for these simulations was the climatic data from the local weather station over the first ten years (simulation period between September 27, 2010 and December 31, 2019) taken on the basis of randomized past data selection and completed by the climatic data provided by the two scenarios of future climate changes (A2 or B1) for the last 30 years of simulation period. Hence, the difference between the two climate change scenarios was only over the last 30 years of simulation period.

In the second case, we artificially increased PHE availability several times, as it might be obtained after the addition of solvents or surfactants. To do so, we run the model over a 5 years period (from September 27, 2010 until September 27, 2015) with increased k_{SW} values (2, 5, 10 folds) corresponding to a 2, 5, 10 fold increase of substrate transfer rate from PAH_{SS} to PAH_{WS}.

In the numerical model, the lysimetric plot was considered as one-dimensional domain with a simulation depth of 40 cm that was discretised into one layer by a finite element mesh. When water flow and heat transport modules were calibrated using data collected from lysimeter, the lysimeter geometry was represented in the model by the same way as in plot but with simulation depth of 200 cm. The upper water flow boundary condition (0 cm depth) was set by the daily atmospheric conditions (rainfall and evapotranspiration) and the lower boundary condition (respectively depth 40 cm in plot and 200 cm in lysimeter) was the free drainage. The potential evapotranspiration values (ETP) were calculated from the collected climatic data using Penman-Monteith equation (FAO 56-Method). The upper solute transport boundary condition was defined as Cauchy boundary condition. The upper heat transport boundary condition was specified as the hourly soil surface temperature and a free temperature condition was applied as boundary condition. The initial conditions for water flow and heat transport were assigned in terms of volumetric water content and soil temperature values at the beginning of each simulation. When PAH dynamics were simulated in plot, we always chose to start our simulations to coincide at one of soil sampling times. The initial conditions for sorption and biodegradation modules were therefore taken as follows: PAH_{CO2}, PAH_{Bs} and PAH_{MET} were all considered null; the initial specific biomass concentration was always taken equal to 0.575 mg C kg_{ds}^{-1} (equivalent to 0.61 mg PHE kg_{ds}^{-1}) as reported by Cébron et al. (2009), while the values of PAH_{WS}, PAH_{AV} and PAH_{SS} were

derived from the PHE measured data described in section (3.1.2). The quantity of PHE extracted with Tenax represented the total bioavailable fraction (PAH_{AV}+PAH_{WS}) found in both aqueous and sorbed phases. The quantity extracted with dichloromethane represented the sum of the total bioavailable fraction and the aged fraction (i.e. PAH_{AV}+PAH_{WS}+PAH_{SS}). Thus, the aged fraction, PAH_{SS}, was obtained from subtracting the total bioavailable fraction from the total extracted PHE fraction at each sampling time. The amount of PHE in solution that was viewed as PAH_{AV} of the model was calculated from the total bioavailable fraction considering that the PHE recovered by Tenax was sorbed on soil (*i.e.* neglecting contribution of soluble PHE, being 1/1000 to 1/960 of the total) using the sorption distribution coefficient K_d (L kg_{ds}^{-1}) as following:

$$K_d = \frac{\text{sorbed PAH compound recovered by Tenax (mg kg}_{\text{ds}}^{1})}{PAH_{AV}} \quad \text{(IV.1)}$$

The K_d value was obtained using:

$$K_d = K_{OC} f_{OC} \quad \text{(IV.2)}$$

Where f_{oc} is the organic carbon content in soil (here 63 g C kgds-1) and *K*oc is the sorption distribution coefficient normalized to *f*oc, which can be calculated using the correlation taken from Nguyen et al. (2005):

$$\text{Log } K_{OC} = 1.14 \text{ Log } K_{ow} \quad 1.02 \quad \text{(IV.3)}$$

Where K_{ow} is the octanol-water partition coefficient and Log K_{ow} value is 4.57 for phenanthrene (Mackay et al., 2006).

As well, we assumed uniform concentrations of the soil microbial biomass and PHE along the soil profile (between 0 and 40 cm) because they were all taken from soil samples collected over the whole profile depth. In the current study and based on the conclusion of our previous work that the specific biodegradation pathway is the most significant at explaining PHE biodegradation (Brimo et al., 2016), the co-metabolism biodegradation pathway was neglected (i.e. $K_{deg} = 0$; $\beta = 0$).

3.4. Goodness of fit criterions

We applied the following statistical criteria in order to assess our model correctness: Nash-Sutcliffe model efficiency index *NS* (Nash and Sutcliffe, 1970), Theil's inequality coefficient U^2 (Power, 1993) and the chi-squared test χ^2 (FOCUS, 2006) as well as the correlation coefficient *corr* (Fisher, 1958). The mathematical formulations of these criteria are given in

appendix (SI). *NS* = 1 indicates a perfect agreement between the simulated and the observed data while *NS* ≤0 indicates that the model provides less accurate predictions than the mean value of the observed data. Conversely best model performance result in $U = 0$, while $U > 1$ indicates that the model performs worse than using past observations to describe future conditions. The χ^2 test considers the deviations between observed and predicted values relative to the uncertainty of the measurements. The χ^2 calculated for a specific fit at a given degree of freedom should be below 15% (at 5% significance error). The correlation coefficient (*corr*) is calculated using the function "corrcoef" in MATLAB where a correlation value of 1 indicates that the model matches the pattern of the observations exactly.

Statistical criteria (SI)

- *Nash-Sutcliffe model efficiency index:* $NS = 1 - \frac{\sum_{i=1}^{n}\left(y_{obs,i} - y_{calc,i}\right)^2}{\sum_{i=1}^{n}\left(\bar{y}_{obs} - y_{obs,i}\right)^2}$

- *Theil's inequality coefficient:* $U^2 = \frac{\sum_{i=1}^{n}\left(y_{obs,i} - y_{calc,i}\right)^2}{\sum_{i=1}^{n}\left(y_{obs,i}\right)^2}$

- *Chi-squared test:* $^2 = \sum_{i=1}^{n}\frac{\left(y_{obs,i} - y_{calc,i}\right)^2}{\left(err.\bar{y}_{obs}\right)^2}$, *where* $err = \sqrt{\frac{1}{^2_{(n\ g,\ )}}\sum_{i=1}^{n}\frac{\left(y_{obs,i} - y_{calc,i}\right)^2}{\bar{y}_{obs}}}$

Where $y_{obs,i}$ *and* $y_{calc,i}$ *are respectively the observed and predicted values at the* i^{th} *observed point,* $\bar{y}_{obs}$ *represents the mean of all observed values.* $^2_{(n\ g,\ )}$ *is the* χ^2 *tabulated value for (n-g) degrees of freedom, with n number of data points and g parameters estimated.* α *is the probability at which the test is performed (*α*=5% in our study)*

4. Results and discussion

4.1. Model calibration and validation

4.1.1. Heat and water flow

The parameters used for simulating the heat and water flow are given in Table IV.1. All heat flow parameters were taken from Garnier et al. (2001). The parameters of the van Genuchten equation, θ_r, *l*, *n*, *Ks,* were predicted from our soil textural properties (sand: 62.9 %, silt 24.1% and clay 13%) using the ROSETTA code (Schaap et al., 2001) whereas the two other ones, θ_s and α, were optimized using the hydraulic data observed in the lysimeter column

(results not shown). θ_s and θ_r are respectively the saturated and residual volumetric water content, *Ks* is the hydraulic conductivity at saturation and α, *l*, *n* are empirical parameters. Once calibrated on the lysimeter column data, these parameters were then used to simulate lysimetric plots hydraulic behavior. For water outflow both the exact timing of the onset of drainage and the peak discharge were generally perfectly simulated (Figure SI IV.3 and 4) as confirmed by *NS, U* and *corr* values close to ideal values (Table SI IV.2). For soil temperature, since no data were available on lysimetric plots, parameters were checked against lysimetric column data. In general, a satisfactory correspondence between observed and model-predicted values was found as confirmed with high *NS* value equals to 0.76. Nevertheless, the model tended to underestimate temperature values at 50 cm depth during dry periods by about 3.28 °C (Figure SI IV.5). We suspect the major reason of this was related to setting ambient air temperature (instead of soil surface temperature) for the upper limit condition, due to lack of data. However, this anomaly should not have a considerable effect on simulation results of PHE degradation as the water content during dry periods is reported to have more significant limitation on biological activity than the temperature (Alletto et al., 2006).

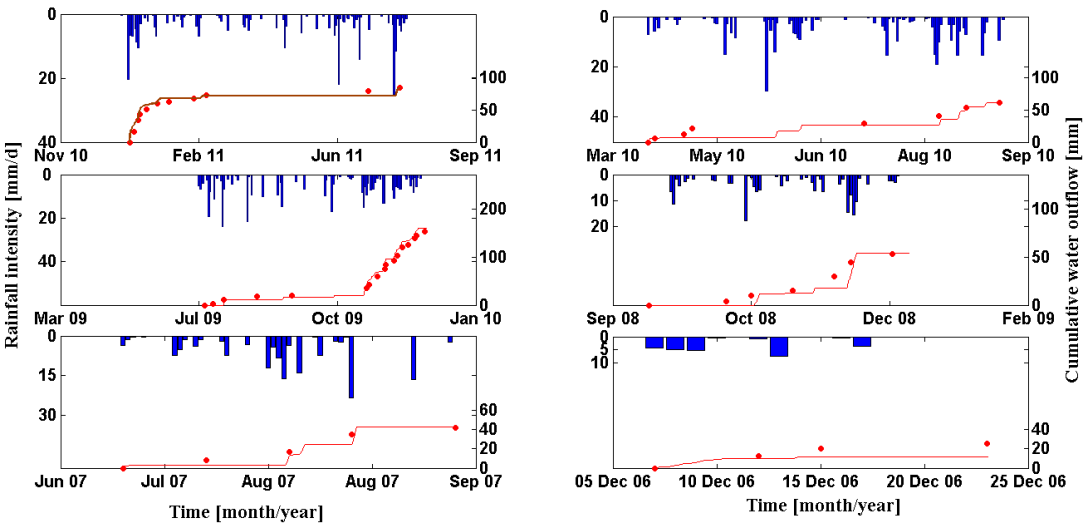

Figure SI IV.3. The measured and simulated average cumulative water outflows obtained in the lysimetric plots (4 replicates) of year 2011, 2010, 2009, 2008, 2007 and 2006. Left y-axes indicate the rainfall intensity (mm d^{-1}) (blue bars), while right y-axes indicate the measured (points) and simulated (line) average water outflows (mm).

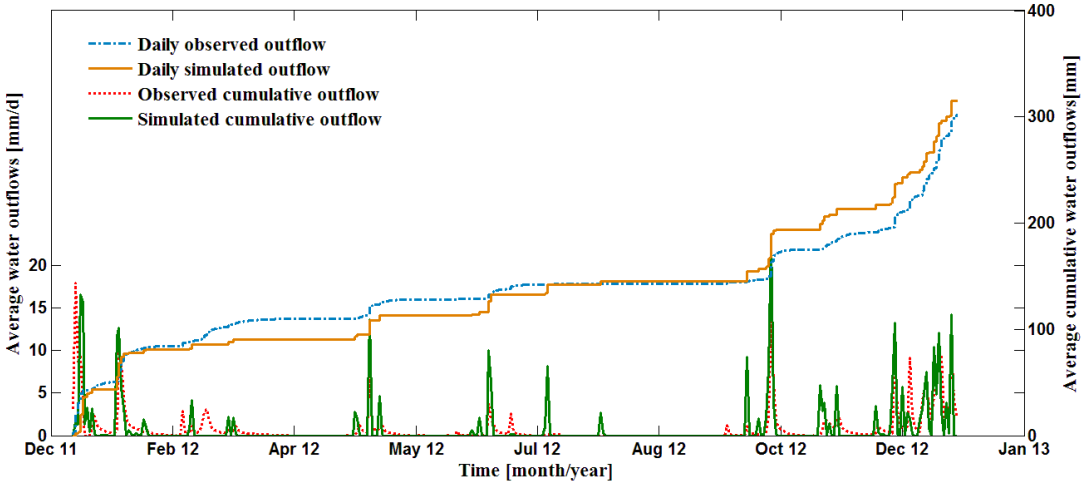

Figure SI IV.4. The measured and simulated average daily and cumulative water outflows of the lysimetric plots (4 replicates) between January 1, 2012 and December 31, 2012.

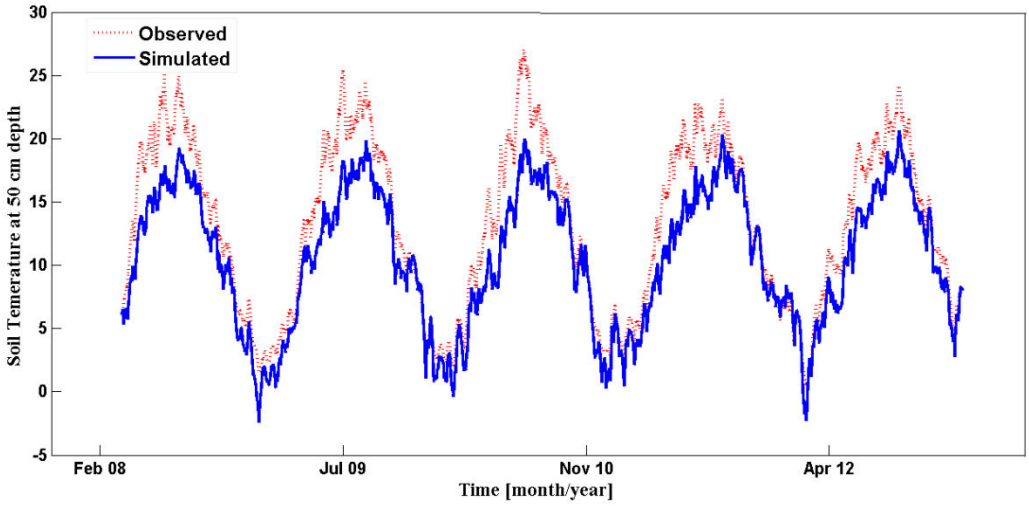

Figure SI IV.5. Comparison between simulated (solid blue line) and observed (red dotted line) temperature values at 50 cm depth of soil profile in the lysimeter column.

Table IV.1. Physical parameters used in PAH coupled model to simulate water, heat, and solute species

Parameters	Values
Water flow	
Saturated volumetric water content, θ_s (m^3 m^{-3})	0.3454
Residual volumetric water content, θ_r (m^3 m^{-3})	0.0471
Inverse of the air-entry value, α (m^{-1})	0.10
Pore-size distribution index, *n* (-)	1.3910
Pore-connectivity parameter, *l* (-)	0.5
Saturated hydraulic conductivity, K_s (m day^{-1})	0.3152
Heat transport	
Heat capacity of the solid phase of each layer (J kg^{-1} K^{-1})	800
Term of degree 0 in the polynomial formulation of the thermal conductivity coefficient as a function of water content (W m^{-1} K^{-1})	0.5
Term of degree 1 in the polynomial formulation of the thermal conductivity coefficient as a function of water content (W m^{-1} K^{-1})	2
Solute transport	
Longitudinal dispersivity (cm)	1
Molecular diffusion coefficient (cm^2 day^{-1})	0.3776*

*Value taken from Gustafson and Dickhut (1994).

Table SI IV.2. Statistical criteria (NS, U and corr) for water flow simulations. Values in bold characters represent poor match between observed and simulated data.

Rainfall event	*NS*	*U*	*corr*
6 - 22 Dec, 2006	**-2.055**	**0.4581**	0.949
9 Jul - 11 Sep, 2007	0.9	0.145	0.987
22 Sep - 19 Dec, 2008	0.897	0.207	0.975
10 Jul - 16 Dec, 2009	0.998	0.127	0.995
30 Mar - 15 Sep, 2010	0.921	0.167	0.977
7 Jan - 21 Jul, 2011	0.592	0.279	0.963
1 Jan - 30 Dec, 2012	0.899	0.102	0.984

4.1.2. Biodegradation and adsorption modules

The parameter sets previously obtained for PAH biodegradation and adsorption modules (in chapter II) did not lead to a satisfactory prediction of *in situ* PHE data (results not shown). This was quite expected since those parameters were determined using short-time laboratory incubation data and therefore at this time scale and under controlled conditions aging time and

effects of varying conditions of soil temperature and water content were not taken into account. Thus, those modules required additional parameter calibration before being used. The new parameter sets are given in Table IV.2, three parameters were optimised. The μs_{max} value was set equal to 0.0171 d^{-1} as reported by Thiele-Bruhn and Brümmer (2005) for long-term PHE biodegradation in former coking plant soil. According to Wick et al. (2001) the mortality rate k_M varied between 5 and 10% of μs_{max}. The estimated k_M value of 0.0015 d^{-1} was within that range. The k_{SW} value was in the ranges of values reported by Johnson et al. (2001).

Figure IV.2 (a to e) present the comparison between the predicted and observed average PHE data over the calibration and validation periods. The simulated surfaces were obtained by stochastic simulations through running the model using the 95% confidence intervals of PHE input data (i.e. the initial concentrations) defined at the beginning of every simulation. The uncertainty in model parameters (i.e. their 95% confidence interval values) could not be included due to excessive simulation time requirements. The quantitative assessment of the model performances for the calibration and validation periods was calculated using the 50^{th} percentile (i.e. median value). In general, the results presented in Figure IV.2 confirm the suitability of the model to describe the *in situ* dynamics of PHE, as confirmed by the good values of the different goodness of fit criteria. Hence, over the calibration period these criteria reached: $\chi^2 = 0.317$, $NS = 0.78$ and $U = 0.31$ whereas over the validation period we obtained: $\chi^2 = 0.294$, $NS = 0.97$ and $U = 0.12$. Thus the model yielded better prediction for the validation period than the calibration one. This unusual result may come from the high uncertainty in measured total PHE data for three successive dates of calibration period (September 2008, April 2009 and September 2009, Figure IV.2a), when the model largely overestimated the amounts measured for PHE.

The total PHE concentration globally displayed a continuous decrease that appeared to slow down with time, when comparing calibration and validation periods (respectively Figure IV.2a and b). The bioavailable amount dynamics appeared more cyclic with increases during the cold seasons (from October to April) and decrease during the warm seasons (from May to September) (Figure IV.2c and d). We suspect that the major reason for this was the reduction and enhancement respectively in the biodegradation process that occurred in cold seasons and warm seasons in accordance with the variations of temperature of the soil profile. Figure SI IV.6 reveals that when the temperature of the soil profile decreases in cold periods, the environmental conditions likely become less favourable for PAH degraders growth, and

reverse in warmer periods. This gives a first evidence that the environmental conditions might impact the biological activity and therefore the fate of PAH in soil.

The solute fraction of PHE was not measured individually but total dissolved PAH concentration was regularly recorded. The predicted soluble PHE concentration and measured total dissolved PAH in leachates behaved similarly. Both breakthrough curves displayed the same onset and tended to run parallel over both calibration and validation periods. This was confirmed by high correlation index between both curves with values greater than 0.97 and 0.99 respectively for calibration and validation periods. The estimated leaching rate of PHE was 1.89 10^{-9} mg m^{-2} d^{-1} (Figure SI IV.7). Simulation results showed that at end of calibration and validation periods respectively, the total leached PHE amount at 40 cm depth of the soil profile represented less than 0.006 and 0.003% of the initial PHE content of the soil profile. Regarding microorganisms, the model predicted a slow increase of PHE degraders over the 2 first years of simulation that tended to stabilize afterwards. Experimental results reported by (Ouvrard et al., 2011) showed no significant increase of PAH-degrading population over the same calibration period. According to our simulations, the most significant dissipation pathway for PHE in the soil is the mineralisation of PHE into CO_2. The model predicted that, at end of the simulation periods, the mineralised quantity of PHE into CO_2 was about 16.3 and 5.8 % of the total initial PHE content in the soil for calibration and validation periods respectively, followed by the amounts of PHE converted into biological bounded residues which represented about 2.1 and 0.78 % respectively. The produced amounts of metabolites represented less than 0.13 and 0.07 % of the total initial PHE content in soil for calibration and validation periods respectively.

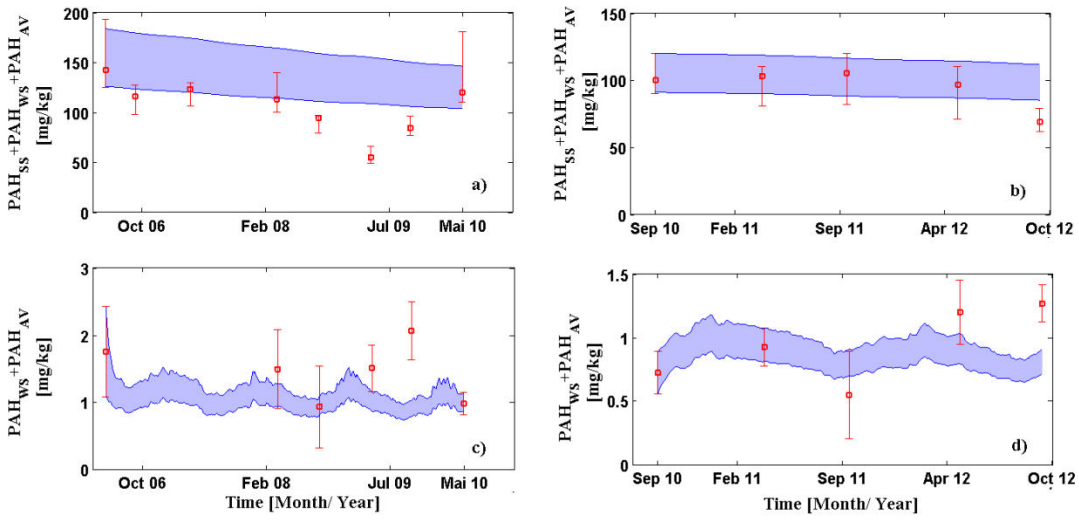

Figure IV.2. Comparison between simulated and measured data over the calibration period (left) and validation period (right) for the total PHE (a, b) and the available fraction (c, d). The shaded areas represent the 95% confidence intervals of simulated values considering only input values uncertainty. (ǫ) represent the mean value and 95% confidence intervals of observed data considering all uncertainties.

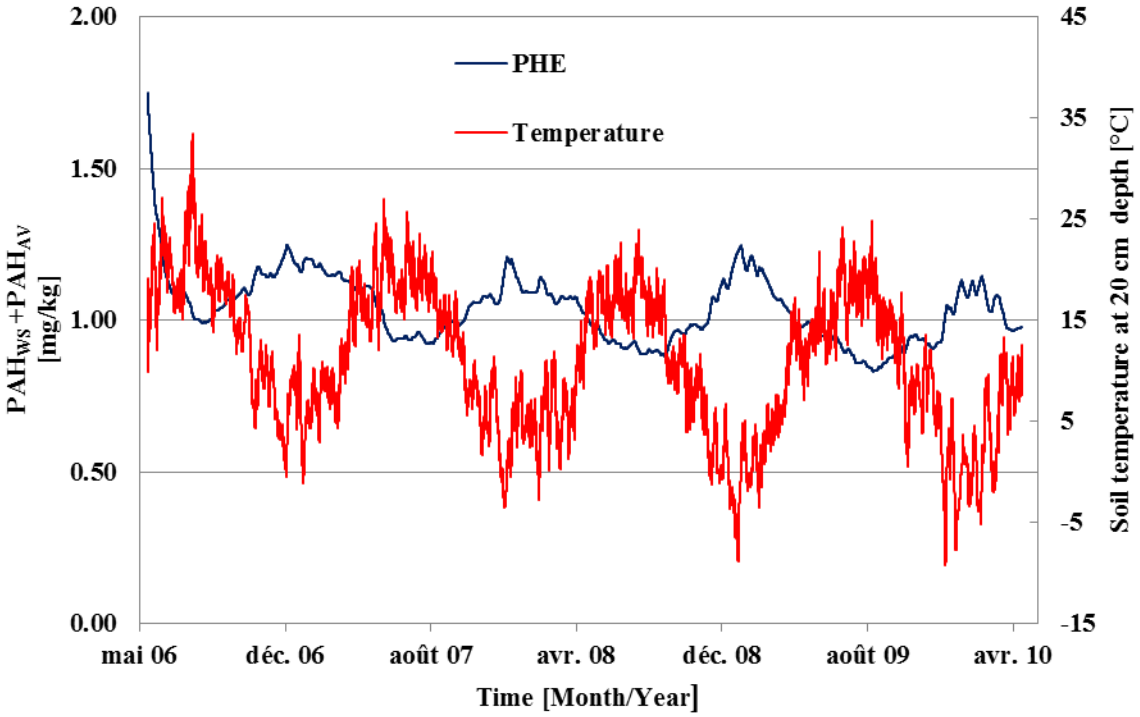

Figure SI IV.6. Dynamics the total bioavailable amount of PHE against the variation of soil temperature at 20 cm depth

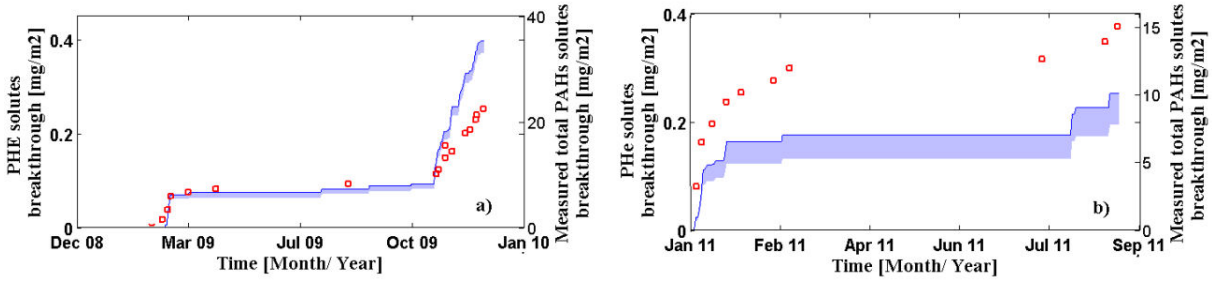

Figure SI IV.7. Comparison between PHE simulated breakthrough and 16 PAH measured breakthrough over the calibration period (a) and validation period (b). The shaded areas represent the 95% confidence intervals of simulated values considering only input values uncertainty. (⊖) represent the mean value and 95% confidence intervals of observed data considering all uncertainties.

Table IV.2. Parameter sets for PAH biodegradation and PAH adsorption modules. Only values in bold characters were optimized in this study, the others were previously validated in Brimo et al. (2016).

Symbol	Description	Value
$\mathbf{k_{AW}}$	First order kinetic constant that goes from PAH_{AV} into PAH_{WS} (day^{-1})	55.7250
$\mathbf{k_{WA}}$	First order kinetic constant that goes from PAH_{WS} into PAH_{AV} (day^{-1})	0.0567
$\mathbf{k_{WS}}$	First order kinetic constant that goes from PAH_{WS} into PAH_{SS} (day^{-1})	0.0582
$\mathbf{k_{SW}}$	First order kinetic constant that goes from PAH_{SS} into PAH_{WS} (day^{-1})	**0.0006**
$\boldsymbol{\mu s_{max}}$	Maximum specific growth rate (day^{-1})	**0.0171***
$\mathbf{ks_{spe}}$	Half saturation of growth substrate for the specific biomass (mg PHE kg_{ds}^{-1})	0.0356
$\mathbf{Y_{spe}}$	Yield of specific biomass (-)	0.1270
$\mathbf{k_M}$	Mortality rate constant (day^{-1})	**0.0015**
$\boldsymbol{\alpha}$	Magnitude of metabolites production by biodegradation for specific biodegradation (-)	0.0121
$\mathbf{k_{MB}}$	First order kinetic constant that goes from PAH_{MET} into PAH_{Bs} (day^{-1})	0.0006
$\mathbf{k_{deg}}$	Pseudo first order kinetic constant of biodegradation for co-metabolism (day^{-1})	-
$\boldsymbol{\beta}$	Magnitude of metabolites production by biodegradation for co-metabolism (-)	-

*μs_{max} value taken from (Thiele-Bruhn and Brümmer, 2005)

4.2. Long-term (2010-2049) prediction of phenanthrene under variable climatic prospective conditions

This prospective simulation aimed at exploring the long-term fate of PHE in the aged soil subject to natural attenuation (without plants and without any efforts at cleanup). An additional goal of the scenario was to analyze the influence of projected future climate changes on PHE fate and behavior in that soil.

Over the 40 years of simulation, both scenarios applied similar climatic data for the 10 first years and differed only for 30 last years. Figure SI IV.8 presents the predicted mean annual air temperatures over time for both scenarios. Both climatic scenarios, A2 and B1 predicted that air temperatures would be higher in the few next years but with a little linear increase in scenario B1 compared to A2 (increasing rates are 0.00512x and 0.0051x for B2 and A1 respectively where x stands for the year at which the future temperature is calculated). They also differed significantly on the amount of water reaching the soil surface (Figure SI IV.9) with cumulated values over the 40 years of 6932 mm and 5178 mm for A2 and B1 respectively (i.e. 1.34 folds more for A2 compared to B2). This latter was calculated by subtracting accumulated evapotranspiration flux (ETP) from accumulated rainfall flux. This increase in volume of water for scenario A2 compared to B1 was related to, respectively, decrease and increase of the predicted ETP and rainfall flux values through the last 30 years simulation periods as was described in Table SI IV.1 (i.e. between 2020 and 2049 the mean annual ETP varied between 593 and 634 mm whereas mean annual rainfall varied between 777 and 760 mm for scenario A2 and scenario B1 respectively). Consequently, the combined effects of metrological factors including precipitations, ETP, and air temperatures contribute in generating more preferential conditions of soil water content and temperature for PHE bacteria degraders in A2 compared to B1. A little increase and decrease respectively in soil water content and temperature was observed in A2 compared to B2 (see Figure SI IV.10).

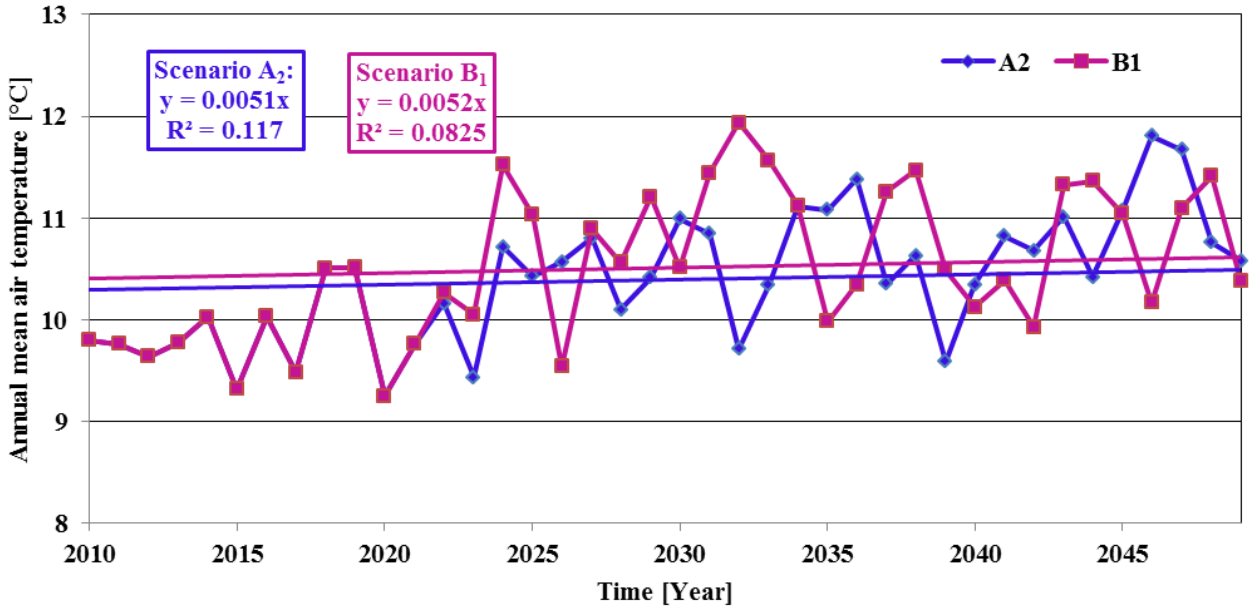

Figure SI IV.8. Comparison mean annual air temperature for the two future climatic change scenarios: A2: the most intense; B2 the most modest

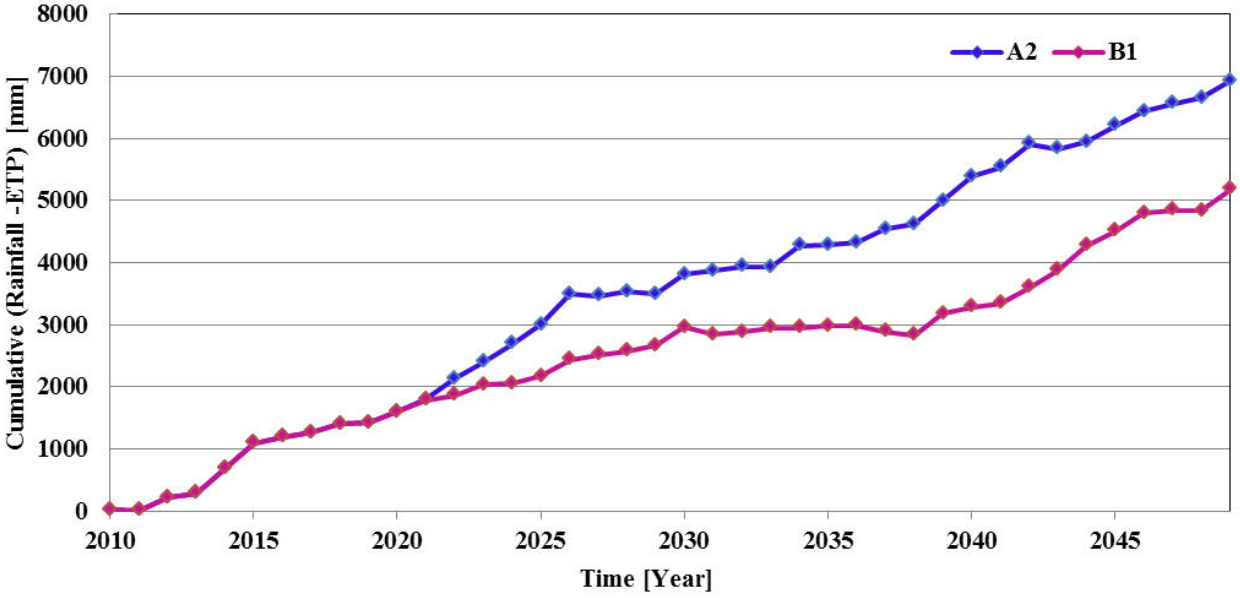

Figure SI IV.9. Comparison annual water volume (i.e..Rainfall – ETP) for the two future climatic change scenarios, A2, the most intense and B2, the most modest

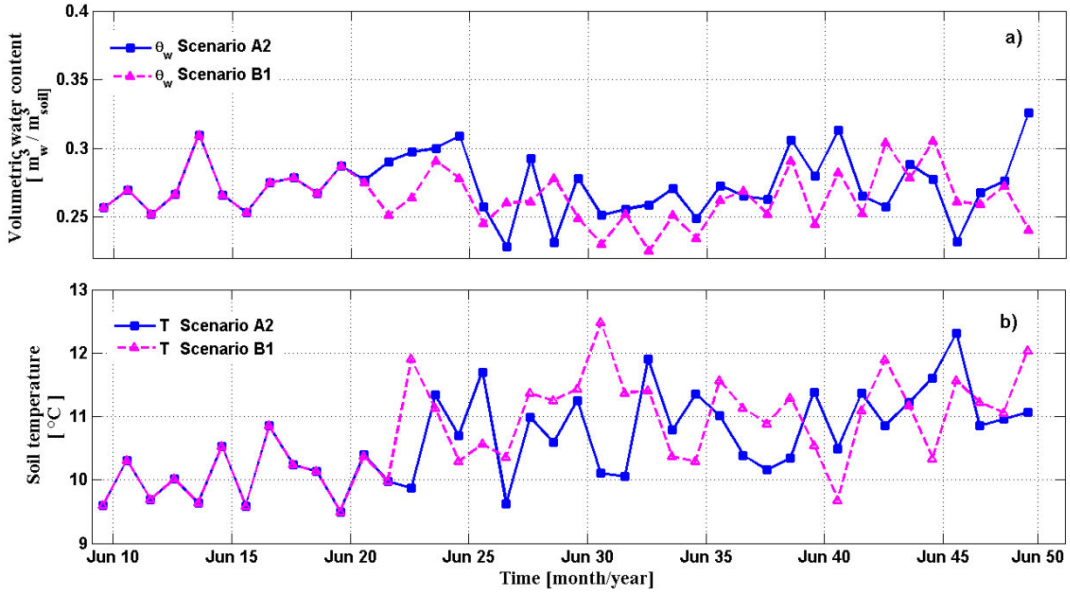

Figure SI IV.10. Mean annual soil water content (a) and mean annual soil temperature (b) over 40 years (2010-2049) predicted at 20 cm depth using the two future climatic change scenarios.

The simulated curves of the dynamics of PHE using the two meteorological data sets (A2 and B1) are given in Figure IV.3 (a to e). All variables are expressed as the percentages of the initial total measured amount of PHE in the soil profile (0 - 40 cm).

For both climatic prospective conditions, simulation results indicated that PHE extractible fraction displayed bi-phasic loss with a first phase of about 39% decrease over the 13 first

years and a second phase with an additional 15% decrease in the 27 following years (Figure IV.3a). Similarly, the production rates of both biological bounded residues (PAH_{BS}) and the mineralized amount into CO_2 (PAH_{CO2}) were found to be much more important in the first phase compared to the second phase (Figure IV.3c and d respectively). The evolution of the specific microbial biomass (B_{SPE}) accumulated in the soil profile (Figure IV.3f) increased over the first 6 years (i.e. from 2010 to 2016) and started declining thereafter to reach a value close to its initial value at the end of the first phase period (around 2022). It further continued to slowly decrease to reach a very low value at the end of the simulation period. The bioavailable fraction (Figure IV.3b) decreased by about 0.0129 mg kg_{ds}^{-1} y^{-1} over the initial 13 years and remained stable over the rest of the simulation time. Indeed, in our model the total bioavailable PHE concentration results from the balance between the sink due to the metabolism of substrate by microorganisms and the supply source including the kinetics of exchanges between the highly adsorbed sites PAH_{SS} and the weakly ones PAH_{WS}. Figure IV.4a and b show respectively the daily absolute exchange kinetics between PAH_{WS} and PAH_{SS} and the daily degradation rate of PHE by microbial biomasses. One would note that both processes display similar patterns suggesting that the translocation of PHE from PAH_{SS} to PAH_{WS} is the dominant process for the supply of PHE to the microbial biomasses. Thus, the two distinct phases for PHE loss are likely caused by the decrease of the transfer rate of PHE with increasing time.

Indeed, translocation might not be only the main process influencing the metabolism of PHE by microorganisms especially in short and medium terms (i.e. from several months to a few years) but it was mostly the limiting factor during all the simulation period. This could explain why for example the shift in microbial communities induced by plant species cultivated on the same soil was not experimentally observed to impact significantly PHE removal in soil. This result supports the conclusion that remediation practices on the basis of increase in PAH bacteria degraders for highly polluted soils may have a significant effect in short to medium term but a little or no effectiveness for longer term.

On the other hand and based on scenarios of future climate changes conditions, it was found that PHE removal efficiency within the scenario B1 was less than that showed by scenario A2. Over the last 29 years of simulation (i.e. from 2021 to 2039) the PHE extractible fraction decreased by 15.97% and 12.65% for scenario A2 and scenario B1 respectively (Figure IV 3a). Thus, the difference observed between both scenarios was 3.32%. This occurrence would therefore be explained by modifying the degradation rate resulting from the difference of temperature and soil water content conditions between the both scenarios.

Figure IV.4e presents PHE leaching for both scenarios. The leaching rate of PHE was found to be higher (by a factor of 1.2) in B1 compared to A2 which was consistent with findings reported for pesticides showing that leaching to groundwater increases with increasing persistence (Soutter and Musy, 1999; Tiktak et al., 1994). These results clearly highlight that climate conditions are factors that can affect the efficiency of the natural remediation of PAH in contaminated soil and should therefore be accounted for in future management practices.

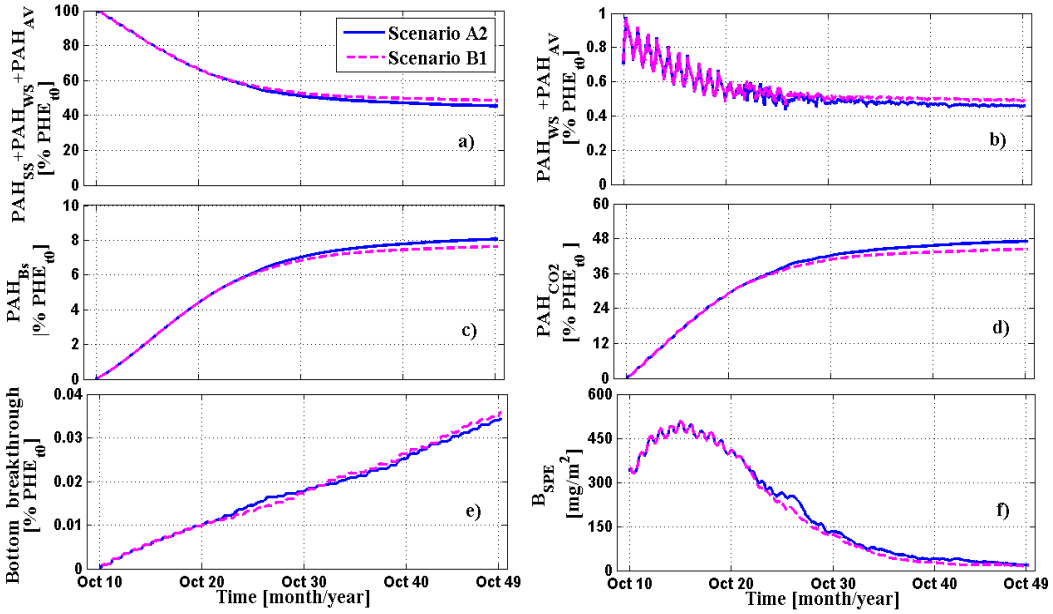

Figure IV.3. Dynamics of phenanthrene in soil between the years 2010 and 2049 using two future climatic change scenarios: A2: the most intense; B2 the most modest. The results in panels (a) to (e) are presented as percentage of the initial total observed amount of phenanthrene in soil profile [0-40 cm] while panel (f) represents the temporal evolution of the specific biomass accumulated in soil profile expressed by unit of mg m^{-2}.

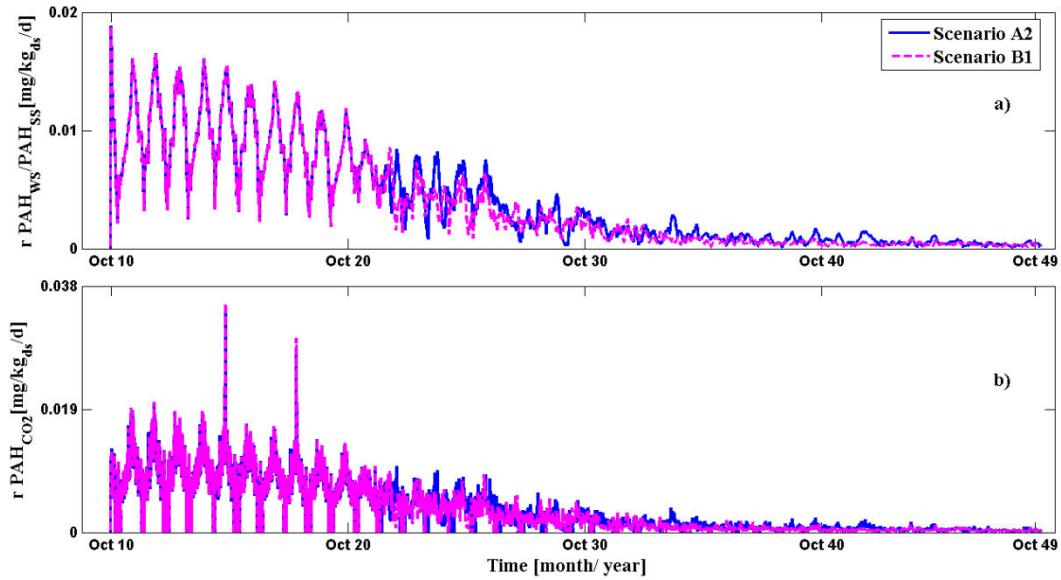

Figure IV.4. (a) kinetics of exchanges of phenanthrene between the weakly sorbed fraction (PAH_{WS}) and the strongly one (PAH_{SS}). (b) PAH_{CO2} production rate by specific biomasses

4.3. Effect of simulated increase in PHE desorption rate

This scenario tried to approximate an alternative strategy that would increase the mass transfer of contaminant substrate such as an addition of solvents or surfactants (e.g. alcohol ethoxylate, glycoside, triton X-100, tween 80). As expected (Laha et al., 2009; Madesen and Kristensen, 1997), simulation results showed an increase in the degradation rate with the increase of the translocation rate of the substrate from the PAH_{SS} into PAH_{WS} compartment (Figure IV.5). It provided further evidence that delivering the substrate to bacteria degraders was the main limitation to biodegradation. Interestingly the increase in degradation was not fully proportional to the increase of the desorption rate. As an example, when the desorption rate was doubled a remediation level was reached in 6 years (including 40% PHE mass loss into PAH_{CO2} and PAH_{BS}) instead of 14 years. Thus any technology achieving this effect of increased desorption rate, when combined with bioremediation strategy enhancing and/or maintaining high biological activity, might be a real asset for remediation of contaminated sites of former industrial activities.

However, this strategy also increases PHE exposure. Indeed, both the concentration of bioavailable fraction (Figure IV.5b) and the leaching rate into groundwater (Figure IV.5e) are enhanced thus increasing the potential toxicity risks. Such factors should be kept in mind when a decision concerning the remediation strategy has to be made. It is also important to indicate that our simulation results for this scenario did not consider the real method by which

such an increase in bioavailability could be achieved. For instance any addition of surfactant or extracting solvents could also have an effect on the biological activity. Such inhibition, including toxicity, of surfactant on the microorganisms growth has already been pointed out (Aronstein et al., 1991; Li and Chen, 2009; Mosche and Meyer, 2002).

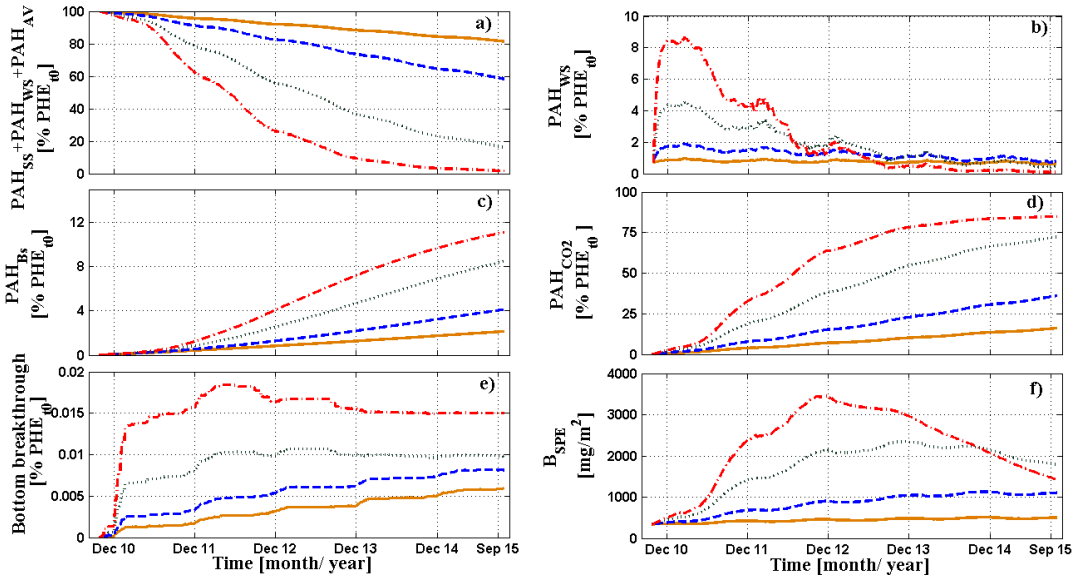

Figure IV.5. Evolution of PHE removal whether the desorption rate of PHE was increased forcefully several times: solid line = k_{SW} x 1; dashed line= k_{SW} x 2; pointed line= k_{SW} x 5; point-dashed line= k_{SW} x 10

5. Conclusion

Based on the experimental data of a long term field experiment, this study was dedicated to predict the fate of phenanthrene (a PAH model compound) *in situ* under two remediation options: strategy based on long term natural attenuation without any efforts at clean up whereby two future climate changes were tested, and by addition of solvents or surfactants to accelerate the substrate transfer rates. To do so, the PAH model was inserted in the Virtual Soil Platform of INRA including other modules describing the water transfer, heat transport and solute transport as well as the climatic conditions. The performance of the coupled model was tested via a calibration and validation process. Simulation results based on long term natural attenuation showed that i) degradation of PHE was characterized by two degradation phase, ii) PHE removal was governed by substrate transfer limitation from the strongly sorbed compartment into the weakly one and not by the microorganisms, and iii) meteorological factors were important and therefore must to be accounted for in each management strategy. The second option emerged that addition solvent or surfactants resulted in significant

increasing in substrate transfer rate, hence reducing time remediation. However, also increases in toxicity and risk of leaching were noticed. In the future, module associated to plant functions and compost fertilization will be integrated in the Virtual Soil platform to simulate the fate of PAH in agricultural soils.

6. Acknowledgements

This research was financially supported by the French Environment and Energy Management Agency (ADEME) and the Environment and Agronomy division of the French National Institute for Agricultural Research (INRA). We are grateful to the development team of the Virtual Soil Platform: Nicolas Moitrier, Nathalie Moitrier and Cédric Nouguier for their technical help and to Erwan Personne for the fruitful discussions.

7. References

Adam, I.K.U., Rein, A., Miltner, A., Fulgêncio, A.C.D., Trapp, S., Kästner, M., 2014. Experimental results and integrated modeling of bacterial growth on an insoluble hydrophobic substrate (phenanthrene). Environ. Sci. Technol. **48**, 8717–8726. doi:10.1021/es500004z

Alletto, L., Coquet, Y., Benoit, P., 2006. Effects of temperature and water content on degradation of isoproturon in three soil profiles. Chemosphere **64**, 1053–1061. doi:10.1016/j.chemosphere.2005.12.004

Andrén, O., Steen, E., Rajkai, K., 1992. Modelling the effects of moisture on barley straw and root decomposition in the field. Soil Biol. Biochem. **24**, 727–736. doi:10.1016/0038-0717(92)90246-T

Aronstein, B.., Calvillo, Y.., Alexander, M., 1991. Effect of surfactants at low concentrations on the desorption and biodegradation of sorbed aromatic-compounds in soil. Environ. Sci. Technol. **25**, 1728–1731.

Barnier, C., Ouvrard, S., Robin, C., Louis, J., 2014. Desorption kinetics of PAHs from aged industrial soils for availability assessment. Sci. Total Environ. **470–471**, 639–645. doi:10.1016/j.scitotenv.2013.10.032

Beulke, S., Dubus, I.G., Brown, C.D., Gottesburen, B., 2000. Simulation of pesticide persistence in the field on the basis of laboratory data : A review. Environ. Qual. **29**, 1371–1379. doi:10.2134/jeq2000.00472425002900050001x

Brimo, K., Garnier, P., Sun, S., Bertrand-krajewski, J., Cébron, A., Ouvrard, S., 2016. Using a Bayesian approach to improve and calibrate a dynamic model of polycyclic aromatic hydrocarbons degradation in an industrial contaminated soil. Environ. Pollut. **215**, 27–37. doi:10.1016/j.envpol.2016.04.094

Broholm, M.M., Jones, I., Torstensson, D., Arvin, E., 1998. Groundwater contamination from a coal carbonization plant. Geol. Soc. London Eng. Geol. Spec. Publ. **14**, 159–165. doi:10.1144/GSL.ENG.1998.014.01.19

Cebron, A., Beguiristain, T., Faure, P., Norini, M.-P., Masfaraud, J.-F., Leyval, C., 2009. Influence of vegetation on the in situ bacterial community and Polycyclic Aromatic

Hydrocarbon (PAH) degraders in aged PAH-contaminated or thermal-desorption-treated soil. Appl. Environ. Microbiol. **75**, 6322–6330. doi:10.1128/AEM.02862-08

Cunningham, S.D., Anderson, T.A., Schwab, A.P., Hsu, F.C., 1996. Phytoremediation of soils contaminated with organic pollutants. Adv. Agron. **56**, 55–114. doi:10.1016/S0065-2113(08)60179-0

Edwards, N.T., 1983. Polycyclic Aromatic Hydrocarbons (PAH's) in the terrestrial environment-a review. J. Environ. Qual. **12**, 427–441.

Fisher, R.., 1958. Statistical methods for research workers, 13th Ed. ed. New York.

FOCUS, 2006. Guidance document on estimating persistence and degradation kinetics from environmental fate studies on pesticides in EU registration" Report of the FOCUS work group on degradation kinetics, EC Document reference.

Fragoulis, G., Trevisan, M., Puglisi, E., Capri, E., 2005. A model assessing bioavailability of persistent organic pollutants in soil, Reactive Transport in Soil and Groundwater. Springer-Verlag, Berlin/Heidelberg. doi:10.1007/3-540-26746-8_3

Garban, B., Blanchoud, H., Motelay-massei, A., Chevreuil, M., Ollivon, D., 2002. Atmospheric bulk deposition of PAHs onto France : trends from urban to remote sites. Atmos. Environ. **36**, 5395–5403.

Garnier, P.., Néel, C., MARY, B., LAFOLIE, F., 2001. Evaluation of a nitrogen transport and transformation model in a bare soil. Eur. J. Soil Sci. **52**, 253–268.

Geng, C., Haudin, C.-S., Zhang, Y., Lashermes, G., Houot, S., Garnier, P., 2015. Modeling the release of organic contaminants during compost decomposition in soil. Chemosphere **119**, 423–431. doi:10.1016/j.chemosphere.2014.06.090

Gustafson, K.E., Dickhut, R.M., 1994. Molecular diffusivity of polycyclic aromatic hydrocarbons in aqueous solution. J. Chem. Eng. Data **39**, 281–285. doi:10.1021/je00014a019

Iarc, 2010. IARC monographs on the evaluation of carcinogenic risks to uumans: some non-heterocyclic polycyclic aromatic hydrocarbons and some related exposures. Iarc Monogr. Eval. Carcinog. Risks To Humans **92**, 1–868.

Johnson, M.D., Keinath, T.M., Weber, W.J., 2001. A distributed reactivity model for sorption by soils and sediments. 14. Characterization and modeling of phenanthrene desorption rates. Environ. Sci. Technol. **35**, 1688–1695. doi:10.1021/es001391k

Lafolie, F., 1991. Modelling water flow , nitrogen transport and root uptake including physical non-equilibrium and optimization of the root water potential. Nutr. Cycl. Agroecosystems **27**, 215–231. doi:10.1007/BF01051129

Lafolie, F., Cousin, I., Marron, P.-A., Mollier, A., Pot, V., Moitrier, N., Moitrier, N., Nouguier, C., 2014. The « VSOIL » modeling platform. Rev. For. Française Fr.], ISSN 0035. doi:10.4267/2042/56287

Laha, S., Tansel, B., Ussawarujikulchai, A., 2009. Surfactant–soil interactions during surfactant-amended remediation of contaminated soils by hydrophobic organic compounds: A review. J. Environ. Manage. **90**, 95–100.

Li, J.-L., Chen, B.-H., 2009. Surfactant-mediated Biodegradation of Polycyclic Aromatic Hydrocarbons. Materials (Basel). **2**, 76–94. doi:10.3390/ma2010076

Mackay, D., Shiu, W.Y., Ma, K., Lee, S.C., 2006. Handbook of physical-chemical properties and environmental fate for organic chemicals, 2nd ed. ed. CRC Press, Boca Raton (FL).

Madesen, T., Kristensen, P., 1997. Effects of bacterial inoculation and nonionic surfactants on degradation of polycyclic aromatic hydrocarbons in soil. Environ. Toxicol. Chem. 16, 631–637.

Mosche, M., Meyer, U., 2002. Toxicity of linear alkylbenzene sulfonate in anaerobic digestion: Influence of exposure time. Water Res. **36**, 3253–3260.

Mualem, Y., 1976. A new model to predicting the hydraulic conductivity of unsaturated porous media. Water Resour. Res. **12**, 513–522.

Nash, J.E., Sutcliffe, J.V., 1970. River flow forecasting through conceptual models part I — A discussion of principles. J. Hydrol. **10**, 282–290. doi:10.1016/0022-1694(70)90255-6

Nguyen, T.H., Goss, K.-U., Ball, W.P., 2005. Polyparameter linear free energy relationships for estimating the equilibrium partition of organic compounds between water and the natural organic matter in soils and sediments. Environ. Sci. Technol. **39**, 913–924. doi:10.1021/es048839s

Ouvrard, S., Barnier, C., Bauda, P., Beguiristain, T., Biache, C., Bonnard, M., Caupert, C., Cébron, A., Cortet, J., Cotelle, S., Dazy, M., Faure, P., Masfaraud, J.F., Nahmani, J., Palais, F., Poupin, P., Raoult, N., Vasseur, P., Morel, J.L., Leyval, C., 2011. In situ assessment of phytotechnologies for multicontaminated soil management. Int. J. Phytoremediation **13**, 245–263. doi:10.1080/15226514.2011.568546

Ouvrard, S., Leglize, P., Morel, J.L., 2014. PAH phytoremediation : rhizodegradation or rhizoattenuation ? Int. J. Phytoremediation 16, 37–41. doi:10.1080/15226514.2012.759527

Peters, C.A., Knightes, C.D., Brown, D.G., 1999. Long-term composition dynamics of PAH-containing NAPLs and implications for risk assessment. Environ. Sci. Technol. 4499–4507.

Power, M., 1993. The predictive validation of ecological and environmental models. Ecol. Model. **68**, 33–50.

Pujol, A.G., Iooss, B., Janon, A., Veiga, D., Fruth, J., Gilquin, L., Guil-, J., Gratiet, L. Le, Lemaitre, P., Ramos, B., Touati, T., 2015. Package " sensitivity " [WWW Document]. URL https://cran.r-project.org/web/packages/sensitivity/sensitivity.pdf

Recous, S., 1995. Soil inorganic N availability: effect on maize residue decomposition. Soil Biol. Biochem. **27**, 1529–1538.

Rein, A., Adam, I.K.U., Miltner, A., Brumme, K., Kästner, M., Trapp, S., 2016. Impact of bacterial activity on turnover of insoluble hydrophobic substrates (phenanthrene and pyrene)— Model simulations for prediction of bioremediation success. J. Hazard. Mater. **306**, 105–114. doi:10.1016/j.jhazmat.2015.12.005

Schaap, M.G., Leij, F.J., Genuchten., M.T. van, 2001. ROSETTA: A computer program for estimating soil hydraulic parameters with hierarchical pedotransfer functions. J. Hydrol. **251**, 163–176.

Séré, G., Ouvrard, S., Magnenet, V., Pey, B., Morel, J.L., Schwartz, C., 2011. Predictability of the evolution of the soil structure using water flow modeling for a constructed technosol es evolution as an indicator of technosol pedogenesis. Vadose Zo. J. **11**, 111–123. doi:10.2136/vzj2011.0069

Soutter, M., Musy, A., 1999. Global sensitivity analyses of three pesticide leaching models using a Monte-Carlo approach. J. Environ. Qual. **28**, 1290–1297.

Takaki, K., Wade, A.J., Collins, C.D., 2014. Assessment of plant uptake models used in exposure assessment tools for soils contaminated with organic pollutants. Environ. Sci. Technol. **48**, 12073−12082.

Thiele-Bruhn, S., Brümmer, G.W., 2005. Kinetics of polycyclic aromatic hydrocarbon (PAH) degradation in long-term polluted soils during bioremediation. Plant Soil **275**, 31–42. doi:10.1007/s11104-004-0265-9

Tiktak, A., Linden, A.M.A. van der, Swartjes, F.., 1994. PESTRAS : a one dimensional model for assessing leaching and accumulation of pesticides in soil.

Tsibart, A.S., Gennadiev, A.N., 2013. Polycyclic aromatic hydrocarbons in soils : sources , behavior , and indication significance (a review). Eurasian Soil Sci. **46**, 728–741. doi:10.1134/S1064229313070090

Van Genuchten, M.T., 1980. A closed-form equation for predicting the hydraulic conductivity of unsaturated soils. Soil Sci. Soc. Am. J. 892±898.

Wick, L.Y., Colangelo, T., Harms, H., 2001. Kinetics of mass transfer-limited bacterial growth on solid PAHs. Environ. Sci. Technol. **35**, 354–61.

Wilcke, W., 2000. SYNOPSIS Polycyclic Aromatic Hydrocarbons (PAHs) in Soil — a Review. J. Plant Nutr. Soil Sci. **163**, 229–248. doi:10.1002/1522-2624(200006)163:3<229::AID-JPLN229>3.0.CO;2-6

Wilson, S.C., Jones, K.C., 1993. Bioremediation of soil contaminated with polynuclear aromatic hydrocarbons (PAHs): A review. Environ. Pollut. **81**, 229–249. doi:10.1016/0269-7491(93)90206-4

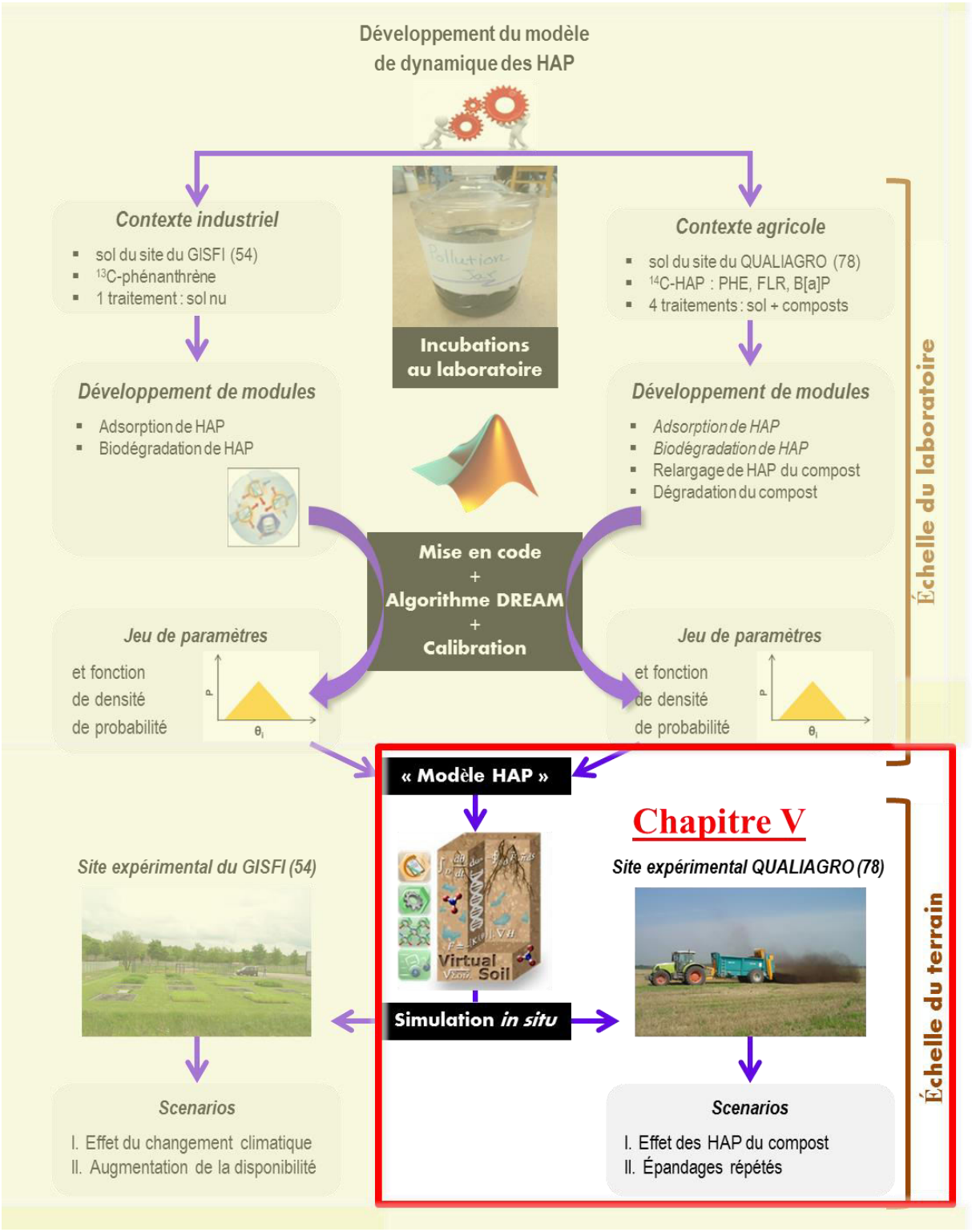

Place du chapitre V dans l'ensemble de travail de thèse

Chapitre V. Simulations de la dynamique *in situ* des HAP dans un sol agricole ; évaluation de l'impact de scenario de l'apport répété de composts urbains sur le long terme.

Résumé du contenu du chapitre en français

Ce chapitre a pour but de réaliser des scenarios numériques avec le modèle de HAP développé au sein de la plateforme SOL VIRTUEL afin de prédire, au champ, les risques associés à l'apport de HAP dû au recyclage des déchets organiques compostés dans un sol agricole. Le modèle couplé de HAP, présenté dans le chapitre précèdent, a été mis à jour pour prendre en compte les modules de HAP, présentés an chapitre 3, décrivant l'effet de la qualité des matières organiques compostées sur le relargage des HAP de ces composts pendant leur décomposition dans le sol. Les données expérimentales du site de Feucherolles (78) acquises dans 2 modalités différentes d'épandage de composts (compost d'ordures ménagères et compost de déchets verts et boues) et un traitement de control ont été utilisées pour affiner la calibration des diffèrent modules de HAP. Le modèle calibré et testé *in situ* a ensuite été utilisé pour réaliser deux scenarios. Un premier scenario est dédié à mieux comprendre comment les HAP ajoutés avec les composts évoluent dans le sol amendé en fonction de la nature des déchets organiques et du type de HAP sur une échelle temporelle de moyen terme (13 ans). Le second scenario simule l'impact d'un apport répété à plus long terme sur 38 ans des déchets organiques compostés sur les teneurs en HAP dans le sol. Les simulations ont montré que la majorité des HAP apportés avec le compost s'accumule et persiste dans le sol en causant une augmentation constante de leurs concentrations dans le sol amendé, mais qui reste à une faible valeur. L'étude n'a montré aucun effet significatif de la nature des composts sur l'état de transformations des HAP dans le sol. Ce chapitre fait l'objet d'un article en cours de préparation pour le Journal *Science of the total Environment*: « In situ

long term modeling of PAHs fate in agricultural soil after repeated applications of urban composts using the "VSOIL" platform »

In situ long term modeling of PAHs fate in agricultural soil after repeated applications of urban composts using the "VSOIL" platform

Khaled Brimo[a,b,c,d], Stéphanie Ouvrard[b,c], Marjolaine Deschamps[a], Pierre Benoit[a], Sabine Houot[a], François Lafolie[e], Patricia Garnier[a]

[a] France

[a]UMR ECOSYS, INRA, AgroParisTech, Université Paris-Saclay, 78850, Thiverval-Grignon, France

[b]INRA, Laboratoire Sols et Environnement, UMR 1120, F-54518 Vandoeuvre-lès-Nancy, France

[c]Université de Lorraine, Laboratoire Sols et Environnement, UMR 1120, F-54518 Vandoeuvre-lès-Nancy, France

[d]Agence de l'Environnement et de la Maîtrise de l'Energie, 20 avenue du Grésillé, BP 90406, F-49004 Angers Cedex 01, France

[e] INRA UAPV, UMR EMMAH 1114, F-84914 Avignon 9, France

*Corresponding authors: Patricia Garnier

Tel: + 33 130 815 314

E-mail: patricia.garnier@inra.fr

Article prepared for submission in Science of the Total Environment

1. Abstract

A potential accumulation of PAH in soils from successive compost applications could imply risks to the environment. Here we apply a global model for PAH that describes the major physical, biochemical and biological processes influencing the fate of PAH in soil under climatic conditions. The model was applied first to simulate the dynamics of PAH observed in situ with different organic amendments applied for 18 years on an agricultural soil and then to predict scenarios of the fate of these chemicals in soil. Our simulations show that the model can adequately predict the fate of PAH in soil and can contribute to clarify some of unexplored aspects regarding the behavior of PAH in soil like their mineralization and accumulation. Scenarios that predict the dynamic of PAHs in soil at long terms showed a low accumulation of extractable fraction of PAH in soil over further 38 years due to a high sequestration of PAH as non extractable fraction that is slightly higher for municipal solid waste composts than for green waste sludge composts.

Keywords: Scenarios, amended soil, model, phenanthrene, benzo (a) pyrene, bioavailability, leaching of PAH, Virtual Soil platform

2. Introduction

Nowadays, the application of urban composts on agricultural soils makes possible the recycling of organic matter in soils and the partial substitution of mineral fertilizers (Annabi et al., 2011). However, urban composts may contain trace elements among them the Polycyclic Aromatic Hydrocarbons (PAHs) present in the initial feedstock materials (Brändli et al., 2005; Houot et al., 2009). Composts are viewed as one of the most important anthropogenic source of PAHs in agricultural soils (Senesil et al., 1999; Wilcke, 2000). In France, the regulation concerning the use of urban composts including the standards NFU 44-095 and NFU 44-051 include the acceptable thresholds of 3 PAH (i.e. fluoranthene, benzo(b)fluoranthene and benzo(a)pyrene) content in compost as well as the acceptable cumulative input of these chemical with repeated applications of compost over the period of 10 successive years (Houot et al., 2002).

Nevertheless, questions remain to determine if these limits are low enough to prevent the adverse effects of PAH accumulation since the bioavailability and mobility of PAH in soil are indeed influenced by several factors like the rate and frequency of compost application, the nature and reactivity of the organic amendments (Houot et al., 2012; Xing, 1997; Xiu-hong et al., 2014), the soil physical-chemical characteristics (Chung and Alexander, 2002; Nam et al., 2003), the nature of PAH (Iarc, 2010) and the climate conditions (Dagois et al., 2015; Noyes et al., 2009). The complex interactions between the various above factors make the long term assessment of the fate and impacts of repeated applications of composts with PAH contents below the authorized maximum thresholds in agricultural soil far difficult. Modeling is a powerful technique to analyze and quantify such complex problem. An integrated numerical model would make possible to estimate the distribution patterns of PAH content among soil fractions. This would provide a more complete picture for understanding and predicting the fate of PAH in soil, which include their potential mobility, bioavailability and even their assimilation by plants in cultivated soil. Several works report PAH behavior during the composting of different organic materials (Houot et al., 2012; Lashermes et al., 2010), or the effects of single compost addition on the behavior of PAH in soil under laboratory conditions (Geng et al., 2015; Haudin et al., 2013; Kästner et al., 1999), but little or no work can be found on quantification and modeling under outdoor conditions of the long term effects of repeated compost applications on the dynamics of PAH in soil.

This study aimed at exploring the long term effects of several successive applications of urban composts on the accumulation and the bioavailability of PAH in an agricultural soil. The

study investigated the fate of two PAH substances: phenanthrene (PHE) and benzo(a) pyrene (B(a)P) within a mature and a non-mature urban composts produced from different feedstocks. The PAH dynamics in soil were simulated through scenarios using Virtual Soil Platform and data from a long term field trial. The objectives of the first scenario was to understand the transformation pathways of PAH substances added with successive applications of compost in soil, and to explore how the origin of the compost and the properties of the PAHs would control their behavior in amended soil. The objectives of the second scenario were to investigate at a long term whether the repeated applications of compost could increase the PAH concentration that might be potentially bioavailable for microbial activity in soil and therefore increase over time some ecotoxic risks.

3. Materials & Methods

3.1. Study site

3.1.1. Field experiment

The QUALIAGRO long term field experiment (INRA-Veolia collaboration) located in Feucherolles near Paris (48°52N, 1°58E), was set up in 1998 in order to explore the benefits and the environmental impacts of repeated application of different urban composts on agricultural soil. The soil was aluvisol with a silty loam texture, neutral pH in the plough layer. Mean annual temperature was 10.9°C and mean annual rainfall 648 mm / year (Average data between 1998 and 2012 recorded with a weather station installed near the site). In this study, we used the plots corresponding to optimal mineral nitrogen (N) fertilization. It included 20 plots of 450 m^2, randomly distributed, with 4 replicates of each treatment (corresponding to 3 urban composts and a farmyard manure in addition to control with no organic amendments). These plots were cultivated with a rotation of wheat and corn maize. The three distinct treatments hold for this study were: i) application of a co-compost of green waste and sludge t (GWS), ii) application of municipal solid waste compost (MSW), and iii) the control treatment receiving no organic amendment. Composts were applied and incorporated in the plough layer of soil (0-29 cm) once every two years in September of the following years: 1998, 2000, 2002, 2004, 2006, 2007, 2009 and 2011 (We had an exception in 2006 and 2007). The compost dose applied on a single plot was at a rate equivalent to 4 tons C/ha which was about 2- 3 times the usual dose applied by farmers. This corresponded to individual compost dose average of 16.36 ton compost.ha^{-1} for GWS compared to only 12.04 ton compost.ha^{-1} for MSW at each application, considering the average organic content of

MSW was 1.16 times superior that of GWS (the overall observed data are summarized in Table SI V.1). All composts were sampled and analyzed for their content in 16 PAHs and other physio-chemical and biochemical parameters before each compost application. For each plot, in August prior to each compost application, a representative soil sample was obtained from 10 sampling points located in the plough layer and distributed within the entire surface of the plot field for monitoring the physical chemical properties including the concentrations of each substance of the16 PAHs in soil. Data regarding PAH content in soil were only available for the following years: 1998, 2002, 2004, 2006, 2007 and 2011. In order to quantitatively and qualitatively assess the quality of soil water in the different treatments, one plot of each treatment was equipped with two lysimeters at depths of 45 cm and 100 cm respectively. The plots were also equipped with tensiometers, Time Domain Reflectometry probes and temperature sensors for monitoring the physical transfers in soil profile. Daily climatic data were recorded onsite. Details of the monitoring devices are described in Chalhoub et al., (2013a). Only the most relevant information related to this study was described here. Further details of the experimental set up, composting processes and chemical analysis protocols could be found in Chalhoub et al.(2013) and Houot et al.(2009, 2002).

3.1.2. PAHs characterization in soil and composts

The 16 EPA-PAHs (acenaphthene, acenaphthylene, anthracene, benzo(a)anthracene, benzo(a)pyrene, benzo(b)fluoranthene, benzo(g,h,i)perylene, benzo(k)fluoranthene, chrysene, dibenzo(a,h)anthracene, fluoranthene, fluorene, indeno(1,2,3-cd)pyrene, naphthalene, phenanthrene and pyrene) were analyzed. An exhaustive extraction of sorbed PAHs in the collected samples of soil and composts were extracted using a pressurized liquid extraction method with an ASE 200 (Dionex-ThermoFisher Scientific) at 150 °C and 104 bar with an organic solvent mixture (acetone/methylene chloride/n-hexane, 50/25/25, v/v). The obtained extracts were concentrated before their analysis. In 2004 for the composts and in 2006 for the soils, additional series of extractions using a pressurized hot water extraction method (ASE) at 50°C were also performed in parallel to the usual exhaustive extraction in order to assess the available sorbed fraction of each PAH in these samples ("PAH_{AV}" fraction of the model). The extracts were analyzed by HPLC-fluorescence detection as described by (Bourdat-Deschamps et al., 2007). Figure V.1 (a, b) respectively showed the measurements for PHE and B(a)P, obtained with the exhaustive extraction method. For soil, the averages of the four replicates of every treatment were reported there. For composts, the averages corresponded to three replicates were reported by unit of dry soil in order to facilitate the comparison of the

sets of data. The standard deviation associated with measured PAHs data in soil and composts was very large. For soil, it is mainly due to the heterogeneity of the field. The concentrations of PAHs in composts remained below the regulatory limits (4 and 1.5 mg/kg_{dw} for PHE and B(a)P, respectively). The experimental data of Figure V.1 show that the composts differ by their content of PAHs and thus by the rates of PAHs that entered into soil at each compost application. The PAHs load entering with each compost application represented from 0.5 to 5 % of the initial stock present in the soil. If we calculate the total amount of PAH added with 8 compost applications, we found the following results expressed in µg/kg soil: 10.44 ± 3.94 for GWS-PHE (dose equivalent to 39.95±15.1 g/ha), 8.47 ± 2.48 for MSW-PHE (dose equivalent to 32.41±9.48 g/ha),, 4.34 ± 1.45 for GWS-BaP (dose equivalent to 16.61±5.57 g/ha),, 1.07± 0.30 for MSW-BaP. (dose equivalent to 4.09±1.157 g/ha), The uncertainties in the previous values were quantified using the law of propagation of uncertainty that applies to the use of a first order Taylor approximation. For most applications, the PAH fluxes were often introduced in higher quantity with GWS compost compared to MSW one, and it was particularly obvious for B(a)P. In 2009, water samples collected from lysimeters were analyzed against PAHs contents, but they were found to be below the detection limit of the instrument, that was 1.3 and 0.7 ng/l for PHE and B(a)P, respectively (Bourdat-Deschamps et al., 2007).

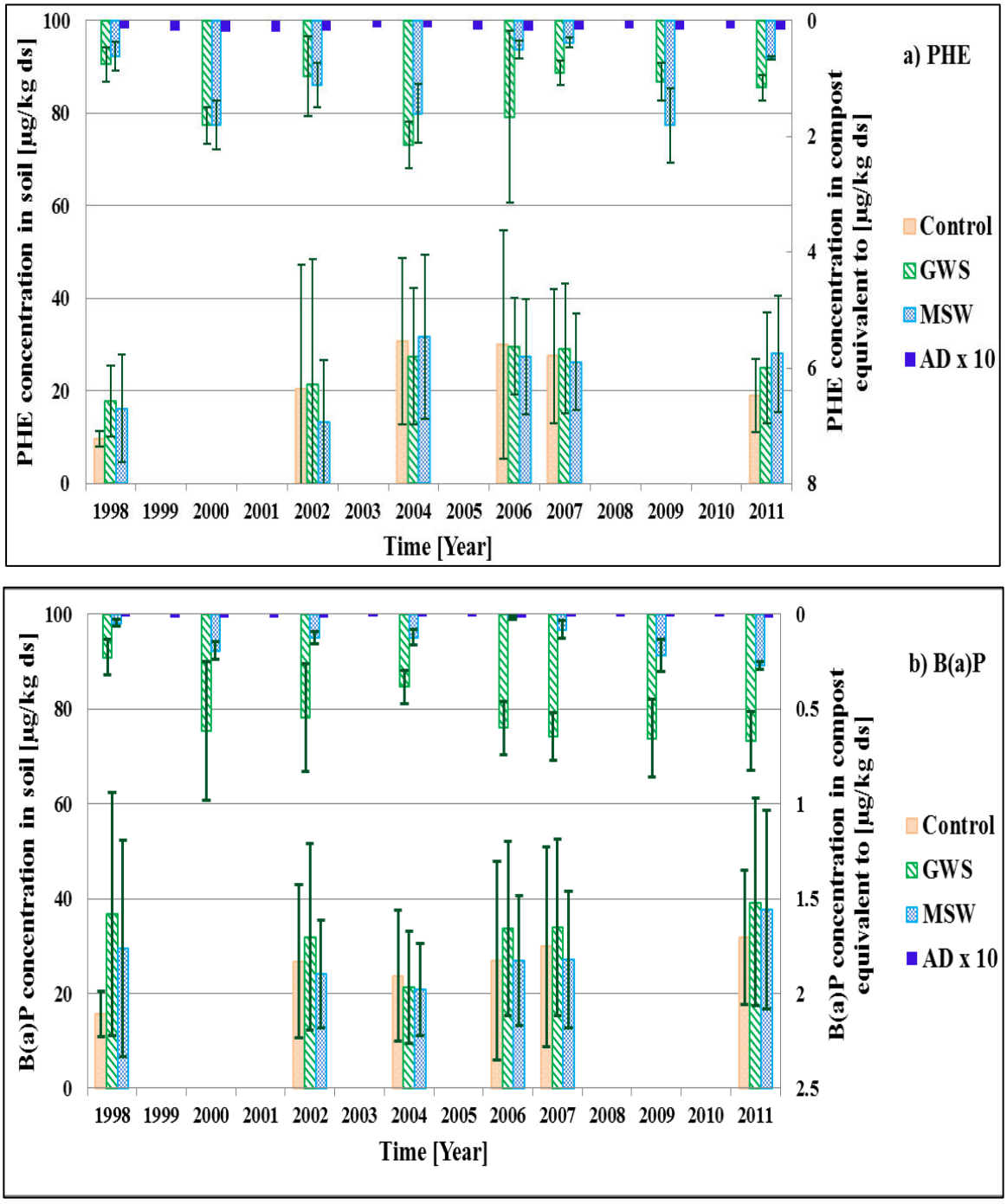

Figure V.1. Evolutions of concentrations of PHE and B(a)P in soils and composts for different treatments: control, GWS and MSW. Bottom bars represent the mean measured concentrations of the PAH in the soil ploughed layer (µg/kg$_{ds}$). The upper bars represent the mean concentration of the relevant PAH in the applied compost (µg/kg$_{ds}$) in addition to the annual atmospheric bulk depositions (AD) for the relevant PAH. Error bars indicate to the standard deviations (4 replicates for soil and 3 for compost).

3.1.3. Climatic data and PAHs data added with rainfall precipitations

Climatic conditions were monitored with a weather station located just 500 m away from the field experiment. Data included air temperature, humidity, global incoming solar radiation, rainfall and wind speed. During a period of 4 years (from 2005 to 2008), monthly samples of rainfall precipitations were analyzed to determine their contents of each of the 16 PAHs. The content of each PAH in rainfall samples was determined using stir bar sorptive extraction followed by HPLC fluorescence detection (Bourdat-Deschamps et al., 2007). The mean flux of PHE and B(a)P added into soil with rainfall precipitations over a two-year period were found to be about 2.6 % and 1.4 %, respectively of the flux of these substances introduced into soil by a single compost application.

3.1.4. Statistical analysis

Statistical analyses were performed using R software (Version 3.2.3). Analysis of variance (ANOVA) and the Tukey Kramer HSD test were performed to test if the PAHs measurements differed significantly among the four replicates of each treatment in the field experiment. The same test was also used out to verify whether a significant difference existed in PAHs measurements between the two halves of field. No significant difference regarding PAH content in soil between the two halves was existed.

Table SI V.1. Main composts characteristics required for the PAH model (the organic fertilization module)

Year[+]	Treatment	Compost dose[†] ton.ha^{-1}	Mean Van Soest fractionation values (%)					OC[*] gC.kg$_{dw}^{-1}$	PHE µg.kg$_{dw}^{-1}$	BaP µg.kg$_{dw}^{-1}$
			Slow	Fast	HCEL	CEL	LIG			
1998	GWS	10.70 ±4.23	48.80	0.00	5.77	13.80	31.63	272.73±11.14	269.95±6.09	81.13±7.70
	MSW	10.01±2.95	0.00	50.80	6.13	29.40	13.67	303.73±17.66	235.24±65.42	17.35±5.41
2000	GWS	19.81±2.70	40.90	0.00	1.90	7.40	49.80	191.13±3.51	349.33±39.5	119.33±68.72
	MSW	19.16±4.10	0.00	48.70	5.00	26.90	19.40	313.22±3.41	360.33±29.67	38.20±5.06
2002	GWS	18.48±3.35	33.7	0.00	4.97	30.80	30.53	349.26±47.18	200±137.47	113.33±55.08
	MSW	9.46±2.46	0.00	46.80	3.77	34.53	14.90	277.45±17.31	453.33±101.2	50.00±0.00
2004	GWS	17.25±3.21	38.50	0.00	8.20	34.07	19.24	310.67±21.94	476.6±7.03	84.91±11.61
	MSW	14.62±4.68	0.00	45.93	10.50	27.03	16.54	263.33±8.62	419.34±7.46	31.90±1.57
2006	GWS	17.74±3.68	55.47	0.00	5.93	20.03	18.57	244.67±4.04	357.94±311.1	129.48±14.00
	MSW	9.99±3.07	0.00	31.83	6.83	47.90	13.44	390.33±12.10	193.87±6.99	7.09±2.10
2007	GWS	15.81±2.90	56.47	0.00	3.80	18.47	21.26	238.34±3.79	217.67±30.56	156.33±11.59
	MSW	10.50±2.27	0.00	31.10	6.37	49.30	12.23	359.33±6.43	136.67±10.41	29.75±16.15
2009	GWS	16.98±5.10	45.53	0.00	7.17	19.03	28.27	256.33±3.51	236.33±19.34	147.33±12.74
	MSW	9.43±3.26	0.00	34.60	10.97	25.67	25.30	310.33±22.37	732.67±60.74	88.14±16.43
2011	GWS	14.14±1.32	44.77	0.00	7.37	24.80	23.06	261.33±17.04	312.67±53.00	180.67±37.87
	MSW	13.12±0.68	0.00	42.17	4.67	29.13	24.03	248.67±13.32	187.67±3.06	78.71±5.10
2013	GWS	15.46	44.77	0.0	7.37	24.8	23.06	244.29	365.70	218.50
	MSW	13.81	0.00	42.17	4.67	29.19	24.03	235.35	190.70	83.82
2015	GWS	12.82	44.77	0.0	7.37	24.8	23.06	244.29	259.70	142.80
	MSW	12.44	0.0	45.93	10.5	27.03	24.03	235.35	184.60	73.63
2017	GWS	20.46	38.5	0.0	8.2	54.07	19.23	288.73	483.70	96.51
	MSW	19.30	0.0	31.1	6.37	49.3	16.54	254.71	426.80	33.67
2019	GWS	15.81	56.47	0.0	3.8	18.47	21.26	238.34	217.70	156.30

Year[+]	Treatment	Compost dose[†] ton.ha^{-1}	Mean Van Soest fractionation values (%)					OC[*] gC.kg$_{dw}^{-1}$	PHE µg.kg$_{dw}^{-1}$	BaP µg.kg$_{dw}^{-1}$
			Slow	Fast	HCEL	CEL	LIG			
	MSW	10.50	0.0	31.1	6.37	49.3	13.23	359.33	136.70	29.75
2021	GWS	12.91	56.47	0.0	3.8	18.47	21.26	234.55	187.10	144.70
	MSW	8.23	0.0	31.1	6.37	49.3	13.23	352.90	126.30	13.60
2023	GWS	22.08	45.53	0.0	7.17	19.03	28.27	252.82	255.70	160.10
	MSW	12.68	0.0	34.6	10.97	25.67	28.76	287.97	793.40	104.60
2025	GWS	17.11	40.9	0.0	1.9	7.4	49.8	187.62	309.80	50.61
	MSW	15.06	0.0	48.7	5.0	26.9	119.4	309.81	330.70	33.14
2027	GWS	21.42	55.47	0.0	5.93	20.03	18.57	240.63	669.10	143.50
	MSW	13.06	0.0	31.83	6.83	47.9	13.44	378.24	200.9	9.182
2029	GWS	20.46	38.5	0.0	8.2	34.07	19.23	288.73	483.70	96.51
	MSW	19.30	0.0	45.93	10.5	27.03	16.54	254.71	426.80	33.47
2031	GWS	10.70	48.8	0.0	5.77	13.8	31.63	272.73	270.00	81.13
	MSW	10.01	0.0	50.8	6.13	29.4	13.67	303.73	235.20	17.35
2033	GWS	18.71	56.47	0.0	3.8	18.47	21.26	234.55	483.70	167.90
	MSW	12.77	0.0	31.1	6.37	49.3	13.23	352.90	147.10	45.90
2035	GWS	20.46	38.5	0.0	8.2	34.07	19.23	288.73	483.70	96.51
	MSW	19.30	0.0	45.93	10.5	27.03	16.54	254.71	426.80	33.47
2037	GWS	15.13	33.77	0.0	4.97	30.8	30.46	302.08	62.53	58.26
	MSW	7.00	0.0	46.8	3.77	34.53	14.9	260.14	352.20	41.50
2039	GWS	15.46	44.77	0.0	7.37	24.8	23.06	244.29	365.70	218.50
	MSW	13.81	0.0	42.17	4.67	29.13	24.03	235.35	190.70	83.82
2041	GWS	14.93	48.8	0.0	5.77	13.8	31.63	261.59	276.00	88.83
	MSW	12.69	0.0	50.8	6.13	29.4	13.67	280.60	300.70	22.76
2043	GWS	17.74	55.47	0.0	5.93	20.03	18.57	244.67	357.90	129.50
	MSW	9.99	0.0	31.83	6.83	4.79	13.44	390.33	193.70	22.76

Year +	Treatment	Compost dose† ton.ha^{-1}	Mean Van Soest fractionation values (%)					OC✱ gC.kg$_{dw}^{-1}$	PHE µg.kg$_{dw}^{-1}$	BaP µg.kg$_{dw}^{-1}$
			Slow	Fast	HCEL	CEL	LIG			
2045	GWS	12.82	44.77	0.0	7.37	24.8	23.06	244.29	259.70	142.80
	MSW	12.44	0.0	42.17	4.67	29.13	24.03	235.35	184.60	73.61
2047	GWS	15.46	44.77	0.0	7.37	24.8	33.06	244.29	259.70	218.50
	MSW	13.81	0.0	50.8	6.13	29.4	13.67	286.07	190.70	11.94
2049	GWS	18.48	33.77	0.0	4.97	30.80	30.46	349.26	259.70	113.30
	MSW	9.46	0.0	46.8	3.77	34.53	14.90	277.45	453.30	50.00

+ The observed mean and standard deviation values for each input data are given between, 1998 and 2010, whereas the extrapolated values determined on the basis of random data selection from the available observed values are given between 2013 and 2049

† Compost dose applied onto soil

✱ The compost organic carbon content, where dw stands to dry weight

3.2. Model description

The PAH model developed within the Virtual Soil platform (Lafolie et al., 2014) was updated in order to simulate the dynamics of PAH in pollutant-soil-compost system using the model described in Chapter 4.

The VSoil platform (Lafolie et al., 2014) simulates water flow, solute transport (potentially PAH) and heat transport under climatic conditions. The platform was applied in our previous chapter 4 to simulate the interactions of PHE in an aged bare contaminated soil by considering PAH sorption to soil particles and PAH biological degradation by microorganisms. In this study two new modules that describe organic carbon decomposition of compost and PAH release from compost were added in the platform (see chapter. 3) inspired by the model of Geng et al. (2014). We did not consider the PAH uptake by roots because we assumed that the flux was too low. An overview of the updated PAH model was presented in Figure SI V.1.

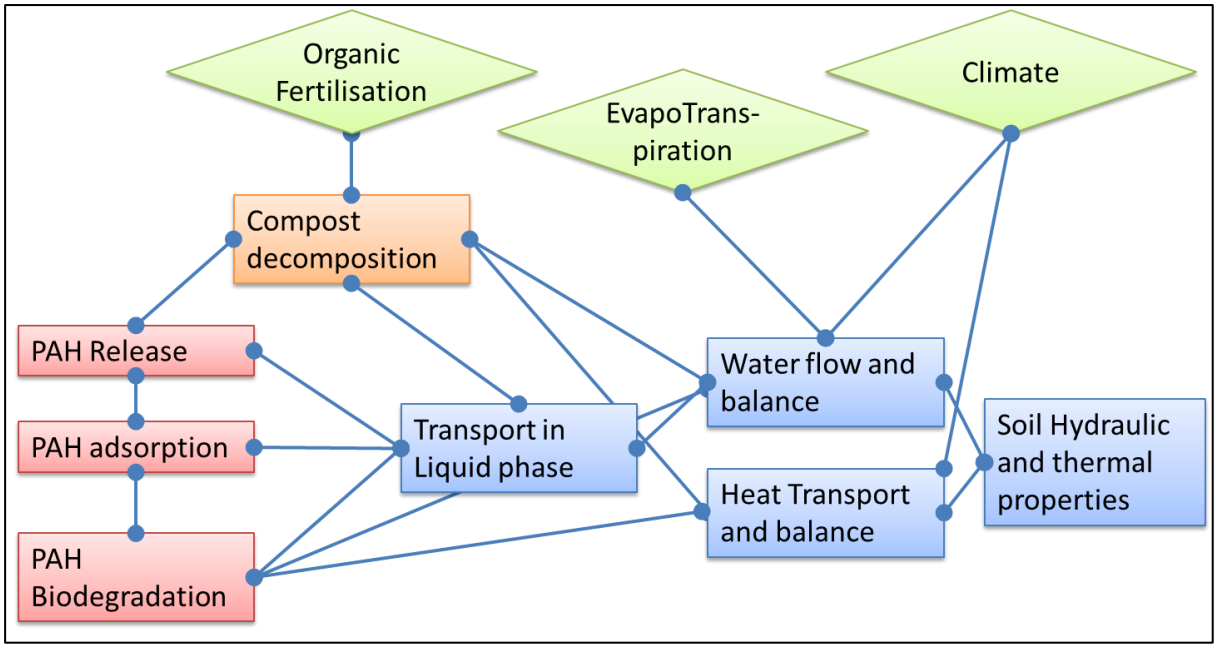

Figure SI V.1. The new PAH model integrated in VSoil platform: Scheme of the interconnections (bold lines) of the different modules considered in PAH model

Three additional modules were integrated in this updated version: the organic carbon module, the PAH release module from compost decomposition and the organic-fertilization module. The OC module simulates the decomposition of composted organic matter in compost-soil mixture system and the associated co-metabolic microbial biomass. In this study, we simplified the organic matter model by considering only the evolution of soil organic carbon

of compost incorporated into soil and not the evolution of the humified organic matter. The PAH release from OC module simulates the release of PAH added with compost as a function of the hydrolysis rates of biochemical pools of the applied compost. It also simulates the portion of PAH added with compost that is directly strongly adsorbed on mineral-organic particles of soil. The organic-fertilization module is viewed as a boundary condition and gives information about the applied compost doses, the biochemical pools of compost (corresponding to. the Van Soest fractions) as well as the organic carbon and PAH contents in compost at each compost application. Some of the data linked to this module are presented in Table SI V.1. Based on the data collected in the field, the PAH data from atmospheric depositions (AD) seemed to be negligible (See Figure V.1 a and b) but it was still included in the model since this process has been observed in recent works (Motelay-Massei et al., 2007; Ollivon et al., 2002). This later was integrated by updating the climatic module, described in our previous work and regarded as boundary condition for the model, to provide data input about the PAH atmospheric depositions rates dependently on the daily rainfall intensities. Detailed descriptions of the structure of these new added modules as well as for the previously existing ones were reported in (Chapters 3 and 4).

3.3. Modeling methodology

In the following, we present the different steps of calibration and the model scenarios. Different periods were selected. For PAH calibration, two years from 2004-2006 were chosen because of the higher precision of the PAH measurements in soils. For both scenarios, we choose one short period of 13 years where PAH were also measured, and a long period of further38 years without PAH measurements.

3.3.1. Calibration of water and heat flow modules

We started the simulations by testing the ability of the water flow module and the heat transport module to produce water contents and temperatures similar to these previously obtained by Chalhoub et al. (2013) using the PASTIS model. The simulations were carried out on the same period (i.e. from September, 15, 2007 to September, 15, 2009) as that of Chalhoub et al. (2013). The Van Genuchten (1980) soil hydraulic functions with the model of Mualem (1976) were used to describe the soil water retention and the hydraulic conductivity functions using the parameters obtained by Chalhoub et al. (2013 a.). The parameter sets for water and heat flows modules are given in Table SI V.2 of the supporting information.

Table SI V.2. Physical parameters of the different soil horizons taken from Chalhoub et al., 2013 and applied in PAH model to simulate water and heat processes

Depth (cm)	0-30	31-51	52-72	73-96	97-118	119-149	150-200
Water flow parameters							
Saturated water content, θ_s , ($cm^3.cm^{-3}$)	0.428	0.378	0.368	0.376	0.371	0.363	0.300
Residual water content, θ_r, ($cm^3.cm^{-3}$)	0.00024	0.00004	0.00060	0.00060	0.00001	0.00001	0.00002
Inverse of the air-entry value, α, (cm^{-1})	0.052	0.017	0.018	0.021	0.014	0.006	0.014
Pore-size distribution index, *n*, (-)	1.140	1.165	1.124	1.122	1.094	1.119	1.100
Pore-connectivity parameter, *l*, (-)	- 0.5 -						
Saturated hydraulic conductivity, K_s, ($cm.day^{-1}$)	87.71	10.35	9.21	14.78	9.80	2.76	12.67
Heat parameters[a]							
Thermal inertia of soil at saturation, ($J.K^{-1}.m^{-2}.s^{-1/2}$)	2108						
Coefficient a_1 in the expression for the thermal conductivity function, (-)	2300						
Coefficient a_2 in the expression for the thermal conductivity function, (-)	1890						
Coefficient a_3 in the expression for the thermal conductivity function, (-)	0.428						

3.3.2. Organic carbon module calibration

Data required for calibration of the organic carbon (OC) module were obtained from the simulation data given by Chalhoub et al. (2013). In their work, the CANTIS module of PASTIS model (Garnier et al., 2003) had been used to simulate N and C balances in the soil of the same field over 2 years (from September 2007 through September 2009), and provided correct predictions of nitrogen dynamics in soil of plots for different treatments. We, therefore, used the PASTIS model computations of the mineralization kinetics of organic C resulting from decomposition of compost for our model calibration based on experimental kinetics of C and N mineralization during incubation of soil-compost mixtures. The mineralization kinetics of compost organic C data was assessed by subtracting the mineralized C simulated data in the control treatment alone from the mineralized C simulated data in amended soil.

The step of model calibration was done for GWS and MSW treatments. The CANTIS model used by Chalhoub et al. (2013) to simulate OM decomposition was slightly different from the OC module used in this work. Starting from the set of parameters obtained from OC module in our previous chapter 3, we chose to re-adjust the two parameters of hydrolysis rate of the slow organic C soluble pool (k_{SLOW}), and the proportion of dead biomasses returning into organic C humified pool (w_{cp}) because the composts added in field here were not exactly the same composts as those used in laboratory experiments described in Chapter 3. This selection

was in accordance with results reported in literature by Zhang et al. (2012) who found that the OC module was very sensitive to parameters characterizing the organic C soluble pool (split into fast soluble and slow soluble) and among them these two selected parameters.

3.3.3. Calibration of PAH modules

For model calibration of PAH modules (corresponding to the biodegradation module/ sorption modules and PAH release from OC module), we started from the default PAH parameters determined in laboratory and described in Chapter 3. We tested the PAH model for a short period of 2 years, from August 15, 2004 to August 15, 2006. This period was chosen because that corresponded to two successive dates of PAH measurement in soil over 2 years with the use of a more exhaustive extraction method in 2006. The test was done for PHE and B(a)P in soil in the different treatments (GWS, MSW and control). However, using the initial set of parameters led to an under estimation by the model of the extractable PAHs measured in field and specially the sorbed fraction that we assumed to be measured with the PAH fraction recovered at 150°C. The discrepancy between this first test of the model and data could be attributed to the difference of the methods used to extract the PAHs, either by pressurized liquid extraction with a mixture of solvents at 150° for samples collected in field, or by shaking mechanically with methanol at room temperature for those measured in laboratory from ^{14}C experiment as presented in chapter3. The increased desorption of the analytes from the matrices and the accelerated dissolution kinetic process at high temperature were probably responsible for higher extraction recoveries with ASE than with shaking extraction (Conte et al., 1997; Gan et al., 1999). A new set of parameters had to be estimated. We chose to increase the adsorption coefficients from the "available" compartment to the weakly "sorbed" compartment in order to increase this compartment. The new parameter set was derived by fitting the parameter k_{WA} (describing the kinetic transfer of PAH from the weakly sorbed compartment (PAH_{WS}) to the available one (PAH_{AV})) from the experimental data of PAH measured in field in 2004-2006. The parameter k_{WA} was chosen because of its large influence on the model outputs as previously was assessed by a global sensitivity test (Chapter 3). The parameter k_{AW} was then calculated from the estimated parameter k_{WA} and the adsorption coefficient K_d using the following equation:

$$K_d = \frac{k_{AW}}{k_{WA}} \quad \text{(V.1)}$$

Where K_d was the sorption distribution coefficient in (L/kg_{ds}, ds refers to dry soil) of PAH. The K_d values (Table SI V.3) were calculated from the 2006 experimental data and the equation V.2:

$$K_d = \frac{\text{PAH recovered at 150 °C}}{\text{PAH recovered at 50 °C}} \quad \text{(V.2)}$$

Where Sorbed PAH recovered at 50 °C and 150 °C were taken from the supplementary extraction analysis data performed on soil samples in 2006.

Table SI V.3. K_d values for the different treatments used in this study and calculated by using PAH analytical data in soil samples in 2006

PAH	Treatment	PAH analysis in soil in 2006 ($\mu g.kg_{ds}^{-1}$)			OC $gC.kg_{ds}^{-1}$	log K_{OC}	K_d† $L.kg_{ds}^{-1}$	K_d ✱ $L.kg_{ds}^{-1}$
		Extracted at 50 °C	Extracted at 125 °C	Extracted at 150 °C				
PHE	Control	0.084±0.073	5.287±5.449	16.632±10.409	10.5	4.33	224	198
	GWS	0.077±0.021	4.650±1.831	23.294±10.594	14	4.35	313	302
	MSW	0.086±0.041	4.848±3.018	22.296±14.424	12	4.23	203	260
B(a)P	Control	0.006±0.000	0.129±0.149	24.547±22.120	10.5	6.49	32448	4091
	GWS	-	0.100±0.047	22.853±11.880	14	6.25	25476+	-
	MSW	0.001±0.000	0.127±0.055	22.080±16.375	12	6.25	21340	22080

† *K*d values calculated from the relationship $K_d = K_{OC}$ .OC where OC : the soil organic carbon taken from Chalhoub et al., 2013 and K_{OC}: the sorption distribution coefficients normalized to organic content taken from Chapter 3

✱ *K*d values calculated using Equation (2) and were selected for the study

\+ The *K*d value selected for the corresponding treatment

3.3.4. Scenario modelling

The calibrated model was further used to carry out two scenarios.

The first scenario aimed to investigate at a middle term (13 years) the degradation pathways of PAH added with the composts following their application in soil according to the compost quality and the physiochemical properties of both PAHs. To do so and starting from the mean initial data measured in August 15, 1998, we run two identical simulations during the period from August 15, 1998 to December 15, 2012 (that included 8 successive compost applications). The only difference between the two simulations concerned the PAH contents in the composts. While the first simulation was performed by considering the PAH contained in compost before its application in soil, the second simulation assumed that no PAH was present in the applied compost. The fate of PAH added with compost was then assessed by subtracting the simulated results without PAH of the second simulation from the simulated

results with PAH obtained with the first simulation. This scenario was repeated for GWS and MSW and for each PAH.

The second scenario aimed to evaluate at a long term the potential accumulation of PAH in soil if the management practices have continued in the field with the same frequency and doses for a further 38 years since the last available PAH sampling date of August 2011. The compost was assumed to be applied once every 2 years. The required data associated with every compost application such as compost quantity, OC content and biochemical composition of compost as well as the PAH content were all chosen randomly from the available collected data during the monitoring period (From 1998 through 2011) and by also taking into account the uncertainties in these values. The overall input data values necessary for the scenario were summarized in Table SI V.1. PAHs added with rainfall precipitations were also taken randomly from the available data. The required climatic data for this scenario were set on the basis of randomized climatic data calculated from the local weather station for the first ten years (from August 15, 2011 through December 31, 2020). The climatic data over the next decades (between the years 2021 and 2050) was taken from the climatic data taken from the future climatic change scenario (B1) over the last 30 years of simulation period (the dataset of ANR-SCAPEI project). Only the meteorological data concerning the future climate conditions under the most modest climate scenario (i.e. scenario B1) of the zone of study (Feucherolles, France) were used. This scenario 2 was repeated for GWS, MSW and control treatments and for each PAH.

3.3.5. Set up the simulations

The soil profile was modelled as one dimensional domain with a simulation depth of 200 cm that was discretized into seven layers (corresponding to the distinct horizons of the soil profile) by a finite element mesh. The upper boundary condition of water flow module (at 0 cm depth) was set by the daily atmospheric conditions (rainfall and evapotranspiration) and the lower boundary condition (at 200 cm depth) was the free drainage. The potential evapotranspiration values (ETP) were calculated from the collected climatic data using Penman-Monteith equation (FAO 56-Method). The upper boundary condition of heat transport module was specified as the daily soil surface temperature and a free temperature condition was applied as lower boundary condition. The initial conditions at t_0 for water flow and heat transport modules were assigned respectively in terms of soil water pressure and soil temperature values measured at beginning of simulations. We always chose the beginning of our simulation period to coincide with one of PAH soil sampling dates.

Before we run the investigated simulations, the PAH model has to be run over 1 year to reach a steady state for the sum of PAH model compartments corresponding to the total extractable amounts of PAH in soil (i.e. the sum of the three model compartments PAH_{WS}, PAH_{AV} and PAH_{COMP}). The model outputs from this transient state provide the boundary conditions of PAH model at the equilibrium state, from which the model has to be re- run again over the investigated simulation period. Simulations were always performed, in the equilibrium state, to account for the uncertainty in the initial concentrations of extractable PAH.

To start the simulation of the transient state, the compartments $PAH_{SS,}$ PAH_{CO2}, PAH_{Bs} and PAH_{MET} were considered null. The initial co-metabolic biomass concentration present in soil was taken equal to 244 mg C /kg $_s$ as reported by Chalhoub et al. (2013). Due to lack of data, the initial specific biomass concentration was taken randomly equal to 1 µg /kg_{ds} (in the range of values found for the specific biomasses in Chapter 3). The values of PAH_{WS}, PAH_{AV} and PAH_{COMP} were derived from the PAH measured data described in section (3.3.3). The quantity of PAH extracted with organic solvent at 150 °C in soil represented the sum of aqueous and sorbed model compartments PAH_{AV} and PAH_{WS} with PAH_{WS} being much higher than PAH_{AV}. The amount of PAH in solution PAH_{AV} was calculated from the only available PAH measurement obtained from organic solvent at 150 C° and the sorption distribution coefficient K_d (L/kg_{ds}) calculated in 2006 and summarized in Table SI V.3 as following:

$$PAH_{AV} = \frac{\text{PAH recovered at 150 °C (µg/kg}_{ds})}{K_d} \qquad \text{(V.3)}$$

The initial value of PAH_{WS} variable at the beginning of the previous transient state was determined using a trial and error approach so that the output of this variable at the end of simulation period should be as closer as possible to the measured value in soil at the initial date of investigated simulation. At each compost application date, PAH_{COMP} was automatically set to the value of PAH data measured in compost. Based on the data measured in field, the initial values for the variables describing the microbial biomass and the biochemical pools of compost as well as all the PAH compartments were set as uniform values in the first 29 cm of the soil profile. Below this depth, they were all fixed to zeros.

4. Results and discussion

4.1. Model calibration

4.1.1. Water and heat flow simulations

The water and temperature transfer simulated by our PAH model were very close to those obtained by Chalhoub et al.(2013), who shown that they were very similar between the three treatments: Control, GWS and MSW (Examples of the simulated results were given in Figure SI V.2 a and b for water and heat flow simulations, respectively).

4.1.2. Calibration of the OC module

The calibration of OC module yielded an estimated value of 0.00365 d^{-1} for the slow organic C soluble pool (k_{SLOW}) and a value of 0.6 (-) for the parameter w_{cp} (proportion of dead biomasses returning into organic C humified pool). The parameter k_{SLOW} was higher than this found in laboratory conditions in the Chapter 3 (0.0001 d^{-1}) and the value of w_{cp} was within the ranges reported for this parameter in laboratory conditions (0.1 and 1 for GWS and MSW, respectively). The updated parameters set of OC module was found to simulate adequately the kinetics of compost organic C mineralization in the treatments GWS and MSW. The MSW compost showed faster and higher organic C mineralization rate compared to GWS, and particularly during the first months after its application in soil (see Figure SI V.3). This result was attributed to the difference in their maturity and then in the biochemical composition of these two composts as reported by Chalhoub et al. (2013) and by Peltre et al.(2012). Nevertheless, the simulation results showed that the total organic C mineralization rate from both composts did not differ significantly at the end of 2 years of simulation (0.23 against 0.21 kg C/m2 for MSW and GWS respectively, where the concentrations were normalized by unit of area).

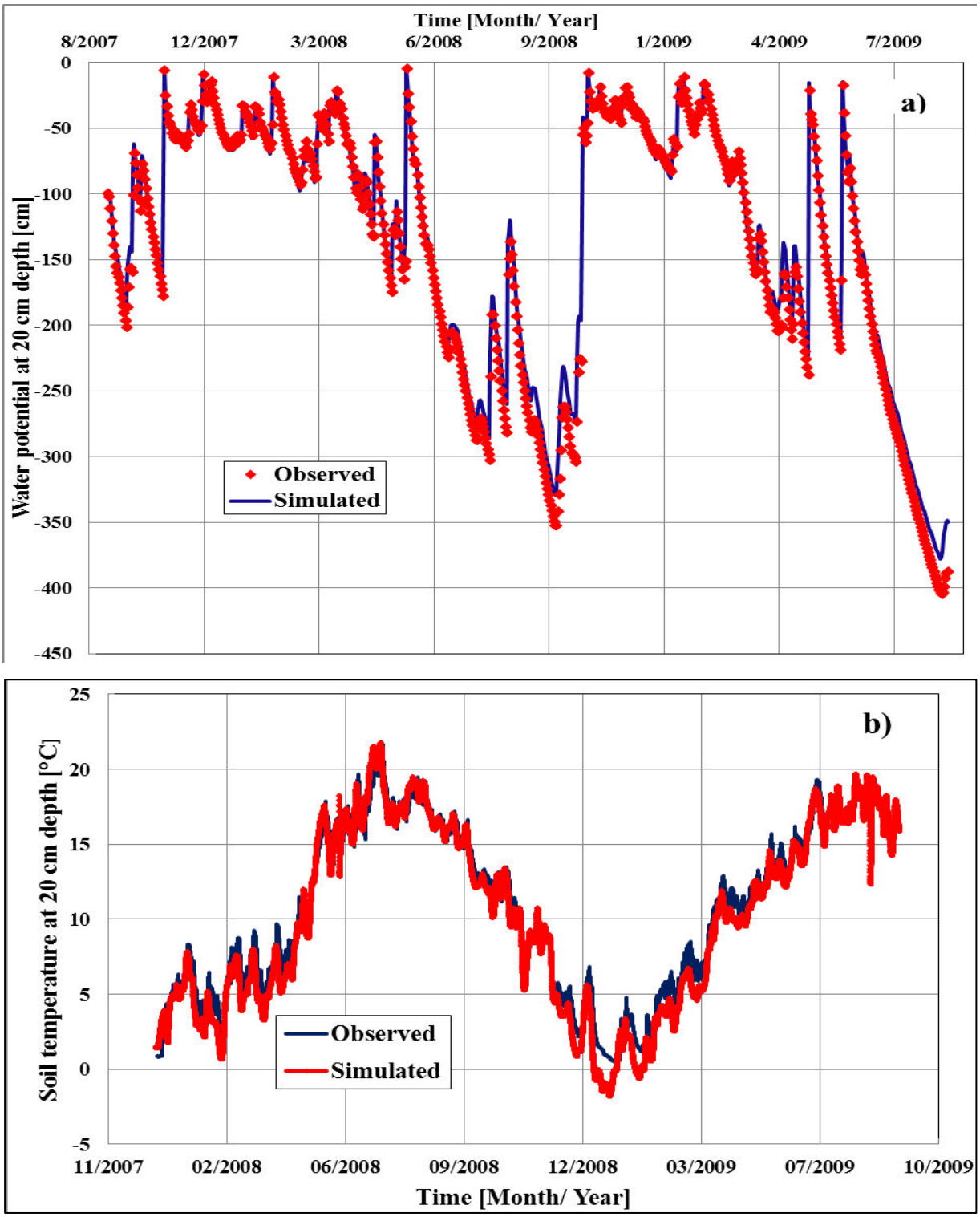

Figure SI V.2. a) Comparison of water potential simulated by Vsoil versus simulated by Chalhoub et al. (2013) at 20 cm depth of soil profile. b) Comparison of temperature simulated by Vsoil versus simulated by Chalhoub et al., (2013) values at 20 cm depth of soil profile

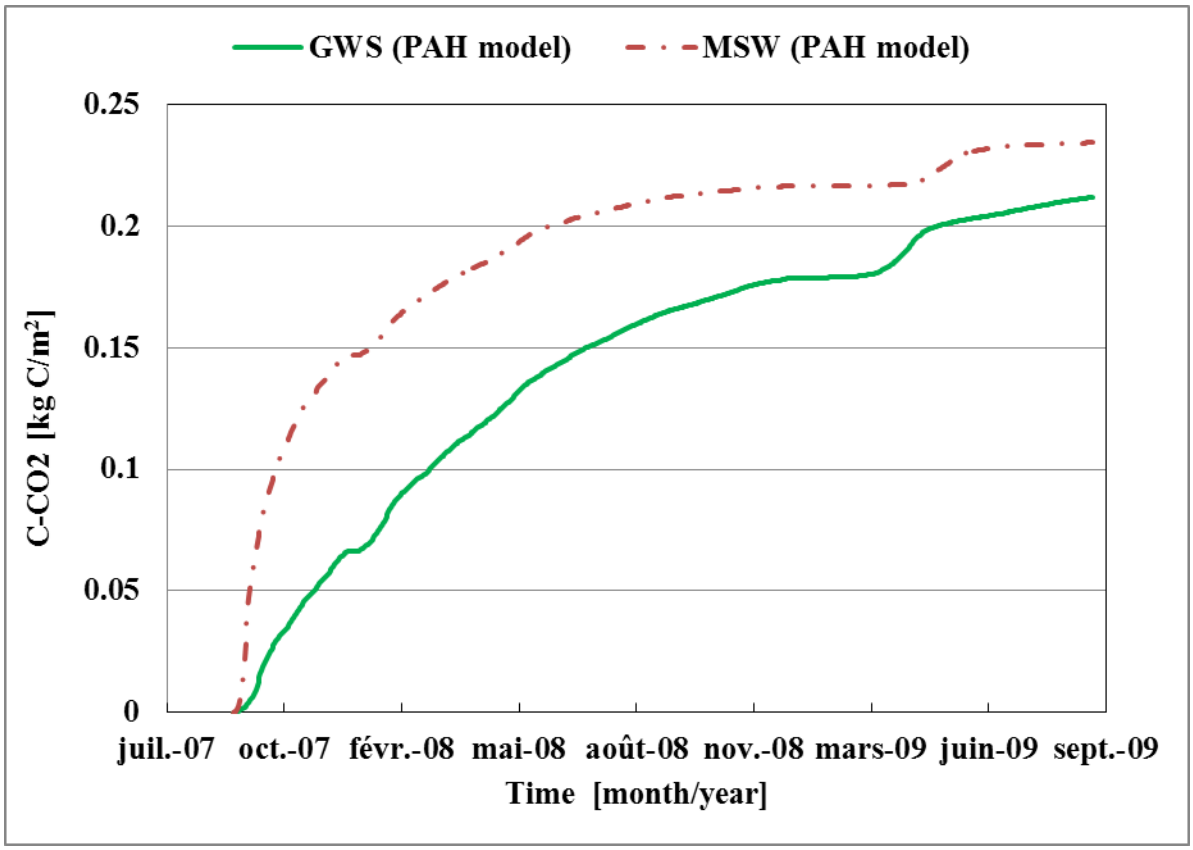

Figure SI V.3. MSW-simulated (dashed-pointed lines) and GWS-simulated results (solid lines) for the organic C mineralization kinetics of applied compost.

4.1.3. Calibration of PAH modules

The model calibration yielded an estimation of the adsorption coefficient k_{WA} value of 0.00001 d^{-1} and 0.00034 d^{-1} for PHE and B(a)P respectively. Each parameter value was valid on the 3 aforementioned treatments. Using the equation (1) and the K_d values given in Table 3SI, a value of the parameter k_{AW} for PHE was set to 0.00215d^{-1}, 0.003 d^{-1} and 0.0025 d^{-1} for control, GWS and MSW treatment, respectively. Similarly, for B(a)P, a value of k_{AW} was set to 1.387 d^{-1}, 8.64 d^{-1} and 7.237 d^{-1} for control, GWS and MSW treatment respectively. Note here that the new estimated values of parameter k_{WA} were 2336 and 640 times lower than their pre-estimated values for PHE and B(a)P obtained in laboratory and presented in chapter 3, respectively. Considering that the parameter k_{WA} represents the kinetic transfer rate of PAH substrate from PAH_{WS} (potentially bioavailable substrate) into PAH_{AV} (bioavailable substrate) in soil solution, most of PAHs remained absorbed on the organic or mineral particles of soil and were not bioavailable immediately for microorganisms. Figure V.2 showed the comparison between the simulated and observed data of the total extractable amounts for the 3 different treatments for PHE (Figure V.2a) and for B(a)P (Figure V.2b) through the

calibration process. Simulated results showed that over period of 2 years, there was nearly no change for the total extractable amount of PAH irrespective the treatment and type of PAH: the model predicted that quantity of PAH in 2006 was almost in the same order as that observed in 2004. The increase observed in the measured data of B(a)P in 2006 compared to 2004 could therefore, be related to uncertainty in the measured data. Finally, the model confirmed that there is negligible leaching of PAH at depths 45cm and 100 cm of soil profile irrespective of the quality of treatment and type of PAH. We simulated the following concentrations in 2009 at 45 cm depths in ng/L: $2.09\ 10^{-2}$, $1.84\ 10^{-2}$, $5.6\ 10^{-6}$, $6.75\ 10^{-6}$, for PHE x GWS, PHE x MSW, B(a)P x GWS, B(a)P x MSW, respectively.

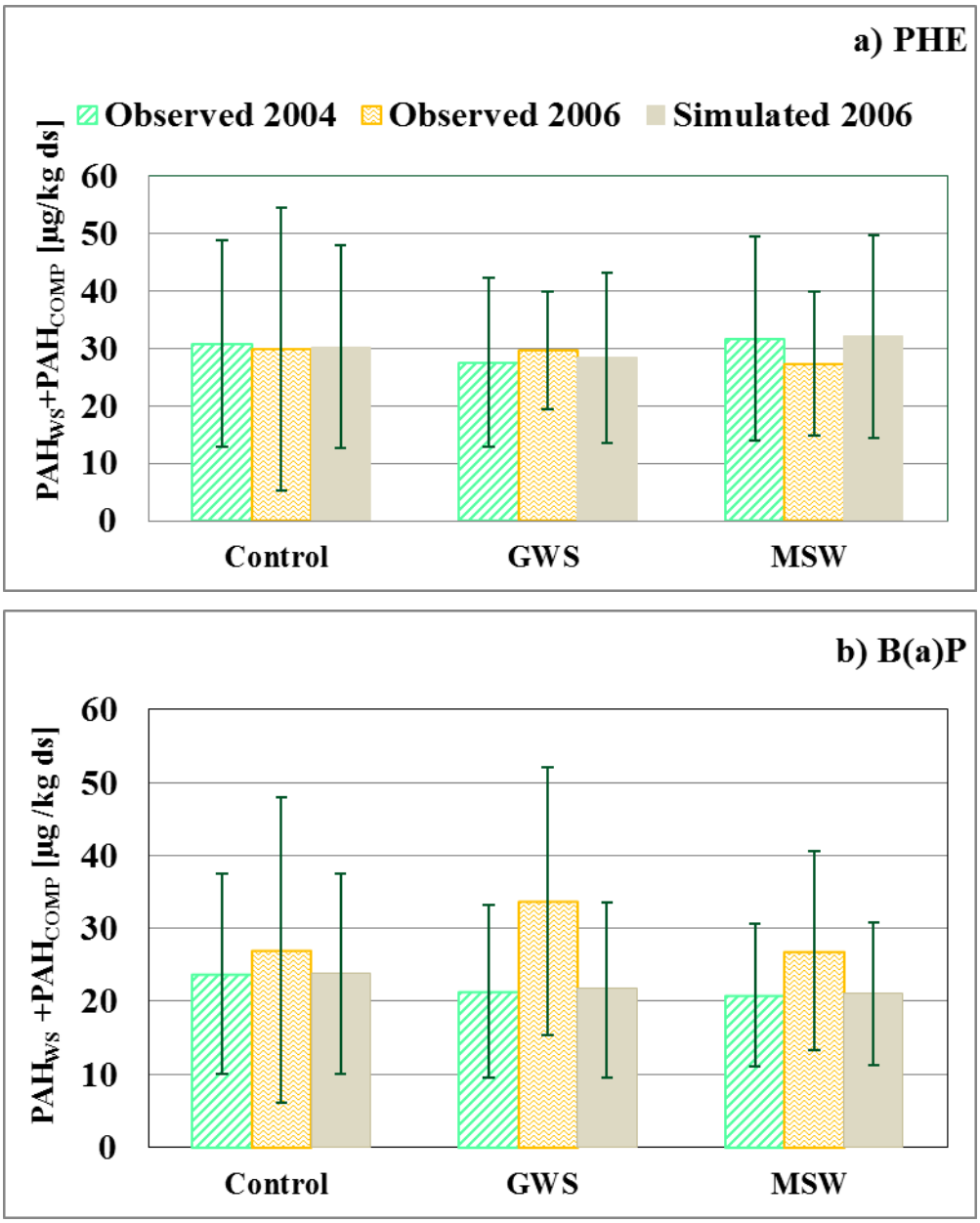

Figure V.2. Calibration results of the PAH model: observed versus simulated values for the sum of 3 model compartments PAH_{AV}, PAH_{WS} and PAH_{COMP} for (a) PHE and (b) B(a)P for different treatments. Error bars indicate to the standard deviations. For the output simulated results, the error bars are obtained by taking into account the standard deviations of the initial concentrations of extractable PAH.

4.2. Scenario 1: how the origin of the compost and the properties of the PAHs would control the behavior of PAHs in amended soil at short terms (13 years)?

First, we checked the ability of the PAH model to simulate the dynamics of observed PAH contents in amended soils from 1998 to 2011 with 8 compost applications (shown in Figure SI V.4). The model was always in the error bars of the experimental data. The final predicted

distributions of PHE and B(a)P in soil added with GWS and MSW after the 8 successive compost applications, are presented in Figure V.3 (a, b). The maximum percentage for PAH_{CO2} was estimated to be less than 3% of the total PAH added with the composts. The percentage of "PAH_{CO2}" was slightly different between GWS and MSW treatments irrespective of type of PAH, and this percentage was higher for the PAH with lower hydrophobicity (i.e. PAH_{CO2} with PHE > PAH_{CO2} with B(a)P). The mineralization of PAH found in field was much lower than that simulated in laboratory (Chapter 3) mainly because of the higher adsorption coefficients (K_{AW}) that decreased the bio availability of the PAH in the field conditions. The model predicted that the bioavailable fraction (PAH_{WS}+PAH_{COMP}) was about 31-33 % of the PAH added with composts irrespective of PAH type and composts. We found no significant effect of the origin of amendments on the total potential bioavailable fraction but the distribution was not the same for PHE and B(a)P with higher PHE adsorbed in the soil particles compare to B(a)P that was still adsorbed on the organic matter of compost after few years of simulation.

The PAH bounded residues fraction was divided into two main sub-fractions: the biogenic sub-fraction "PAH_{BS}" and the sequestrated (aging) sub-fraction "PAH_{SS}". The model predicted that only a few minor part of the PAH added in soil was transferred into "PAH_{BS}" (less than one percent). The low bioavailability of PAH lead to low microbial activity of degradation and that explained in turn the very few microbial degradation by-products. Once again, the biogenic bound fraction of PAH found in field was much lower than that simulated in laboratory (Chapter 3) because of the lower bio availability of the PAH simulated in the field conditions. The model predicted that the major part of PAH residues resulted from "PAH_{SS}", ranged between 63 and 68 % of the PAH added with the composts irrespective of the quality of treatment and type of PAH.

Consequently, because of the low mineralization of PAH, the model simulated that PAHs may accumulate in soil and increase the PAH stock in amended soil. The high contribution of PAH_{SS} compared to other PAH forms makes the sequestrating (aging) of the pollutant in soil the major way of PAH transformation in the amended soil.

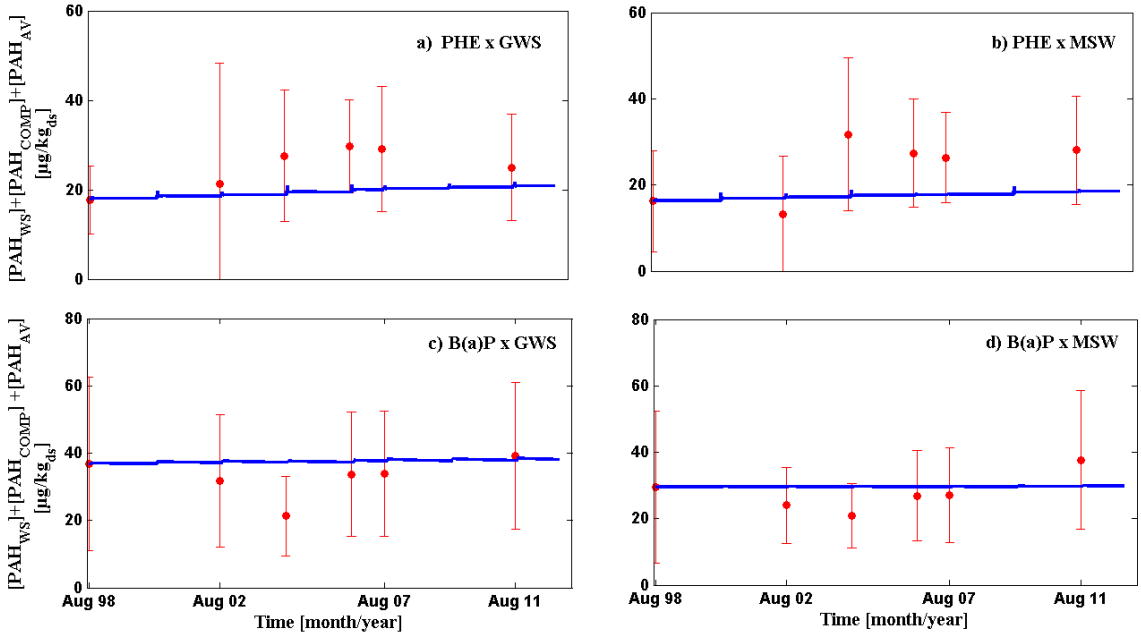

Figure SI V.4. Comparison of simulated versus observed for the total extractable fractions "PAH_{WS}+PAH_{COMP}+PAH_{AV}" in the top soil of the two treatments: GWS and MSW. The bold solid line represents the simulation results by taking into account 50 % confidence intervals (i.e. the median) of observed PAH data as initial conditions. (ǒ) indicates ± standard deviations of observed data.

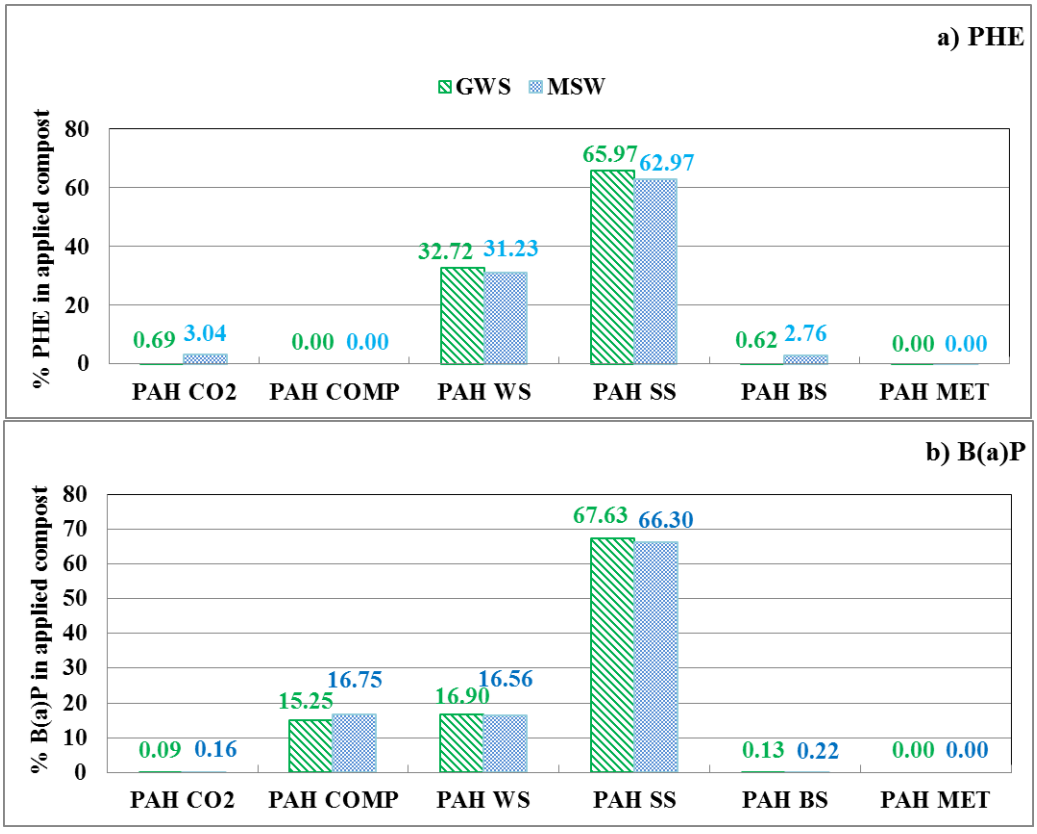

Figure V.3. Overall patterns distribution of PAH included in compost following repeated applications in amended soil for the treatments MSW and GWS respectively

4.3. Scenario 2: What are the effects of repeated applications of PAH contained in composts on PAH stock in soil over further38 years?

The simulated data representing the actual and theoretical accumulations of the total PAH extractable fractions "PAH_{AV}+PAH_{WS}+PAH_{COMP}" in soil for PHE and B(a)P through the three different treatments, Control, GWS and MSW, presented at depth of 20 cm are shown in Figure V.4 a to f. The theoretical accumulation of PAH concentration (plotted in dashed lines Figure V.4) in the amended soil was expressed as the increase of the initial observed concentration of the PAH in amended soil resulting from the PAH added with the repeated applications and assuming that no PAH dissipation had occurred in the amended soil. As expected, simulated results estimated a decrease of the total extractable fraction of PAH in control treatment because no organic amendments were added. The flux of PAHs entering the soil through the atmospheric deposition was too low to increase the PAH concentration in soil. Consequently, the model predicted a slight decrease of the total extractable fraction at the end of the simulation period by 4.3 % and 2.2 % for PHE and B(a)P in the control treatment (Figure V.4 a and d). The model predicted an increase in the extractable fraction by up to 33 % over further38 years for PHE in GWS (from 25.01 through 33.46 µg/kg_{ds}). This fraction would have reached a theoretical concentration value of 50.77 µg/kg_{ds} with the assumption of no PHE dissipation. Thus, a cumulative extractable fraction of 17.31 µg/kg_{ds} (50.77-33.46) of PHE (decrease rate equivalent to 0.45 µg/kg_{ds}/year) was obtained with the model from the repeated applications of GWS compost. This decrease in the bioavailable fraction was due mainly by the formation of bound residue strongly sorbed to the soil (see Figure V.4b: 64.94%). Similarly, the model predicted an increase in the cumulative concentration by up to 17 % over further 38 years (from 27.85 through 32.67 µg/kg_{ds}) for PHE in MSW (Figure V.4c). Assuming no PHE dissipation, this fraction would have reached a theoretical concentration value of 46.27 µg/$kg_{ds,}$ and thus, a cumulative non extractable fraction of 13.6 µg/kg_{ds} for PHE resulting from the repeated applications of MSWat end of simulation period (dissipation rate equivalent to 0.35 µg/kg_{ds}/year). By the same way, we also analyzed the simulation results of B(a)P in both GWS treatment (Figure V.4e) and MSW treatment (Figure V.4f). We obtained analogous results, with cumulative non extractable fraction of 11.17 and 2.80 µg/kg_{ds} for B(a)P resulting respectively from the repeated applications of GWS and MSW during the same simulation period (dissipation rate equivalent to 0.29 and 0.073 µg/kg_{ds}/year with GWS and MSW treatments respectively). Comparison of the results obtained by the two different composts irrespective of the PAH type shows evidence that

GWS compost posed a higher risk to environment than MSW does when considering the current average doses of compost applied in situ. That was because of an increase in both the rate of formation of extractable fraction and the amount of PAH added with compost in GWS compare to MSW compost.

The simulation results gave very low amount of PAH leached in the soil profile (<1%). They also gave estimations of the leaching rates. While the leaching rates were estimated to be negligible in control treatment irrespective of the PAH type, the leaching rate values of PHE and B(a)P at 200 cm depth of soil profile were estimated to be as follows: the leaching rates for PHE were 1.09 10^{-3} to 1.64 10^{-3} µg/m^2/year whereas for B(a)P the leaching rates were 3.5 10^{-7} to 1.06 10^{-6} µg/m^2/year, in GWS and MSW treatments respectively. These results indicated that the leaching rates were higher for PHE than for B(a)P because of its lower hydrophobicity and the leaching rates were higher with MSW than with GWS because of the higher adsorption coefficients in GWS than in MSW (see Table SI V.3).

The distribution of PAH expressed in percentage obtained for PHE in scenario 1 (Figure V.3) were very similar to those obtained in scenario 2. We found an increase of PAH_{SS} fraction by about 5-9 % for B(a)P in the both treatments compare to scenario 1. This increase in PAH_{SS} fraction resulted in a decrease by the same order of magnitude in the potential bioavailable fraction "PAH_{COMP}". We suspected the major reason of this was related to the PAH properties considering the high hydrophobicity of B(a)P compared to PHE in soil.

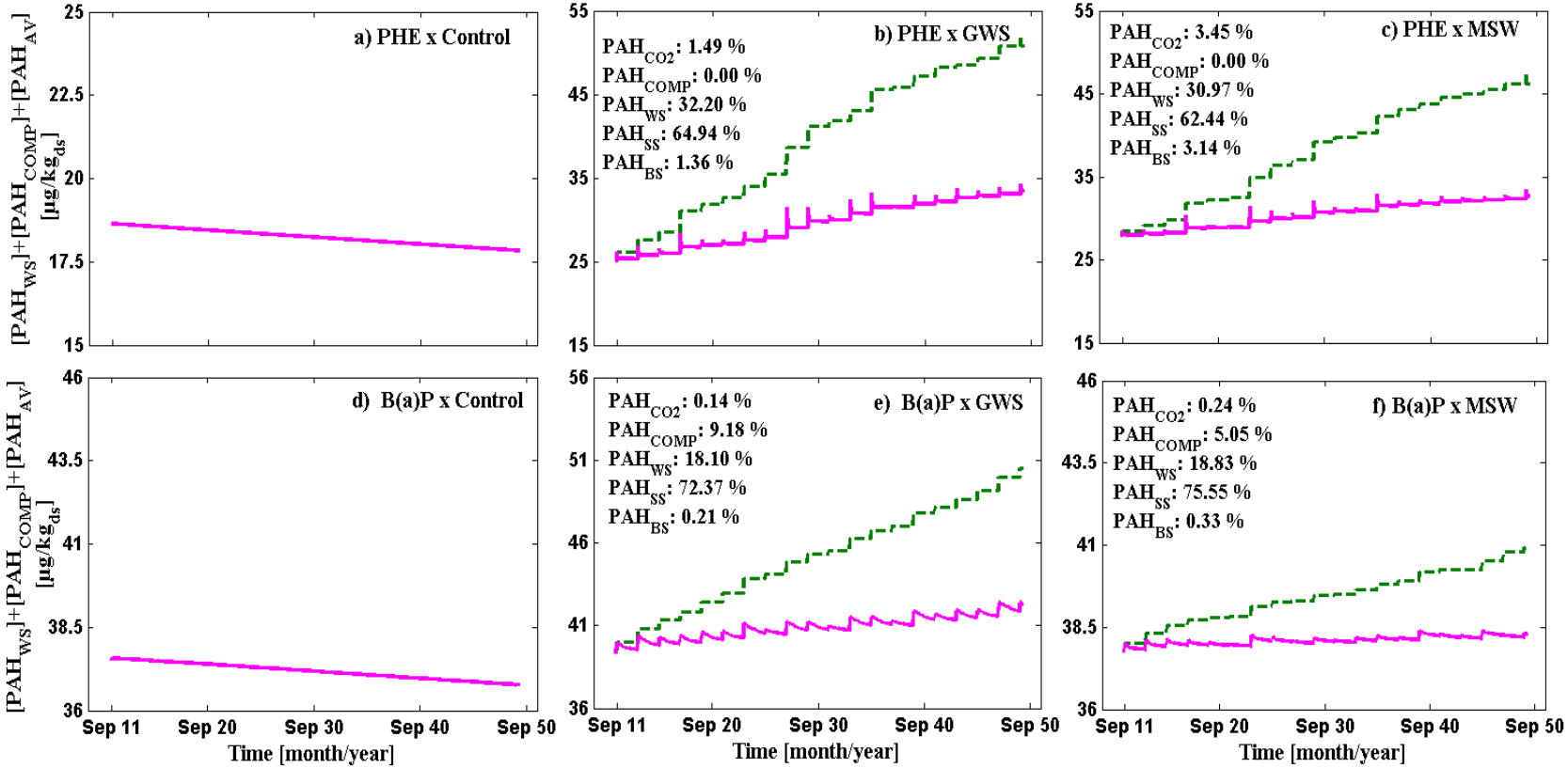

Figure V.4. For scenario 2 (further 38 years of applied compost every two years), the simulated (solid lines) and the theoretical (dashed lines) cumulative PAH extractable fraction "PAH_{AV}+PAH_{WS}+PAH_{COMP}" in soil for PHE and B(a)P for the three treatments : Control, GWS and MSW respectively. The textural parts in panels (b, c, e and f) represent the pattern forms of the relative PAH added with repeated applications in the amended soil at end of simulation period

5. Conclusion

Using the updated PAH model developed in Virtual Soil Platform based on data from a long term field trial, this paper addresses two main questions: i) what is the fate in soil of the PAH brought with the compost and ii) what is the amount of cumulative PAHs in soil from repeated applications of composts over a long period of time? According to this study, the sequestrated fraction resulting from aging of PAH in soil matrix was the major transformation pattern of PAH in amended soil. However, about one quarter-one third of the added PAH was still potentially bioavailable. All fractions made from biological activity were minor. The PAH mineralization was governed by substrate transfer limitation rather than microbial activity. Very little effect of compost quality on the transformation of PAH in soil was found. On the basis of the current average compost doses applied in situ, simulations based on long term repeated applications of PAH contaminated composts have showed that cumulative PAHs in soil are slightly higher in composts made from green wastes and sludge rather than those made from municipal solid wastes compost.

Nomenclature

ds dry soil

dw dry weight

GWS Green Sludge and Waste compost

k_{AW} first order kinetic constant that goes from PAH_{AV} into PAH_{WS} compartment

K_d sorption distribution coefficient

k_{SLOW} hydrolysis rate of the slow organic C soluble pool

k_{WA} first order kinetic constant that goes from PAH_{WS} into PAH_{AV} compartment

MSW Municipal Solid Waste compost

PAH polycyclic aromatic hydrocarbons

PAH_{AV} PAH as available in soil solution

PAH_{BS} PAH as biogenic non extractable residues

PAH_{CO2} carbon dioxide gas produced from the mineralization of PAH

PAH_{COMP} PAH weakly sorbed in compost

PAH_{MET} PAH as metabolites

PAH_{SS} PAH strongly sorbed in soil

PAH_{WS} PAH weakly sorbed in soil

w_{cp} proportion of dead biomasses into organic C humified pool

6. Acknowledgements

This research was financially supported by the French Environment and Energy Management Agency (ADEME) and the Environment and Agronomy division of the French National Institute for Agricultural Research (INRA). The authors would like to thank Nathalie BERNET for her technical assistance.

7. References

Annabi, M., Bissonnais, Y. Le, Villio-poitrenaud, M. Le, Houot, S., 2011. Improvement of soil aggregate stability by repeated applications of organic amendments to a cultivated silty loam soil. "Agriculture, Ecosyst. Environ. **144**, 382–389. doi:10.1016/j.agee.2011.07.005

Bourdat-Deschamps, M., Daudin, J.-J., Barriuso, E., 2007. An experimental design approach to optimise the determination of polycyclic aromatic hydrocarbons from rainfall water using stir bar sorptive extraction and high performance liquid chromatography-fluorescence detection. J. Chromatogr. A **1167**, 143–153.

Brändli, R.C., Bucheli, T.D., Kupper, T., Furrer, R., Stadelmann, F.X., Tarradellas, J., 2005. Persistent organic pollutants in source-separated compost and its feedstock materials--a review of field studies. J. Environ. Qual. **24**, 735–60. doi:10.2134/jeq2004.0333

Brimo, K., Garnier, P., Sun, S., Bertrand-krajewski, J., Cébron, A., Ouvrard, S., 2016. Using a Bayesian approach to improve and calibrate a dynamic model of polycyclic aromatic hydrocarbons degradation in an industrial contaminated soil. Environ. Pollut. **215**, 27–37. doi:10.1016/j.envpol.2016.04.094

Chalhoub, M., Coquet, Y., Vachier, P., 2013a. Water and bromide dynamics in a soil amended with Different urban composts. Vadose Zo. J. **12**, 1–11.

Chalhoub, M., Garnier, P., Coquet, Y., Mary, B., Lafolie, F., Houot, S., 2013b. Increased nitrogen availability in soil after repeated compost applications : Use of the PASTIS model to separate short and long-term effects. Soil Biol. Biochem. **65**, 144–157. doi:10.1016/j.soilbio.2013.05.023

Chung, N., Alexander, M., 2002. Effect of soil properties on bioavailability and extractability of phenanthrene and atrazine sequestered in soil. Chemosphere **48**, 109–115. doi:10.1016/S0045-6535(02)00045-0

Conte, E., Mllam, R., Morah, G., Abballe, F., 1997. Comparison between accelerated solvent extraction and traditional extraction methods for the analysis of the herbicide diflufenican in soil. J. Chromatogr. A **765**, 121–125.

Dagois, R., Schwartz, C., Coussy, S., Lorgeoux, C., Ouvrard, S., Faure, P., 2015. Climatic influence on mobility of organic pollutants in Technosols from contrasted industrial activities. J. Soils Sediments. doi:10.1007/s11368-015-1108-4

Gan, J., Papiernik, S.., Koskinen, W.., Yates, S.., 1999. Evaluation of Accelerated Solvent Extraction (ASE) for analysis of pesticide residues in soil. Environ. Sci. Technol. **33**, 3249–3253.

Geng, C., Haudin, C.-S., Zhang, Y., Lashermes, G., Houot, S., Garnier, P., 2015. Modeling the release of organic contaminants during compost decomposition in soil. Chemosphere **119**, 423–431. doi:10.1016/j.chemosphere.2014.06.090

Haudin, C.S., Zhang, Y., Dumény, V., Lashermes, G., Bergheaud, V., Barriuso, E., Houot, S., 2013. Fate of 14C-organic pollutant residues in composted sludge after application to soil. Chemosphere **92**, 1280–1285. doi:10.1016/j.chemosphere.2013.02.041

Houot, S., Cambier, P., Benoit, P., Deschamps, M., Jaulin, a., Lhoutellier, C., 2009. Effet d ' apports de composts sur la disponibilité de micropolluants métalliques et organiques dans un sol cultivé. Etude Gest. des Sols **16**, 255–274.

Houot, S., Clergeot, D., Michelin, J., Francou, C., Bourgeois, S., Caria, G., Ciesielski, H., 2002. Agronomic value and environmental impacts of urban composts used in agriculture, in: Insam, U.D.D.H., Sc., N.R.M., Klammer, M.S. (Eds.), Microbiology of Composting. Springer Berlin Heidelberg, pp. 457–472. doi:10.1007/978-3-662-08724-4_38

Houot, S., Verge-Leviel, C., Poitrenaud, M., 2012. Potential mineralization of various organic pollutants during composting. Pedosphere **22**, 536–543. doi:10.1016/S1002-0160(12)60038-1

Iarc, 2010. IARC monographs on the evaluation of carcinogenic risks to uumans: some non-heterocyclic polycyclic aromatic hydrocarbons and some related exposures. Iarc Monogr. Eval. Carcinog. Risks To Humans **92**, 1–868.

Kästner, M., Streibich, S., Beyrer, M., Richnow, H.H., Fritsche, W., 1999. Formation of bound residues during microbial degradation of [14C]anthracene in soil. Appl. Environ. Microbiol. **65**, 1834–1842.

Lafolie, F., Cousin, I., Marron, P.-A., Mollier, A., Pot, V., Moitrier, N., Moitrier, N., Nouguier, C., 2014. The « VSOIL » modeling platform. Rev. For. Française Fr.], ISSN 0035. doi:10.4267/2042/56287

Lashermes, G., Houot, S., Barriuso, E., 2010. Sorption and mineralization of organic pollutants during different stages of composting. Chemosphere **79**, 455–462. doi:10.1016/j.chemosphere.2010.01.041

Motelay-Massei, A., Ollivon, D., Garban, B., Tiphagne-Larcher, K., Chevreuil, M., 2007. Fluxes of polycyclic aromatic hydrocarbons in the Seine estuary , France : mass balance and role of atmospheric deposition. Hydrobiologia **588**, 145–157. doi:10.1007/s10750-007-0659-9

Mualem, Y., 1976. A new model to predicting the hydraulic conductivity of unsaturated porous media. Water Resour. Res. **12**, 513–522.

Nam, K., Kim, J.Y., Oh, D.I., 2003. Effect of soil aggregation on the biodegradation of phenanthrene aged in soil. Environ. Pollut. **121**, 147–51.

Noyes, P.D., Mcelwee, M.K., Miller, H.D., Clark, B.W., Tiem, L.A. Van, Walcott, K.C., Erwin, K.N., Levin, E.D., 2009. The toxicology of climate change : Environmental contaminants in a warming world. Environ. Int. **35**, 971–986. doi:10.1016/j.envint.2009.02.006

Ollivon, D., Blanchoud, H., Garban, B., Curie, M., 2002. Atmospheric deposition of PAHs to an urban site ,. Atmos. Environ. **36**, 2891–2900.

Peltre, C., Christensen, B.T., Dragon, S., Icard, C., Kätterer, T., Houot, S., 2012. RothC simulation of carbon accumulation in soil after repeated application of widely different organic amendments. Soil Biol. Biochem. **52**, 49–60. doi:10.1016/j.soilbio.2012.03.023

Senesil, G.S., Baldassarre, G., Senesi, N., Radina, B., 1999. Trace element inputs into soils by anthropogenic activities and implications for human health. Chemosphere **39**, 343–77.

Van Genuchten, M.T., 1980. A closed-form equation for predicting the hydraulic conductivity of unsaturated soils. Soil Sci. Soc. Am. J. 892±898.

Wilcke, W., 2000. SYNOPSIS Polycyclic Aromatic Hydrocarbons (PAHs) in Soil — a Review. J. Plant Nutr. Soil Sci. **163**, 229–248. doi:10.1002/1522-2624(200006)163:3<229::AID-JPLN229>3.0.CO;2-6

Xing, B., 1997. The effect of the quality of soil organic matter on sorption of naphthalene. Chemosphere **35**, 633–642.

Xiu-hong, Y., Garnier, P., Shi-zhong, W., Bergheaud, V., Xiong-fei, H., 2014. PAHs sorption and desorption on soil influenced by pine needle litter-derived dissolved organic matter. Pedosphere **24**, 575–584. doi:10.1016/S1002-0160(14)60043-6

Zhang, Y., Lashermes, G., Houot, S., Doublet, J., Steyer, J.P., Zhu, Y.G., Barriuso, E., Garnier, P., 2012. Modelling of organic matter dynamics during the composting process. Waste Manag. **32**, 19–30. doi:10.1016/j.wasman.2011.09.008

CONCLUSION

Rappel de la démarche

Pour mieux décrire et quantifier la dynamique des HAP dans les sols contaminés allant de parcelles agricoles amendées avec des matières organiques faiblement contaminées jusqu'à d'anciens sites industriels fortement contaminés, dont les concentrations vont d'environ de 0.5 mg/kg_{ds} à 1500 mg/kg_{ds}, une démarche numérique de modélisation a été menée dans ce travail de thèse. Un nouveau modèle dynamique de HAP (à 1 dimension) qui couple l'ensemble des processus physiques, biologiques et biochimiques contrôlant la dissipation des HAP dans le sol a été développé sous la plateforme VSoil de l'INRA. Dans un premier temps, et sur la base de **données expérimentales de laboratoires** obtenues avec des polluants marqués en **^{14}C ou ^{13}C, le modèle a été calibré** en utilisant une approche Bayésienne « DREAM » sur les deux contextes d'études. Cela a permis d'identifier le jeu de paramètres du modèle pour trois différents types de HAP concernant le contexte faiblement contaminé tandis que le jeu des paramètres pour un seul HAP a été identifié pour le contexte fortement contaminé. Dans un deuxième temps, le modèle calibré **a été évalué** pour estimer sa capacité à restituer les données expérimentales observées **au champ** sous des conditions climatiques réelles dans les deux sites d'étude. Dans un troisième temps, le modèle validé a été utilisé pour tester différentes hypothèses de variation de disponibilité et **scenarios** climatiques ou d'apports répétés de différents composts sur le devenir de HAP dans le sol **sur des temps plus longs**. Les principales caractéristiques des systèmes d'étude pour les deux sites concernés, les HAP et les traitements étudiés, et pour les deux échelles d'étude ainsi que les méthodes d'extraction utilisées pour quantifier les HAP dans les sols sont résumés dans le **Tableau C1.**

Tableau C1. Comparaison entre les deux systèmes d'études

	Contexte industriel, site du GISFI		**Contexte agricole, site de QUALIAGRO**	
	Echelle du laboratoire	**Echelle du terrain**	**Echelle du laboratoire**	**Echelle du terrain**
Description	Sol industriel anciennement contaminé		Sol agricole (Taux d'application de compost 4 ton C/ha/2 ans)	
Teneur en 16 HAP d	1500 mg/kg_{ds}		0.5 mg/kg_{ds}	
Traitements étudiés	Sol nu sans plante		Sol control Sol + DVB Sol + MSW[b] Sol + BioW[c]	Sol control Sol + GWS Sol + MSW
HAP étudié	^{13}C-PHE	PHE	^{14}C-PHE ^{14}C-BaP ^{14}C-FLT	PHE BaP
Périodes d'observation	13 jours	2005-2012	28 j en compost + 55 j en (compost + sol)	1998-2011
Méthode d'analyse	Extraction ASE (dichlorométhane, DCM)	Extraction ASE DCM + Extraction sur phase solide Tenax	Extractions successives au méthanol	Extraction ASE (acétone / DCM / n-hexane)
	Chapitre II	**Chapitre III**	**Chapitre IV**	**Chapitre V**

Les cinétiques des HAP dans les sols

Les cinétiques des HAP au champ sont mal ou trop peu connues dans la littérature. Au cours de cette étude, un jeu de paramètres pour le phénanthrène a été établi sur sol nu (sans plante) sur le site du GISFI, tandis que 3 jeux de paramètres pour le phénanthrène (PHE), le fluoranthène (FLT) et benzo(a)pyrene (BaP) ont été établis pour le sol du site QUALIAGRO pour différents traitements d'apport de compost (Tableau C1). Le Tableau C2 résume l'ensemble des jeux de paramètres du modèle obtenus pour le PHE qui est le HAP commun aux deux sites d'études, GISFI et QUALIAGRO et la Figure C1 rappelle la structure complète du modèle utilisé. Pour chacun des sites d'étude, une étape complémentaire de calibration pour certains paramètres du modèle a été nécessaire car les paramètres du modèle optimisés à l'échelle du laboratoire n'étaient pas capables de reproduire de manière correcte les dynamiques des HAP observées à l'échelle du terrain. En effet, les paramètres ont été déterminés en utilisant des incubations de molécules de HAP marquées sur des périodes relativement courtes (13 et 55 jours pour la situation du GISFI et QUALIAGRO, respectivement). A cette échelle de temps, l'effet du vieillissement, le temps de maintenance

des biomasses microbiennes et les effets des varaitions des conditions de température du sol et de teneur en eau ne peuvent pas être pris en compte. Une autre raison qui explique l'échec partiel des jeux de paramètres déterminés au laboratoire à reproduire les observations à l'échelle de terrain est liée aux différences dans les méthodes d'extractions entre les deux échelles pour un même site d'étude (Tableau C1). Cela a conduit à imposer des conditions initiales et des hypothèses de démarrage différentes en fonction du type de données expérimentales disponibles. Par exemple, dans le site GISFI et à l'échelle du laboratoire (Chapitre II), la distribution de ^{13}C-PHE dans le sol a été évaluée par la méthode d'extraction de solvant accélérée (par dichlorométhane). Lors de l'étape de calibration et afin d'adapter les données expérimentales aux différents compartiments du modèle, la quantité de ^{13}C récupérée par extraction a été attribuée (en utilisant le coefficient de distribution K_d) aux compartiments du modèle PAH_{AV} et PAH_{WS} représentant respectivement la fraction biodisponible de PHE dans la solution du sol et la fraction faiblement adsorbée dans la matrice du sol. Le compartiment du modèle PAH_{SS} représentant la fraction de HAP fortement adsorbés a été attribuée avec l'autre compartiment du modèle PAH_{BS} aux données de PHE non extractibles obtenues par bilan de masse (le paramètre k_{SW} représentant la cinétique de retour de HAP de PAH_{SS} à PAH_{WS} a été considéré nul). A l'échelle du terrain et pour le même site d'étude (Chapitre IV), la méthode d'extraction de solvant accélérée (Dichlorométhane) est accompagnée d'une extraction en phase solide avec Tenax. Nous avons alors attribué les compartiments du modèle aux données expérimentales de manière différente à celle du chapitre II. Etant donnée que la fraction non extractible de PHE ne peut être identifiée analytiquement au terrain et que la fraction de HAP mesurée par Tenax est considéré comme accessible aux biomasses microbiennes, nous avons choisi d'attribuer la fraction HAP identifiée par Tenax aux deux compartiments du modèle PAH_{WS} et PAH_{AV}, tandis que la fraction extraite par dichlorométhane a été considéré comme fraction fortement adsorbée et elle a donc été attribuée au compartiment du modèle PAH_{SS} (le paramètre k_{SW} n'était donc plus nul et une étape de calibration supplémentaire a été donc nécessaire).

En revanche, pour la situation du site QUALIAGRO, nous avons attribué les données expérimentales aux différents compartiments du modèle de manière similaire dans les deux échelles d'études (ici le compartiment PAHss a été considéré non extractible aux deux échelles, le laboratoire « chapitre III » , et le terrain « chapitre IV »). Cependant, une nouvelle étape de calibration a été quand même nécessaire lors du changement d'échelle. L'échec ici peut être expliqué par les mêmes raisons que celles présentées ci-dessus ainsi que

par la différence dans les rendements d'extraction des HAP obtenus par les méthodes d'extractions, comme expliqué dans le chapitre V (section 5.3.3.3).

D'autre part, les résultats obtenus par ce travail ont montré que pour un HAP il n'y a pas un jeu de paramètres qui peut être valide pour les deux sites d'études GIFI et QUALIAGRO et qui produirait ainsi un modèle générique. En plus des raisons mentionnées ci-dessus, la différence entre les jeux des paramètres des deux sites d'étude peut être attribuée à la différence dans les conditions qui contrôlent ces sites : nature du sol, nature des matières organiques, temps de contact entre les HAP et le sol et/ou les matières organiques et les valeurs des teneurs en HAP initiales qui représente un facteur 3000 entre les deux sites d'étude (Johnson et al., 2001) (Tableau C1).

Tableau C2. Jeux de paramètres du modèle pour le phénanthrène dans les deux situations d'étude

Paramètre	Unité	Situation de site de GISFI		Situation de site de QUALIAGRO	
		[d,✱]Echelle du laboratoire	Echelle du terrain	[d]Echelle du laboratoire	Echelle du terrain
k_{AW}	d^{-1}	55.725		1.770	0.0022[a] 0.0025[b] 0.0030[c]
k_{WA}	d^{-1}	0.0567		0.230	0.00001
k_{WS}	d^{-1}	0.0582		0.065	
k_{SW}	d^{-1}	0.0	0.0006	0.032	
k_{MB}	d^{-1}	0.0006		0.037	
k_{CS}	d^{-1}	-		0.238	
k_{deg}	($mg\,C/kg_{dw.}d$)	-		0.0027	
β	-	-		0.478	
μs_{max}	d^{-1}	4.89	0.0171	2.606	
ks_{spe}	$\mu g/kg_{dw}$	35.6		36.627	
Y_{spe}	-	0.127		0.251	
k_M	d^{-1}	0.0	0.0015	0.035	
		Chapitre II	Chapitre III	Chapitre IV	Chapitre V

a : traitement sol control
b : traitement sol + GWS compost
c : traitement sol+ MSW compost
d : Seulement les valeurs les plus ont données ici ;
✱ Les paramètres obtenus par le biais de scénario de biodégradation par spécifique biomasse

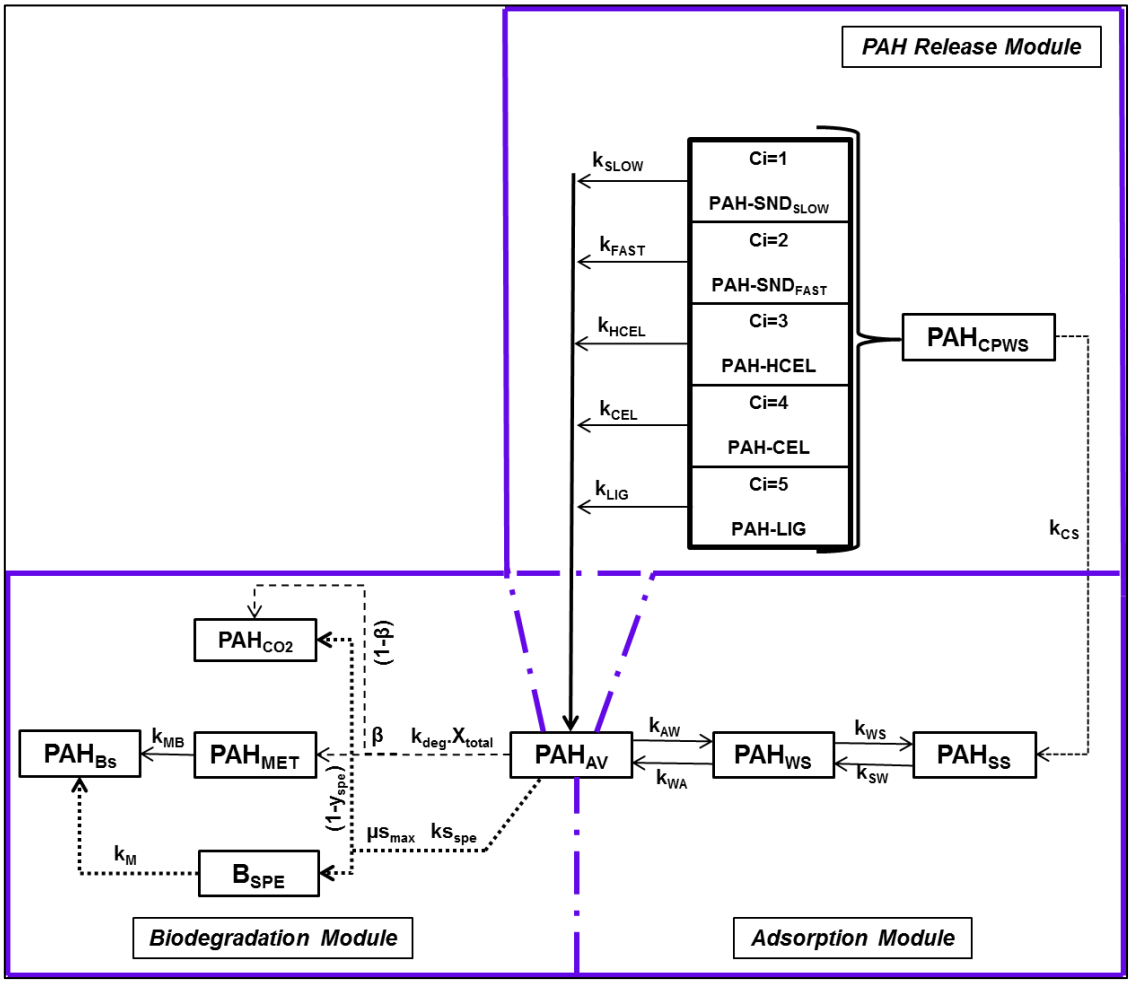

Figure C.1. Schéma du couplage entre les modules HAP

Influence des conditions climatiques sur la gestion du sol contaminé

L'effet des paramètres environnementaux de température et humidité du sol sur le devenir des HAP dans le sol a été étudié via un scénario au long terme sur le site du GISFI (chapitre IV). L'effet de deux futures scénarios de changement climatiques du GIEC (Groupe d'experts Intergouvernemental sur l'Evolution du Climat) A2 et B1 simulés pour la zone d'étude sur la dissipation des HAP dans le sol a été examiné. En générale les deux scénarios climatiques A2 (le plus intense) et B1 (le plus modeste) prédisaient que les températures de l'air seraient plus élevées dans les prochaines années, mais avec une légère augmentation dans le scénario B1 par rapport à A2. Mais cela est accompagné par une augmentation dans la quantité d'eau atteignant la surface du sol pour le scenario A2 en comparaison à B2 (soit 1,34 fois plus pour A2 que pour B2). Notre résultat de simulation a montré que la différence dans les facteurs météorologiques entre les deux scénarios a conduit à une augmentation environ 3.32% (au profit de A2) de la quantité dissipée de PHE dans le sol au bout 20 ans de simulations.

L'augmentation de la température améliore donc la dissipation des HAP dans le sol du fait de l'augmentation des taux de dégradation du polluant dans le sol. Notre résultat est en accord avec les résultats déjà publiés dans la littérature pour les pesticides (Noyes et al., 2009). D'après notre résultat, les facteurs météorologiques sont importants et devraient donc être pris en compte dans chaque future stratégie de gestion.

Biodégradation HAP dans les sols

Dans notre modèle, les deux voies classiques de biodégradation ont été couplées. Dans le cadre de l'étude du sol contaminé du site de GISFI (chapitre II), diffèrentes hypothèses de biodégradation du PHE dans le sol ont été testées afin d'identifier la voie de biodégradation la plus pertinente dans les différents systèmes étudiés (via le cométabolisme, via le métabolisme spécifiques, ou par les deux voies de biodégradation ensemble). Les résultats de la simulation ont mis en évidence que la voie de biodégradation spécifique était la plus efficace pour expliquer les données expérimentales. Nos résultats confirment des résultats expérimentaux précédents effectués sur le même sol contaminé qui ont montré qu'une modification de la diversité de la population bactérienne dégradant le phénanthrène n'augmente pas le taux de minéralisation du phénanthrène dans le sol (Cébron et al., 2011). En revanche, dans les sols amendés (situation de QUALIAGRO, chapitre III), les résultats pour le PHE et le BAP, ont mis en évidence que la biodégradation des HAP était principalement due à la biomasse microbienne co-métabolique alors que la dégradation des HAP était due à la biomasse microbienne spécifique dans le sol control. Pour FLT, le modèle prédit qu'une partie importante de la fraction de minéralisée a été formée par la voie de biodégradation spécifique pour les sols amendés par des composts matures (i.e. GWS et BIOW). Ce dernier résultat est en accord avec les résultats reportés que la croissance des biomasses spécifiques affectant la minéralisation d'un HAP peut être plus élevée dans les composts matures (Houot et al., 2012).

Processus biologiques ou physiques, lequel est le plus limitant ?

L'utilisation de notre modèle couplé pour représenter les processus majeurs contrôlant le devenir des HAP dans le sol nous a permis de montrer que la dissipation des HAP dans le sol était plutot régie par des interactions physico-chimiques et par la limitation du transfert du substrat plutôt que par une activité biologique. Cette conclusion a été confirmée plusieurs fois dans les différents chapitres de cette étude. Un test de sensibilité globale fait sur les paramètres du module d'adsorption couplé avec le module de biodégradation (chapitre II)

nous a montré que les paramètres k_{WA}, k_{AW} (qui sont les cinétiques réciproques entre le compartiment PAH_{AV} représentant la fraction HAP dans la solution du sol et le compartiment PAH_{WS} représentant la fraction HAP faiblement adsorbé) sont, tous les deux seuls ou en interactions avec les autres paramètres du modèle, les deux principaux paramètres déterminant la quantité HAP dégradé par les biomasses microbiennes. Un autre test de sensibilité effectué sur ces deux modules précédents couplés avec le module de décomposition de la matière organique compostée et un autre décrivant la libération des HAP du compost (chapitre III, section 3.4.4.1) a montré que le taux de minéralisation est principalement contrôlé par la limitation de la biodisponibilité des HAP plutôt que par la biomasse microbienne dégradante des HAP dans le système sol-compost. Les résultats des chapitres III et V ont également mis en évidence l'effet de hydrophobie des HAP sur leur minéralisation dans le sol (diminution dans l'ordre suivante PHE> FLT> BAP).

Lors de la simulation de scenario de modification de la disponibilité sur le long terme (chapitre IV), les résultats ont montré que l'augmentation de la disponibilité du polluant, toutes choses égales par ailleurs, conduit à une réduction significative des HAP au cours du temps.

Effet du compost sur le devenir des HAP dans le sol

Les résultats expérimentaux obtenus par les incubations des HAP marqués (chapitre III) montrent que les processus qui ont lieu avant l'application du compost dans le sol influencent fortement le devenir des HAP dans les différents sols amendés au laboratoire. Nos simulations ont montré que la dissipation des HAP pendant le compostage était plus élevée dans les composts matures alors que la dissipation des HAP dans le sol amendé était plus élevée dans les cas d'incorporation de compost non mature.

Nos résultats ont également permis de mieux comprendre le devenir et la biodisponibilité des HAP rajoutés au sol agricole avec l'application des composts à l'échelle de terrain (chapitre V). Les simulations ont montré que la majorité des HAP apportés avec le compost s'accumule et persiste dans le sol en causant une augmentation constante de leurs concentrations dans le sol amendé, mais qui reste à une faible valeur. La fraction séquestrée (i.e. PAH_{SS}) résultant du vieillissement des HAP dans la matrice du sol était la principale forme de stockage des HAP dans les sols amendés. Cependant, environ 25-30 % des HAP ajoutés étaient encore potentiellement biodisponibles. Toutes les fractions issues de l'activité biologique (i.e. minéralisé sous forme CO_2, transformé en métabolites ou biogéniques) sont mineures.

Une application de deux types différents de composts : un compost mature GWS et non mature MSW, à 4 ton C / ha / 2 an pendant 38 ans a entraîné une augmentation de la teneur en HAP dans les sols agricoles très faible et dans l'ordre suivante PHE > BaP. Par ailleurs, l'étude n'a pas montré d'effet significatif de la nature des composts sur l'état de transformation des HAP dans le sol. Ainsi l'accumulation de HAP dans les sols due à l'application de compost n'a pas augmenté de façon significative et les concentrations finales au bout de 38 ans de simulation sont inférieures à celles trouvées dans des directives réglementaires françaises pour l'application de composts contaminés par les HAP aux terres agricoles quel que soit le HAP et le compost appliqué.

Perspectives

La modélisation de la dynamique des HAP dans les sols a mis en évidence que la disponibilité du polluant pour les biomasses microbiennes dégradantes des HAP était la majeure contrainte affectant la performance de gestion des sols contaminés. Nous avons montré que l'amplitude de la dégradation dépendait principalement de l'amplitude de la disponibilité du polluant dans la solution du sol, et donc ce sont plutôt les processus physiques et non biologiques qui agissent sur la dissipation des HAP dans les sols pollués. Si ces résultats doivent être confirmés par des simulations numériques complémentaires, les recherches doivent aujourd'hui être poursuivies en intégrant dans notre modèle HAP (implanté dans VSoil) d'autres modules qui simulent le rôle que les plantes peuvent jouer dans les sols pollués et cultivés (particulièrement les modules qui simulent le processus d'absorption des HAP dissouts par les racines des plantes, l'impact de la teneur en matière organique dissoute produite dans la rhizosphère). Il serait aussi utile d'intégrer dans le modèle HAP un module décrivant l'interaction entre les HAP et les matières organiques dissoutes (MOD) du sol et le rôle de ces dernières sur la désorption et le transport des polluants dans le profil du sol (par exemple, le nouveau module proposé dans la thèse de Chabauty, (2015)). L'étude des effets de processus supplémentaires sur la dissipation des HAP en conditions climatiques réelles permettrait d'aboutir à une fiabilité raisonnable de nos différents résultats acquis dans ce travail.

Une procédure de modification du code du modèle de manière à ce que le modèle nous permette de faire des scénarios avec plusieurs HAP en même temps dans le sol serait nécessaire. Cela nous permettrait dans le future de vérifier certains problèmes comme par exemple la compétition entre les différents HAP pour les sites d'adsorption dans la matrice du

sol ainsi que l'effet multi-HAP sur la croissance de la biomasse microbienne et sa minéralisation dans le sol.

D'autre part, à cause du manque de données expérimentales, la prédiction des fractions biogéniques des résidus liés non-extractibles et leur pourcentage par rapport aux quantités totales des résidus liées non-extractibles a été réalisée avec une certaine incertitude, et nos résultats de simulation du site QUALIAGRO ne sont pas vérifiables sur ce point. Cette information est importante pour estimer le risque environnemental potentiel lié aux HAP. Cependant la fraction biogénique n'est pas mesurable facilement. La quantification de la fraction biogéniques des résidus liés au cours du temps peut être réalisée par l'application de méthodes d'analyses recommandées dans la littérature (comme par exemple celles, citées par Nowak et al.(2013) ou Richnow et al.(2000)). Les méthodes chimiques d'extraction ont montré un effet important sur la répartition des fractions mesurées des HAP dans les compartiments du modèle initialement et au cours du temps. Il serait imortant d'utiliser des méthodes d'analyse communes au laboratoire et au champ afin d'améliorer la comparaison entre les deux systèmes d'échelle.

Références

Cébron, A., Louvel, B., Faure, P., France-lanord, C., Chen, Y., Murrell, J.C., Leyval, C., 2011. Root exudates modify bacterial diversity of phenanthrene degraders in PAH-polluted soil but not phenanthrene degradation rates. Environ. Microbiol. **13**, 722–736. doi:10.1111/j.1462-2920.2010.02376.x

Chabauty, F., 2015. Effets des matières organiques dissoutes sur le transport de différents contaminants organiques dans l'horizon illuvié (Bt) de sols limoneux profonds : approche expérimentale et modélisation.

Houot, S., Verge-Leviel, C., Poitrenaud, M., 2012. Potential mineralization of various organic pollutants during composting. Pedosphere **22**, 536–543. doi:10.1016/S1002-0160(12)60038-1

Johnson, M.D., Keinath, T.M., Weber, W.J., 2001. A distributed reactivity model for sorption by soils and sediments. 14. Characterization and modeling of phenanthrene desorption rates. Environ. Sci. Technol. **35**, 1688–1695. doi:10.1021/es001391k

Nowak, K.M., Girardi, C., Miltner, A., Gehre, M., Schäffer, A., Kästner, M., 2013. Contribution of microorganisms to non-extractable residue formation during biodegradation of ibuprofen in soil. Sci. Total Environ. **445–446**, 377–384. doi:10.1016/j.scitotenv.2012.12.011

Noyes, P.D., Mcelwee, M.K., Miller, H.D., Clark, B.W., Tiem, L.A. Van, Walcott, K.C., Erwin, K.N., Levin, E.D., 2009. The toxicology of climate change : Environmental contaminants in a warming world. Environ. Int. **35**, 971–986. doi:10.1016/j.envint.2009.02.006

Richnow, H.H., Annweiler, E., Koning, M., Lüth, J.C., Stegmann, R., Garms, C., Francke, W., Michaelis, W., 2000. Tracing the transformation of labelled [1-13C]phenanthrene in a soil bioreactor. Environ. Pollut. 108, 91–101. doi:10.1016/S0269-7491(99)00205-5

LISTE DES FIGURES

LISTE DES TABLEAUX

université PARIS-SACLAY
ÉCOLE DOCTORALE
Agriculture, alimentation, biologie, environnement, santé (ABIES)

Titre : Modélisation de la dynamique des hydrocarbures aromatiques polycycliques (HAP) dans des sols soumis à un gradient de contamination allant d'un contexte agricole à un contexte industriel

Mots clés : modélisation, compost, sols agricoles, sols de friche industrielle, plateforme Sol Virtuel

Résumé : Du fait des activités industrielles anciennes et du recyclage croissant des produites résiduaires organiques d'origine urbaine dans les sols agricoles, des composés organiques persistants, parmi lesquels les hydrocarbures aromatiques polycycliques (HAP) se retrouvent présents dans les sols français. Dans le cadre de la gestion des sites et sols pollués et de l'évaluation des risques associés aux HAP dans l'environnement, une meilleure connaissance du comportement, de la dissipation, du transfert ou de l'accumulation des HAP dans les sols est alors indispensable. Dans ce but, il est utile de développer une nouvelle génération de modèles numériques basés sur le couplage flexible de l'ensemble des processus majeurs contrôlant la dynamique des HAP dans le sol. Notre travail repose sur la mise en œuvre, dans le cadre de la plateforme VSoil de l'INRA (https://www6.inra.fr/vsoil/The-Project), d'un modèle global interdisciplinaire de dynamique des HAP dans les sols, applicable à l'échelle du terrain et couplant des modules décrivant les principaux processus physiques, biochimiques et biologiques. Ce modèle associe d'une part des modules déjà publiés simulant la décomposition des matières organiques exogènes apportées, le transfert d'eau, le transfert de chaleur et le transport de solutés dans des conditions climatiques réelles, et d'autre part, un nouveau modèle représentant spécifiquement la réactivité des HAP.La démarche numérique adoptée dans ce travail a alors été de i) calibrer le modèle de terrain en utilisant des paramètres déterminés à partir de données expérimentales obtenues au laboratoire et complétées avec une partie des données de terrain obtenues sur une courte période, ii) tester et valider le modèle calibré au terrain à l'aide des données de terrain complémentaires sur des périodes plus longues, iii) tester différentes hypothèses de variation de disponibilité et scenarios climatiques ou d'apports répétés de différents composts sur le devenir de HAP dans le sol. Nos résultats montrent que le modèle peut prédire de manière satisfaisante le devenir des HAP dans le sol sur une gamme de contamination allant de parcelles agricoles amendées avec des matières organiques faiblement contaminées jusqu'à d'anciens sites industriels fortement contaminés et permettent alors de mieux appréhender les processus contrôlant la dynamique des HAP dans ces différents systèmes.

Title : Modeling the dynamic of polycyclic aromatic hydrocarbons (PAH) in soils impacted by a gradient of contamination ranging from agricultural to industrial contexts

Keywords : modeling, compost, agricultural soil, industrial soil, Virtual Soil platform

Abstract: Due to former industrial activities and the increasing recycling of organic waste products from urban areas in agricultural soils, increasing amounts of persistent organic compounds, among them polycyclic aromatic hydrocarbons (PAH), are to be found in French soils. In the framework of the management of polluted sites and soils and the risk assessment of PAH transfer in the environment, it is essential to better understand the behavior, dissipation, transfer or accumulation of PAH in soils. For this purpose, there is a need to develop a new generation of numerical models based on the flexible coupling between the processes describing PAH dynamics in soil. Our work presents the development and assessment of such model. It is based on the implementation of an interdisciplinary global model, and applicable at the field scale, for PAH in soil by coupling modules describing the major physical, biochemical and biological processes influencing the fate of PAH in soil, with modules that simulate water transfer, heat transfer, solute transport, and organic matter transformation under real climatic conditions. The coupling is performed using the «VSoil» modeling platform of INRA (https://www6.inra.fr/vsoil/The-Project). The steps of our modelling study are the following: i) calibrate the model at the field scale using previously estimated parameters at the lab-scale and completed with field data on a short period of time, ii) test and validate the calibrated model using field experimental data on mid term periods, iii) test different hypotheses of variation of availability and climatic scenarios or repeated applications of different composts on the fate of PAH in soil. Our results show that the model can adequately predict the fate of PAH in soil over a wide range of contamination ranging from agricultural plots amended with weakly contaminated composted organic wastes to old industrial sites heavily contaminated. This new tool allows, therefore, a better understanding of the processes controlling the dynamics of PAH in these different systems.

Université Paris-Saclay
Espace Technologique / Immeuble Discovery
Route de l'Orme aux Merisiers RD 128 / 91190 Saint-Aubin, France